# STUDIES ON CHEMICALLY MODIFIED BIOLOGICAL POLYMERS AS ENVIRONMENT-FRIENDLY CORROSION INHIBITORS

**THESIS**

SUBMITTED IN PARTIAL FULFILMENT OF THE REQUIREMENTS

FOR THE AWARD OF THE DEGREE OF

*Doctor of Philosophy*

IN

**CHEMISTRY**

BY

**VIMAL KUMAR K**

**(Roll No. 701162)**

RESEARCH SUPERVISOR

**Dr. B. V. APPA RAO**

**PROFESSOR OF CHEMISTRY (RETD.)**


**DEPARTMENT OF CHEMISTRY**

**NATIONAL INSTITUTE OF TECHNOLOGY WARANGAL**

**WARANGAL – 506 004, TELANGANA, INDIA**

**APRIL – 2018**

# DECLARATION

This is to declare that the work presented in the thesis entitled ***"Studies on Chemically Modified Biological Polymers as Environment-friendly Corrosion Inhibitors"***, is a bonafide work done by me under the supervision of **Dr. B. V. Appa Rao**, Professor of Chemistry (Retd.), Department of Chemistry, and was not submitted elsewhere for the award of any degree.

I declare that this written submission represents my ideas in my own words and where others' ideas or words have been included, I have adequately cited and referenced the original sources. I also declare that I have adhered to all principles of academic honesty and integrity and have not misrepresented or fabricated or falsified any idea/data/fact/ source in my submission. I understand that any violation of the above will be a cause for disciplinary action by the Institute and can also evoke penal action from the sources which have thus not been properly cited or from whom proper permission has not been taken when needed.

Date: **(VIMAL KUMAR K.)**

Place: **NIT Warangal** Roll Number: **701162**

Dr. B. V. APPA RAO
Professor of Chemistry (Retd.)
Department of Chemistry
National Institute of Technology
Warangal - 506 004

# CERTIFICATE

This is to certify that the work presented in the thesis entitled ***"Studies on Chemically Modified Biological Polymers as Environment-friendly Corrosion Inhibitors",*** is a bonafide work carried out by **Mr. Vimal Kumar K** under my supervision and was not submitted elsewhere for the award of any degree.

Place: Warangal **(B. V. APPA RAO)**

Date: **(Research Supervisor)**

# A C K N O W L E D G E M E N T S

It is with immense pleasure that I express my deep sense of gratitude to ***Prof. B. V. Appa Rao,*** Professor of Chemistry (Retd.), National Institute of Technology, Warangal for his inspiring guidance and invaluable cooperation in the course of my research. The fruitful discussions I had with him on the subject gave me the needed insight into the subject and were very helpful in the preparation of this thesis. I consider myself as very fortunate for being his student and it would have been impossible to achieve this goal without his sturdy support and care.

I am grateful to ***The Director***, National Institute of Technology, Warangal for giving me the opportunity to carry out the work and allowing me to submit in the form of thesis. I greatly acknowledge ***Ministry of Human Resource Development, Govt. of India*** for the financial support in the form of Institute fellowship.

I express my gratitude to the Doctoral Scrutiny Committee members, namely ***Prof. K. V. Gobi,*** Chairman and Head, Department of Chemistry, NIT Warangal and ***Prof. M. Krishna Mohan,*** Department of Metallurgical and Materials Engineering, NIT Warangal for their insightful suggestions.

My sincere thanks are due to the ***former Heads*** of the Department of Chemistry during the period of my research work.

I would like to thank all the faculty members from Chemistry Department namely ***Prof. A. Ramachandraiah, Prof. P. Nageswara Rao, Prof. K. Laxma Reddy***, ***Prof. P. V. Srilakshmi***, ***Dr. Vishnu Shanker***, ***Dr. D. Kasinath, Dr. Venkatathri Narayanan***, ***Dr. B. Srinivas, Dr. K. Hari Prasad*** and the ***other faculty members*** for their valuable advice and encouragement throughout the research work.

I would like to thank ***Dr. Neha Yeshwanta Hebalkar,*** Scientist 'D', ARCI, Hyderabad. For helping me in the XPS analysis.

I convey my special thanks to my seniors ***Dr. S. Srinivara Rao, Dr. Md. Yakub Iqbal, Dr. K. Chaitanya kumar, Dr. M. Nooka Raju, Dr. Narsihma Reddy Miryala*** *and* ***Dr. K. Koteswar Reddy,*** for their continuous support and encouragement in each and every step of my research work.

I would like express my deep sense of gratitude to my friends ***Dr. Satyanarayana Moru, Dr. O. Surender Reddy, Dr. Venkatrajam Marka, Dr. T. Surendar, Dr. V. Krishnaiah, Dr. K. Yugendar Goud, Dr. Mallishwar Reddy*** *and* ***Dr. Punnam chander, N. Kishore Kumar.***

With all happiness I acknowledge the cheerful assistance rendered by all my research colleagues *Dr. B. Janardhan, Dr. S. Kanakaraju, Dr. B. Santhosh Kumar, Dr. G. Srinivasa Rao, Dr. L. Suresh, Dr. P.srinu, Mr. A. Ajay Kumar, Mr. Ashutosh Kumar Yadav, Mr. E. Hari Mohan, Mr. Phani Kumar, Mr. M. Sai Kumar, Mr. Chirra Suman, Mr. V. Sunil kumar, Ms. P. Soumya, Ms. Hitavani, Ms. Mayuri, Ms. S. Manasa, Ms. Pallavi Varanasi, Mr. Suresh Siliveri, Mr. Shekar Kummari, Mr. Ambedkar G.* and other co-research scholars for their munificent support.

I am grateful to the lab assistants *Mr. Praveen, Mr. Srinivas* and *other supporting staff* of the Department of Chemistry, NIT Warangal for their cooperation.

My heart goes to my beloved ***Family Members*** who with all their patience, prayers and faith in the Almighty, waited all these long years to see me reaching this stage. Their blessings and care always gave me new fervour and gusto to do something more with perfection.

I always remember and cherish the encouragement and inspiration provided by all my friends and well-wishers during the course of my research work.

Date: **Vimal Kumar K.**

# List of Symbols and Abbreviations used in this thesis

| | |
|---|---|
| EIS | Electrochemical Impedance Spectroscopy |
| SEM | Scanning Electron Microscopy |
| EDX | Energy Dispersive X-ray spectroscopy |
| XPS | X-ray Photoelectron Spectroscopy |
| XRD | X-ray Diffraction |
| $\beta_a$ | Anodic Tafel slope |
| $\beta_c$ | Cathodic Tafel slope |
| dec. | Decade |
| CPE | Constant Phase Element |
| $C_{dl}$ | Double layer capacitance |
| $E_{corr}$ | Corrosion potential |
| eV | Electron Volt |
| I.E. | Inhibition Efficiency |
| $j_{corr}$ | Corrosion current density |
| kHz | Kilohertz |
| mmpy | Millimeter per year |
| µA | Microampere |
| mV | Millivolt |
| ppm | Parts per million parts |
| Z' | Real Impedance |
| Z'' | Imaginary Impedance |
| W | Warburg impedance |
| $R_{ct}$ | Charge transfer resistance |
| $R_s$ | Solution resistance |
| Cps | Counts per second |
| Ω | Ohm |
| $^oC$ | Degree centigrade |
| nm | Nanometer |
| PCT | Phosphorylated Chitin |
| CX | Chitin Xanthate |
| CAK | Chitosan Ascorbate Ketimine |
| PXG | Phosphorylated Xanthan Gum |

# TABLE OF CONTENTS

## CHAPTER – I



## CHAPTER – II



## CHAPTER III

## CHAPTER IV

# CHAPTER-I

# INTRODUCTION

# TABLE OF CONTENTS

## CHAPTER – I

### INTRODUCTION

# CHAPTER – I

# INTRODUCTION

## I.1 Definition of corrosion

'Corrosion' may be defined as the deterioration of a materials (metal or alloy) due to a chemical or electrochemical reaction with its environment[1,2]. Most of the metals in nature exist in the combined state as minerals in the form of compounds with different anions such as oxides, sulphides, halides etc. In this state they are thermodynamically more stable than the pure form of the metal. The pure metals are extracted from their respective ores through a process called extractive metallurgy[3]. As the pure metal is thermodynamically unstable, it reverts back to the relatively more stable state. Hence, the process of corrosion of metals can be considered as the reverse process of extractive metallurgy[4]. Figure I.1 explains the reason behind the spontaneity of the corrosion process of metals.

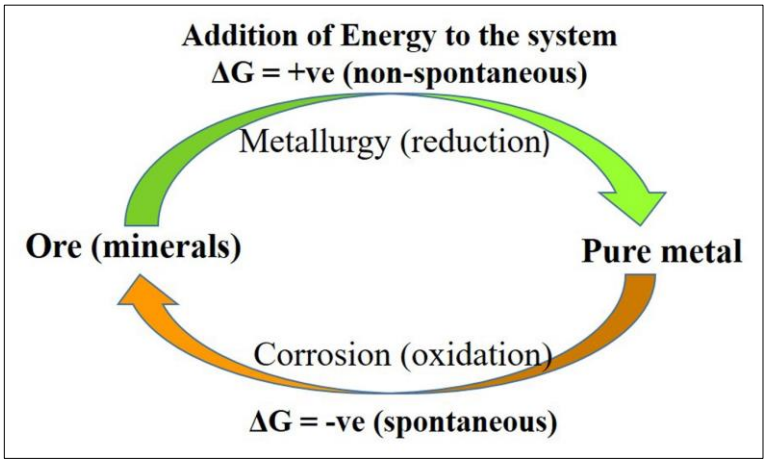


**Figure I.1:** schematic representation of extractive metallurgy and corrosion process.

## I.2 Economic consequences of corrosion

Research in the field of corrosion control mostly revolves around control of corrosion cost (economic factors). The cost of corrosion globally is estimated to be US$ 2505 billion per year, which is equivalent roughly to 3.4% of the global GDP (2013)[5].The cost of corrosion in united states of America, which has an advanced industrial and service economy is US$ 451 billion per year, which is equivalent to 2.7 % of the Nation's GDP[6]. A country like India, which has a significant agricultural economy has the corrosion cost of US$ 70.3 billion, which is equivalent to 4.2 % of the Nation's GDP[6]. Countries like Kuwait, which have a significant oil industry economy, have

different corrosion cost profile. It has been reported in many studies, that the cost of corrosion is in the order of 1 to 5 % of the Gross National Product (GNP) for any country.[7]

It is apparent from the available literature that the economic consequences due to corrosion and estimated savings in various fields can be acquired by the use of corrosion resistant materials (judicious selection of material) along with the corrosion control measures[8]. By implementing the available corrosion control measures, it is estimated that the cost of corrosion to the extent of 15- 35% could be saved, precisely between US$ 375 to $875 billion on a global basis annually[5].

Corrosion of materials holds a significant threat to the safety of human life, which has far greater significance than the economic consequences. Most often tragic news hits the headlines of print and electronic media caused by the sudden failure of equipment due to corrosion resulting in the loss of life and property. A few of such tragic calamities are worth mentioning. The 'Bhopal gas tragedy' in India due to the leakage of methyl isocyanate (MIC) from a pesticide plant storage tank, claimed thousands of lives and even many more became permanently blind [9]. It could have been due to corrosion and, if such is the case, it may well be stated as the biggest fatal accident due to corrosion ever recorded in the history.

A major tragedy occurred at HPCL refinery in Vishakhapatnam, India in 1997 due to corrosion of pipelines[10]. It has resulted in 50 fatalities. Failure in periodic monitoring of the pipelines and poor maintenance was the prime cause for the calamity.

In April 22, 1992, in Guadalajara city, situated in Jalisco state, Mexico a series of gasoline explosions took place in a sewer system. This tragedy has claimed 206 fatalities and estimated financial damage of around 76 million euros[8,11].

Explosion in a GAIL-operated gas pipeline passing through Nagaram village in East Godavari district of Andhra Pradesh on June 27, 2014 is also an example of poor corrosion management.

Conservation of limited and finite resources like metals is also another important concern. Wastage of materials also includes the corresponding losses of energy and water reserves associated with the production and fabrication of metal structures.

### I.3 Methods of corrosion control

Several techniques have been employed to manage, slowdown, or even stop the corrosion of metals. Corrosion prevention can take a number of forms depending on the

circumstances of the metal being corroded. Corrosion prevention techniques can be generally classified into three groups:

A) Alteration of metal:

i) Selection of metal and surface condition plays an important role in prevention the corrosion. Based on the environmental conditions, the type of metal being used can also lead to significant reduction in corrosion. Appropriate alloys can be used for specific environments in order to reduce the corrosion.

ii) Surface modification is an another way of corrosion control in which, the surface of the material is modified either by coatings (organic, metallic) or by surface alloying (phosphating, chromising) to protect against corrosion.

B) Alteration of the environment:

i) The basic cause of corrosion is the chemical or electrochemical interaction between metal and the environment. By altering or manipulation the environment through deaeration and dehumidification, the corrosion process can be hindered.

ii) By adding the corrosion inhibitors to the environment, the problem of corrosion of metals can be tackled.

C) Electrochemical protection:

i) Cathodic protection: This method works by converting the active (anodic) sites into passive (cathodic) sites on metal surface through the application of an opposing current. Cathodic protection can also be done by introducing galvanic anodes (sacrificial anodes) into the electrolytic environment to corrode themselves in order to protect the cathode (metal) from corrosion.

ii) Anodic protection: This method is generally employed when the cathodic protection and coating methods are not suitable.

**I.4 Corrosion control by inhibitors**

According to the American Society for Testing of Materials' corrosion glossary, a corrosion inhibitor is defined as a chemical substance or combination of substances that, when present in the proper concentration and forms in the environment, prevents or reduces corrosion [12]. The definition of a corrosion inhibitor favored by National

Association of Corrosion Engineers (NACE)[13] is that the corrosion inhibitor is 'a substance which retards corrosion when added to an environment in small concentrations'.

The corrosion Inhibitor adsorbs itself on the metal surface and forms a protective film, which enables the corrosion protection. The inhibitor can be employed in the form of solution or as a protective coating via dispersion technique.

### I.4.1 Classification of inhibitors

While there are various inhibitor classifications listed in the literature, there is no completely satisfactory way to categorize. One of the common ways is to classify them according to their reaction at the metal surface[14].

i) Anodic inhibitors: compounds that reduce the metal dissolution (anodic reaction).
ii) Cathodic inhibitors: compounds that reduce the rates of the cathodic reactions (the hydrogen evolution or oxygen reduction reactions).
iii) Mixed inhibitors: compounds that retard both the anodic and cathodic corrosion processes simultaneously.

This classification can also be explained on the basis of electrode polarization behaviour in the presence of an inhibitor. Polarization refers to the change of potential from a stabilized state. In the context of corrosion, it is the shift of the electrode potential away from the open circuit potential (free corroding potential). If the potential shifts in the 'positive' direction (above $E_{corr}$), it is called 'anodic polarization'. If the potential shifts in the 'negative' direction (below $E_{corr}$), it is called 'cathodic polarization'. A schematic representation of perturbation of a system from equilibrium in terms of potential is given in the figure I. 2,

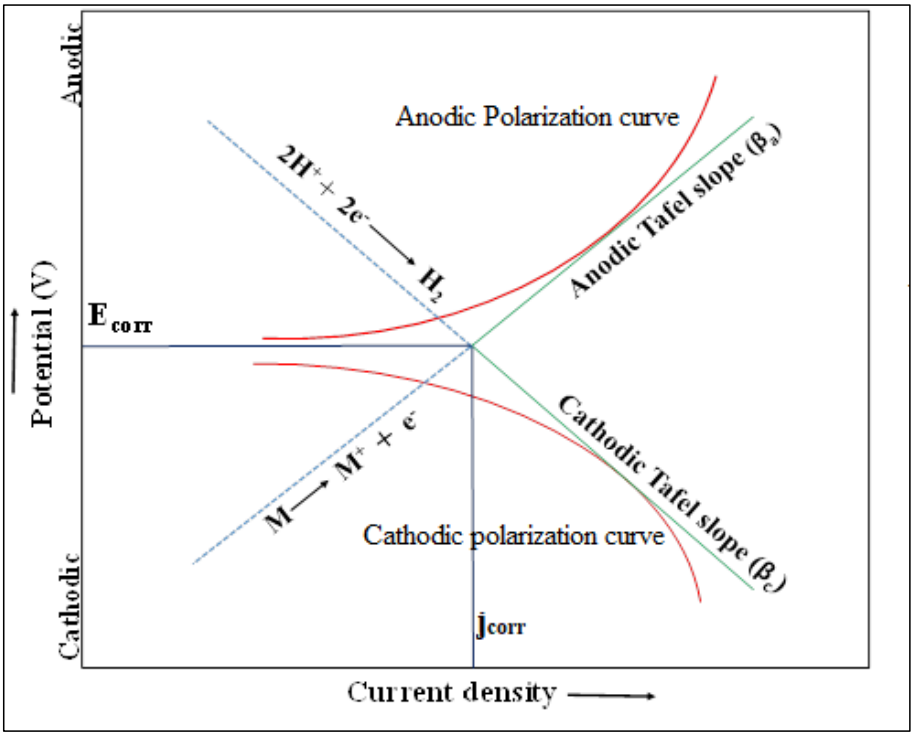


**Figure: I.2**: Schematic diagram showing the anodic and cathodic polarisation curves.

Those inhibitors which increase only the anodic polarization are said to be anodic inhibitors, whereas those inhibitors which increase only the cathodic polarization are considered as cathodic inhibitors. Some inhibitors increase both the anodic and cathodic polarization and such inhibitors are said to be mixed type inhibitors.

When a metal is in equilibrium with the environment (electrolyte solution) the anodic currents($i_a$) and the cathodic currents($i_c$)which flow through the system are equal and opposite[15]and there will be no net current flow in the system. When this equilibrium is perturbed by means of an external potential, the metal will be polarized and a finite amount of net current flow can be observed in the system. When the perturbation induces the electron withdrawal from the metal, then the metal is said to be anodically polarized. In contrary when the perturbation pushes the electrons into the metal, then the metal is said to be cathodically polarized.

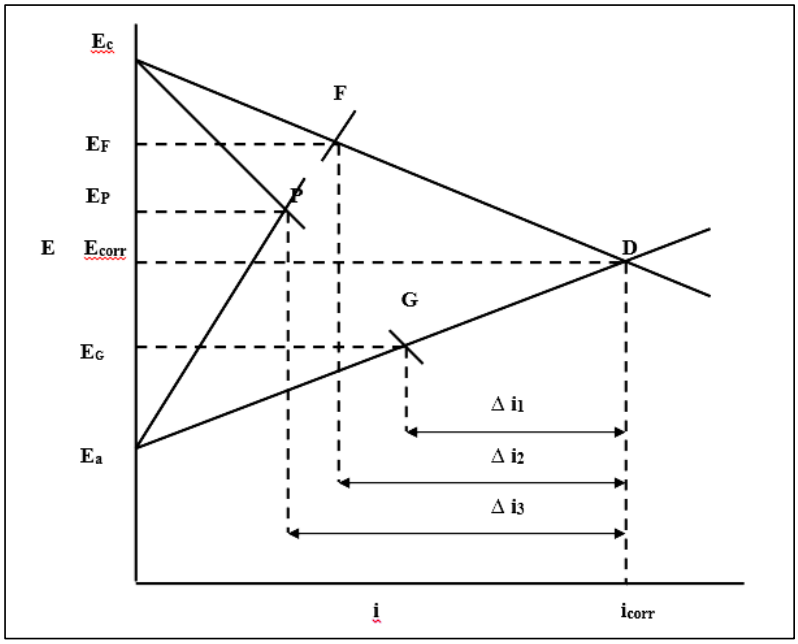


**Figure I.3:** Anodic and cathodic polarization curves when the inhibition is under anodic control, cathodic control and mixed control.

Fig. I.3 is a schematic diagram showing the anodic and cathodic polarization curves when the inhibition is under anodic control, cathodic control and mixed control. When polarization occurs mostly at anodes, it is said that the corrosion reaction is anodically controlled. An anodic inhibitor increases the anodic polarisation and moves the corrosion potential closer to the open circuit potential (OCP) of the cathode ($E_aD$ to $E_aF$ in the Figure I.3). Anodic inhibition results in greater shift in the anodic Tafel slope ($\beta_a$) relative to the cathodic Tafel slope ($\beta_c$). A cathodic inhibitor increases the cathodic polarisation, displacing the corrosion potential towards the OCP of the anode ($E_cD$ to $E_cG$ in the Figure I.3). Cathodic inhibition causes greater shift in $\beta_c$ than in $\beta_a$.

Mixed inhibitors retard both the anodic and cathodic reactions simultaneously. The corrosion potential is more or less unchanged, or changed to a lesser extent. In this case, the change in corrosion potential is smaller and its direction is determined by the relative magnitudes of the anodic and cathodic polarisation effects. In figure I.3, the anodic polarisation curve is shown by $E_aP$ and the cathodic polarisation curve by $E_cP$. Both $\beta_a$ and $\beta_c$ are either shifted equally or are unchanged in the case of mixed inhibitors. It can be found from this figure that in presence of a mixed inhibitor, the decrease in corrosion current density, $\Delta i_3$ is higher than that in case of an anodic and cathodic inhibitors, indicated as $\Delta i_2$ and $\Delta i_1$ respectively.

There is another grouping which is broadly acknowledged based on the mechanism and the mode of protection. According to this classification there are four types of corrosion inhibitors namely Film forming inhibitors, adsorption inhibitors, chemical passivators and vapour phase inhibitors.

**I.5 Synergistic effect of corrosion inhibitors**

The phenomenon of synergism is defined as an effect in which the combined inhibitive effect of the compounds is higher than the sum of the individual inhibitive effect of each of the compounds[16]. This effect mainly occurs either by the interaction between the components of the inhibitor formulation or by interaction between the inhibitor and one of the species present in the aqueous medium. In one case of synergism, corrosion inhibition of the mixture of substances is much higher than the inhibition effect of the individual compounds. There is another case of synergism in which, the substances when added individually, accelerate corrosion, but in combination inhibit corrosion. For instance, some phosphonates and $Zn^{2+}$ ions accelerate corrosion of mild steel when they are added individually. But, the mixture of those phosphonates and $Zn^{2+}$ ions inhibits the corrosion of carbon steel[17]. When the inhibition effect of the mixture of compounds is less than that of the sum of the individual compounds, it is known as antagonistic effect. Very few reports are there in the literature on antagonistic effect[18,19].

There are many reports in literature that addition of both cationic (metal ions) and anionic (halides) species to inhibitors can synergistically improve the inhibition efficiency of the inhibitor. Particularly transition metal cations can synergistically improve the inhibition efficiency of organic inhibitors. For instance, S. Rajendran et al.[20] studied the synergistic effect between sodium salt of phenyl phosphonic acid (PPA) and a transition metal ion, $Zn^{2+}$in inhibiting the corrosion of mild steel in a neutral aqueous environment. They have achieved a 95 % of inhibition efficiency when $Zn^{2+}$ ions are used as synergist.

The synergistic inhibition effect of rare earth cerium(IV) ions (transition metal ion)and 3,4-dihydroxybenzaldehye (DHBA) has been studied by Xianghong Li et al.[21]on corrosion of cold rolled steel in $H_2SO_4$ corrosive environment. They have reported that, the synergistic formulation has obtained an inhibition efficiency of 93 % in $H_2SO_4$, which is significantly much higher than the sum of the inhibition efficiencies obtained when they were used separately.

Da-Quan Zhang et al.[22] reported the synergistic inhibition effect of $Zn^{2+}$ ions and methionine (MTI) on the corrosion of copper in 0.5 M HCl solution. They concluded that the addition of $Zn^{2+}$ enhances the protection efficiency significantly and an inhibition efficiency of 92 % was observed in presence of $Zn^{2+}$ ions.

H. Amar et al.[23] have studied the effect by $Zn^{2+}$ on piperidin-1-yl-phosphonic acid (PPA) in controlling the corrosion of Armco iron in 3% chloride environment. They have concluded that the combination between PPA and $Zn^{2+}$exhibits excellent synergism in controlling the corrosion. An inhibition efficiency of 90.2 % was observed in presence of $Zn^{2+}$ ions. They have interpreted that the film formed on the surface consisting of $Fe^{2+}$-PPA complex and $Zn(OH)_2$ is the main reason for inhibition.

The synergistic relationship between zinc ions and bis(phosphonomethyl) glycine (BPMG) in controlling the corrosion of mild steel in 200 ppm NaCl environment has been studied by B. V. Appa Rao[24] et al. They have reported that excellent synergism exists between $Zn^{2+}$ ions and BPMG in controlling the corrosion of mild steel; formation of a protective film on the metal surface is the main reason for the inhibition. The Potentiodynamic polarization studies revealed that the binary formulation acts as mixed-type inhibitor. The effect of tungstate on the inhibitive action of BPMG and $Zn^{2+}$ ions in controlling the corrosion of mild steel in low chloride environment has also been reported by the same authors B. V. Appa Rao[25]et.al. They have concluded that the ternary inhibitor system works very effectively in neutral, slightly acidic and also slightly alkaline medium. The polarization studies revealed that the formulation works as a mixed type inhibitor. The authors interpreted that there is formation of a protective film on the metal surface, which consists of a polynuclear complex [Fe(III), Zn(II)–BPMG], $WO_3$, $Zn(OH)_2$ and iron oxide.

S. Rajendran et al.[26] studied the effect of a synergistic inhibitor formulation containing 1-hydroxyethane-1, 1-diphosphonic acid (HEDP) and $Zn^{2+}$ ions on the corrosion of mild steel in cooling water system. They have inferred that there exists a synergistic relationship between HEDP and $Zn^{2+}$ ions. The formulation acts as a mixed type inhibitor.

Apart from cations, anions have also received considerable attention as primary synergists. Synergistic effect of halide ions like $Cl^-$, $Br^-$, $I^-$, along with different types of inhibitors such as dyes, surfactants, natural products, polymers and drugs has been widely studied[27].

The action of halide ions on the corrosion inhibiting action of organic dyes has been studied widely. Salah Merah et al.[28] studied the synergistic effect of anionic synergist, $I^-$ ions on the inhibitive action of methyl red (MR) in combating the corrosion of mild steel in 0.5 M $H_2SO_4$ environment. They concluded that addition of $I^-$ ions synergistically enhanced the inhibition efficiency of methyl red. This is due to the adsorption of methyl red on the mild steel surface which has been stabilized when $I^-$ ions are added to the environment. Similarly, Emeka Oguzie et al. [29] reported that a synergistic relationship exists between anionic additive ($I^-$) and methyl green (MG) on the inhibition of mild steel corrosion in 0.5 M $H_2SO_4$ environment.

E.E. Oguzie[30] reported the influence of halide ions ($Cl^-$, $Br^-$, $I^-$) on congo red dye (CR) in combating the corrosion of mild steel in sulfuric acid solution. They observed that synergistic relationship between the halide ions and CR at 60 °C, whereas at 30°C the formulation worked antagonistically in inhibiting the corrosion of mild steel. They have also reported that in the absence of halide ions the corrosion inhibition mechanism by CR works by physisorption, while in the presence of halide ions it follows the chemisorption mechanism.

The effect of halide ions on the corrosion inhibiting action of surfactants has also been studied. Surfactants have better metal corrosion inhibitory effect. But they are toxic, and carcinogenic. Moreover, surfactants are very expensive when compared to other organic inhibitors. Hence, in the presence of halide ions, the amount of surfactant needed for inhibition could be reduced. Mohammed et al.[31] have reported that addition of halide ions as synergists will be a useful way to minimize the shortcomes of surfactants as corrosion inhibitors. They have reported that the inhibitive effect of nonionic surfactant namely nonylphenoxy poly (ethyleneoxy) ethanol (NPPE) on the corrosion of carbon steel in oilfield formation water has increased synergistically when halides ions are added.

Xueming Li et al.[32] reported that a synergistic relationship exists between cetyl trimethyl ammonium bromide (CTAB) and $Cl^-$ ions in combating the corrosion of steel in 1M $H_3PO_4$ environment. They have emphasized that the halide ions act as adsorption mediator for bonding metal surface and CTAB, and the inhibitor formulation acts as a mixed type.

Songqing Hu et al.[33] have studied the effect of 2-oleyl-1-oleylamidoethyl imidazoline ammonium methylsulfate (ODD) and halide ions on corrosion inhibition of mild steel in HCl environment. They have observed synergistic effect between ODD and

halide ions. From the molecular dynamic simulations they have emphasized that the synergistic effect of halide ions with ODD was increased in the order $Cl^- < Br^- < I^-$.

The effect of halide ions on the corrosion inhibiting action of Drugs like β-lactam antibiotics, histamines, barbiturates also was studied by several researchers. For instance, Nnabuk O. Eddy et al.[34] studied the inhibition effect of Cloxacillin (CLX) on the corrosion of mild steel in 1.0 M $H_2SO_4$ and the effect of halide ions on the inhibition efficiency. They have found that Cloxacillin (CLX) acts as a good inhibitor for mild steel corrosion and in combination with halides (KCl, KBr and KI). The inhibitive capability of CLX has enhanced to a greater extent indicating synergistic relationship. Geethanjali et al.[35] reported the studies on the inhibition effect of amodiaquine (anti- malarial and anti-inflammatory drug) on the mild steel corrosion in 0.5 M $H_2SO_4$ solution. They have reported that amodiaquine (AMQ) acquired low inhibition efficiencies when used alone as inhibitor the inhibitive effect has increased hugely when certain cation and anion species ($Mg^{2+}$, $Na^+$, $Cl^-$, $Br^-$, and $I^-$) were added to AMQ. All the tested cations and anions exhibited excellent synergism with AMQ. Among all the primary synergists used $I^-$ ions exhibited greater synergism.

There are reports in the literature on the effect of anions on the corrosion inhibition effect of some naturally occurring and synthetic polymers. For instance, S. A. Umoren et al.[36] reported that the inhibition effect of carboxyl methyl cellulose (CMC) on the corrosion of mild steel in 2M $H_2SO_4$ environment has different influence with different halide ions ($Cl^-$, $Br^-$, $I^-$). With the addition of $Cl^-$ions, the inhibition efficiency of CMC has decreased when compared to CMC alone (Antagonistic effect), whereas carboxyl methyl cellulose (CMC) has synergistic relationship with $I^-$ ions in controlling the corrosion of mild steel in $H_2SO_4$.

Arukalam I. O. et al.[37] studied the influence of $I^-$ ions on the inhibition effect of ethyl hydroxyethyl cellulose on the corrosion of mild steel in 1M $H_2SO_4$ environment. They have reported that the inhibition efficiency of ethyl hydroxyethyl cellulose has increased to a greater extent in presence of $I^-$ ions due to synergistic effect.

**I.6 Corrosion of mild steel and copper**

Mild steel is used in the fabrication of recirculating cooling water systems, heat exchangers and various other materials in the industry. In cooling water systems corrosion of mild steel is a major problem. Copper is generally utilized as a material for tubing and pipelines in industry for storage and distribution of hot and cold water [38,39].

Copper is less corrosive when compared to mild steel. But, it tends to corrode in certain environments. The main problem associated with the use of these metals or alloys in the above mentioned utilities is their susceptibility to corrosion in aqueous chloride environment[40]. There are two most important consequences of corrosion in cooling water systems. Failure of equipment is the first consequence, which leads to the increase in the maintenance cost due to replacement of corroded equipment. The second consequence is the loss of heat transfer capability of heat exchanger tube due to accumulation of corrosion products.

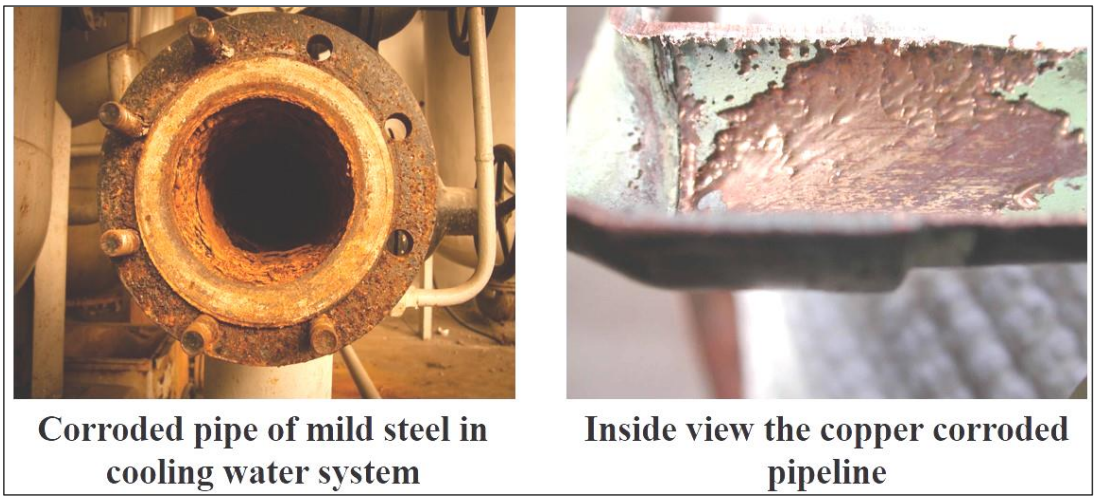


**Figure I.4:** Corroded pipelines in cooling water system (source: internet).

Figure I.4 shows the corroded mild steel pipeline in cooling water system and a cut view of a corroded copper pipeline. This problem of corrosion can be tackled and minimized by the addition of a variety of organic and inorganic compounds as corrosion inhibitors to the environment. Though, most of the conventional corrosion inhibitors may be satisfactory with respect to corrosion mitigation, they are known to be environmentally hazardous. In recent years, considerable efforts have been made to develop environmentally friendly corrosion inhibitors.

## I.7 Review of literature on Environment-friendly corrosion inhibitors

In recent years, the growing interest and attention towards the protection of the environment have made the focus of the researchers in corrosion towards the development of environmentally friendly corrosion inhibitors. A thorough literature survey has been made in this regard.

In pursuit of developing eco-friendly corrosion inhibitors scientists have worked extensively on phosphonate based inhibitors for mild steel[41]. They have worked on various drugs as eco-friendly corrosion inhibitors[42]. They have also studied on a variety of surfactants and ionic liquids which are eco-friendly in nature. But, corrosion inhibition by natural products and biopolymers as eco-friendly corrosion inhibitors is the most recent and most important area of research because of abundant and cheap renewable resources.

### I.7.1. Natural products as environment- friendly corrosion inhibitors

**Plant extracts, amino acids, vitamins** etc. have been extensively studied for their use as environment- friendly corrosion inhibitors for various metals in different corrosive environments. Some examples are given below

Plant extracts are the main focus of researchers for use in corrosion protection of metals in different environments. For instance, Avci, G. et al. [43] studied the aqueous extract of 'Acacia cyanophylla' leaves as environment-friendly inhibitor for mild steel 1 M $H_2SO_4$ solution. They have inferred that the extract has high inhibition effect towards mild steel corrosion and obtained an inhibition efficiency of 93 %. The inhibition efficiency decreased with the increase in temperature.

M. Behpour et al.[44] studied the extract of Punica granatum (PG) containing ellagic acid (EA) and tannic acid (TA), as eco-friendly corrosion inhibitor for mild steel in 2 M HCl and 1 M $H_2SO_4$ environments. They concluded that the Punica granatum (PG) peel extract and ellagic acid (EA) work well in controlling the corrosion of mild steel in both the test environments. But, the efficiency is to some extent better in HCl environment than in $H_2SO_4$.

Omar Benali et al.[45] studied the effect of extract of Anacyclus pyrethrum as corrosion inhibitor for corrosion of mild steel in sulfuric acid environment. The extract acts as an anodic inhibitor by retarding the anodic corrosion reaction. Adsorption of the Anacyclus pyrethrum on mild steel surface follows Langmuir adsorption isotherm model.

Janaina Cardozo da Rocha et al.[46] studied the inhibition effect of the aqueous extracts of fruit peels towards the corrosion of mild steel in 1M HCl solution. They have studied the aqueous extracts of mango, orange, passion fruit and cashew peels in different concentrations and concluded that the extracts act as good corrosion inhibitors for mild steel. The inhibition efficiency increased with increase in concentration and decreased with an increase in temperature.

Krishnegowda, P. M. et al.[47] reported that the ethanol extract of Acalypha torta leaves (EAL) works as excellent inhibitor towards the corrosion of mild steel in 1 M HCl environment. They have also interpreted that the EAL acts as a mixed type inhibitor and the adsorption of the extract on mild steel follows Langmuir adsorption isotherm.

Another plant extract, namely Cannabis plant extract has been studied for the inhibition effect of copper corrosion in 0.5 M $H_2SO_4$ corrosive environment by Abd-El-Nabey BA et al.[48]. From the results they have reported that the Cannabis plant extract solution works as an efficient inhibitor for the corrosion of copper in sulfuric acid environment. The extract works as a cathodic type inhibitor. The adsorption of Cannabis plant extract on mild steel follows Langmiur, Flory-Huggins isotherms and kinetic-thermodynamic model.

S.A. Umoren et al.[49] studied the corrosion inhibition of aluminium using coconut coir dust extract (CCDE) in 1 M HCl solution. From the results they found that the CCDE inhibits efficiently the corrosion of aluminium in acidic chloride environment. The inhibition is achieved by the adsorption of the extract on aluminium. The adsorption process follows Langmuir adsorption isotherm model.

Argemone mexicana plant extract has been tested as an inhibitor for the corrosion of mild steel in acidic environment by Gopalji et al. [50]. From the results of weight loss and electrochemical studies they have found that the extract has the potential to inhibit the corrosion of mild steel. The inhibition occurs through adsorption mechanism and the adsorption follows Langmuir adsorption isotherm model.

Amino acids and their derivates are some of the most studied natural isolated compounds as environment-friendly corrosion inhibitors. Some examples are mentioned here under. Oezcan M et al.[51] studied the effect of cysteine, an amino acid on the corrosion of mild steel in acidic chloride solution. From the results they have concluded that cystine acts as an effective inhibitor for corrosion of mild steel in 0.5 M $H_2SO_4$. The inhibition efficiency increases with the increase in concentration of cystine. Adsorption

phenomenon is the cause of corrosion inhibition and the adsorption of cystine on mild steel surface follows Langmuir adsorption isotherm model.

Morad M. S.[52] studied four sulfur containing amino acids as inhibitors for the corrosion of mild steel in 40% $H_3PO_4$ solution with and without $Cl^-$, $F^-$, $Fe^{3+}$ ions. The four amino acids are cysteine (RSH), methionine ($CH_3SR$), cystine (RSSR) and N-acetylcysteine (ACC). They found that in presence of S-containing amino acids the corrosion of mild steel was hindered significantly and the amino acids behaved as anodic type corrosion inhibitors. The presence of $Cl^-$, $F^-$, $Fe^{3+}$ ions in the corrosive environment increased the corrosion. The inhibition is an outcome of the adsorption phenomenon of amino acids on the mild steel surface. The adsorption mechanism for cysteine (RSH) and N-acetylcysteine (ACC) follows Temkin's isotherm model, whereas the adsorption mechanism for methionine ($CH_3SR$), cystine (RSSR) follows Frumkin and Langmuir isotherm models.

Another green corrosion inhibitor based on L-Tryptophan has been developed by Jia-Jun Fu et al.[53] They have studied the effect of L-Tryptophan on the corrosion of mild steel in 1M HCl solution. It was inferred that L-Tryptophan afforded very good inhibition of corrosion of mild steel in acidic chloride environment. The maximum inhibition efficiency was found to be 90 % at the concentration of $1 \times 10^{-2}$ mol $L^{-1}$. Polarization measurements inferred that this amino acid acts as cathodic inhibitor. The inhibition mechanism involves chemisorption as well as physisorption of the molecules on the metal surface.

Mohammed A. Amin et al.[54] also developed some environment friendly corrosion inhibitors using amino acids. They have investigated the inhibitive effect of alanine (Ala), cysteine (Cys) and S-methyl cysteine (S-MCys) on the corrosion of iron in 1M HCl solution. From the results they have concluded that the inhibition performance of the three selected amino acids is quite satisfactory. From the polarization studies they have inferred that alanine (Ala) acts as cathodic type inhibitor, whereas cysteine (Cys) and S-methyl cysteine (S-MCys) act as mixed type inhibitors. Although all the tested amino acids work well, the highest inhibitive performance was observed for S-containing amino acids ((Cys and S-MCys) with 90 % inhibition efficiency.

G. Moretti et al.[55] developed an eco-friendly corrosion inhibitor for copper in 0.5 M sulfuric acid solution using an amino acid called tryptophan. They have found that it was effective at a concentration of $10^{-2}$ M for copper corrosion inhibition in sulfuric acid

environment in a temperature range of 20–50 °C. The adsorption of tryptophan followed Bockris–Swinkels' isotherm model.

Zhang DQ et al.[56] studied the inhibition action of amino acids namely, DL-alanine and DL-cysteine on the corrosion of copper in aerated 0.5 M HCl environment. They have employed the gravimetric and electrochemical techniques to study the nature of the corrosion inhibition. From the results they have inferred that among the tested inhibitors, DL-cysteine works more efficiently in controlling the corrosion. They have also reported that the inhibition efficiencies of DL-alanine and DL-cysteine are higher than that of benzotriazole.

Barouni, K. et al.[57] developed five inhibitors based on amino acids for copper corrosion in nitric acid solution. The amino acids are, Arginine (Arg), Cysteine (Cys), Glycine (Gly), Lysine (Lys) and Valine (Val). They have reported that among all the amino acids studied, cysteine is the most effective one in controlling the corrosion. The order of inhibition efficiency is given as Valine<Glycine<Arginine<Lysine<Cysteine. Vitamins like vitamin $B_1$, vitamin C, vitamin $B_{12}$, vitamin $B_6$, were also tested as eco-friendly corrosion inhibitors. For instance, Fuchs-Godec R et al. developed a green corrosion inhibitor using vitamin C (ascorbic acid) for corrosion of stainless-steel in aqueous HCl solution (0.01M - 5M HCl). They have inferred that considerable inhibitive efficiency was observed for vitamin C in the concentration range of $10^{-2}$ and $10^{-3}$mol $L^{-1}$ stainless-steel in 0.1 M HCl. Vitamin C was also tested as corrosion inhibitor for steel in saturated $Ca(OH)_2$ solution containing $Cl^-$ ions by L. Valek et al.[58] They have reported that it inhibited pitting corrosion of steel.

S. Malhotra et al.[59] studied the inhibitive effect of vitamins $B_1$, $B_6$ and C for the corrosion of nickel in 1 M $HNO_3$ corrosive environment. They have reported that all the tested vitamins are excellent corrosion inhibitors for Ni in $HNO_3$ solution.

### I.7.2. Naturally occurring polymers as eco-friendly corrosion inhibitors

Application of natural polymers as environment-friendly corrosion inhibitors constitutes an attractive and significant approach to the development of green corrosion inhibitors. Researchers have given a lot of importance in exploring this area and a significant number of articles have been published in the literature on natural gums (guar gum, gum acacia and natural polymers namely, cellulose, starch, chitosan, pectin, alginate, etc. as inhibitors.

Mohammad M. Fares et al.[60] developed an eco-friendly corrosion inhibitor based on a biopolymer namely, pectin. They have studied the inhibitive effect of pectin on the corrosion of aluminium in acidic chloride medium (2M HCl). They reported that pectin successfully inhibited the corrosion of Al in HCl environment. The inhibition efficiency has reached to 91 % at a pectin concentration of 8.0 g $L^{-1}$ at a temperature of 10 °C and decreased to 31 % at a temperature of 40 °C. The adsorption phenomenon of pectin on Al surface follows Langmuir isotherm model.

M.M. Solomon et al.[61] studied the inhibitive effect of carboxymethyl cellulose (CMC), a chemically modified biopolymer towards the corrosion of mild steel in $H_2SO_4$ solution. They reported that CMC is found to be a good inhibitor and the inhibition efficiency increases with an increase in concentration of CMC. With the increase in temperature the inhibition efficiency is decreased. Adsorption of CMC on mild steel surface is the main reason for the inhibition. The adsorption of CMC on mild steel surface follows Langmuir and Dubinin–Radushkevich isotherm models. S. A. Umoren et al.[36] studied the effect of halide ions on the inhibition effect of CMC in controlling the corrosion of mild steel in sulfuric acid solution.

Arukalam IO et al.[62] studied the inhibitive effect of a modified biopolymer namely, hydroxyethylcellulose (HEC) on the corrosion of mild steel and aluminium in 0.5 M HCl solution. From the results they concluded that HEC is found to be excellent corrosion inhibitor. However, HEC works more efficiently in controlling the corrosion of mild steel than aluminium.

Cassava starch derivatives namely activated cassava starch (AS) and carboxymethylated cassava starch (CMS) were tested as eco-friendly corrosion inhibitors for the corrosion of carbon steel in 200 ppm NaCl solution by Nathalie Ochoa et al[63]. They concluded that the cassava starch derivatives, AS and CMS work as efficient inhibitors for the corrosion of carbon steel in 200 ppm NaCl. The inhibition efficiency of these modified starches was found to increase with increase in concentration. The inhibition takes place by virtue of the formation of a protective film on the carbon steel surface.

Natural gums are another class of naturally occurring polymers, which are studied extensively as corrosion inhibitors for metals. Gum Acacia is the most studied gum as the corrosion inhibitor for various metals and alloys. S.A. Umoren et al. studied the inhibitive action of gum arabic (GA) on the corrosion of aluminium in alkaline (NaOH) solution. They have concluded that the GA exhibits considerable inhibitive effect on the

corrosion of aluminium in alkaline NaOH environment by affording 75 % inhibition efficiency. The GA molecules get adsorbed on the metal surface and block the contact of the metal with the corrosive environment. They have also explained that the type of adsorption is mainly chemisorption. The adsorption of GA follows Langmuir and Freundlich adsorption isotherm models.

Hamza Bentrah et al.[64] studied gum arabic (GA) as an inhibitor for API 5L X42 pipeline steel in 1M HCl corrosive environment. They have reported that GA is a very good corrosion inhibitor in acidic chloride environment for the alloy studied and a maximum inhibition efficiency of 92 % was obtained when 2000 ppm of GA was used. They have found that the adsorption behavior of GA on API 5L X42 pipeline steel follows Langmuir adsorption isotherm model. Based on the standard free energy of adsorption ($\Delta G^{\circ}$) value they have confirmed the adsorption of GA is physical adsorption. Potentiodynamic polarization studies showed that GA works as a mixed type inhibitor.

M. Abdallah[65] has studied guar gum (GG) as corrosion inhibitor for mild steel in 1M $H_2SO_4$ solution. He reported that guar gum works efficiently in controlling the corrosion of mild steel in sulfuric acid medium. The inhibition action is a consequence of the adsorption of GG on mild steel surface and the adsorption process follows Langmuir adsorption isotherm model. Pialee Roy et al.[66] have studied the inhibition effect of polyacrylamide grafted Guar gum (GG-g-PAM) on the corrosion of mild steel in 1 M HCl solution. They have studied this effect with various grafting percentages of polyacrylamide (PAM) in guar gum. They have found that PAM grafting on GG increased the inhibition efficiency of mild steel corrosion. The GG-g-PAM works as a mixed type inhibitor and it imparts highest inhibition efficiency for 86 % grafting. They have also concluded that adsorption is the main cause of the inhibition and the adsorption fits best with Langmuir adsorption isotherm model.

S. A. Umoren et al.[67] studied the inhibition effect of raphia hookeri gum (RH) on the corrosion of mild steel in 0.1 M $H_2SO_4$ solution. They have concluded that RH exudate gum acts as a good inhibitor for mild steel in acidic environment by achieving an inhibitions efficiency of 71 %. The inhibition efficiency is directly proportional to the concentration of the RH gum. Langmuir adsorption isotherm model fits well for the adsorption of RH gum on mild steel.

Chitosan and modified chitosans have been studied as corrosion inhibitors for various metals and alloys. For instance, A. Jmiai et al.[68] studied the inhibition effect of the biopolymer namely chitosan on the corrosion of copper in acidic medium. They have

concluded that chitosan has a good inhibitory effect on copper corrosion in 1 M HCl solution, with a maximum inhibition efficiency of 87 %. The adsorption of chitosan on copper follows Langmuir adsorption isotherm model. They have also found that the adsorption process on copper took place through nitrogen and oxygen atoms present in chitosan. Mahmoud N. El-Haddad [69] has also studied the effect of chitosan in controlling copper corrosion in 0.5 M HCl solution. Umoren S. A. et al.[70] studied the inhibitive effect of chitosan on the corrosion of mild steel in 0.1 M HCl solution.

Fekry A.M. et al.[71] studied a modified chitosan namely, acetyl thiourea chitosan (ATUCS) for the corrosion inhibition of mild steel in 0.5 M $H_2SO_4$ environment. They have reported that ATUCS is an excellent inhibitor for mild steel in sulfuric acid solution and obtained an inhibition efficiency of 94.5 % at 0.76 mM concentration. The inhibition efficiency increases with an increase in concentration of ATUCS.

Amino thiourea-modified chitosan was synthesized and its inhibition effect on the corrosion of 304 stainless steel in 2% acetic acid solution was studied by Manlin Li et al.[72] From the results they have concluded that the synthesized chitosan derivative performs very well in controlling the corrosion of 304 stainless steel in 2 % acetic acid environment with a maximum inhibition efficiency of 92 %.

Sha Cheng et al.[73] reported that carboxymenthylchitosan (CM-chitosan) can be a potenialt inhibitor for the corrosion of mild steel in 1 M HCl solution and an inhibition efficiency of 93 % was obtained when 200 ppm of CM-chitosan was used as inhibitor. They have also reported that the adsorption of CM-chitosan on mild steel is the reason for inhibition and the adsorption phenomenon follows Langmuir adsorption isotherm model. The same group have also studied the effect of $Cu^{2+}$ ions as an additive on CM-chitosan[74]. They have found that the addition of $Cu^{2+}$ ions increases the inhibition efficiency.

**References:**


1. Revie, R. W. & Uhlig, herbert H. *corrosion and corrosion control: An Introduction to Corrosion Science and Engineering, fourth edition*. (2008).
2. Cramer, S. D. & Covino, B. S. ASM Handbook Vol. 13a: Corrosion - Fundamentals, Testing, and Protection. *Asm* **13,** 1135 (2003).
3. Fontana, M. Corrosion Engineering. 1987. *McGraw-Hill* 173 (1987).
4. Cicek, V. *Corrosion Engineering and Cathodic Protection Handbook*. *Corrosion Engineering* (John Wiley & Sons, Inc., 2017). doi:10.1002/9781119284338
5. Koch, G. *et al.* International Measures of Prevention , Application , and Economics of Corrosion Technologies Study. *NACE Int.* 1–3 (2016).
6. Bhaskaran, R. *et al.* An analysis of the updated cost of corrosion in India. *Mater. Perform.* **53,** 56–65 (2014).
7. Javaherdashti, R. How corrosion affects industry and life. *Anti-Corrosion Methods Mater.* **47,** 30–34 (2000).
8. Roberge, P. R. *Handbook of Corrosion Engineering*. *New York* **9,** (2000).
9. Sharma, D. C. Bhopal: 20 years on. *Lancet* **365,** 111–112 (2005).
10. Shaluf, I. M., Ahmadun, F.-R. & Said, A. M. Fire incident at a refinery in West Malaysia: the causes and lessons learned. *J. Loss Prev. Process Ind.* **16,** 297–303 (2003).
11. Andersson, N. & Morales, A. Mexico: Disaster in Guadalajara. *Lancet* **339,** 1103 (1992).
12. Cicek, V. & Al-Numan, B. *Corrosion Chemistry*. *Corrosion Chemistry* (2011). doi:10.1002/9781118232163
13. ASTM & NACE International. NACE/ASTM G193-10a: Standard Terminology and Acronyms Relating to Corrosion. *Annu. B. ASTM Stand.* 1–18 (2010). doi:10.1520/G0193-10A.2
14. Rosenfeld, I. L. Whitney Award Lecture—1981: New Data on the Mechanism of Metals Protection with Inhibitors. *CORROSION* **37,** 371–377 (1981).
15. Sastri, V. S. *Green Corrosion Inhibitors*. *Green Corrosion Inhibitors: Theory and Practice* (John Wiley & Sons, Inc., 2011). doi:10.1002/9781118015438
16. Umoren, S. A. & Solomon, M. M. Synergistic corrosion inhibition effect of metal cations and mixtures of organic compounds: A Review. *J. Environ. Chem. Eng.* **5,** 246–273 (2017).

17. Rao, B. V. A. & Rao, S. S. Electrochemical and surface analytical studies of synergistic effect of phosphonate, Zn 2+ and ascorbate in corrosion control of carbon steel. *Mater. Corros.* **61,** NA-NA (2009).
18. Singh, D. D. N. & Dey, A. K. Synergistic effects of inorganic and organic cations on inhibitive performance of propargyl alcohol on steel dissolution in boiling hydrochloric acid solution. *Corrosion* **49,** 594–600 (1993).
19. Rajendran, S., Apparao, B. V. & Palaniswamy, N. Synergistic, antagonistic and biocidal effects of amino (trimethylene phosphonic acid), polyacrylamide and Zn 2+ on the inhibition of corrosion of mild steel in neutral aqueous environment. *Anti-Corrosion Methods Mater.* **44,** 308–313 (1997).
20. Rajendran, S., Apparao, B. V. & Palaniswamy, N. Corrosion inhibition by phenyl phosphonate and Zn 2+. *Anti-Corrosion Methods Mater.* **45,** 158–161 (1998).
21. Li, X., Deng, S., Fu, H. & Mu, G. Synergistic inhibition effect of rare earth cerium(IV) ion and 3,4-dihydroxybenzaldehye on the corrosion of cold rolled steel in H2SO4 solution. *Corros. Sci.* **51,** 2639–2651 (2009).
22. Zhang, D.-Q., Cai, Q.-R., He, X.-M., Gao, L.-X. & Kim, G. S. Corrosion inhibition and adsorption behavior of methionine on copper in HCl and synergistic effect of zinc ions. *Mater. Chem. Phys.* **114,** 612–617 (2009).
23. Amar, H. *et al.* Synergistic corrosion inhibition study of Armco iron in sodium chloride by piperidin-1-yl-phosphonic acid–Zn2+ system. *Corros. Sci.* **50,** 124–130 (2008).
24. Rao, B. V. A., Rao, M. V., Rao, S. S. & Sreedhar, B. Synergistic effect of N,N-bis(phosphonomethyl) glycine and zinc ions in corrosion control of carbon steel in cooling water systems. *Chem. Eng. Commun.* **198,** 1505–1529 (2011).
25. Appa Rao, B. V., Venkateswara Rao, M., Srinivasa Rao, S. & Sreedhar, B. Tungstate as a synergist to phosphonate-based formulation for corrosion control of carbon steel in nearly neutral aqueous environment. *J. Chem. Sci.* **122,** 639–649 (2010).
26. Rajendran, S., Apparao, B. V. & Palaniswamy, N. HEDP-Zn 2+ : a potential inhibitor system for mild steel in low chloride media. *Anti-Corrosion Methods Mater.* **47,** 83–87 (2000).
27. Umoren, S. A. & Solomon, M. M. Effect of halide ions on the corrosion inhibition efficiency of different organic species – A review. *J. Ind. Eng. Chem.* **21,** 81–100 (2015).

28. Merah, S., Larabi, L., Benali, O. & Harek, Y. Synergistic effect of methyl red dye and potassium iodide on inhibition of corrosion of carbon steel in 0.5 M H 2 SO 4. *Pigment Resin Technol.* **37,** 291–298 (2008).
29. Oguzie, E., Akalezi, C. & Enenebeaku, C. Inhibitive effect of methyl green dye on the corrosion of low carbon steel in acidic media. *Pigment Resin Technol.* **38,** 359–365 (2009).
30. Umoren, S. A., Ebenso, E. E. & Ogbobe, O. Synergistic effect of halide ions and polyethylene glycol on the corrosion inhibition of aluminium in alkaline medium. *J. Appl. Polym. Sci.* **113,** 3533–3543 (2009).
31. Mohammed, K. Z., Hamdy, A., Abdel-wahab, A. & Farid, N. . A. Temperature Effect on Corrosion Inhibition of Carbon Steel in Formation Water by Non-ionic Inhibitor and Synergistic Influence of Halide Ions. *Life Sci. Journa* **9,** 424–434 (2012).
32. Li, X., Tang, L., Liu, H., Mu, G. & Liu, G. Influence of halide ions on inhibitive performance of cetyl trimethyl ammonium bromide in various concentrations of phosphoric acid for cold rolled steel. *Mater. Lett.* **62,** 2321–2324 (2008).
33. Hu, S. *et al.* Synergistic effect of 2-oleyl-1-oleylamidoethyl imidazoline ammonium methylsulfate and halide ions on the inhibition of mild steel in HCl. *Mater. Chem. Phys.* **134,** 54–60 (2012).
34. Eddy, N. O. & Ebenso, E. E. Adsorption and quantum chemical studies on cloxacillin and halides for the corrosion of mild steel in acidic medium. *Int. J. Electrochem. Sci.* **5,** 731–750 (2010).
35. Geethanjali, R., Leelavathi, S., Subhashini, S. & Rajalakshmi, R. The synergisticeEffects of halide ions and cations on the corrosion inhibition of mild steel in H2SO4 using amodiaquine. *Chem. Sci. Trans.* **2,** 1296–1303 (2013).
36. Umoren, S. A., Solomon, M. M., Udosoro, I. I. & Udoh, a. P. Synergistic and antagonistic effects between halide ions and carboxymethyl cellulose for the corrosion inhibition of mild steel in sulphuric acid solution. *Cellulose* **17,** 635–648 (2010).
37. Arukalam, I. O., Madu, I. O., Ijomah, N. T., Ewulonu, C. M. & Onyeagoro, G. N. Acid Corrosion Inhibition and Adsorption Behaviour of Ethyl Hydroxyethyl Cellulose on Mild Steel Corrosion. *J. Mater.* **2014,** 1–11 (2014).
38. Lanford, W. A., Ding, P. J., Wang, W., Hymes, S. & Murarka, S. P. Alloying of copper for use in microelectronic metallization. *Mater. Chem. Phys.* **41,** 192–198

(1995).

39. Lokesh, K. S. *et al.* Adsorption of cobalt (II) 5,10,15,20-tetrakis(2-aminophenyl)-porphyrin onto copper substrates: Characterization and impedance studies for corrosion inhibition. *Corros. Sci.* **62,** 73–82 (2012).
40. Antonijević, M. M., Milić, S. M. & Petrović, M. B. Films formed on copper surface in chloride media in the presence of azoles. *Corros. Sci.* **51,** 1228–1237 (2009).
41. Mosayebi, B., Kazemeini, M., Badakhshan, A. & Safekordi, A. Effect of phosphonate based corrosion inhibitors in a cooling water system. *Br. Corros. J.* **37,** 217–224 (2002).
42. Gece, G. Drugs: A review of promising novel corrosion inhibitors. *Corros. Sci.* **53,** 3873–3898 (2011).
43. AVCI, G. & KELEŞ, Y. Aqueous extract of Acacia cyanophylla leaves as environmentally friendly inhibitor for mild steel corrosion in 1 M H2SO4 solution. *Surf. Interface Anal.* **43,** 1311–1317 (2011).
44. Behpour, M., Ghoreishi, S. M., Khayatkashani, M. & Soltani, N. Green approach to corrosion inhibition of mild steel in two acidic solutions by the extract of Punica granatum peel and main constituents. *Mater. Chem. Phys.* **131,** 621–633 (2012).
45. Benali, O., Selles, C. & Salghi, R. Inhibition of acid corrosion of mild steel by Anacyclus pyrethrum L. extracts. *Res. Chem. Intermed.* **40,** 259–268 (2014).
46. da Rocha, J. C., da Cunha Ponciano Gomes, J. A. & D'Elia, E. Corrosion inhibition of carbon steel in hydrochloric acid solution by fruit peel aqueous extracts. *Corros. Sci.* **52,** 2341–2348 (2010).
47. Krishnegowda, P. M., Venkatesha, V. T., Krishnegowda, P. K. M. & Shivayogiraju, S. B. Acalypha torta Leaf Extract as Green Corrosion Inhibitor for Mild Steel in Hydrochloric Acid Solution. *Ind. Eng. Chem. Res.* **52,** 722–728 (2013).
48. Abd-El-Nabey, B. A., Abdel-Gaber, A. H., Ali, M. E. S., Khamis, E. & El-Housseiny, S. Inhibitive Action of cannabis plant extract on the corrosion of copper in 0.5 M H2SO4. *Int. J. Electrochem. Sci.* **8,** 7124–7137 (2013).
49. Umoren, S. A., Eduok, U. M., Israel, A. U., Obot, I. B. & Solomon, M. M. Coconut coir dust extract: a novel eco-friendly corrosion inhibitor for Al in HCl solutions. *Green Chem. Lett. Rev.* **5,** 303–313 (2012).

50. ji, G., Shukla, S. K., Dwivedi, P., Sundaram, S. & Prakash, R. Inhibitive Effect of Argemone mexicana Plant Extract on Acid Corrosion of Mild Steel. *Ind. Eng. Chem. Res.* **50,** 11954–11959 (2011).
51. Özcan, M. AC impedance measurement of cystine adsorption at mild steel/sulfuric acid interface as corrosion inhibitor. *J. Solid State Electrochem.* **12,** 1653–1661 (2008).
52. Morad, M. S. Effect of amino acids containing sulfur on the corrosion of mild steel in phosphoric acid solutions containing Cl−, F− and Fe3+ ions: Behavior under polarization conditions. *J. Appl. Electrochem.* **35,** 889–895 (2005).
53. Fu, J.-J. *et al.* l-Tryptophan as green corrosion inhibitor for low carbon steel in hydrochloric acid solution. *J. Mater. Sci.* **45,** 979–986 (2010).
54. Amin, M. A., Khaled, K. F., Mohsen, Q. & Arida, H. A. A study of the inhibition of iron corrosion in HCl solutions by some amino acids. *Corros. Sci.* **52,** 1684–1695 (2010).
55. Moretti, G. & Guidi, F. Tryptophan as copper corrosion inhibitor in 0.5 M aerated sulfuric acid. *Corros. Sci.* **44,** 1995–2011 (2002).
56. Zhang, D., Gao, L. & Zhou, G. Inhibition of copper corrosion in aerated hydrochloric acid solution by amino-acid compounds. *J. Appl. Electrochem.* **35,** 1081–1085 (2005).
57. Barouni, K. *et al.* Some amino acids as corrosion inhibitors for copper in nitric acid solution. *Mater. Lett.* **62,** 3325–3327 (2008).
58. Valek, L., Martinez, S., Mikulić, D. & Brnardić, I. The inhibition activity of ascorbic acid towards corrosion of steel in alkaline media containing chloride ions. *Corros. Sci.* **50,** 2705–2709 (2008).
59. Malhotra, S. & Singh, G. Vitamins: potential inhibitors for nickel in acidic media. *Surf. Eng.* **21,** 187–192 (2005).
60. Fares, M. M., Maayta, A. K. & Al-Qudah, M. M. Pectin as promising green corrosion inhibitor of aluminum in hydrochloric acid solution. *Corros. Sci.* **60,** 112–117 (2012).
61. Solomon, M. M., Umoren, S. A., Udosoro, I. I. & Udoh, A. P. Inhibitive and adsorption behaviour of carboxymethyl cellulose on mild steel corrosion in sulphuric acid solution. *Corros. Sci.* **52,** 1317–1325 (2010).
62. Arukalam, I. O., Nleme, I. K. & Anyanwu, A. E. Comparative Inhibitive Effect of Hydroxyethylcellulose on Mild Steel and Aluminium Corrosion in 0 . 5M Hcl

Solution. *Acad. Res. Int.* **1,** 492–498 (2011).

63. Ochoa, N. *et al.* Modified cassava starches as potential corrosion inhibitors for sustainable development. *Mater. Res.* **16,** 1209–1219 (2013).
64. Bentrah, H., Rahali, Y. & Chala, A. Gum Arabic as an eco-friendly inhibitor for API 5L X42 pipeline steel in HCl medium. *Corros. Sci.* **82,** 426–431 (2014).
65. Abdallah, M. Guar Gum as Corrosion Inhibitor for Carbon Steel in Sulfuric Acid Solutions. *Port. Electrochim. Acta* **22,** 161–175 (2004).
66. Roy, P., Karfa, P., Adhikari, U. & Sukul, D. Corrosion inhibition of mild steel in acidic medium by polyacrylamide grafted Guar gum with various grafting percentage: Effect of intramolecular synergism. *Corros. Sci.* **88,** (2014).
67. Umoren, S. a., Obot, I. B. & Obi-Egbedi, N. O. Raphia hookeri gum as a potential eco-friendly inhibitor for mild steel in sulfuric acid. *J. Mater. Sci.* **44,** 274–279 (2009).
68. Jmiai, A. *et al.* Chitosan as an eco-friendly inhibitor for copper corrosion in acidic medium: protocol and characterization. *Cellulose* **24,** 3843–3867 (2017).
69. El-Haddad, M. N. Chitosan as a green inhibitor for copper corrosion in acidic medium. *Int. J. Biol. Macromol.* **55,** 142–149 (2013).
70. Umoren, S. A., Banera, M. J., Alonso-Garcia, T., Gervasi, C. A. & Mirífico, M. V. Inhibition of mild steel corrosion in HCl solution using chitosan. *Cellulose* **20,** 2529–2545 (2013).
71. Fekry, A. M. & Mohamed, R. R. Acetyl thiourea chitosan as an eco-friendly inhibitor for mild steel in sulphuric acid medium. *Electrochim. Acta* **55,** 1933–1939 (2010).
72. Li, M. *et al.* Simple preparation of aminothiourea-modified chitosan as corrosion inhibitor and heavy metal ion adsorbent. *J. Colloid Interface Sci.* **417,** 131–136 (2014).
73. Cheng, S., Chen, S., Liu, T., Chang, X. & Yin, Y. Carboxymenthylchitosan as an ecofriendly inhibitor for mild steel in 1 M HCl. *Mater. Lett.* **61,** 3276–3280 (2007).
74. Cheng, S., Chen, S., Liu, T., Chang, X. & Yin, Y. Carboxymethylchitosan+Cu2+ mixture as an inhibitor used for mild steel in 1M HCl. *Electrochim. Acta* **52,** 5932–5938 (2007).

# CHAPTER-II

# NEED, OBJECTIVES AND SCOPE OF THE PRESENT STUDY

# TABLE OF CONTENTS

## CHAPTER – II

# CHAPTER – II

# NEED, OBJECTIVES AND SCOPE OF THE PRESENT STUDY

## II.1: Need of the present study

Mild steel is used in the fabrication of recirculating cooling water systems, heat exchangers and various other materials in the industry. Whereas, copper is generally utilized as a material for tubing and pipelines in the industry for storage and distribution of hot and cold water. The main problem associated with the use of these metals is corrosion in a variety of aqueous environments. The problem of corrosion can be controlled by the addition of a variety of organic and inorganic compounds as corrosion inhibitors to the environment. However, most of the traditionally employed corrosion inhibitors are known to be toxic and lethal to the environment. There is a need to minimize the use of these toxic chemicals and make an effort to conserve our environment from the present vulnerable condition. Therefore, attention was drawn to the development of novel corrosion inhibitors based on ecological approaches.

In recent years, considerable efforts have been made to study the corrosion inhibition efficiency of some natural products[1]. Application of natural polymers as environment-friendly corrosion inhibitors constitutes an attractive and significant approach to the development of green corrosion inhibitors. A significant number of reports have been published in the literature on natural gums (guar gum, gum acacia, etc.,), natural polymers (cellulose, starch, chitosan, pectin, alginate, etc.,) as inhibitors[2–5]. Biological polymers such as chitin, chitosan and polysaccharides constitute an important class of environmentally friendly corrosion inhibitors on which a few studies were reported in the literature. For instance, carboxymethyl and hydroxyethyl cellulose, chitosan and substituted/modified chitosans for corrosion protection applications[4], carboxymethyl chitosan and its synergism with $Cu^{2+}$ ions for mild steel in acidic chloride environment[2,3], polyacrylamide grafted with okra mucilage, a natural grade polysaccharide[6] have been reported in the literature. Until now there are no studies reported in the literature on using chemically modified chitin, as a corrosion inhibitor.

In this background, chitin, a natural polymer has been selected in the present study for the following reasons. Chitin is the second most abundant polysaccharide next to cellulose on the earth. Chitin and chitosan are non-toxic and are inert in the gastrointestinal tract of mammals. These are also biodegradable. Chitin is the main component in the shells of

crustaceans such as shrimps, crab, and lobster, and is also found in the exoskeleton of mollusks, insects and the cell walls of some fungi[7]. Every year, around 6 to 8 million tons of waste from crab, shrimp and lobster shells are produced globally[8]. These waste shells are often just dumped, and cause a lot of environmental problems. There is a large scope of research in using this abundant and cheap renewable resource by developing new application methods. But, the problem associated with the use of these biological polymers is their insoluble nature in most of the aqueous solvents due to the presence of intra and inter molecular hydrogen bonding between adjacent biopolymer chains[9]. This problem can be overcome by chemical modification of these biopolymers. Another natural polymer selected in the present study is xanthan gum. Xanthan gum is a naturally occurring high molecular weight polysaccharide produced by microorganisms such as xanthomonas campestris[10].

The chemical modification on these polymers is only used to increase its solubility. The basic skeleton (cellulosic backbone) of these polymers is unaffected after the chemical modification and hence the retention of properties after modification besides acquiring some additional properties like increased solubility. The non-toxicity and biocompatibility of phosphorylated chitin are already reported in the literature[11–13]. Phosphorylated chitin is also used in biomedical applications. Moreover, it is known that phosphates are non-toxic. The non-toxic nature of phosphorylated cellulosic compounds is reported in the literature by Illy et al.[14] and suflet et al.[15].

The xanthan gum is chemically modified to phosphorylated xanthan gum in order to increase its ability to form complexes with metal ions, by using a method reported in the literature[16]. Phosphorylated xanthan gum which is also a cellulosic compound comes under this category. In another system we have used chitosan and ascorbic acid, both of which are non-toxic and biodegradable.

As far as xanthates are concerned, it is known that sodium ethyl xanthate and sodium isopropyl xanthate are toxic. But, in the present study, the derivative of environmentally friendly chitin, namely chitin xanthate is used. Xanthate introduction on the cellulosic backbone of chitin is only for the increase in solubility. The toxicity of chitin xanthate is expected to be relatively very less due to less degree of substitution of xanthate group on the chitin backbone. It may also be noted that chitin xanthate is also used in biomedical applications. Appropriate references[17,18] are added.

## II.2: Objectives of the present study:

1. To develop corrosion inhibitors based on naturally occurring polymers, which are non-toxic, biodegradable and biocompatible.
2. To investigate the nature of the corrosion inhibition process (anodic, cathodic or mixed type) in the presence of the inhibitors.
3. To investigate the composition of the surface film formed on the metal surface in the corrosion environment in the presence of the inhibitors.
4. To discuss the mechanistic aspects of the corrosion inhibition process by the chosen inhibitors.

## II.3: Scope of the present study:

Mild steel and copper have been used in the present study as materials for which we have developed new inhibitor formulations. These inhibitor formulations have been tested for their corrosion inhibition efficiencies at a temperature of 30±0.1°C. The corrosive environments in which these inhibitor formulationsare tested are 200 ppm NaCl for four inhibitor formulations and 1M HCl solution for one inhibitor formulation.

The inhibitor systems developed by the investigator are listed below.

1) Phosphorylated chitin alone and phosphorylated chitin in combination with $Zn^{2+}$ as corrosion inhibitor for mild steel in water containing 200 ppm sodium chloride.
2) Phosphorylated chitin as a corrosion inhibitor for copper in water containing 200 ppm sodium chloride.
3) Chitosan- ascorbic acid- $Cu^{2+}$system as a corrosion inhibitor for mild steel in one molar hydrochloric acid.
4) Chitin xanthate (CX) as a corrosion inhibitor for copper in water with 200 ppm sodium chloride.
5) Phosphorylated xanthan gum (PXG) as a corrosion inhibitor for mild steel in water with 200 ppm sodium chloride.

## References

1. Gece, G. Drugs: A review of promising novel corrosion inhibitors. *Corros. Sci.* **53,** 3873–3898 (2011).
2. Cheng, S., Chen, S., Liu, T., Chang, X. & Yin, Y. Carboxymenthylchitosan as an ecofriendly inhibitor for mild steel in 1 M HCl. *Mater. Lett.* **61,** 3276–3280 (2007).
3. Cheng, S., Chen, S., Liu, T., Chang, X. & Yin, Y. Carboxymethylchitosan+Cu2+

mixture as an inhibitor used for mild steel in 1M HCl. *Electrochim. Acta* **52,** 5932–5938 (2007).

4. Umoren, S. A. & Eduok, U. M. Application of carbohydrate polymers as corrosion inhibitors for metal substrates in different media: A review. *Carbohydr. Polym.* **140,** 314–341 (2016).
5. El-Haddad, M. N. Chitosan as a green inhibitor for copper corrosion in acidic medium. *Int. J. Biol. Macromol.* **55,** 142–9 (2013).
6. Banerjee, S., Srivastava, V. & Singh, M. M. Chemically modified natural polysaccharide as green corrosion inhibitor for mild steel in acidic medium. *Corros. Sci.* **59,** 35–41
7. Ravi Kumar, M. N. . A review of chitin and chitosan applications. *React. Funct. Polym.* **46,** 1–27 (2000).
8. Yan, N. & Chen, X. Sustainability: Don't waste seafood waste. *Nature* **524,** 155–157 (2015).
9. Sashiwa, H. *et al.* Chemical Modification of Chitosan. 14: 1 Synthesis of Water-Soluble Chitosan Derivatives by Simple Acetylation. *Biomacromolecules* **3,** 1126–1128 (2002).
10. Katzbauer, B. Properties and applications of xanthan gum. *Polym. Degrad. Stab.* **59,** 81–84 (1998).
11. Wang, X. H., Zhu, Y., Feng, Q. L., Cui, F. Z. & Ma, J. B. Responses of Osteo- and Fibroblast Cells to Phosphorylated Chitin. *J. Bioact. Compat. Polym.* **18,** 135–146 (2003).
12. Ripamonti, U. & Duneas, N. Tissue Engineering of Bone by Osteoinductive Biomaterials. *MRS Bull.* 36–39 (1996).
13. Jayakumar, R., Reis, R. L. & Mano, J. F. Chemistry and Applications of Phosphorylated Chitin and Chitosan. *e-Polymers* **6,** 1–16 (2006).
14. Illy, N. *et al.* Phosphorylation of bio-based compounds: the state of the art. *Polym. Chem.* **6,** 6257–6291 (2015).
15. Suflet, D. M., Chitanu, G. C. & Popa, V. I. Phosphorylation of polysaccharides: New results on synthesis and characterisation of phosphorylated cellulose. *React. Funct. Polym.* **66,** 1240–1249 (2006).
16. Shogren, R. L. Flocculation of kaolin by waxy maize starch phosphates. *Carbohydr. Polym.* **76,** 639–644 (2009).
17. Dong, T.-T., Chen, G.-H. & Gao, C.-J. Preparation of chitin xanthate/polyacrylonitrile NF composite membrane with cross-linking agent hydrogen peroxide and its characterization. *J. Memb. Sci.* **304,** 33–39 (2007).
18. Hirano, S., Usutani, A. & Zhang, M. Chitin xanthate and some xanthate ester derivatives. *Carbohydr. Res.* **256,** 331–6 (1994).

# CHAPTER-III

# MATERIALS AND METHODS

# TABLE OF CONTENTS

## CHAPTER III

# CHAPTER III

# MATERIALS AND METHODS

## III.1: Preparation of mild steel and copper specimens

The Chemical composition of mild steel specimens used in the present study is 0.1 to 0.2 % carbon, 0.02 to 0.03 % sulphur, 0.04 to 0.05 % phosphorus, 0.4 to 0.5 % manganese and the rest iron. Whereas, copper samples were taken from a copper sheet of 99.9 % purity. The mild steel specimens of the dimensions, 3.5 cm x 1.5 cm x 0.2 cm and copper specimens of the dimensions, 4 cm x 1 cm x 0.2 cm were used in the weight-loss studies and electrochemical investigations. In all the investigations, before each experiment, the samples were polished with a series of emery polishing papers in a systematic manner (grade 1/0, grade 2/0, grade 3/0 and grade 4/0 respectively). Furthermore, a mirror like finish was obtained by polishing on a rotating disk with alumina slurry. Then, the samples were washed with double distilled water, rinsed with acetone and dried with hot air. The mild steel and copper specimens of the dimensions, 1 cm x 1 cm x 1 mm, were used in the surface examination studies by scanning electron microscopy equipped with energy dispersive X-ray spectroscopy (SEM-EDX), X-ray photoelectron spectroscopy (XPS) and X-ray diffractometry.

## III.2 Chemicals used in the present study

All the other chemicals used in the present study were of the analytical reagent grade.

| S. No. | Chemical | Formula | Grade | Company |
|---|---|---|---|---|
| 1 | Sodium chloride | NaCl | AnalaR | S.D.fine-Chem. Ltd., Mumbai, India |
| 2 | L-Ascorbic acid | $C_6H_8O_6$ | AnalaR | S.D.fine-Chem. Ltd., Mumbai, India |
| 3 | Zinc sulphate heptahydrate | $ZnSO_4.7H_2O$ | AnalaR | S.D.fine-Chem. Ltd., Mumbai, India |
| 4 | Sodium hydroxide | NaOH | AnalaR | S.D.fine-Chem. Ltd., Mumbai, India |
| 5. | Chitin | - | AnalaR | Sigma Aldrich |
| 6. | Chitosan | - | AnalaR | Sigma Aldrich |
| 7. | Hydrochloric acid | HCl | AnalaR | Thermo Fischer Scientific Pvt. Ltd, India |
| 8. | Xanthan gum | - | AnalaR | Himedia laboratories Pvt. Ltd., India |

### III.3: Synthesis of the inhibitor molecules used in the present study:

The inhibitor molecules used in the present study were synthesized by using the methods reported in the literature. The corrosion inhibition ability of these molecules has been evaluated using various methods.

### III.3.1: Preparation of phosphorylated chitin (PCT):

Chitin has been chemically modified to phosphorylated chitin using phosphorous pentoxide ($P_2O_5$) – methane sulphonic acid method, reported in the literature [1–4]**.** The reaction product is found to have a high degree of substitution of phosphonate group and is soluble in water. The structure of PCT is shown in figure III.1.

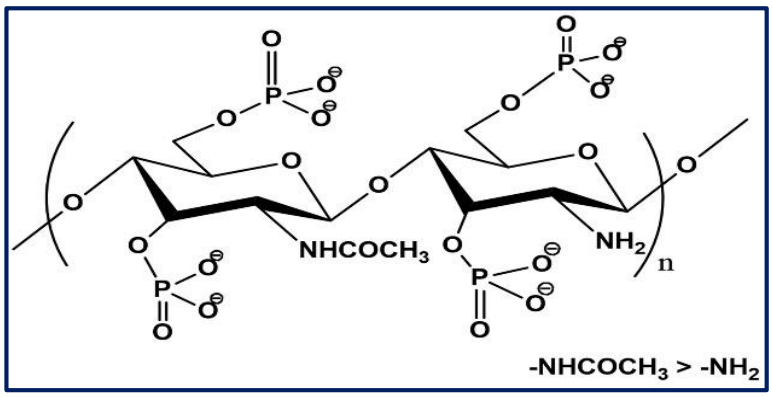


**Figure III.1:** Phosphorylated chitin

### III.3.2 Preparation of Chitin Xanthate (CX):

Chitin has been chemically modified to chitin xanthate using the method reported in the literature[5,6]. The modified derivative is prepared using carbon disulphide in alkaline conditions. The synthetic procedure is illustrated in the figure III.2.

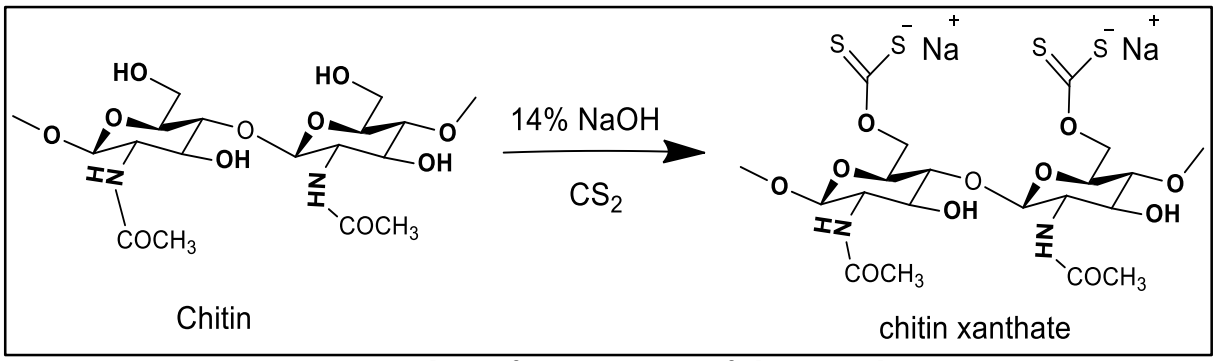


**Figure III.2:** Scheme for preparation of chitin xanthate

### III.3.3: Synthesis of Chitosan ascorbate ketimine

Chitosan ascorbate ketimine has been synthesized according to the procedure reported in the literature[7,8]. Upon addition of ascorbic acid to chitosan present in the solution phase, it will dissolve to form chitosan ascorbate. This solution was kept as such

for 6 h in order to obtain chitosan ascorbate ketimine and the resulting solution was precipitated in acetone.

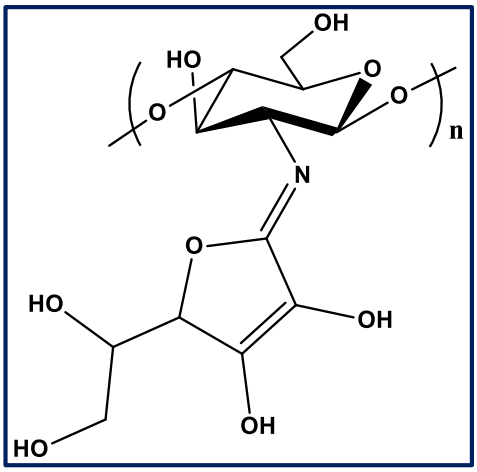


**Figure III.3:** Chitosan ascorbate ketimine

### III.3.4: Synthesis of phosphorylated xanthan gum (PXG):

The phosphorylated Xanthan gum has been synthesized using the method available in the literature[9,10]. The phosphate groups were added on the backbone of xanthan gum using sodium phosphate method.

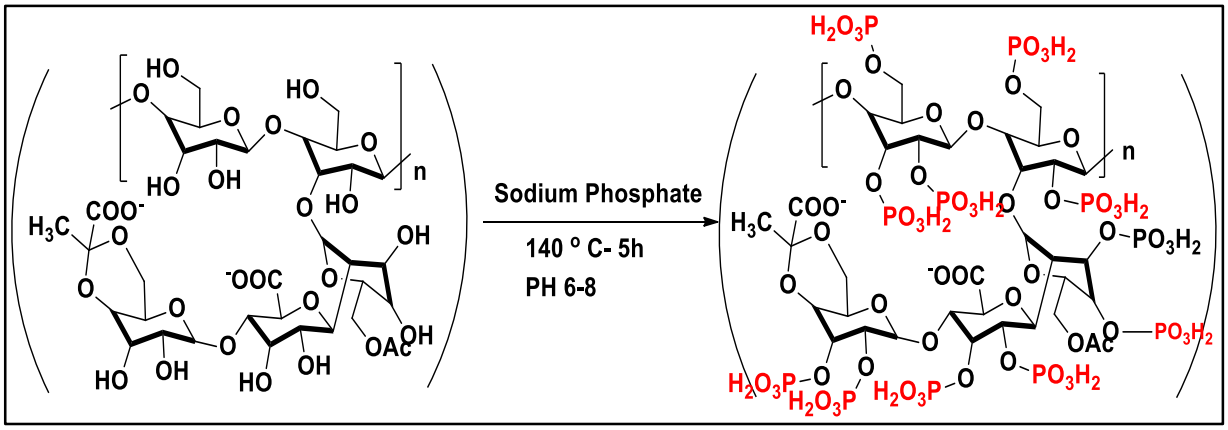


**Figure III.4** Scheme for the preparation of phosphorylated xanthan gum.

### III.4: Preparation of the stock solutions

### III.4.1 Preparation of stock solution of sodium chloride:

Exactly 1.0000 g of sodium chloride was dissolved in double distilled water and made up to one liter mark in a standard measuring flask with double distilled water. This solution consists of 1000 ppm of sodium chloride. A fivefold dilution of this stock solution yields exactly 200 ppm of sodium chloride.

**III.4.2 Preparation of Stock solution of PCT:**

1000 ppm of phosphorylated chitin (PCT) stock solution was prepared by dissolving exactly 1.000 g of PCT in 1000 mL of double distilled water. The pH of this solution was adjusted to 7 by adding appropriate amount of NaOH solution. A fivefold dilution of this stock solution of PCT yields exactly 200 ppm PCT.

Appropriate volumes of PCT and NaCl solutions were taken from the respective stock solutions and mixed in order to achieve various concentrations of PCT inhibitor in the presence of 200 ppm NaCl environment.

**III.4.3: Stock solution of zinc sulphate:**

1000 ppm of a solution of zinc ions solution was prepared by dissolving 4.4000 g of $ZnSO_4$. $7H_2O$ in double distilled water and then making up the solution to 1000 mL in a standard flask. A hundred fold dilution of this stock solution yields exactly 10 ppm of zinc ions.

**III.4.4: Preparation of Stock solution of CX:**

100 ppm of chitin xanthate (CX) stock solution was prepared by dissolving exactly 0.1000 g of CX in 1000 mL of double distilled water. The pH of this solution was adjusted to 7 by adding appropriate amount of NaOH solution. A fivefold dilution of this stock solution of CX yields exactly 20 ppm of CX.

Appropriate volumes of CX and NaCl were taken from the respective stock solutions and mixed in order to achieve various concentrations of CX inhibitor in the presence of 200 ppm NaCl environment.

**III.4.5 Preparation of chitosan ascorbate ketimine inhibitor solutions:**

Various mole ratios of chitosan and ascorbic acid have been used in the preparation of Chitosan ascorbate ketimine solution.

**III.4.6 Preparation of Stock solution of PXG:**

1000 ppm of phosphorylated xanthan gum (PXG) stock solution was prepared by dissolving exactly 1.000 g of PXG in 1000 mL of double distilled water. A fivefold dilution of this stock solution of PCT yields exactly 200 ppm PCT.

**III.4.7: Preparation of corrosive environments and different concentrations of inhibitor:**

Before finalizing the range of concentrations of PCT, chitosan, ascorbic acid, copper, zinc ions, several trial experiments were carried out in different concentration ranges. Based on the results, the range of concentrations has been chosen as there is effect of inhibitor concentration on corrosion inhibition. While studying with mixtures of inhibitors, concentration of one synergist is fixed and concentration of the other species are varied. In this way best combinations, which acquired highest inhibition efficiencies could be arrived at.

**III.4.7.1: corrosive environment: 200 ppm NaCl- mild steel, Inhibitor: PCT+$Zn^{2+}$.**

| S.No | Final concentration of inhibitor solution (100 mL) with 200 ppm of NaCl | Volume of 1000 ppm NaCl | Volume of 1000 ppm $Zn^{2+}$ ions | Volume of 1000 ppm PCT | Vol. of distilled water |
|---|---|---|---|---|---|
| 1 | 0 ppm PCT | 20 mL | 0 mL | 0 mL | 80 mL |
| 2 | 50 ppm PCT | 20 mL | 0 mL | 5 mL | 75 mL |
| 3 | 100 ppm PCT | 20 mL | 0 mL | 10 mL | 70 mL |
| 4 | 150 ppm PCT | 20 mL | 0 mL | 15 mL | 65 mL |
| 5 | 200 ppm PCT | 20 mL | 0 mL | 20 mL | 60 mL |
| 6 | 50 ppm PCT+ 100 ppm $Zn^{2+}$ | 20 mL | 10 mL | 5 mL | 65 mL |
| 7 | 100 ppm PCT+ 100 ppm $Zn^{2+}$ | 20 mL | 10 mL | 10 mL | 60 mL |
| 8 | 150 ppm PCT+ 100 ppm $Zn^{2+}$ | 20 mL | 10 mL | 15 mL | 55 mL |
| 9 | 200 ppm PCT+ 100 ppm $Zn^{2+}$ | 20 mL | 10 mL | 20 mL | 50 mL |

**III.4.7.2: corrosive environment: 200 ppm NaCl-copper, Inhibitor: PCT**

| S.No. | Final concentration of inhibitor solution (100 mL) with 200 ppm of NaCl. | Volume of 1000 ppm NaCl | Volume of 1000 ppm PCT | Volume of distilled water |
|---|---|---|---|---|
| 1 | 0 ppm PCT | 20 mL | 0 mL | 80 mL |
| 2 | 50 ppm PCT | 20 mL | 5 mL | 75 mL |
| 3 | 100 ppm PCT | 20 mL | 10 mL | 70 mL |
| 4 | 150 ppm PCT | 20 mL | 15 mL | 65 mL |
| 5 | 200 ppm PCT | 20 mL | 20 mL | 60 mL |

**III.4.7.3: corrosive environment: 200 ppm NaCl- copper, Inhibitor: CX**

| S.No. | Final concentration of inhibitor solution (100 mL) with 200 ppm of NaCl | Volume of 1000 ppm NaCl | Volume of 1000 ppm CX | Volume of distilled water |
|---|---|---|---|---|
| 1 | 0 ppm CX | 20 mL | 0 mL | 80 mL |
| 2 | 10 ppm CX | 20 mL | 1 mL | 79 mL |
| 3 | 20 ppm CX | 20 mL | 2mL | 78 mL |
| 4 | 30 ppm CX | 20 mL | 3 mL | 77 mL |
| 5 | 40 ppm CX | 20 mL | 4 mL | 76 mL |

**III.4.7.4: corrosive environment: 200 ppm NaCl- mild steel, Inhibitor: PXG.**

| S.No. | Final concentration of inhibitor solution (100 mL) with 200 ppm of NaCl. | Volume of 1000 ppm NaCl | Volume of 1000 ppm PXG | Volume of distilled water |
|---|---|---|---|---|
| 1 | 0 ppm PXG | 20 mL | 0 mL | 80 mL |
| 2 | 50 ppm PXG | 20 mL | 5 mL | 75 mL |
| 3 | 100 ppm PXG | 20 mL | 10 mL | 70 mL |
| 4 | 150 ppm PXG | 20 mL | 15 mL | 65 mL |
| 5 | 200 ppm PXG | 20 mL | 20 mL | 60 mL |

**III.5: Determination of corrosion rate by gravimetric method (weight-loss studies):**

The weight- loss studies were carried out using a Shimadzu AY 120 balance (readability 0.01 mg). In each experiment, the specimen (copper or mild steel) was weighed before and after immersion in the corrosive environment without and with different concentrations of the inhibitor formulations. The immersion period was 7 days for mild steel specimens and 10 days for copper specimens. After completion of the specified immersion time, the specimens were removed and cleaned according to the procedure given in ASTM- G1 specifications[11,12]. Then, the specimens were weighed again. Accuracy in weighing is 0.01 mg and accuracy in surface area measurement is 0.1 $cm^2$, which are in accordance with the recommendations of ASTM G31[13]. Each specimen was weighed three times and the mean value was reported in order to minimize the uncertainty in weighing. The corrosion rates and inhibition efficiencies were calculated from the observed difference in weights. Every experiment was performed in duplicate and the mean value was taken as the final value. The standard error in determination of corrosion rate is found to be less than or equal to two percent, which is in compliance with the standard laboratory practice [14].

From the difference in the weights of the specimens, the corrosion rates were calculated using the following formula given in the equation (1).

$$\text{Corrosion rate (mdd)} = \frac{\text{Weight loss in mg}}{\text{Surface area of specimen (dm}^2\text{)X Period of immersion in days}} \ldots (1)$$

When **mdd** refers to the corrosion rate in milligrams per square decimeter area per day.

The mdd unit of corrosion rate has been converted into **mmpy** (millimeter per year) using the equation given in (2),

$$\text{Corrosion rate (mmpy)} = \frac{\text{Corrosion rate(mdd) X } 0.0365}{\text{D}} \ldots\ldots\ldots\ldots (2)$$

Where 'D' refers to the density of the metal (mild steel or copper as the case may be). The corresponding inhibition efficiencies are obtained using the equation (3)

$$\text{Inhibition efficiency (\%)} = [(\emptyset_{control} - \emptyset_i)/\emptyset_{control}\,]X100 \ldots\ldots\ldots\ldots (3)$$

Here, $\emptyset_{control}$ =corrosion rate in control without inhibitor, $\emptyset_i$ = corrosion rate in the presence of inhibitor.

**III.6: Electrochemical Studies**

Electrochemical Impedance studies (EIS) and potentiodynamic polarization studies were employed to investigate the corrosion inhibition efficiency of the inhibitor formulations. These studies were performed using a three-electrode cell assembly with the appropriate specimen (mild steel or copper) as the working electrode. The dimensions of the specimen were 3.5 cm x 1.5 cm x 0.2 cm for mild steel and 4 cm x 1 cm x 0.2 cm for copper respectively. Only one $cm^2$ surface area of the specimen has been exposed to the corrosive environment and the rest is coated with epoxy resin. An Ag| AgCl| 3M KCl electrode was used as a reference electrode and a platinum plate electrode was used as the counter electrode. All the studies were carried out using ZAHNER IM6e Electrochemical Workstation (Germany). All the investigations were performed at a temperature of 30 ± 0.1°C by taking 500 mL of 200 ppm NaCl solution as corrosion environment for four inhibitor formulations and 1 M HCl as corrosive environment for one inhibitor formulation. The pH of all the solutions in case of aq. NaCl corrosive environment was adjusted to 7.0 using 0.1 N NaOH solution. While performing the experiments the solutions were maintained in a stagnant condition (naturally aerated).

**III.6.1: Electrochemical impedance studies (EIS)**

The electrochemical impedance studies were carried out at the open circuit potential (OCP) in the frequency range of 10 mHz to 60 kHz with an ac signal of 10 mV, peak to peak. In all the experiments the OCP was achieved after 1 h of sample immersion in the corrosive environment. Both the Nyquist and Bode plots were recorded in the present study for the analysis of the corrosion phenomenon.

Impedance parameters such as solution resistance ($R_s$), charge transfer resistance ($R_{ct}$), double layer capacitance ($C_{dl}$), CPE exponent (n) and Warburg impedance (W) etc, were obtained by fitting the experimental data with appropriate equivalent circuit models. The three different equivalent circuit models which were used in the present study are depicted in figures III.5 and III.6.

From the charge transfer resistance values, the inhibition efficiency was calculated for each inhibitor concentration using the equation (4).

$$\boldsymbol{I.E.\%} = \frac{(\boldsymbol{R_{ct}})_i - (\boldsymbol{R_{ct}})_{control}}{(\boldsymbol{R_{ct}})_i} \boldsymbol{X\ 100} \ldots\ldots\ldots\ldots\ldots\ldots\ldots (4)$$

$(R_{ct})_i$= charge transfer resistance in the presence of inhibitor

$(R_{ct})_{control}$= charge transfer resistance without inhibitor

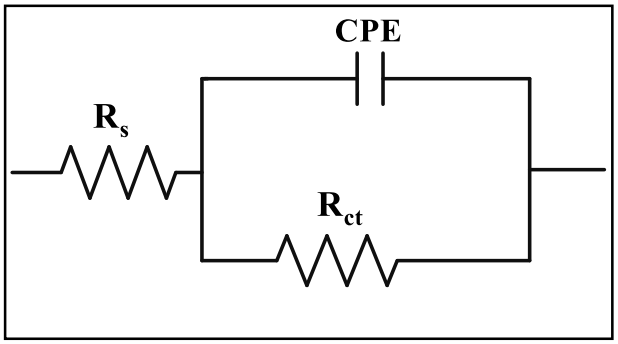


**Figure III.5:** Equivalent circuit used in impedance measurements for mild steel specimen (in aq. NaCl) in control and in the presence of inhibitor formulation.

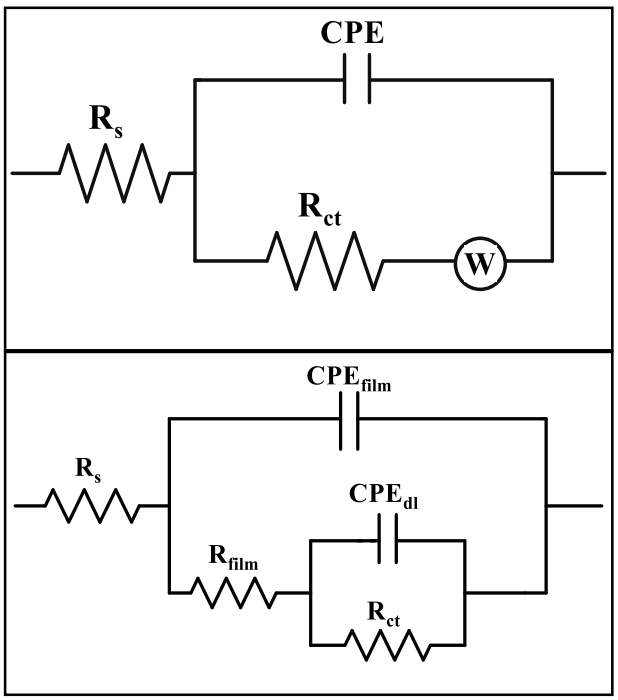


**Figure III.6:** Equivalent circuit used in impedance measurements of A) copper specimen with Warburg behaviour B) copper specimen in presence of inhibitor formulation and for mild steel specimen in 1M HCl. in control and in the presence of inhibitor formulation

Where, $R_s$ = Solution resistance

$R_{ct}$ = Charge transfer resistance

$R_{film}$ = Resistance of the film

$CPE_{film}$ = Constant phase element of the film

$CPE_{dl}$ = Constant phase element of the electrical double layer

W = Warburg impedance

The Nyquist plots obtained in the present study exhibited depressed semicircles rather than ideal semicircles. This phenomenon is called dispersing effect[15]. When the depressed semicircle with centre below the real axis occurs in the EIS results, it is often ascribed to the roughness and non-homogeneous nature of the metal surface, which is also a characteristic for solid electrodes[16]. It is also attributed to the distribution of active sites, adsorption of inhibitor molecules and formation of porous layers [17].

At high frequencies the $R_s$ determines the impedance and at very low frequencies the cell impedance is equal to the sum of $R_s$ and $R_{ct}$.

### III.6.2 Potentiodynamic polarization studies

Potentiodynamic polarization experiments were performed on mild steel or copper specimen surface immersed in the corrosive environment without and with different concentrations of inhibitor formulation. The potential range was between -750 mV to +250 mV for mild steel and -700 mV to +700 mV for copper. The scan rate was 0.1 mV $sec^{-1}$.

Corrosion potential ($E_{corr}$) and corrosion current density ($j_{corr}$) were determined from the polarization curves by the Tafel extrapolation method.

From the corrosion current density values, the inhibition efficiency was calculated for each inhibitor concentration using the equation (5).

$$\boldsymbol{I.E.\%} = \frac{(\boldsymbol{J_{corr}})_{\boldsymbol{control}} - (\boldsymbol{J_{corr}})_{\boldsymbol{i}}}{(\boldsymbol{J_{corr}})_{\boldsymbol{control}}} \boldsymbol{X\ 100}) \ldots\ldots\ldots\ldots\ldots\ldots\ldots\ldots (5)$$

Where $(J_{corr})_{control}$, $(J_{corr})_i$ represent the corrosion current density values without, and with inhibitor formulation, respectively.

### III.7 Surface morphological studies by Scanning Electron Microscopy (SEM):

The surface morphology of the metal samples immersed in corrosive environment with and without inhibitor formulations was investigated by scanning electron microscopy (SEM). Initially the specimens (copper or mild steel) were polished, degreased, dried and then immersed in the corrosive environment with inhibitor formulations. After immersion for 7 days for mild steel and 10 days for copper specimen the specimens were removed from the solutions and gently washed with doubly distilled water and dried. Then, the SEM images were recorded using a VEGA 3 TESCAN, USA model scanning electron microscope

### III.8: Analysis of the surface films using energy dispersive X-ray spectroscopy:

The surface films formed after corrosion were characterized using an energy dispersive X-ray spectrometer (Oxford instruments make).

### III.9: surface characterization by X-ray photoelectron spectroscopic studies (XPS):

The X-ray photoelectron spectroscopic studies were performed using X-ray photoelectron spectrometer model ESCA 2SR, Omicron Nano Technology, GmbH, Germany with a base vacuum of $1\times 10^{-6}$ Pa. Al Kα radiation (1486.6 eV) was used for primary excitation. Survey scan spectra were recorded at pass energy of 187.9 eV and the individual high resolution spectra were taken at pass energy of 20.0 eV with an

energy step of 0.1 eV. The deconvolution spectra were recorded with a step of 0.1 eV for the elements of interest namely Fe 2p, Cu 2p, Zn 2p, O 1s, P 2p, N 1s, C 1s and S 2p. The XPS instrument was calibrated using Au foil for which the characteristic binding energy value of 4f electron is 84.1 eV.

X-ray photoelectron spectroscopic studies were performed in the binding energy range of 0 eV to 1200 eV. The binding energy values of the peaks present in the spectrum of the samples under study were then compared with the literature values and analyzed. Based on the shift in the binding energy values of the basic elemental peaks, the surface analysis has been carried out. The chemical shift can be in the range of 0.1 to 10 eV. The list of chemical shift values for various oxidation states for most of the elements is available in literature[18].

In the present study the films formed on the metal surface immersed in corrosive environment (mild steel- 7 days, copper- 10 days) in presence or absence of inhibitor formulations were characterized by XPS studies.

**III.10: Analysis of the surface films using powder X-ray diffractometry:**

The surface film formed on the metals after corrosion process in the absence as well as in the presence of inhibitor systems were characterized using X-ray diffraction studies. The XRD instrument, Bruker D8-advance, Germany was used to perform the XRD experiments. The X-ray source is Cu-Kά ($\lambda$ = 1.5418 Aº (in 2$\theta$)) radiation. The spectrum was recorded in the range of 10 to 80°.

**References:**


1. Nishi, N., Maekita, Y., Nishimura, S., Hasegawa, O. & Tokura, S. Highly phosphorylated derivatives of chitin, partially deacetylated chitin and chitosan as new functional polymers: metal binding property of the insolubilized materials. *Int. J. Biol. Macromol.* **9,** 109–114 (1987).
2. Nishi, N. *et al.* Highly phosphorylated derivatives of chitin, partially deacetylated chitin and chitosan as new functional polymers: preparation and characterization. *Int. J. Biol. Macromol.* **8,** 311–317 (1986).
3. Jayakumar, R., Selvamurugan, N., Nair, S. V., Tokura, S. & Tamura, H. Preparative methods of phosphorylated chitin and chitosan-An overview. *Int. J. Biol. Macromol.* **43,** 221–225 (2008).
4. Tachaboonyakiat, W., Netswasdi, N., Srakaew, V. & Opaprakasit, M. Elimination of inter- and intramolecular crosslinks of phosphorylated chitosan by sodium salt formation. *Polym. J.* **42,** 148–156 (2009).
5. Hirano, S., Usutani, A. & Zhang, M. Chitin xanthate and some xanthate ester derivatives. *Carbohydr. Res.* **256,** 331–336 (1994).
6. Sankararamakrishnan, N. & Sanghi, R. Preparation and characterization of a novel xanthated chitosan. *Carbohydr. Polym.* **66,** 160–167 (2006).
7. Muzzarelli, R., Tanfani, F. & Emanuelli, M. Chelating derivatives of chitosan obtained by reaction with ascorbic acid. *Carbohydr. Polym.* **4,** 137–151 (1984).
8. Muzzarelli, R. A. A. Removal of uranium from solutions and brines by a derivative of chitosan and ascorbic acid. *Carbohydr. Polym.* **5,** 85–89 (1985).
9. Shogren, R. L. Flocculation of kaolin by waxy maize starch phosphates. *Carbohydr. Polym.* **76,** 639–644 (2009).
10. Granata, A. & Perlin, A. S. Use of O-thallium(I) salts in the synthesis of phosphate, sulfite, and related ester derivatives of carbohydrates. *Carbohydr. Res.* **94,** 165–171 (1981).
11. ASTM NACE/ASTMG31-12a. *Standard guide for laboratory immersion corrosion testing of metals*. *ASTM International* (ASTM International, 2012). doi:10.1520/G0031-12A.
12. ASTM International. Standard Practice for Preparing , Cleaning , and Evaluating Corrosion Test. *Significance* **90,** 1–9 (1999).
13. Astm. *ASTM Standards: G31-72*. *Annual Book of ASTM Standards* **72,** (2012).

14. Freeman, R. A. & Silverman, D. C. Technical Note: Error Propagation in Coupon Immersion Tests. *Corrosion* **48,** 463–466 (1992).
15. Li, S. L. *et al.* Inhibition of Copper Corrosion with Schiff Base Derived from 3-Methoxysalicylaldehyde and O-Phenyldiamine in Chloride Media. *CORROSION* **54,** 947–954 (1998).
16. Jüttner, K. Electrochemical impedance spectroscopy (EIS) of corrosion processes on inhomogeneous surfaces. *Electrochim. Acta* **35,** 1501–1508 (1990).
17. El Hosary, A. A., Saleh, R. M. & Shams El Din, A. M. Corrosion inhibition by naturally occurringsubstances—I. The effect of Hibiscus subdariffa (karkade) extract on the dissolution of Al and Zn. *Corros. Sci.* **12,** 897–904 (1972).
18. Castle, J. E. Practical surface analysis by Auger and X-ray photoelectron spectroscopy. D. Briggs and M. P. Seah (Editors). John Wiley and Sons Ltd, Chichester, 1983, 533 pp., £44.50. *Surf. Interface Anal.* **6,** 302–302 (1984).

# CHAPTER-IV

## Section IV.1: Phosphorylated Chitin (PCT) – $Zn^{2+}$ system to combat the corrosion of mild steel in neutral chloride environment

## Section IV.2: Phosphorylated chitin (PCT) as an inhibitor to control corrosion of copper in neutral chloride environment

# TABLE OF CONTENTS

## CHAPTER IV

# Chapter IV

This chapter has been divided into two sections. Section IV.1 deals with the experimental results and discussion of the corrosion protection of mild steel in neutral chloride environment using Phosphorylated Chitin (PCT) – $Zn^{2+}$ system and section IV.2 consists of the experimental results and discussion of the corrosion protection of copper in neural chloride environment using Phosphorylated Chitin (PCT).

## Section IV.1: Phosphorylated Chitin (PCT) – $Zn^{2+}$ system to combat the corrosion of mild steel in neutral chloride environment.

### IV.1.1. Characterization of Phosphorylated Chitin (PCT):

The synthesized phosphorylated derivative of chitin was characterized by Fourier Transform Infrared spectroscopy (FTIR). Figure IV.1.1 presents the FTIR spectra of pure chitin and phosphorylated chitin (PCT). In the spectrum of PCT, a broad peak at 3428 $cm^{-1}$ is because of P-OH groups [1–3]. Due to phosphorylation, a shoulder peak appeared around 1220 $cm^{-1}$and this peak is assigned to phosphate group (P=O asymmetric stretching)[4]. The Peak at 1050 $cm^{-1}$ is because of C-O-P stretching in phosphate ester and the peak at 975 $cm^{-1}$is due to P-OH stretching. A broad band between 900 $cm^{-1}$ to 1100 $cm^{-1}$ is also an indication of phosphorylation[5].

The synthesized derivative of chitin was also characterized by $^{13}C$ NMR spectroscopy. The $^{13}C$ NMR spectrum of phosphorylated chitin is shown in **figure IV.1.2.** From the results we can infer that the $^{13}C$ NMR spectrum of PCT exhibits characteristic chemical shift values for the non-equivalent carbons at appropriate positions with respect to tetramethylsilane (TMS). The carbon atoms attached to the functionalised amine and hydroxyl groups appeared in the spectrum. The $^{13}C$ NMR signal at δ 53.87 ppm corresponds to the $C_2$ carbon of pyranose ring (–CH-NH-). The signal at δ 66.68 ppm corresponds to $C_3$ carbon of pyranose ring (-CH-O-P). The signals at δ 38.35 ppm, δ 68.23 ppm and δ 69.04 ppm correspond to the $C_4$, $C_5$ and $C_6$ carbons of pyranose ring respectively.

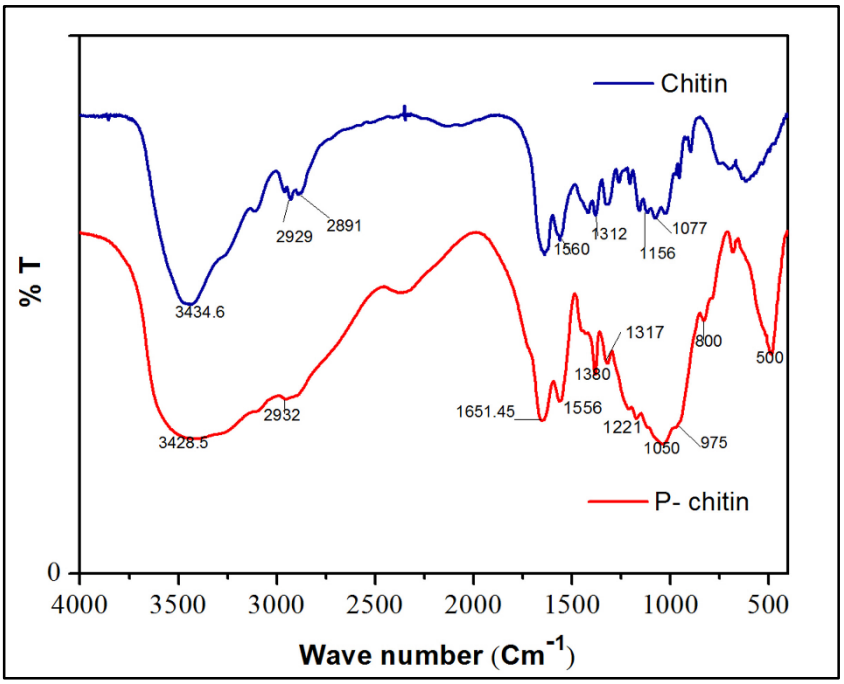


**Figure IV.1.1:** FTIR spectra of pure chitin and Phosphorylated Chitin (PCT).

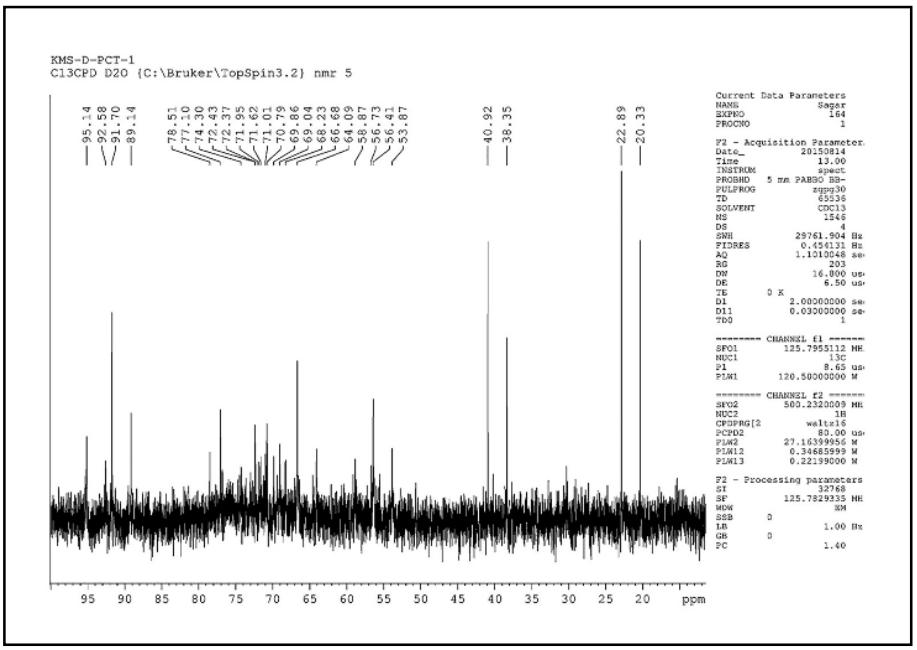


**Figure IV.1.2:** $^{13}$C- NMR spectrum of Phosphorylated Chitin (PCT).

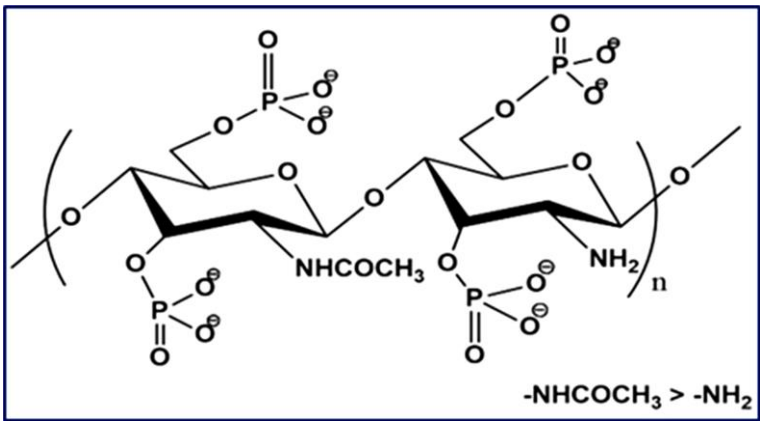


**Phosphorylated chitin**

Weight-loss studies, electrochemical impedance studies and potentiodynamic polarization studies were carried out to investigate the corrosion inhibition ability. SEM-EDX and XPS studies were employed for analysis of the surface films.

**IV.1.2: Analysis of the results of weight-loss Studies:**

The corrosion inhibition efficiency of the chemically modified chitin (PCT) and the synergism of this modified polymer and $Zn^{2+}$ have been investigated using the weight-loss studies at 30 °C after 7 days immersion period. The experimental data of the corrosion rates and the inhibition efficiencies are given in the table IV.1.1. The results showed that the corrosion rate decreased and the inhibition efficiency increased appreciably by the addition of phosphorylated chitin as inhibitor. It is very clear that the PCT inhibits corrosion of mild steel in neutral aqueous chloride environment at all the tested concentrations. The inhibition efficiency increased with increasing concentration of the modified polymer and the highest inhibition efficiency of 73% was obtained at 150 ppm concentration of the polymer. When the concentration of PCT is further increased to 200 ppm, the weight-loss of mild steel is slightly increased and slight increase in corrosion rate is observed. This result could be the consequence of an increase in the number of molecules of phosphorylated chitin adsorbed on mild steel surface and 150 ppm PCT is the sufficient concentration to form a protective film. From the literature, it is known that $Zn^{2+}$ alone accelerates the corrosion rate of mild steel in neutral chloride environment[6,7]. It is also known that $Zn^{2+}$ functions as a synergists in combination with phosphates in protecting mild steel from corrosion in chloride environment. The inhibition efficiency of PCT at all concentrations increased considerably when $Zn^{2+}$(100 ppm) was added as a synergist. The inhibition efficiency reached up to 93 % for 200 ppm PCT in presence of 100 ppm $Zn^{2+}$. The synergistic

parameter (S) values for various PCT concentrations have been calculated using the equation (1) given below to confirm the existence of synergistic effect between PCT and $Zn^{2+}$.

The synergistic parameter (S) has been calculated using the equation (1) given below[8],

$$S = \frac{1 - Ø_{1+2}}{1 - Ø'_{1+2}} \ldots\ldots\ldots\ldots\ldots\ldots (1)$$

Here $Ø_{1+2} = Ø_1 + Ø_2 - (Ø_1.Ø_2)$

$Ø_1$= surface coverage by $Zn^{2+}$ when used alone, $Ø_2$= surface coverage by PCT when used alone, $Ø'_{1+2}$ = surface coverage by PCT in combination with $Zn^{2+}$.

**Table.IV.1.1:** Corrosion parameters for mild Steel in 200ppm NaCl (aq) in absence and presence of different concentrations of phosphorylated chitin obtained from the gravimetric method.

| S.No. | Concentration(ppm) | | Weight - loss(mg) | Corrosion Rate(mdd) | Corrosion Rate (mmpy) | I.E.% |
|---|---|---|---|---|---|---|
| | P-Chitin | $Zn^{2+}$ | | | | |
| 1 | 0 | 0 | 12.14 | 17.47 | 0.08111 | - |
| 2 | 50 | 0 | 8.94 | 11.92 | 0.05534 | 26 |
| 3 | 100 | 0 | 5.83 | 7.78 | 0.03612 | 51 |
| 4 | 150 | 0 | 3.22 | 4.29 | 0.01991 | 73 |
| 5 | 200 | 0 | 4.75 | 6.34 | 0.02943 | 61 |
| 6 | 0 | 100 | 14.15 | 20.36 | 0.09455 | -16 |
| 7 | 50 | 100 | 5.43 | 7.24 | 0.03361 | 55 |
| 8 | 100 | 100 | 3.96 | 5.28 | 0.02451 | 67 |
| 9 | 150 | 100 | 3.14 | 4.18 | 0.01940 | 74 |
| 10 | 200 | 100 | 0.83 | 1.10 | 0.00513 | 93 |
| 11 | 300 | 100 | 1.50 | 2.00 | 0.00928 | 88 |
| 12 | 400 | 100 | 1.55 | 2.07 | 0.00961 | 87 |

The ‘S’ values are listed in table IV.1.2. The S value is greater than one for all

PCT concentrations, which suggests that there is a synergistic effect between PCT and $Zn^{2+}$. Similar results on synergistic effects of synthetic phosphonates and $Zn^{2+}$ in controlling corrosion of carbon steel have been reported in the literature[9,10].

**Table.IV.1.2:** Synergistic parameters for different concentrations of phosphorylated chitin as inhibitor.

| S.No. | Concentration (ppm) | | I.E.% | Synergistic parameter (S) |
|---|---|---|---|---|
| | P-Chitin | $Zn^{2+}$ | | |
| 1 | 50 | 100 | 55 | 1.9 |
| 2 | 100 | 100 | 67 | 1.7 |
| 3 | 150 | 100 | 74 | 1.2 |
| 4 | 200 | 100 | 93 | 7.3 |

### IV.1.3: Analysis of the results of Electrochemical Studies:

### Electrochemical Impedance Studies

The electrochemical impedance studies were performed at the open circuit potential in the absence and presence of various concentrations of phosphorylated chitin (PCT) and PCT in combination with $Zn^{2+}$ ions in neutral aqueous chloride environment. The studies were performed at various immersion times namely 1h, 6h, 12h and 24h. Figure IV.1.3 depicts the Nyquist plots for mild steel sample immersed in 200 ppm sodium chloride solution in the absence and in presence of various concentrations of PCT at 24 h immersion period. Similarly figure IV.1.4 presents the Nyquist plots for mild steel sample in the absence and in presence of various concentrations of PCT in combination with 100 ppm $Zn^{2+}$ions. The corresponding Bode plots are depicted in figures IV.1.5 and IV.1.6 respectively. The experimental values were fitted with different equivalent circuits in order to obtain the corrosion parameters. The experimental data fitted well with the simple Randles equivalent circuit shown in the figure IV.1.7. The equivalent circuit consists of solution resistance ($R_s$), charge transfer resistance ($R_{ct}$), and a constant phase element (CPE). Similar equivalent circuit was also reported by other researchers[11–13] The calculated parameters from EIS data are presented in the table IV.1.3.

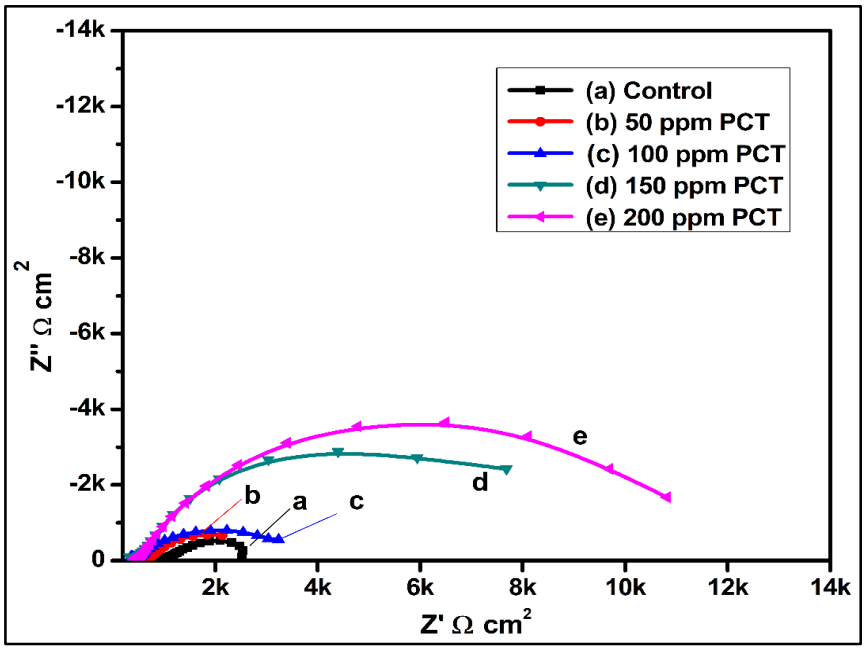


**Figure IV.1.3**: Nyquist plots of mild steel sample in 200 ppm NaCl (a) in the absence (b) in presence of 50 ppm PCT (c) 100 ppm PCT (d) 150 ppm PCT (e) 200 ppm PCT (24 h immersion period). [Points- experimental data, solid line- fitted using the equivalent circuit mode].

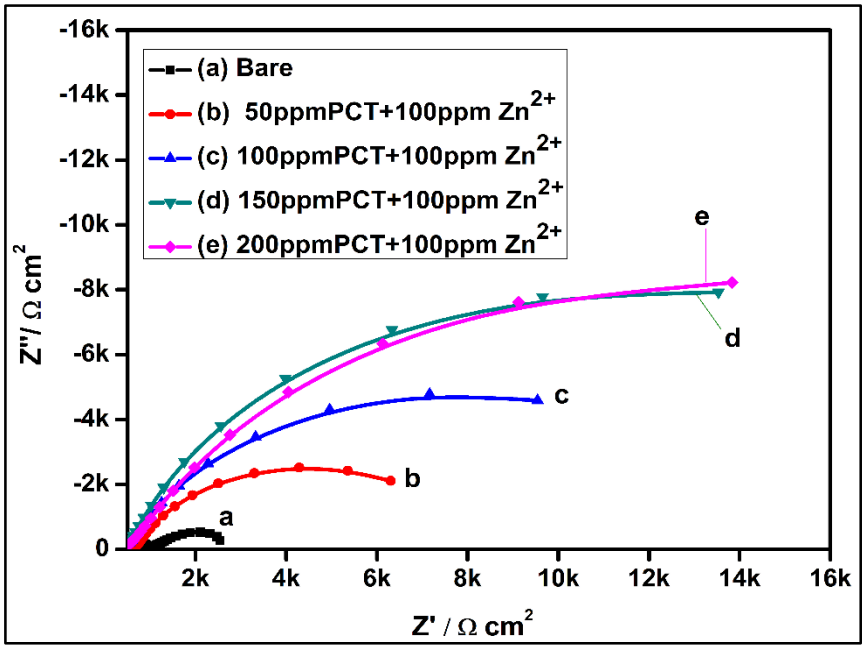


**Figure IV.1.4**: Nyquist plots of mild steel sample in 200 ppm NaCl (a) in the absence (b) in presence of 50 ppm PCT along with 100 ppm $Zn^{2+}$ (c) 100 ppm PCT along with 100 ppm $Zn^{2+}$ (d) 150 ppm PCT along with 100 ppm $Zn^{2+}$ (e) 200 ppm PCT along with 100 ppm $Zn^{2+}$ (24 h immersion period). [Points- experimental data, Solid line- fitted using the equivalent circuit mode].

In the case of control, a small depressed semicircle is observed in the Nyquist plots with an $R_{ct}$ value of 1.9 kΩ $cm^2$. When PCT alone is used as an inhibitor, despite the fact that the semicircle is depressed the diameter of the semicircle is increased with an increase in concentration of the inhibitor. An $R_{ct}$ value of 10.7 kΩ $cm^2$ is obtained for 200 ppm of PCT, which afforded an inhibition efficiency of 83 %. When a small concentration of $Zn^{2+}$ (100 ppm) is used as synergist in combination with 200 ppm PCT, the $R_{ct}$ is increased to 32.9 kΩ $cm^2$, which accounts for an inhibition efficiency of 94 %. These results indicate the significance of the synergism between zinc ions and P- chitin in enhancing inhibition efficiency. From the data given in the table it is established that $Zn^{2+}$ ions function as synergist at all the concentrations of PCT in controlling the corrosion of mild steel.

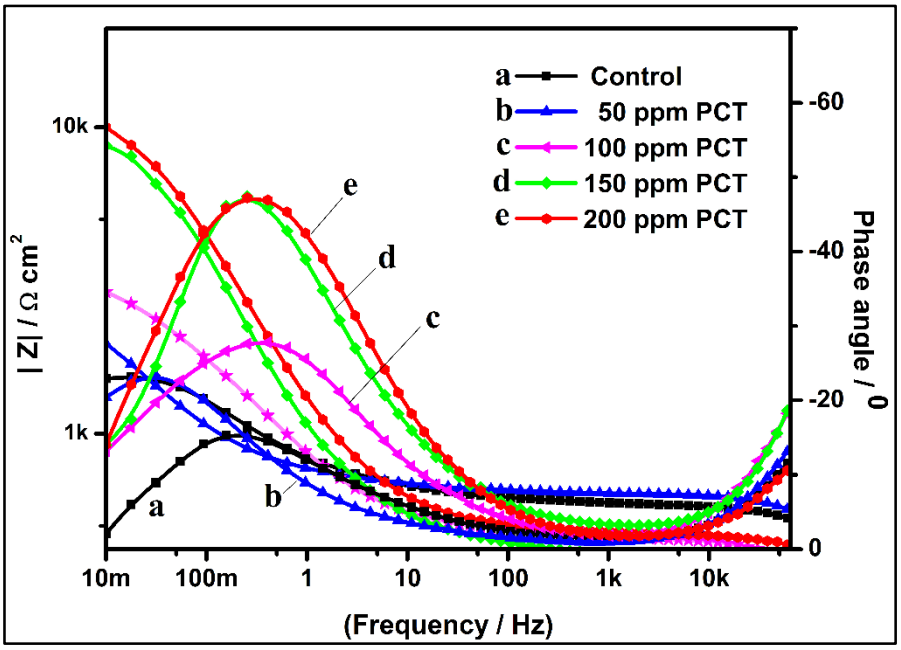


**Figure IV.1.5:** Bode plots of of mild steel sample in 200 ppm NaCl (a) in the absence (b) in presence of 50 ppm PCT (c) 100 ppm PCT (d) 150 ppm PCT (e) 200 ppm PCT (24 h immersion period). [Points- experimental data, solid line- fitted using the equivalent circuit mode].

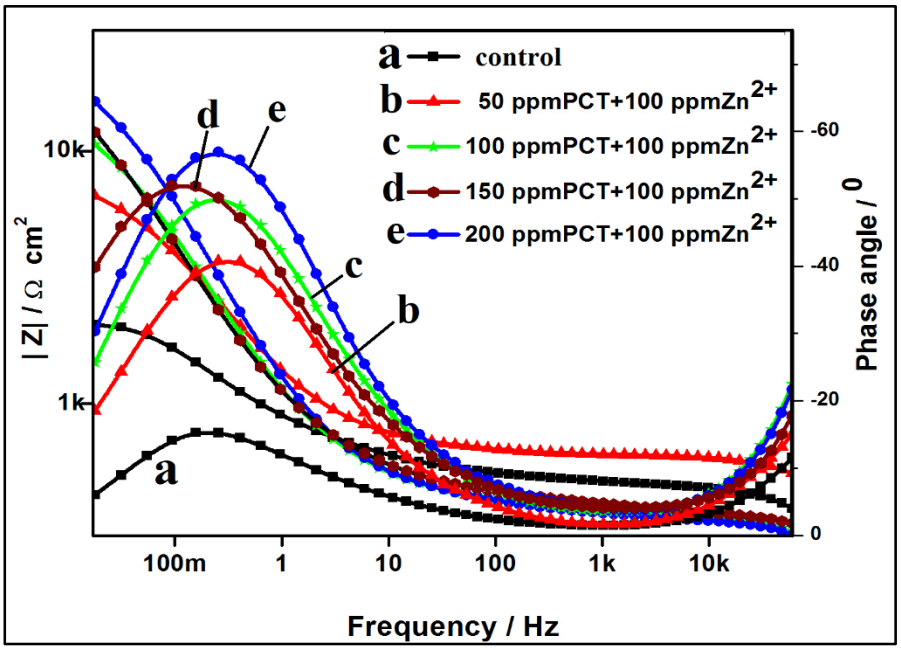


**Figure IV.1.6**: Bode plots of mild steel sample in 200 ppm NaCl (a) in the absence (b) in presence of 50 ppm PCT along with 100 ppm $Zn^{2+}$ (c) 100 ppm PCT along with 100 ppm $Zn^{2+}$ (d) 150 ppm PCT along with 100 ppm $Zn^{2+}$ (e) 200 ppm PCT along with 100 ppm $Zn^{2+}$ (24 h immersion period). [Points- experimental data, Solid line- fitted using the equivalent circuit mode].

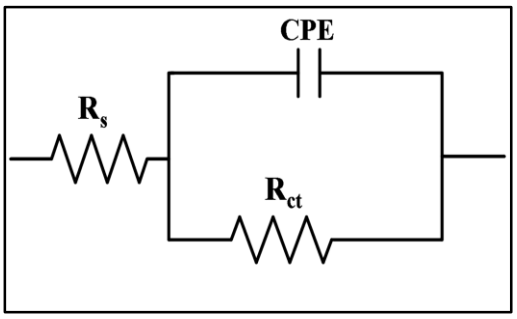


**Figure IV.1.7:** Equivalent circuit used (Simple Randles Circuit)

$R_s$- Solution Resistance, $R_{ct}$ - Charge transfer resistance, CPE - Constant phase element.

In Bode plots it can be seen that the phase angle maximum is only 15° in the presence of control and is increased to a value of around 60° in the presence of binary inhibitor formulation, namely 200 ppm PCT + 100 ppm $Zn^{2+}$. The total impedance of the system is also increased from 2.50 kΩ $cm^2$ to 35.02 kΩ $cm^2$ in the presence of binary inhibitor system. This result is indicative of the protective film formation on the metal surface. It is interesting to note that the charge transfer region is in the low frequency range namely 10 Hz to 10 mHz in the presence of the binary inhibitor formulation, which

affords the highest inhibition efficiency. The total impedance vs. frequency plot showed a clear tendency for an increase in impedance even at the lowest frequency namely 10 mHz.

**Table IV.1.3**: Impedance parameters for mild steel in 200ppm aq. NaCl solution in the absence and presence of different concentrations of inhibitor formulation.

| S.No. | Concentration(ppm) | | $R_{ct}$(kΩ $cm^2$) | $C_{dl}$(µF $cm^{-2}$) | n | I.E.% |
|---|---|---|---|---|---|---|
| | PCT | $Zn^{2+}$ | | | | |
| 1 | 0 | 0 | 1.9 | 14.3 | 0.580 | - |
| 2 | 50 | 0 | 2.9 | 13.8 | 0.568 | 37 |
| 3 | 100 | 0 | 3.3 | 12.7 | 0.593 | 44 |
| 4 | 150 | 0 | 9.1 | 12.1 | 0.713 | 80 |
| 5 | 200 | 0 | 10.7 | 12.0 | 0.758 | 83 |
| 6 | 50 | 100 | 7.7 | 14.3 | 0.733 | 76 |
| 7 | 100 | 100 | 15.0 | 13.9 | 0.699 | 88 |
| 8 | 150 | 100 | 24.5 | 11.1 | 0.735 | 92 |
| 9 | 200 | 100 | 32.9 | 10.2 | 0.782 | 94 |

From the impedance parameters, we can also observe a change in the 'n' value. The 'n' value is shifted towards higher values in the presence of the inhibitor formulation. In the case of control, the 'n' value is 0.580, which is increased to 0.782 when the binary inhibitor formulation of PCT (200 ppm) + $Zn^{2+}$ (100 ppm) is used. The value of n is close to 0.5 in the case of control and in the presence of inhibitor formulations, which afforded low inhibition efficiency. Such a low value of n indicates mass transport also. When the value of 'n' is very close to 1, it indicates that the protective film is highly homogeneous. Even in the presence of inhibitor, which afforded the highest efficiency, the value of n is not very close to 1. This result is indicates that the protective film is not perfectly homogeneous.

The double layer capacitance ($C_{dl}$) value is decreased in presence of all the combinations inhibitor formulation; but the decrease is not in a linear manner with increase in concentration of the inhibitor formulations. This decrease can be attributed to the replacement of the adsorbed water molecules on the mild steel surface by the

inhibitor formulation. The capacitance of the inhibitor formulation film is less because of the less dielectric constant of the inhibitor molecules when compared to water molecules.

Thus, all the results of the impedance studies indicate that there is formation of a protective film on the metal surface in presence of the binary inhibitor formulation.

**Potentiodynamic polarization studies:**

Figures IV.1.8 and IV.1.9 represent the anodic and cathodic polarization curves of mild steel immersed in 200 ppm NaCl solution at pH=7 and temperature 30±0.1ºC in the absence and presence of different inhibitor formulations.

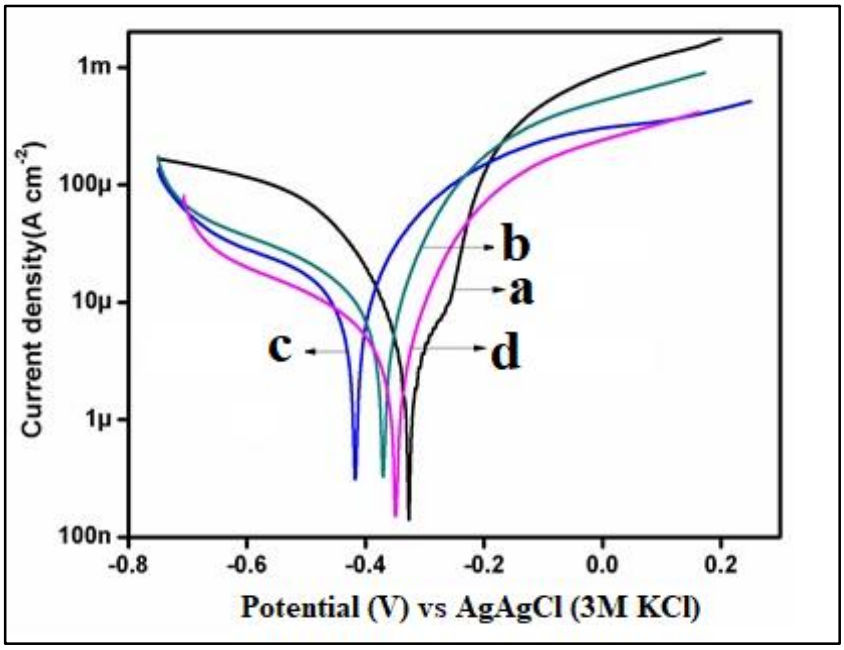


**Figure IV.1.8**: Potentiodynamic polarization curves mild steel sample in 200 ppm NaCl (a) in the absence (b) in presence of 50 ppm PCT (c) 150 ppm PCT (d) 200 ppm PCT.

From the **figure IV.1.8** it can be inferred that in the presence of PCT the corrosion current density values decreased, and the corrosion potential is shifted towards more negative side when compared to control.

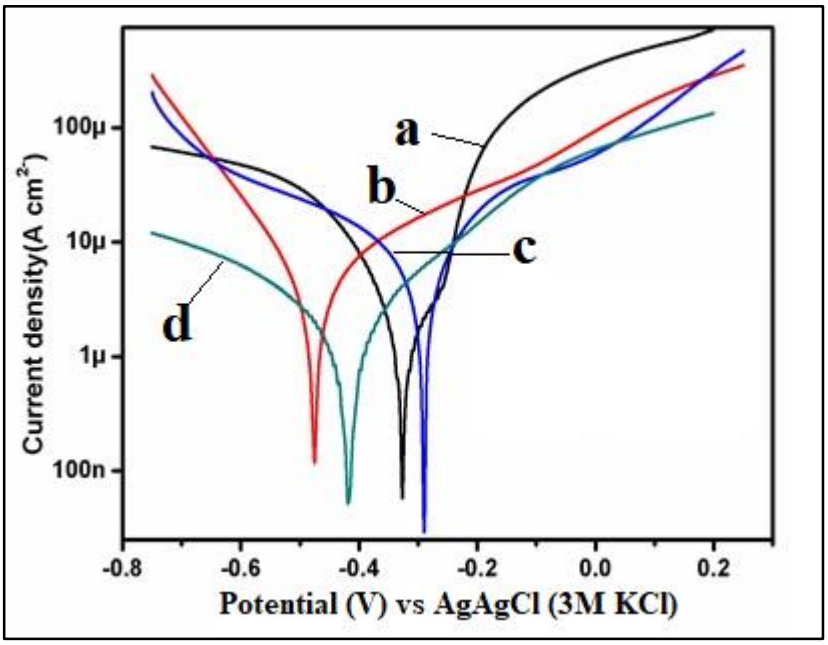


**Figure IV.1.9:** Potentiodynamic polarization curves of mild steel sample in 200 ppm NaCl (a) in the absence (b) in presence of 50 ppm PCT along with 100 ppm $Zn^{2+}$ (c) 150 ppm PCT along with 100 ppm $Zn^{2+}$ (d) 200 ppm PCT along with 100 ppm $Zn^{2+}$.

The corrosion parameters were calculated from the polarization curves by extrapolating the cathodic and anodic Tafel regions. The potential range, which has been used to extrapolate the Tafel regions is between ±30 mV from the corrosion potential value. The corrosion potential ($E_{corr}$), corrosion current density ($i_{corr}$), anodic Tafel slope (βa) and cathodic Tafel slopes (βc) and the calculated corrosion inhibition efficiencies are presented in the table IV.1.4. In the control system, a corrosion potential ($E_{corr}$) of -323.0 mV is observed and the corresponding corrosion current density ($J_{corr}$) is 11.8 µAcm$^{-2}$. When PCT alone was used as the inhibitor, the corrosion potential is shifted towards more negative side with respect to control, and the corresponding corrosion current density is decreased with increasing concentration of PCT. This result infers that indicating PCT can inhibit the corrosion of mild steel in 200 ppm NaCl. The lowest corrosion current density of 3.2 µAcm$^{-2}$ is obtained when 200 ppm PCT was used and the inhibition efficiency is 72 %. It has been reported in the literature that when $Zn^{2+}$ ions alone are added to the control, they increase in corrosion current density[14]. In the present study when $Zn^{2+}$ ions are added along with different concentrations of PCT the inhibition efficiencies increased considerably, which are higher when compared to the inhibition efficiencies in presence of PCT alone as inhibitor. This result indicates the presence of a synergistic effect between PCT and $Zn^{2+}$ ions in controlling the corrosion

of mild steel in aqueous sodium chloride environment. For instance, the inhibition efficiency is increased from 72 % to 93 % when 100 ppm of $Zn^{2+}$ ions were added to 200 ppm PCT.

**Table IV.1.4:** Corrosion parameters obtained for mild steel in 200 ppm NaCl (aq) in absence and presence of different concentrations of the inhibitor by potentiodynamic polarization studies.

| S.No. | Concentration(ppm) | | $E_{corr}$ (mV) | $J_{corr}$ ($\mu Acm^{-2}$) | βc (mV $dec^{-1}$) | βa (mV $dec^{-1}$) | I.E.% |
|---|---|---|---|---|---|---|---|
| | PCT | $Zn^{2+}$ | | | | | |
| 1 | 0 | 0 | -323.0 | 11.8 | -441 | 189 | - |
| 2 | 50 | 0 | -395.6 | 9.7 | -102 | 59.5 | 17 |
| 3 | 150 | 0 | -412.4 | 3.7 | -106 | 53.2 | 68 |
| 4 | 200 | 0 | -365.5 | 3.2 | -102 | 51.7 | 72 |
| 5 | 50 | 100 | -476.0 | 2.3 | -190 | 88.8 | 80 |
| 6 | 150 | 100 | -294.0 | 1.7 | -184 | 95 | 85 |
| 7 | 200 | 100 | -413.5 | 0.8 | -245 | 155 | 93 |

Form the figure IV.1.9 it is quite evident that the combination of PCT and $Zn^{2+}$ (100 ppm) significantly decreases the corrosion of mild steel by decreasing both the anodic and cathodic current densities. Highest inhibition efficiency was obtained for the combination of PCT (200 ppm) + $Zn^{2+}$ (100 ppm) with a corrosion current density of 0.8 $\mu Acm^{-2}$, which is 6.79 % of the $J_{corr}$ value of the control. It is observed that both the anodic and cathodic curves showed lower current densities in the presence of all binary inhibitor formulations. By adding inhibitor formulation to the control solution, the βa and βc values decreased significantly. From the results it is evident that, although both the anodic and cathodic corrosion processes are retarded by the inhibitor, the cathodic process is relatively more affected. Taking into account the decrease in Tafel slopes and corrosion current densities, it can be said that the present inhibitor formulation affects the kinetics of both iron dissolution and oxygen reduction. From these results, we can infer that the inhibitor formulation acts as a mixed type inhibitor. Zinc ions form zinc

hydroxide on the cathodic sites and inhibit the cathodic reaction. Consequently, the cathodic current densities are affected more[15]. An Inhibition efficiency of 93 % was obtained with the combination of 200 ppm PCT and 100 ppm $Zn^{2+}$. Thus, the results of weight-loss studies, impedance studies and potentiodynamic polarization studies established the synergistic effect of PCT and $Zn^{2+}$ ions in controlling the corrosion of mild steel in 200 ppm chloride environment. In conclusion, the PCT+$Zn^{2+}$ system functions as a good inhibitor for protection of mild steel from corrosion in neutral chloride environment.

**IV.1.4: Analysis Surface morphology by scanning electron microscopy (SEM):**

Scanning electron microscopic images of the surface of mild steel samples were recorded in order to study the surface morphology after immersion in the corrosive environment for seven days in the absence and presence of inhibitor formulation.

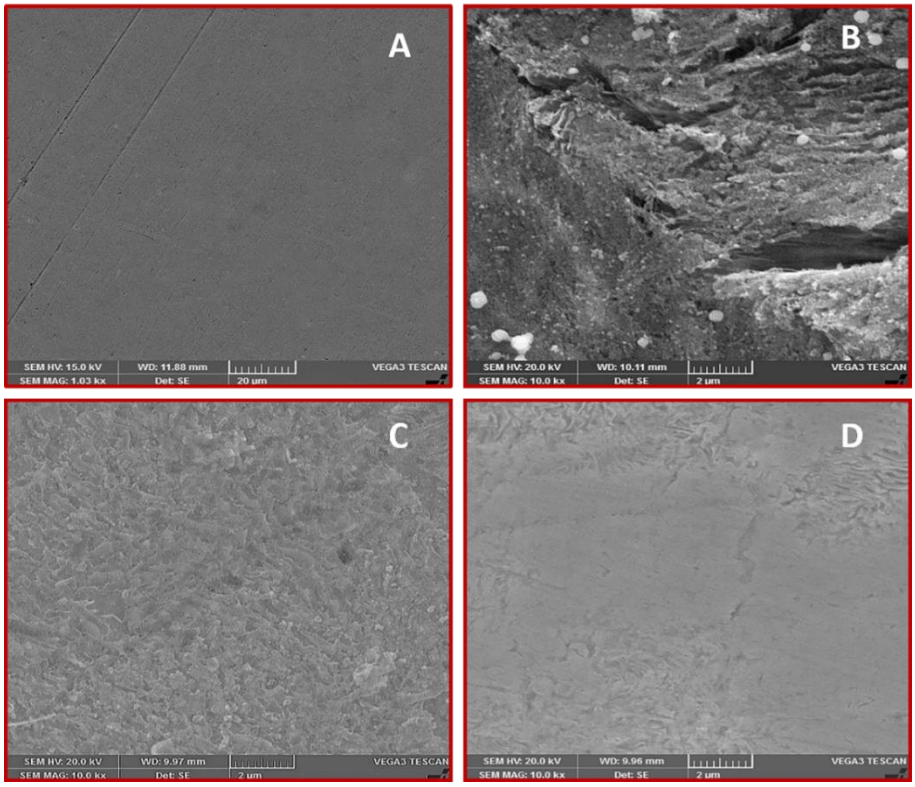


**Figure IV.1.10:** SEM images (10,000X magnification) of (A) polished specimen, (B) Control, (C) PCT (200 ppm), (D) PCT (200 ppm) +$Zn^{2+}$ (100 ppm) in 200 ppm NaCl environment after seven days immersion.

Figure IV.1.10A represents the SEM micrograph of the polished mild steel specimen. Figure IV.1.10B represents the SEM micrograph of the surface of mild steel immersed in the control without inhibitor, which clearly shows the corrosion products

and deep cracks on the surface. Figure IV.1.10C and IV.1.10D are the SEM images of mild steel after immersion in 200 ppm PCT, and in the synergistic mixture of 200 ppm PCT and 100 ppm $Zn^{2+}$ respectively. In Figure IV.1.10C, it can be seen that in presence of 200 ppm PCT the surface of the mild steel shows a film, which may consist of adsorbed inhibitor molecules. This film formation contributes to the minimization of corrosion. Figure IV.1.10D also reveals that the mild steel surface consists of an inhibitor film which is relatively more uniform than that of the film formed in presence of 200 ppm PCT alone. However, these two figures show the surface smoothness and the absence of any corrosion product on mild steel surface due to the formation of a protective film on the mild steel surface[15].

**IV.1.5: Surface analysis by X-ray photoelectron spectroscopic studies (XPS):**

The XPS survey spectra of the surface films formed on mild steel in the absence and presence of the binary inhibitor formulation containing PCT (200 ppm) and $Zn^{2+}$ (100 ppm) are shown in the figures IV.1.11A and IV.1.11B respectively.

The XPS survey spectrum of the surface film formed on the mild steel surface in the absence of the binary inhibitor system exhibits peaks for Fe 2p, O 1s, C 1s and the Cl 2p. Whereas, the XPS survey spectrum of the surface film in presence of the inhibitor formulation (Figure IV.1.11B) shows peaks for P 2p, N 1s, Zn 2p, along with Fe 2p, O 1s and C 1s, which give the evidence for the adsorption of the inhibitor on the mild steel surface.

The computer deconvolution spectra for iron (Fe2p) and oxygen (O1s) of the film formed on the mild steel surface in the corrosive environment in the absence and in the presence of inhibitor formulation (200 ppm PCT + 100 ppm $Zn^{2+}$) are shown in figure IV.1.12 and figure IV.1.13 respectively. Figures IV.1.14 – IV.1.17 present the deconvolution spectra for carbon, phosphorus, nitrogen and zinc present in the film formed in the absence and presence of inhibitor.

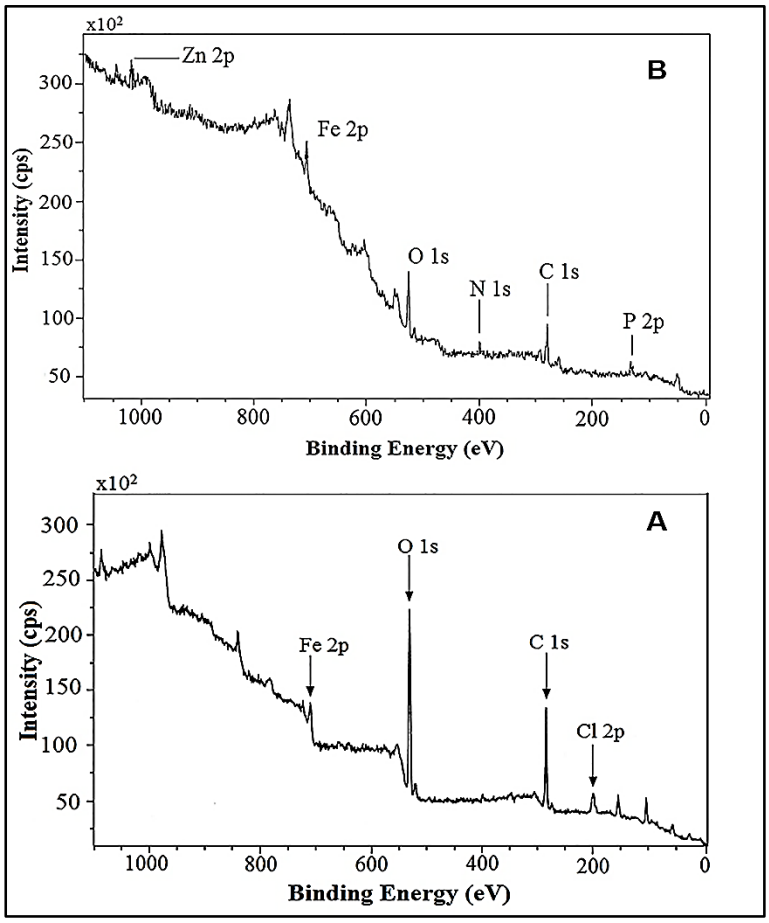


**Figure IV.1.11:** XPS Survey spectrum of mild steel specimen immersed in **(A)** 200 ppm NaCl and **(B)** in presence of PCT (200 ppm) +$Zn^{2+}$ (100 ppm) along with 200 ppm NaCl.

The deconvolution spectrum of the Fe2p of control consists of two peaks, one at 710.8 eV corresponding to Fe $2p_{3/2}$ electron and the other one at 724.2 eV corresponding to the Fe $2p_{1/2}$ electron (Figure IV.1.12A). There is a large shift in the binding energy value of Fe $2p_{3/2}$ from the characteristic elemental binding energy value of 707.0 eV. This shift of 3.8 eV suggests that iron is present as $Fe^{3+}$ in the form of ferric oxide and hydroxide. Indeed, the peak at a binding energy of 710.8 eV was attributed to ferric compounds such as $Fe_2O_3$, $Fe_3O_4$ and FeOOH in the literature[16,17]. The peak located at 724.2 eV was attributed to the presence of a small concentration of $FeCl_3$ on the metal surface[18]. In the presence of binary inhibitor system, the Fe 2p deconvolution spectrum consists of two peaks, one at 711 eV, which is due to Fe $2p_{3/2}$, and the other at 724.3 eV which is due to Fe $2p_{1/2}$ (Figure IV.1.12B). The Fe $2p_{3/2}$ peak may be interpreted due to the presence of ($Fe^{3+}$- PCT complex) along with small amount of oxides and hydroxides ($Fe_2O_3$, $Fe_3O_4$ and FeOOH) present in the surface film. There is no peak due to elemental iron in the case of control or in the presence of the inhibitor formulation. This result is an

indication for the formation of a film in both the cases. The film is non- protective in the case of control and is protective in the presence of the inhibitor formulation[19].

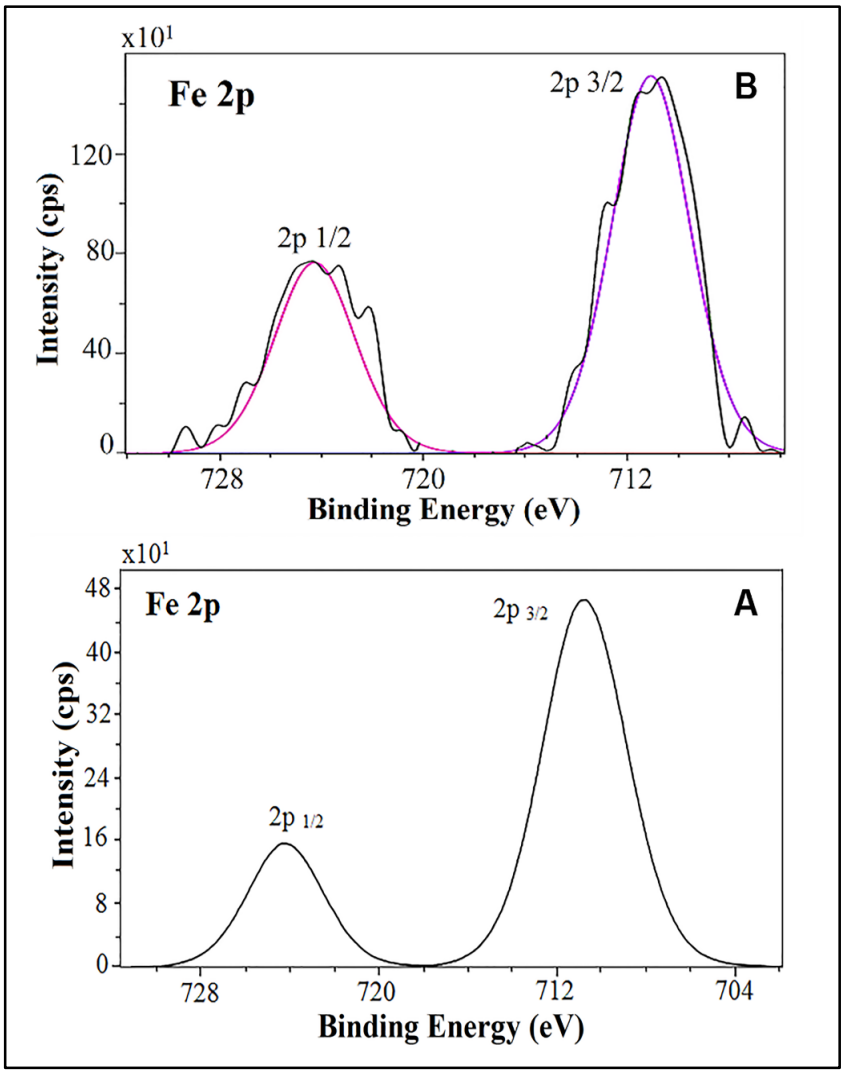


**Figure IV.1.12:** XPS deconvolution spectra of Fe 2p for mild steel sample immersed in **(A)** 200 ppm NaCl **(B)** PCT (200 ppm) + $Zn^{2+}$ (100 ppm) along with 200 ppm NaCl.

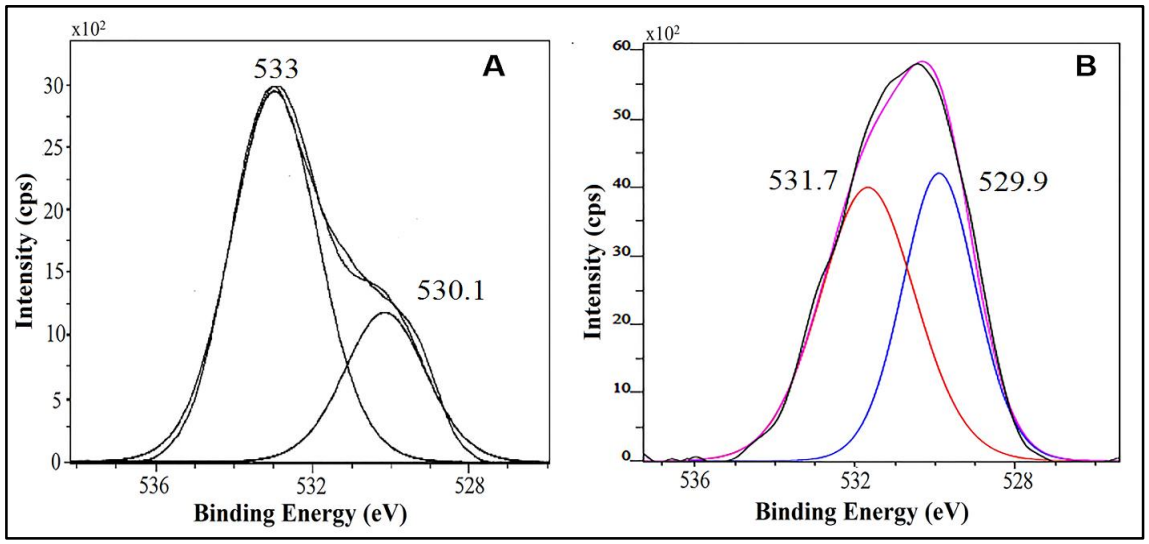


**Figure IV.1.13:** XPS deconvolution spectra of O1s for mild steel sample immersed in **(A)** 200 ppm NaCl **(B)** PCT (200 ppm) + $Zn^{2+}$ (100 ppm) along with 200 ppm NaCl.

The deconvolution spectrum of O 1s in the case of control consists of two peaks (Figure IV.1.13A), one peak at a binding energy value of 530.1 eV and the other one at a binding energy value of 533.0 eV. The peak located at lower binding energy value (530.1 eV) can be attributed to $O^{2-}$ and can be related to the bond with $Fe^{3+}$ in iron oxides and hydroxides ($Fe_2O_3$, $Fe_3O_4$). The peak located at higher binding energy value (533.0 eV) can be ascribed to oxygen atoms of the adsorbed water molecules. Whereas, the deconvolution spectrum of O 1s in the presence of binary inhibitor formulation (Figure IV.1.13B) consists of two peaks, one at 529.9 eV and the other one at 531.1 eV. The former one can be interpreted due to oxygen present in the oxides and hydroxides of Fe (III), in the form of $O^{2-}$. The later one (peak at 531.7 eV) is ascribed to $OH^-$ and is attributable to oxygen in hydrous iron oxides, such as FeOOH and $Fe(OH)_3$ [20], $Zn(OH)_2$ and some contribution from the oxygen present in the inhibitor molecule (PCT). The peak at 533.0 eV is absent in the case of binary inhibitor system, which means that there are no adsorbed water molecules on the metal surface, as a consequence of the replacement of adsorbed water molecules by the inhibitor molecules.

Figure IV.1.14A represents the computer deconvolution spectrum of C 1s in the case of control, which shows a single peak at 284.6 eV. This peak can be interpreted as a contaminant carbon peak, which arises due to the cracking of vacuum oil used in the instrument[21].In the case of binary inhibitor formulation the carbon deconvolution spectrum consists of three peaks (Figure IV.1.14B), one peak at the binding energy value of 284.6 eV with high intensity and two peaks of lower intensities at 286.1 eV and 288.3

eV. These peaks can be interpreted as follows. The inhibitor, PCT has different types of carbon environments like C – N, C – C and C – H, which explain the presence of three different peaks in the deconvolution spectrum. These carbon peaks show an evidence for the presence of the PCT molecules in the surface film.

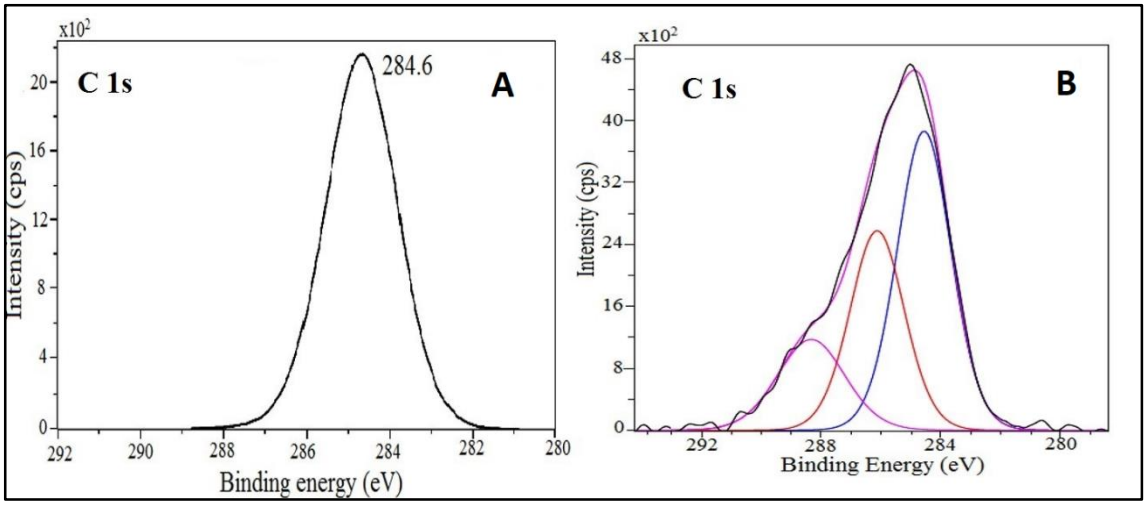


**Figure IV.1.14:** XPS deconvolution spectra of C1s for mild steel sample immersed in **(A)** 200 ppm NaCl **(B)** PCT (200 ppm) + $Zn^{2+}$ (100 ppm) along with 200 ppm NaCl.

The XPS deconvolution spectrum for P 2p in the presence of the inhibitor formulation is shown in the Figure IV.1.15. The spectrum shows two peaks, one at 132.9 eV and the other one at 134.6 eV. The former peak is mainly because of phosphate group present in the PCT molecule. The second peak is mainly attributed to phosphates of iron(III) and zinc (II) which are the main components of the complex in the protective film formed on the mild steel surface[22–25]. Based on the literature reports, the characteristic binding energy value of this coordinate phosphate is around 134.2 eV[26–28]. With all these evidences, the P 2p peak observed in the present study suggests the presence of PCT in the surface film formed in presence of the binary inhibitor system.

Figure IV.1.16 represents the deconvolution spectrum of N 1s in the presence of inhibitor formulation. Three different peaks are observed at 398.7 eV, at 399.8 eV and at 400.8 eV respectively. The characteristic elemental binding energy of N 1s is 398.0 eV [29]. That means, all the peaks observed in the spectrum are shifted from the characteristic elemental binding energy value. These peaks are mainly because of three different nitrogen environments present in the PCT molecule (C-$NH_2$, -$NHCOCH_3$ and Nitrogen participated in the complexation by virtue of its lone pair of electrons). This result

indicates that the PCT present in the surface film is probably in the form of a complex with Fe (III) and Zn (II) ions.

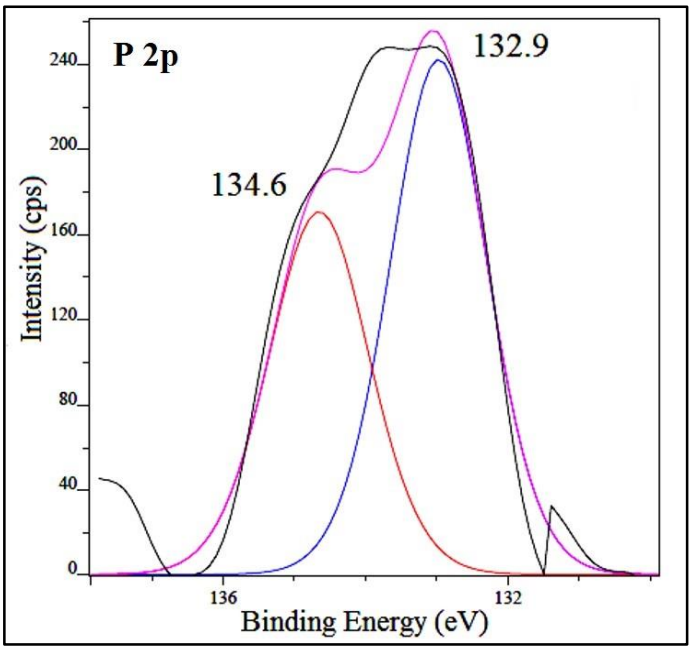


**Figure IV.1.15:** XPS deconvolution spectra of P 2p for mild steel sample immersed in 200 ppm NaCl along with PCT (200 ppm) + $Zn^{2+}$ (100 ppm).

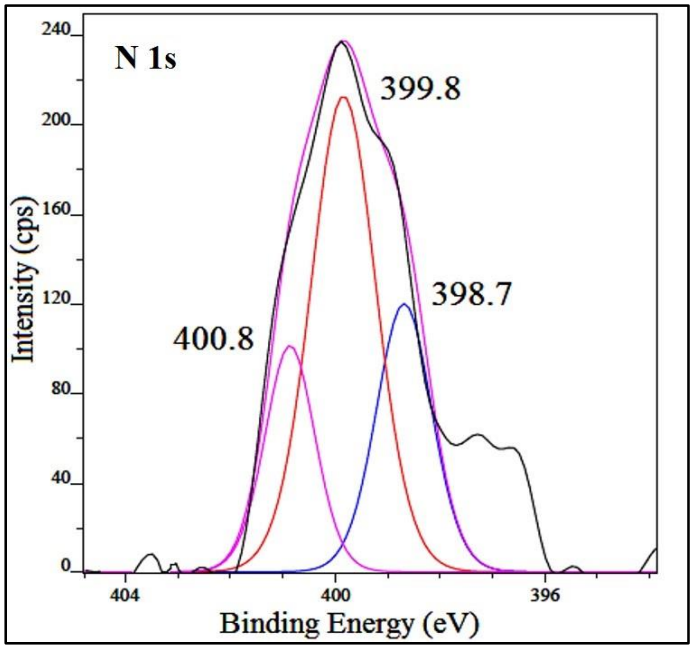


**Figure IV.1.16:** XPS deconvolution spectra of N 1s for mild steel sample immersed in 200 ppm NaCl along with PCT (200 ppm) + $Zn^{2+}$ (100 ppm).

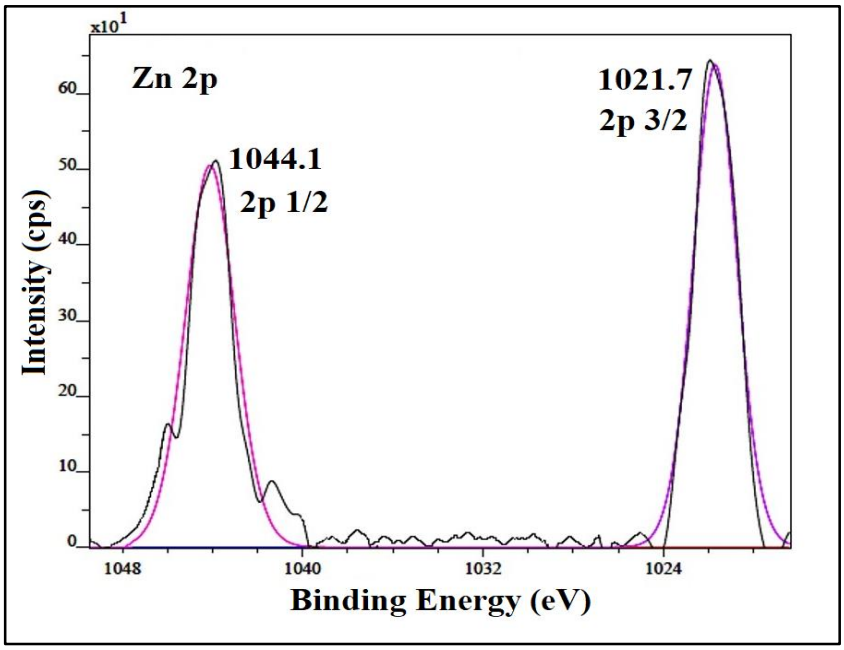


**Figure IV.1.17:** XPS deconvolution spectra of Zn 2p for mild steel sample immersed in 200 ppm NaCl along with PCT (200 ppm) + $Zn^{2+}$ (100 ppm).

Figure IV.1.17 presents the deconvolution spectrum of Zn 2p in presence of the inhibitor formulation. This spectrum shows two peaks, one at 1021.7 eV, which represents Zn $2p_{3/2}$, and another peak at 1044.1 eV, which represents Zn $2p_{1/2}$. The presence of intense Zn $2p_{3/2}$ peak is assigned to $Zn(OH)_2$ [30] present in the surface film and also possibly because of $Zn^{2+}$ involvement in the complex formation with PCT[26,29,31].

**IV.1.6: Analysis of the surface film by X- ray diffraction studies (XRD):**

Figures IV.1.18(A) and IV.1.18(B) depict the X-ray diffractograms of the surface of mild steel immersed in 200 ppm NaCl environment in the absence and presence of the inhibitor formulation (PCT+$Zn^{2+}$) respectively. The XRD pattern shows prominent iron (Fe) peaks at (1 1 0) and (2 0 0) planes in both the cases, since mild steel is the base material of the sample under study. The intensity of the iron peak for (1 1 0) plane is so high that all the other peaks present in the spectrum are relatively low intensed. Along with these iron peaks, the XRD pattern in control also shows peaks for corrosion product, $Fe_3O_4$ [32,33]. The planes present in the spectrum for $Fe_3O_4$ are (3 1 1), (4 4 0), (4 0 0) and (5 1 1).

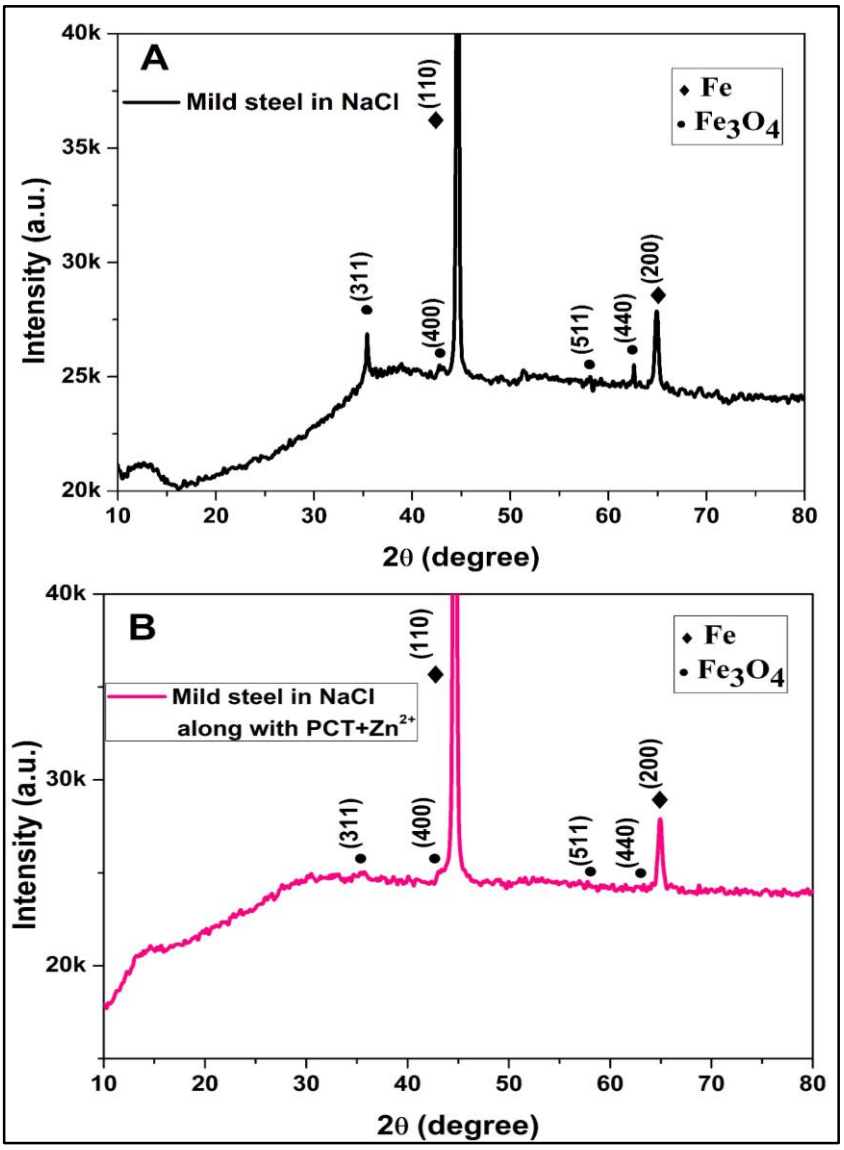


**Figure IV.1.18:** The X-ray diffraction patterns of the surface film formed on mild steel sample immersed in 200 ppm NaCl (A) in the absence (B) in the presence of PCT (200 ppm) + $Zn^{2+}$ (100 ppm).

The XRD pattern of mild steel surface in presence of inhibitor formulation also shows peaks for corrosion product, $Fe_3O_4$ for the planes (311), (440), (400) and (511). But, the intensities of these peaks are relatively far less than the peaks for $Fe_3O_4$ in case of control. This result indicates that the surface of mild steel contains relatively less amount of corrosion product on the surace in the presence of inhibitor. The film may contain small amounts of other corrosion products like $Fe_2O_3$, oxides and hydroxides of of zinc, etc,. But, relative to the intensity of iron peaks, their intensities are too small to be able to be distinguished from in the spectrum. From this analysis, we can infer that the

surface is less corroded in presence of PCT and $Zn^{2+}$ formulation when compared with control.

### IV.1.7: Langmuir adsorption isotherm:

The inhibition mechanism can be understood from the interaction between the inhibitor molecules and metal surface. Different adsorption isotherm models were taken into consideration to understand the inhibition mechanism of PCT + $Zn^{2+}$ formulation. Among them Langmuir adsorption isotherm model is well fitted (based on the correlation coefficient value). The Langmuir adsorption isotherm is given in equation 2.

$$\frac{C}{\emptyset} = \frac{1}{K_{ads}} + C \ldots\ldots\ldots\ldots\ldots\ldots\ldots\ldots\ldots (2)$$

Here, $\emptyset$ is the surface coverage of the inhibitor molecules, which is obtained by the relation, $I.E.\% = \emptyset\, X\, 100$. The I.E. % values are taken from the results of weight-loss studies. C is the concentration of PCT (mg $L^{-1}$). $Zn^{2+}$ concentration is not taken into consideration since it is constant and $K_{ads}$ is the equilibrium constant.

Figure IV.1.19 presents the $C/\emptyset\ Vs\ C$ plot for adsorption of PCT on mild steel surface. A linear curve is obtained with a good correlation coefficient value ($R^2$= 0.9998). This result suggest that the adsorption process follows Langmuir adsorption isotherm model. From the plot it can be seen that the $\emptyset$ value increases with the increase in the PCT concentration ($Zn^{2+}$ concentration being constant). This result can be attributed to the increase in the surface coverage of the metal with inhibitor molecules (PCT) and as a consequence higher inhibition efficiencies are obtained.

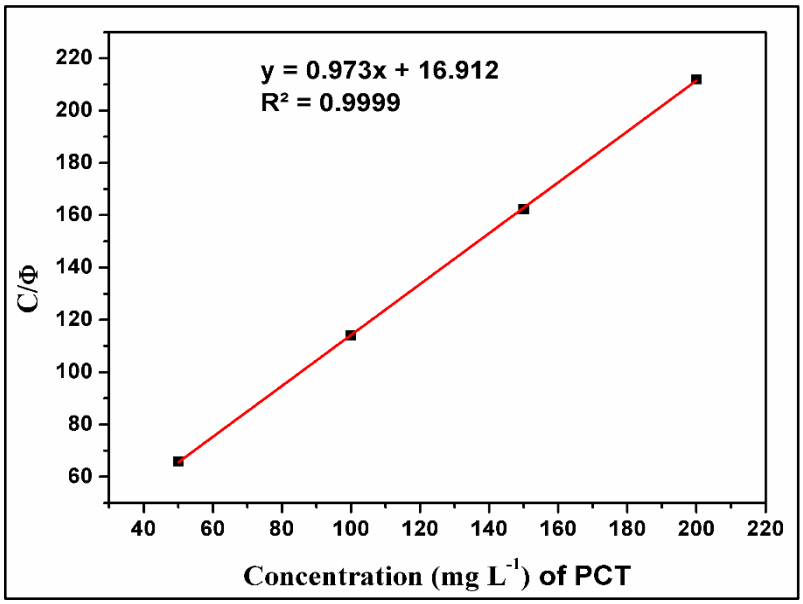


**Figure IV.1.19:** Langmuir adsorption isotherm for PCT on mild steel.

We have calculated the adsorption equilibrium constant and standard free energy of adsorption ($\Delta G^0_{ads}$) from the equation 3,

$$\Delta G^0{}_{ads} = -RTln(55.5K_{ads}) \ldots\ldots\ldots\ldots\ldots\ldots (3)$$

The adsorption equilibrium constant ($K_{ads}$) is found to be 23648 $M^{-1}$ (viscosity-average molecular weight for the phosphorylated chitin is taken as 4 X $10^5$). The standard free energy of adsorption ($\Delta G^0{}_{ads}$) is found to be –35.488 $kJmol^{-1}$. The negative value of $\Delta G^0{}_{ads}$ indicates the spontaneity of the adsorption process of the inhibitor molecule on to the metal surface. It is well known from the literature that when the value of $\Delta G^0_{ads}$ is between -20 kJ $mol^{-1}$ and - 40 kJ $mol^{-1}$ the process may involve charge transfer from the inhibitor molecule to the metal surface to form a coordination bond[34,35]. A $\Delta G^0_{ads}$ value of -35.488 found in the present case suggests that the adsorption process involves chemisorption of PCT on the metal surface and then formation of a coordinate complex between PCT and metal ions.

**IV.1.8: Mechanistic aspects of corrosion and corrosion inhibition:**

The mechanism of corrosion of mild steel in nearly neutral aqueous medium in the absence of any inhibitor is well established[36,37]. However, the anodic and cathodic reactions are reproduced below.

At anode $\quad Fe \longrightarrow Fe^{2+} + 2e^-$ (4)

At cathode $\quad H_2O + 1/2\ O_2 + 2e^- \longrightarrow 2OH^-$ (5)

$$Fe^{2+} + 2OH^- \longrightarrow Fe(OH)_2 \quad (6)$$

$$Fe(OH)_2 \xrightarrow{[O_2]} Fe(OH)_3 \quad (7)$$

When only PCT is used as inhibitor the inhibition efficiency increases with an increase in concentration up to 150 ppm, at which the highest inhibition efficiency (IE%) of 73 % is obtained. When the concentration of PCT is further increased to 200 ppm the IE% value is decreased to 60 %. This result can be explained as follows. PCT gets chemisorbed on the metal surface and the optimum concentration to form a thin an adherent film is 150 ppm. At this concentration all the $Fe^{3+}$ present on the metal surface is converted into [Fe(III)-PCT] complex, which acts as a barrier to corrosive environment and no more PCT is needed. When the PCT concentration is increased beyond 150 ppm, the extra PCT which is present in the solution diffuses to the metal surface and may induces some dissolution of iron to form a complex with PCT. As a

consequence, less corrosion inhibition efficiency is observed beyond the concentration of 150 ppm PCT.

**Plausible inhibition mechanism in presence of PCT and $Zn^{2+}$**

When Phosphorylated chitin (PCT) and $Zn^{2+}$ ions are added to the aqueous solution, $Zn^{2+}$ coordinates through N, O and P donors present in PCT to form [$Zn^{2+}$ – PCT] complex. This complex diffuses to the metal surface and binds to Fe(III) ions already present on the surface due to initial corrosion of iron.

Anodic reaction in the presence of inhibitor:

$$[Zn\ (II)\ –PCT] + Fe\ (III) \longrightarrow [Fe\ (III), Zn\ (II)\ –PCT] \ldots. (8)$$

The resulting bimetallic complex, [Fe(III), Zn(II) – P- chitin] covers the anodic sites and controls the corresponding anodic reaction.

Free $Zn^{2+}$ ions diffuse to the metal surface and react with $OH^-$ ions produced at the cathodic sites to form a precipitate of $Zn(OH)_2$ [30], which controls the cathodic partial reaction.

Cathodic reaction in the presence of inhibitor:

$$Zn^{2+} + 2OH^- \longrightarrow Zn(OH)_2\downarrow \qquad (9)$$

Now a question arises about the need for 200 ppm PCT along with 100 ppm $Zn^{2+}$ to provide higher inhibition efficiency of 93.16 % against 74.13 % IE for the mixture of 150 ppm PCT and 100 ppm $Zn^{2+}$. As mentioned in the mechanism, PCT and $Zn^{2+}$ first form a soluble complex in the solution. So, the optimum concentration of PCT is 200 ppm for the formation of adequate amount of soluble PCT- $Zn^{2+}$ complex, which diffuses to the metal surface in order to form the bimetallic complex (equation 8) with a higher surface coverage of the metal.

This protective film consists of [Fe (III), Zn (II) –PCT], $Zn(OH)_2$ and small amounts of oxides and hydroxides of Fe(III)

# Chapter IV

## Section IV.2 Phosphorylated chitin (PCT) as an inhibitor to control corrosion of copper in neutral chloride environment.

Results of the studies on Phosphorylated chitin as a corrosion inhibitor to control the corrosion of copper in neutral chloride environment using various methods are presented here under.

### IV.2.1: Results of weight-loss Studies (gravimetric studies):

The weight-loss studies were performed for copper samples immersed in sodium chloride (200 ppm) solution for 10 days at a temperature of 30 ± 0.1 °C without and with different concentrations of PCT as inhibitor. Table 1 presents the corresponding corrosion rate values. The results showed that the addition of PCT to control decreased the corrosion rate of copper very significantly. In the absence of inhibitor the weight of the copper sample is reduced by 6.52 mg after 10 days of immersion in 200 ppm NaCl and the corresponding corrosion rate is 0.0698 mmpy. The weight-loss of copper has decreased in the presence of PCT at all concentrations, indicating that PCT can inhibit the corrosion of copper. Increase in concentration of PCT afforded greater decrease in the corrosion rate of copper. The weight-loss of copper was the lowest at a concentration of 200 ppm PCT which afforded the highest inhibition efficiency of 88 %. The inhibitor molecules may have got chemisorbed on the copper surface and formed a protective film in the form of a coordination complex. This film acts as a barrier between copper and the corrosive environment and as a consequence a decrease in corrosion rate occurred. Increase in concentration of PCT increases the extent of the surface coverage of PCT and the larger the surface coverage, higher is the inhibition efficiency. When the concentration of PCT is increased beyond 200 ppm, the observed weight-loss remained the same. This result infers that 200 ppm PCT is the lowest concentration which can afford the highest inhibition efficiency for copper in 200 ppm NaCl environment.

**Table.IV.2.1:** Corrosion Rates of copper in 200ppm NaCl in the absence and presence of different concentrations of PCT obtained from gravimetric method.

| S. No. | Concentration of PCT (ppm) | Weight - loss(mg) | Corrosion Rate (mmpy) | I.E.% |
|---|---|---|---|---|
| 1 | 0 | 6.52 | 0.0698 | - |
| 2 | 50 | 1.37 | 0.0154 | 79 |
| 3 | 100 | 1.07 | 0.0142 | 83 |
| 4 | 150 | 1.02 | 0.0135 | 84 |
| 5 | 200 | 0.77 | 0.0102 | 88 |
| 6 | 300 | 0.77 | 0.0102 | 88 |
| 7 | 400 | 0.77 | 0.0102 | 88 |

### IV.2.2: Analysis of the results of Electrochemical Studies:

### Electrochemical Impedance Studies

Impedance spectroscopy is a non-destructive technique and can be employed to analyse the corrosion processes[38]. In the present context this technique was used to investigate the ability of phosphorylated chitin as copper corrosion inhibitor in aq. 200 ppm NaCl environment. The impedance studies were performed initially at various immersion times in the range, 1 hour – 48 hours. The results showed that 24 h immersion time is adequate to obtain the highest inhibition efficiency and therefore, 24 h immersion period was fixed in the impedance studies.

The Nyquist plots for copper specimen immersed in 200 ppm sodium chloride environment without and with different concentrations of PCT are shown in the figure IV.2.1. The plots exhibit a profile of depressed capacitive loop (semi-circular pattern). In the absence of the inhibitor the plot shows Warburg impedance (straight line at lower frequencies), which is primarily due to diffusion of ionic species to the interface causing corrosion. Whereas, in presence of the inhibitor the Nyquist plot does not show any Warburg impedance. As the concentration of PCT increased the diameter of the capacitive loop increased to a considerable extent. The capacitive loop that appeared at higher frequencies can be attributed to the double layer, and the loop at lower frequency range may be due to the chemisorbed layer of inhibitor. Figure IV.2.2 presents the Bode plots for control and the inhibitor system at various concentrations. Two distinct phase

angle maxima are seen in the presence of inhibitor, which indicate two time constant. The total impedance and phase angle maximum are increased with an increase in the concentration of the inhibitor. There is shift in phase angle maximum to the higher frequency with an increase in concentration of the inhibitor. Impedance vs frequency plots showed that the charge transfer region is increased with an increase in the concentration of PCT. These results infer the formation of a protective surface film.

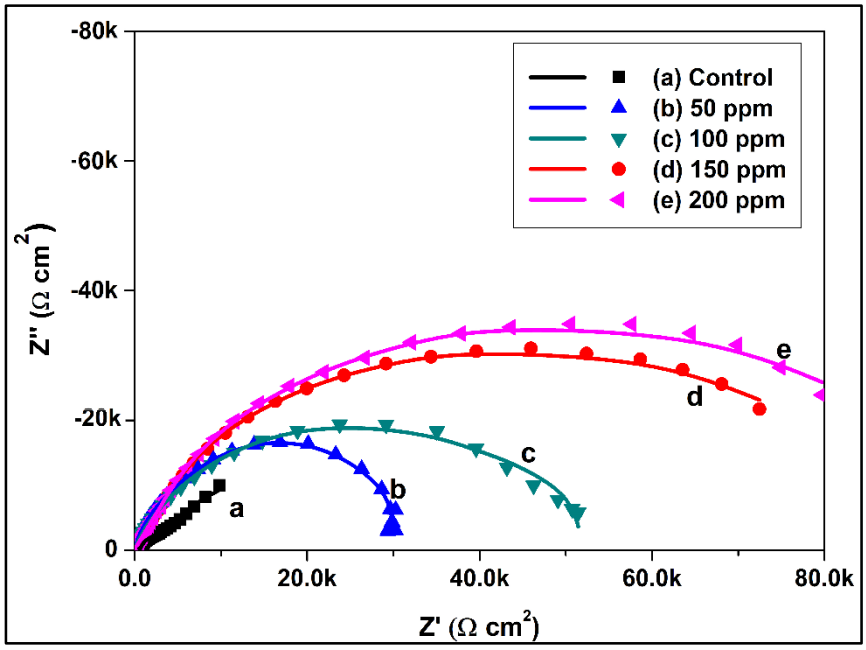


**Figure IV.2.1:** Nyquist Plots for copper specimen immersed in 200 ppm NaCl (a) in the absence (b) in presence of 50 ppm PCT (c) 100 ppm PCT (d) 150 ppm PCT (e) 200 ppm PCT (24 h immersion period). [Points- experimental data, Solid line- fitted using the equivalent circuit mode].

The impedance parameters such as charge-transfer resistance ($R_{ct}$), double layer capacitance ($c_{dl}$) were calculated from the experimental data using a theoretical fit with the help of equivalent circuit shown in the figure IV.2.3. The equivalent circuit was selected based on the physical model of the system and least error after fitting the data. Two different equivalent circuits were used to fit the experimental data for the systems in the absence of the inhibitor (control) and in the presence of PCT inhibitor. The impedance parameters are tabulated in the table IV.2.2.

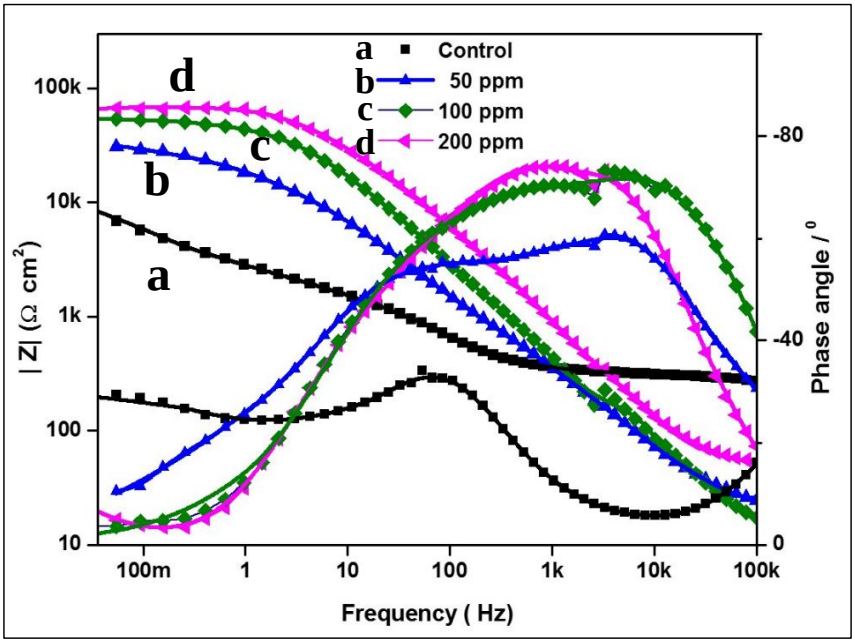


**Figure IV.2.2:** Bode Plots for copper specimen immersed in 200 ppm NaCl (a) in the absence (b) in presence of 50 ppm PCT (c) 100 ppm PCT (d) 200 ppm PCT (24 h immersion period). [Points- experimental data, Solid line- fitted using the equivalent circuit mode].

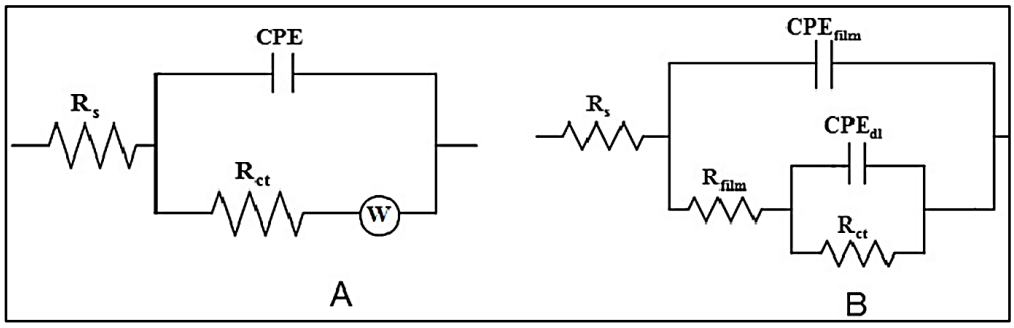


**Figure IV.2.3:** Equivalent circuits used for copper immersed in 200 ppm NaCl (A) without inhibitor (B) with the PCT inhibitor.

It is inferred from the results that addition of PCT to the corrosive environment increases the charge transfer resistance ($R_{ct}$) of the system and causes less dissolution of metal. This result is an indication of the formation of a protective film that hindered corrosion. Moreover, as the concentration of PCT increased, the $R_{ct}$ value is increased and a maximum $R_{ct}$ value of 82.1 kΩ $cm^2$ is obtained at 200 ppm PCT. The inhibition efficiency is found to be 92 %. Furthermore, addition of inhibitor also triggered a decrease in the double layer capacitance, which is a consequence of the chemisorption process of PCT molecules on the metal surface by replacing the water molecules. A lower 'n' value is representative of non- homogeneity of the surface and a significant

increase in 'n' value infers that the surface retained its smoothness in presence of PCT due to much less corrosion when compared to the control. It may be noted that the resistance of the film ($R_{film}$) is also increased with an increase in the concentration of PCT.

**Table IV.2.2**: Corrosion rates obtained from impedance studies for copper in 200 ppm NaCl in absence and presence of different concentrations of PCT (immersion time 24 h).

| Conc. of PCT (ppm) | $R_{ct}$ (kΩ cm$^2$) | $C_{dl}$ (µF cm$^{-2}$) | n | $R_{film}$ (kΩ cm$^2$) | $CPE_{film}$ (µF cm$^{-2}$) | $n_{film}$ | I.E. % |
|---|---|---|---|---|---|---|---|
| 0 | 6.5 | 5.5 | 0.538 | - | - | - | - |
| 50 | 36.7 | 3.3 | 0.781 | 15.2 | 0.7 | 0.41 | 82 |
| 100 | 52.2 | 2.6 | 0.790 | 17.2 | 0.6 | 0.53 | 87 |
| 150 | 55.4 | 2.2 | 0.754 | 17.5 | 0.6 | 0.54 | 88 |
| 200 | 82.1 | 1.8 | 0.778 | 17.9 | 0.6 | 0.57 | 92 |

**Potentiodynamic polarization studies:**

The cathodic and anodic Tafel curves for copper specimen immersed in aqueous sodium chloride environment without and with various concentrations of PCT at pH 7 and temperature of 30±0.1 ºC are depicted in figure IV.2.4. The corresponding calculated corrosion parameters are shown in the table IV.2.3.

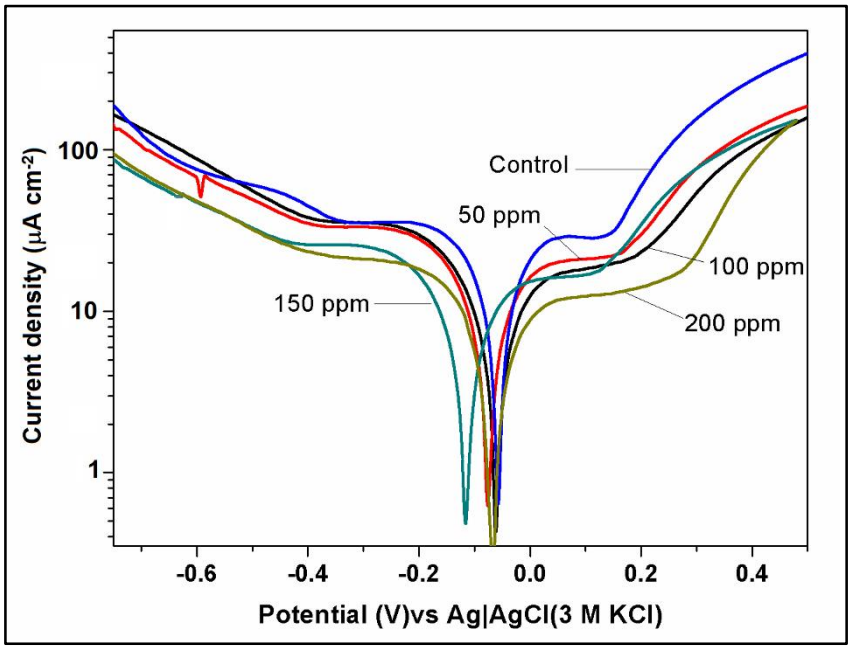


**Figure IV.2.4:** Potentiodynamic polarization curves of copper specimens immersed in 200 ppm NaCl without and with different concentrations of PCT.

**Table IV.2.3:** Corrosion parameters obtained from potentiodynamic polarization studies for copper specimen immersed in 200 ppm NaCl in absence and presence of different concentrations of PCT.

| **Concentration of P- Chitin (ppm)** | **$E_{corr}$ (mV) Vs Ag\|AgCl (3M KCl)** | **$J_{corr}$ ($\mu A\ cm^{-2}$)** | **Bc ($mV\ dec^{-1}$)** | **βa ($mV\ dec^{-1}$)** | **I. E.%** |
|---|---|---|---|---|---|
| 0 | -62.0 | 11.5 | -373 | 197 | - |
| 50 | -78.2 | 4.2 | -245 | 120 | 64 |
| 100 | -62.2 | 3.7 | -202 | 98 | 68 |
| 150 | -112.2 | 3.2 | -200 | 97 | 72 |
| 200 | -77.5 | 1.6 | -189 | 88 | 89 |

The profiles of the Tafel curves indicated that both the anodic and cathodic current densities decreased in presence of PCT. In the case of control, the corrosion current density ($j_{corr}$) was 11.55 $\mu A\ cm^{-2}$. Whereas, in the presence of PCT the '$J_{corr}$' values decreased significantly and were found to be in the range of 4.2-1.6 $\mu A\ cm^{-2}$. This result infers a decrease in corrosion rate of copper as a consequence of the adsorption of large quantities of PCT molecules on the copper surface and formation of a protective film. As both the anodic and cathodic current densities are reduced in the presence of phosphorylated chitin, it is interpreted that PCT works as a mixed type inhibitor. The lowest corrosion current density was observed when 200 ppm of PCT was used as inhibitor, with an inhibition efficiency of 89 %.

The polarization curve in case of control shows that at a potential of around 0.15 V the current density has increased suddenly. This indicates that after initial corrosion, a passive film on the copper surface consisting of CuCl is formed. With a further increase in anodic potential, CuCl is further oxidised to form soluble Cu(II) species. As a consequence the current density value has increased suddenly. Whereas, in presence of inhibitor this film breakdown potential increased to higher values and the highest potential is obtained for 200 ppm PCT. This result also infers that protective nature of the film in presence of PCT inhibitor.

**IV.2.3: Analysis Surface morphology by scanning electron microscopy and Energy dispersive X-ray spectroscopy (SEM-EDX):**

The surface topography of the copper specimens immersed in 200 ppm NaCl for 10 days with and without 200 ppm PCT has been studied using SEM. The surface films have been analyzed by energy dispersive X-ray spectroscopy. The surface morphology of the polished specimen is depicted in figure IV.2.5A. After immersing the sample in 200 ppm NaCl for 10 days, the resulting specimen's surface morphology is shown in the figure IV.2.5B, which reveals the damage of the surface and presence of corrosion products. The EDX spectrum shows an increase in the oxygen peak intensity due to cuprous and cupric oxides. Figure IV.2.5C presents the surface morphology of the copper specimen immersed in 200 ppm NaCl along with 200 ppm PCT as inhibitor and the surface film composition is inferred from the EDX spectrum depicted in figure IV.2.6.

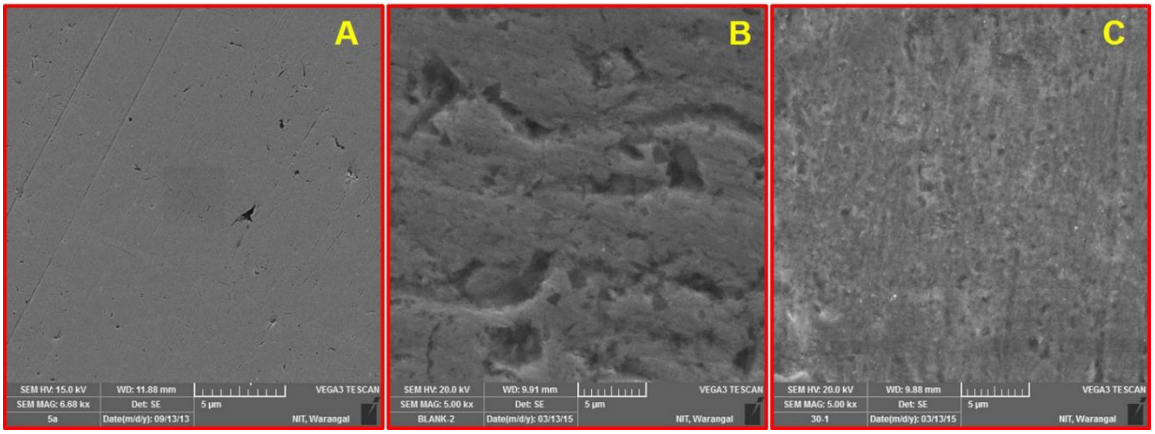


**Figure IV.2.5:** (A) SEM image of copper polished sample, (B) **S**EM image of copper specimen immersed in 200 ppm NaCl, (C) **S**EM image of copper specimen immersed in 200 ppm NaCl with 200 ppm PCT.

The micrograph clearly reveals the retention of the smoothness of the surface even after 10 days immersion in the corrosion environment. This result is because of the protective nature of the surface film, which constitutes the inhibitor molecule. This protective film prevents the metal surface from exposure to the corrosive environment. It is evident from the EDX spectrum that the composition of the protective film consists of phosphorous, nitrogen, carbon and oxygen, which are present in the adsorbed inhibitor molecule. The oxygen peak intensity also decreased considerably when compared to blank. This result infers the presence of less amount of oxide, which means less corrosion rate. It may be noted that the oxygen peak is due to oxygen present in the

inhibitor and oxygen in the copper corrosion products. But, the relative quantities cannot be quantified from this result.

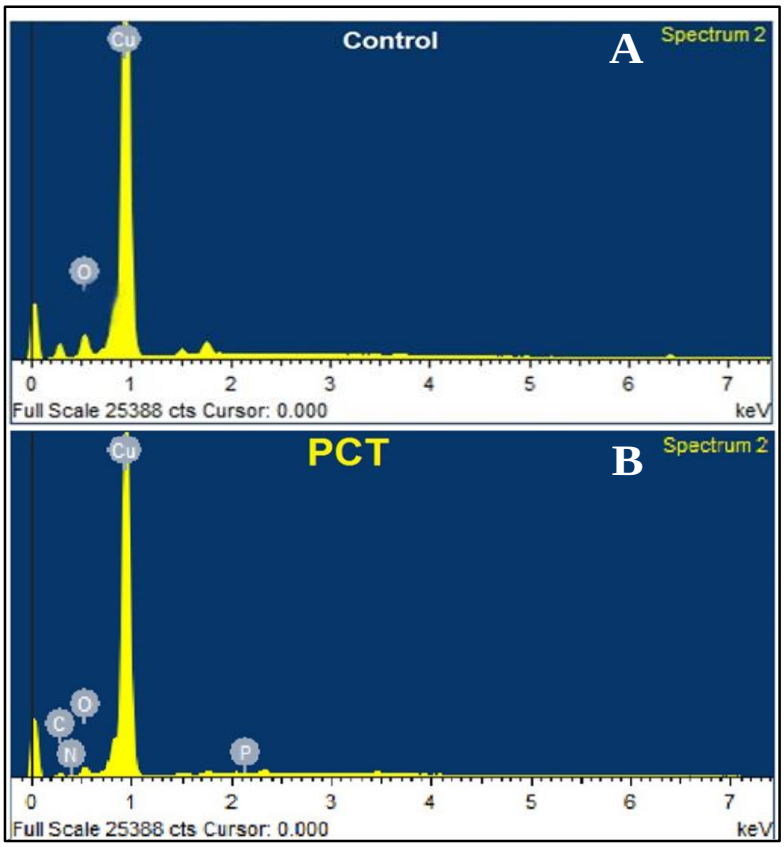


**Figure IV.2.6:** EDX spectrum of Cu specimen immersed in 200 ppm NaCl environment (A) without inhibitor (B) With 200 ppm PCT.

**IV.2.4: Surface analysis by X-ray photoelectron spectroscopic studies (XPS):**

Chemical composition of the surface film formed on copper during ten days immersion in 200 ppm NaCl without and with 200 ppm PCT has been studied using X-ray photoelectron spectroscopy. Figures IV.2.7A and IV.2.7B represent the survey spectra of the films formed in the absence and presence of PCT respectively. The survey spectrum of the control indicates that the surface film consists of carbon, oxygen and copper. The peak due to carbon is ascribed to the contaminant carbon due to cracking of vacuum oil during the measurement[39]. Whereas, the survey spectrum of copper immersed in the corrosive environment in presence of inhibitor infers that the surface film contains carbon, oxygen, copper, phosphorous, and nitrogen. The corresponding deconvolution spectra for each of the elements are shown in the subsequent figures.

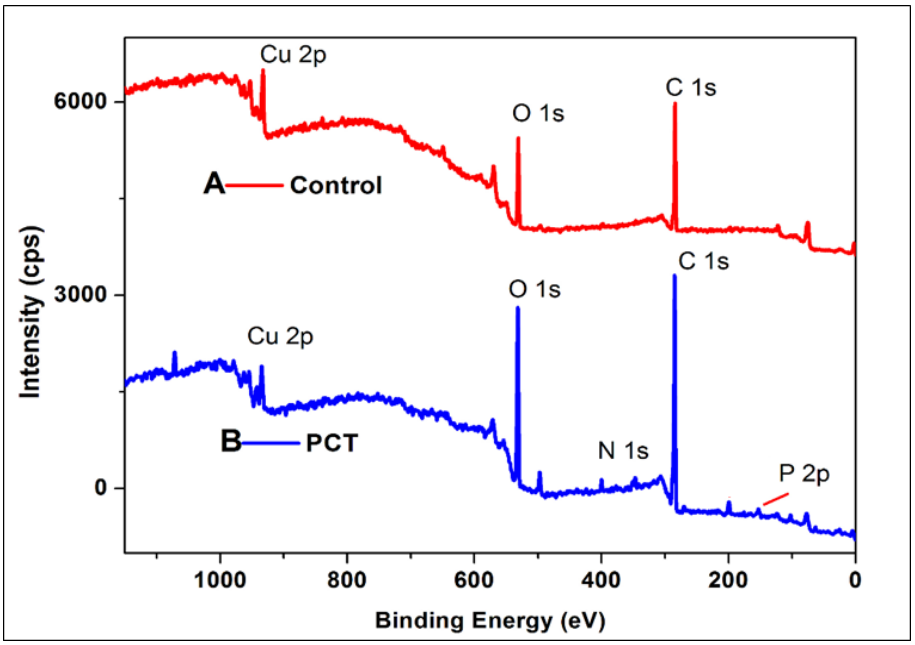


**Figure IV.2.7:** (A) XPS survey spectrum of copper specimen immersed in 200 ppm NaCl in the absence of inhibitor, (B) in the presence of PCT (200ppm).

Figure IV.2.8A represents C 1s deconvolution spectrum for control. It consists of a single peak at a binding energy value of 284.6 eV, which is attributed to the contaminant carbon due to cracking of vacuum oil during the measurement [29]. In the case of inhibitor the C 1s deconvolution spectrum consists of three distinguishable peaks (Figure IV.2.8B), one peak at the binding energy value of 284.7 eV with high intensity and two peaks of lower intensities at 285.4 eV and 288.3 eV. These peaks can be interpreted as follows. The inhibitor, PCT has three different types of carbon environments such as carbon bound to oxygen, carbon, bound to carbon and carbon bound to hydrogen, which explain the occurrence of three different peaks. These carbon peaks show an evidence for the presence of PCT molecules in the surface film formed after immersing in the corrosive environment with 200 ppm PCT.

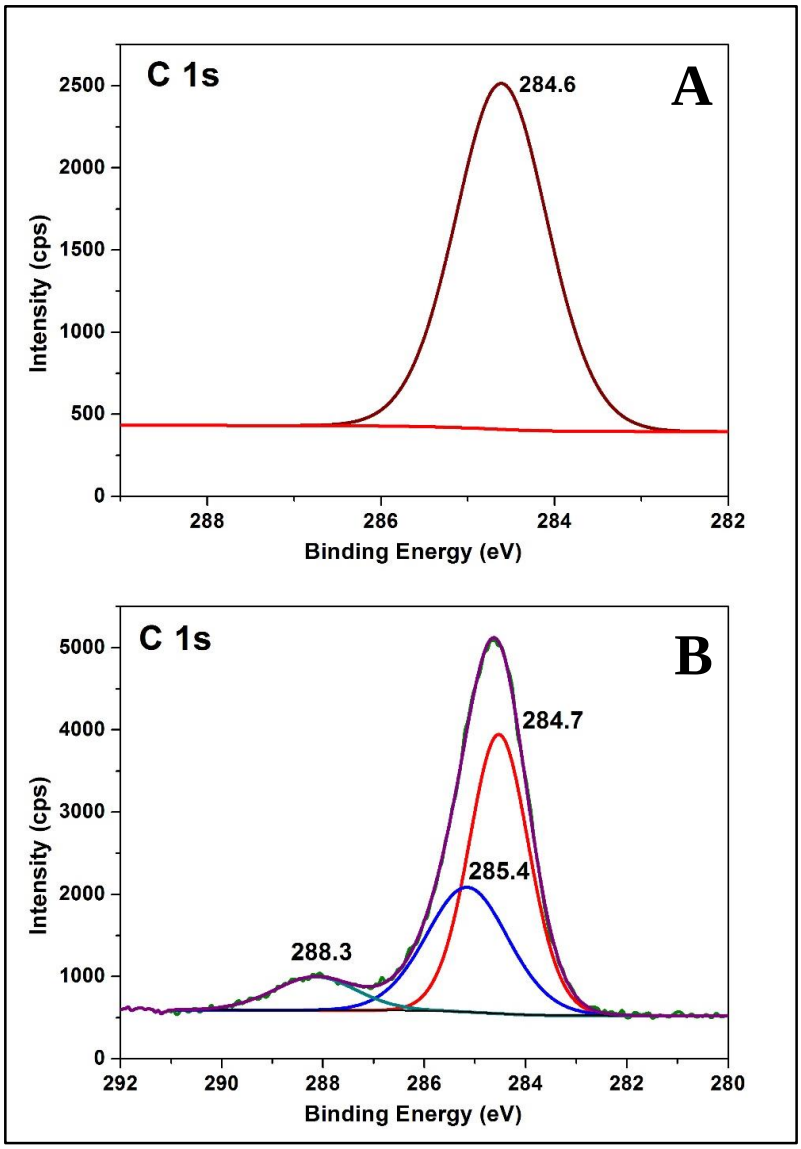


**Figure IV.2.8:** XPS deconvolution spectra of C 1s for copper sample immersed in (A) 200 ppm NaCl (B) PCT (200 ppm) along with 200 ppm NaCl.

Figure IV.2.9 shows the O 1s deconvolution spectra for copper in 200 ppm NaCl in the absence and presence of PCT. Figure IV.2.9A represents the deconvolution spectrum of O 1s in the case of blank, which consists of two peaks at 531.1 eV and 532.6 eV. These peaks can be attributed to $O^{2-}$, and can be related to the bond with Cu (II) in cupric oxide (CuO). Whereas, in the presence of PCT inhibitor as shown in figure IV.2.9B, the O 1s deconvolution spectrum consists of two distinct peaks at 531.6 eV and 533.1 eV. The former one can be due to oxygen present in the oxides and hydroxides of Cu (II) in the form of $O^{2-}$. The later one is assigned to oxygen present in metal hydroxide ($Cu(OH)_2$) as well as the oxygen present in the inhibitor molecule, which is bound to copper[40].

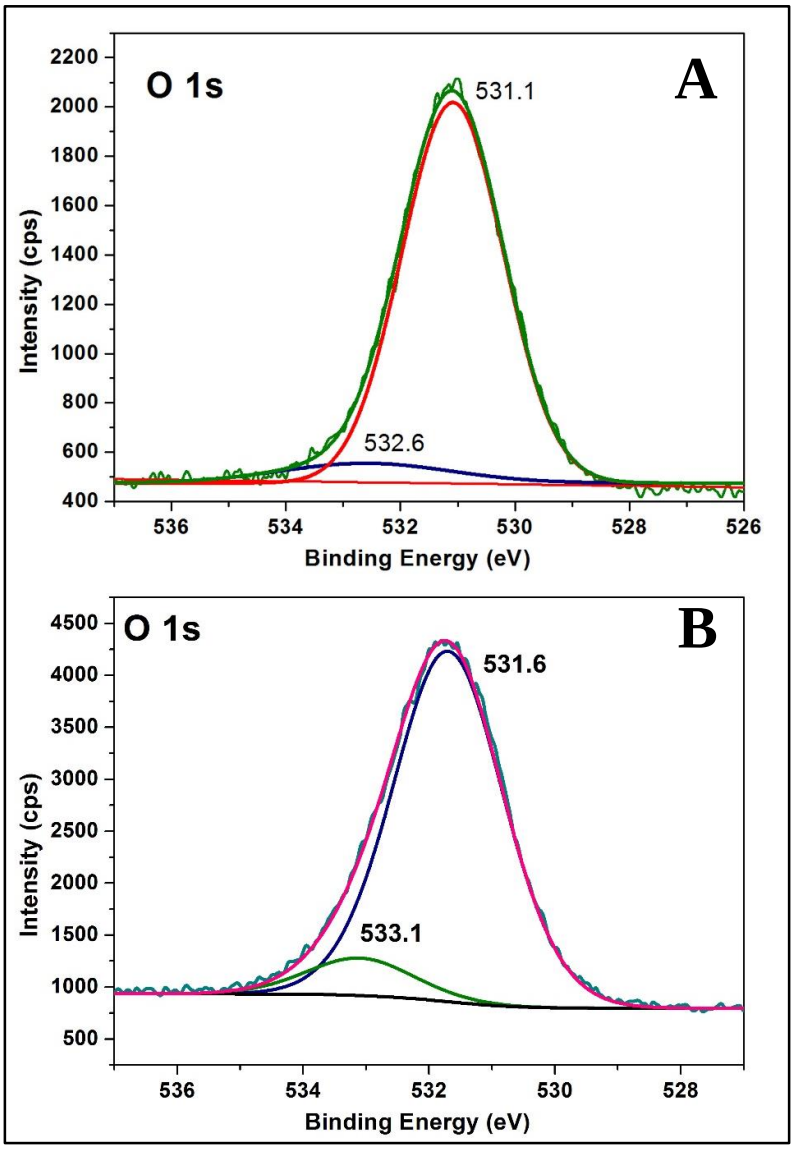


**Figure IV.2.9:** XPS deconvolution spectra of O 1s for copper sample immersed in (A) 200 ppm NaCl (B) PCT (200 ppm) along with 200 ppm NaCl.

The Cu 2p deconvolution spectra for the control and the inhibitor system are shown in figure IV.2.10A and figure IV.2.10B respectively. According to the standard reference data base the Cu $2p_{1/2}$ and Cu $2p_{3/2}$ peaks for pure Cu appear at a binding energy of 952.45–952.56 eV and 932.20–933.1 eV, respectively[21]. We generally interpret the Cu $2p_{3/2}$ peaks for analysis. For control we have observed the Cu $2p_{3/2}$ peak at 933.9 eV and approximately a 2 eV shift from the characteristic elemental binding energy, indicates the presence of Cu in its double oxidation state. Moreover, the presence of strong satellite peaks further confirms the presence of Cu (II). It may be noted that the

Cu $2p_{3/2}$ peak for the CuO was reported in the literature at 932.7-934.6 eV, which was interpreted due to CuO and not $Cu_2O$ [41,42].

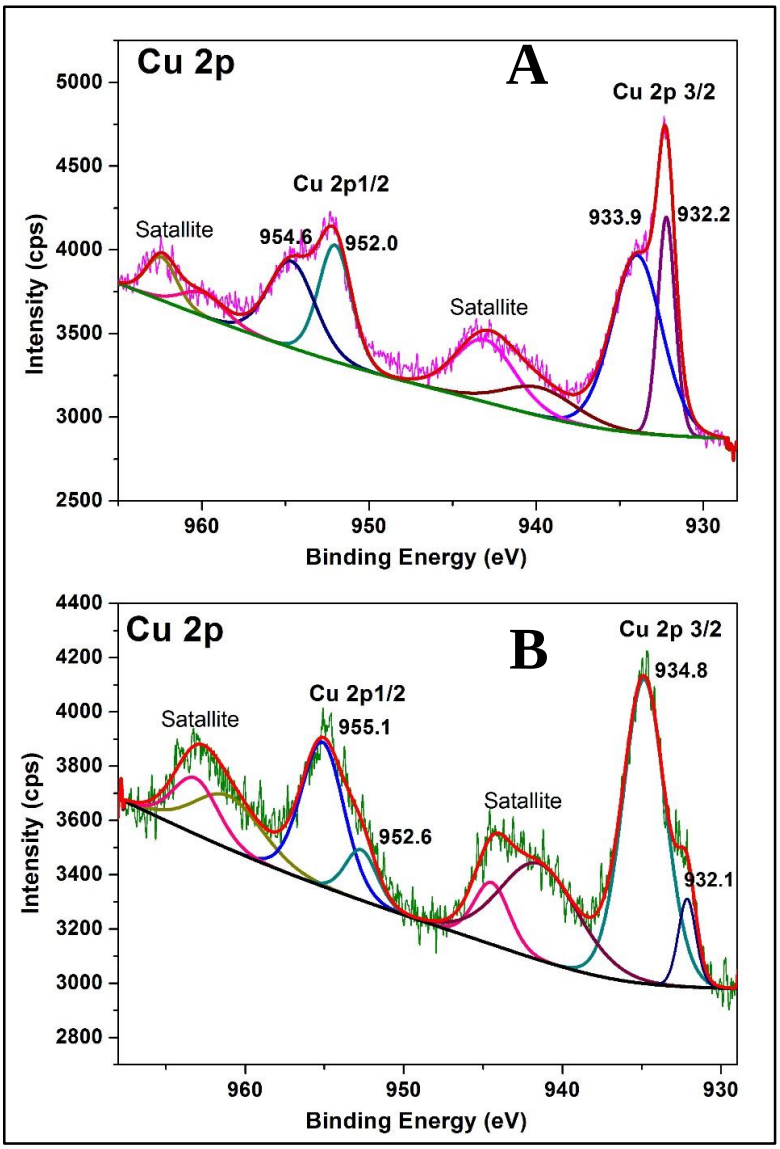


**Figure IV.2.10:** XPS deconvolution spectra of Cu 2p for copper sample immersed in **(A)** 200 ppm NaCl **(B)** PCT (200 ppm) along with 200 ppm NaCl.

In the presence of inhibitor we have observed the Cu $2p_{3/2}$ peak at 934.2 eV with a clear shift of 2 eV from that of pure Cu indicating the presence of Cu in Cu (II) form. Moreover, the presence of the shake-up satellites in the Cu 2p spectrum indicates the presence of Cu (II). Under the present experimental condition (Cu in aqueous chloride solution containing inhibitor) the most probable Cu (II) containing species are the [Cu(II)-PCT] complex, $Cu(OH)_2$ and CuO.

In addition to the above elements, the survey spectrum of the surface film on copper in presence of inhibitor consists of phosphorous and nitrogen. The corresponding deconvolution spectra are shown in the figures IV.2.11 and IV.2.12 respectively.

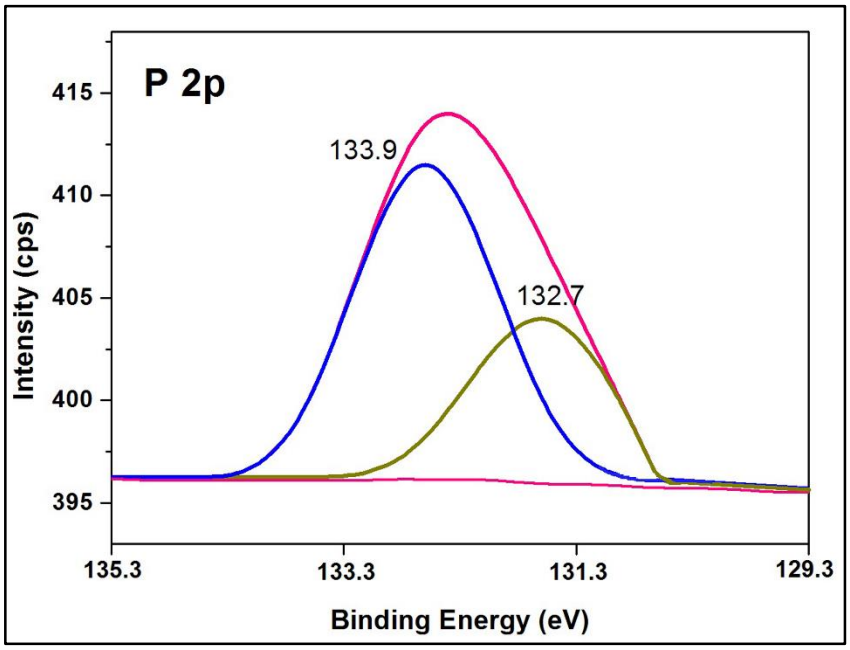


**Figure IV.2.11:** XPS deconvolution spectra of P 2p for copper sample immersed in 200 ppm NaCl along with PCT (200 ppm).

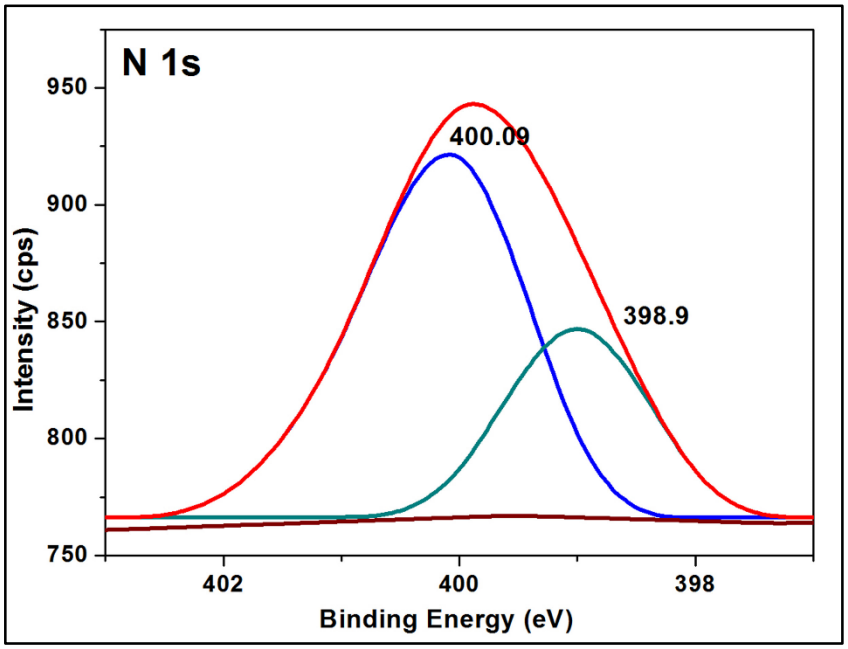


**Figure IV.2.12:** XPS deconvolution spectra of N 1s for copper sample immersed in 200 ppm NaCl along with PCT (200 ppm).

The P 2p spectrum consists of two distinct peaks, one at 132.7 eV and the other one at 133.9 eV. These peaks are mainly because of the two different environments of 'P' atom, which are present in the PCT molecule adsorbed on copper, namely the phosphate group attached to primary carbon and the phosphate group bound to the secondary carbon in PCT molecule. The chemisorption process of PCT molecule on copper can occur through both the phosphorous environments. Here we can interpret that the former peak at 132.7 eV is because of phosphorous in phosphate (attached to 1° carbon) and the later peak at 133.9 eV is because of phosphorous in phosphate (attached to 2° carbon). The N 1s deconvolution spectrum consists of two different peaks at 398.9 eV and 400.09 eV, indicating two different nitrogen environments in PCT. The former peak is assigned to nitrogen bound to carbon[43] which is a possibility in the present case (C-$NH_2$) and the later one is assigned to the nitrogen bound to copper[44].

**IV.2.5: Analysis of the surface film by X- ray diffraction studies (XRD):**

Figure IV.2.13(A) and IV.2.13(B) represents the XRD patterns of the copper specimen immersed in 200 ppm NaCl environment in the absence and presence of phosphorylated chitin (PCT) inhibitor respectively. In both the diffractograms the patterns show the presence of corrosion product $Cu_2O$ and base material copper on the surface[45,46]. The planes which are observed for $Cu_2O$ are (1 1 0), (1 1 1) and (2 2 0). The planes observed for base materail copper are (1 1 1), (2 0 0) and (2 2 0). The XRD pattern does not show any peak for CuO which is the predominant corrosion product and XPS results have also shown that the CuO is present on the surface. This can be explained by the fact that the CuO is only present in the topmost layers of the film whose thickness may be at nanometer level. XRD can however, analyse the material within about 10 μm depth of the surface[47]. Which means that the XRD can analyse the inner layers of the surface. Since, the inner layers of the corrosion product on the copper surface contain $Cu_2O$, the XRD pattern shows the $Cu_2O$ peaks only[48]. On the other hand, the XPS spectrum detects only the topmost surface layer and hence detected the presence of CuO in the top surface layer.

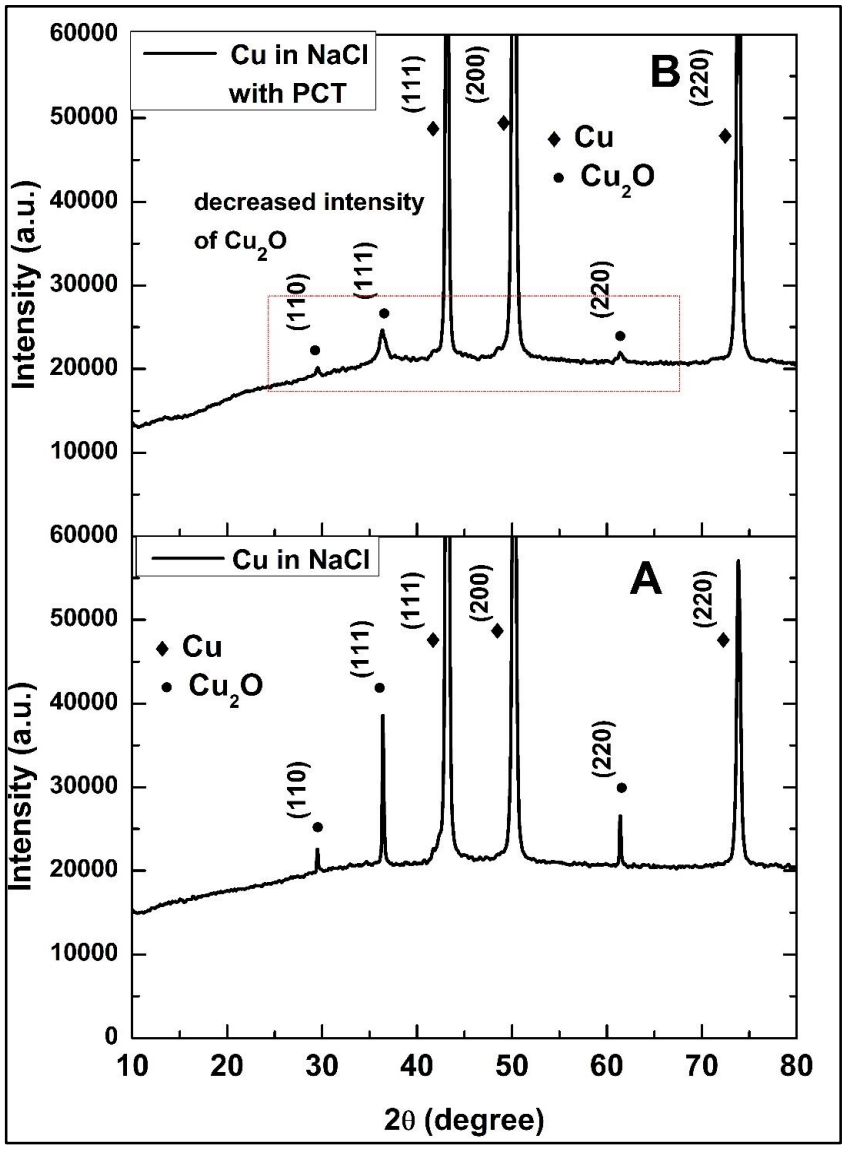


**Figure IV.2.13:** The X-ray diffraction patterns of the surface film formed on copper sample immersed in 200 ppm NaCl (A) in the absence (B) in the presence of PCT (200 ppm).

From the intensities of the $Cu_2O$ peaks it can be observed that in presence of PCT the intensities are significantly decreased when compared to the peaks of $Cu_2O$ in the absence of any inhibitor. This result infers that in the presence of PCT the corrosion of copper is decreased considerably.

### IV.2.6: Langmuir adsorption isotherm

The interaction between the inhibitor molecule and the metal surface can give an idea about the inhibition mechanism. Different adsorption isotherm models were taken into consideration to understand the inhibition mechanism of PCT and among them the Langmuir adsorption isotherm model is well fitted (based on the correlation coefficient

value). The Langmuir adsorption isotherm equation has already given in the equation (2) of this chapter.

In this case, $\emptyset$ is the surface coverage of the inhibitor molecule (Which is obtained by the relation, $\text{I.E.}\% = \emptyset X\ 100$), C is the concentration of PCT (the monomer molecular weight is taken to calculate the concentration ) and $K_{ads}$ is the equilibrium constant.

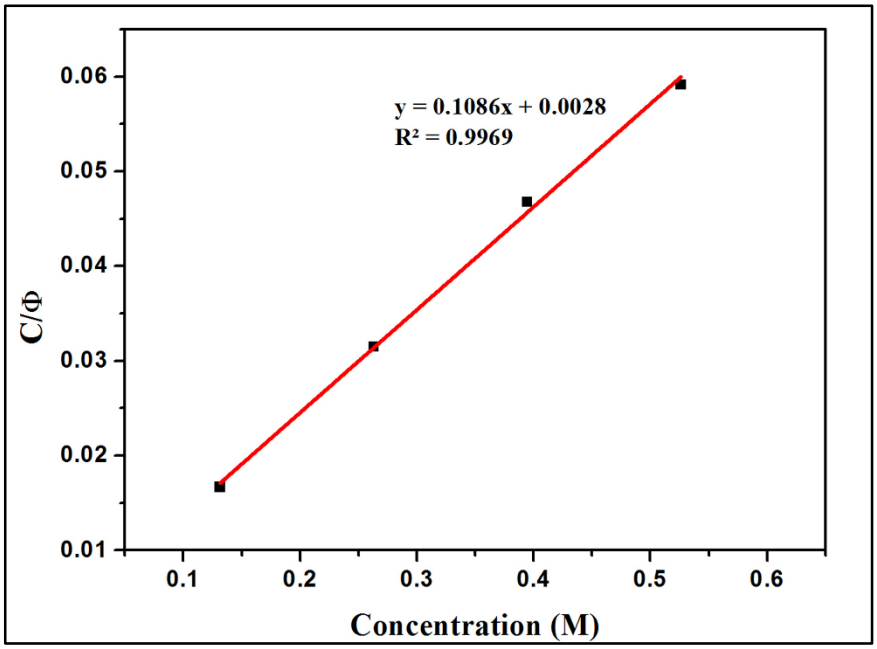


**Figure IV.2.14:** Langmuir adsorption isotherm plot for adsorption of PCT on copper surface.

Figure IV.2.14 illustrates the $C/\emptyset\ Vs\ C$ plot for adsorption of PCT on copper surface. A linear curve is obtained with a good correlation coefficient value ($R^2$= 0.9969), which infers that the adsorption process follows the Langmuir adsorption isotherm model. From the plot it can be seen that the $\emptyset$ value increases with an increase in the PCT concentration, which can be attributed to the increase in the metal surface coverage with the inhibitor molecules (PCT) and as a consequence attaining higher inhibition efficiency.

**IV.2.7: Mechanistic Aspects of Corrosion Inhibition:**

The corrosion of metals whether it is mild steel or copper in neutral environment is well established [49,50]. However, the anodic and cathodic reactions in case of corrosion of copper in neutral chloride environment are reproduced below.

at anode

$$Cu + Cl^- \rightleftharpoons CuCl + e^- \quad (10)$$ film formation reaction

$$CuCl + Cl^- \rightleftharpoons CuCl_2^- \quad (11)$$ film dissolution reaction

at cathode

$$H_2O + 1/2O_2 + 2e^- \longrightarrow 2OH^- \quad (12)$$

This cupric chloride complex further dissolved to form,

$$CuCl_{2\,(ads)}^- \rightleftharpoons Cu^{2+} + 2Cl^- + e^- \quad (13)$$

$$Cu^{2+} + 2OH^- \rightleftharpoons Cu(OH)_2 \quad (14)$$

Surface analytical studies gave evidence for the composition of the surface film, which was formed in the process of corrosion inhibition by PCT. Carbon, oxygen, nitrogen and phosphorous constitute the film. Corrosion inhibition occurs by the chemisorption of the PCT inhibitor molecules on the metal surface and formation of a coordinate complex with copper (II) through donor atoms like N, O present in PCT. The linkage in the chelation is predominantly dependant on electronegativity. The O, N donor atoms have relatively higher electronegativity when compared to P. Moreover, in PCT, O and N donor atoms possess lone pairs of electrons and hence the linkage with copper ions could occur through N and O atoms. Thus, the inhibitor film on copper surface blocks the contact between metal and corrosive environment, minimizes the diffusion of ions or molecules to and from the metal surface and thus, imparts corrosion protection to copper[51]. The plausible interaction mechanism of PCT with copper surface is shown in figure IV.2.15.

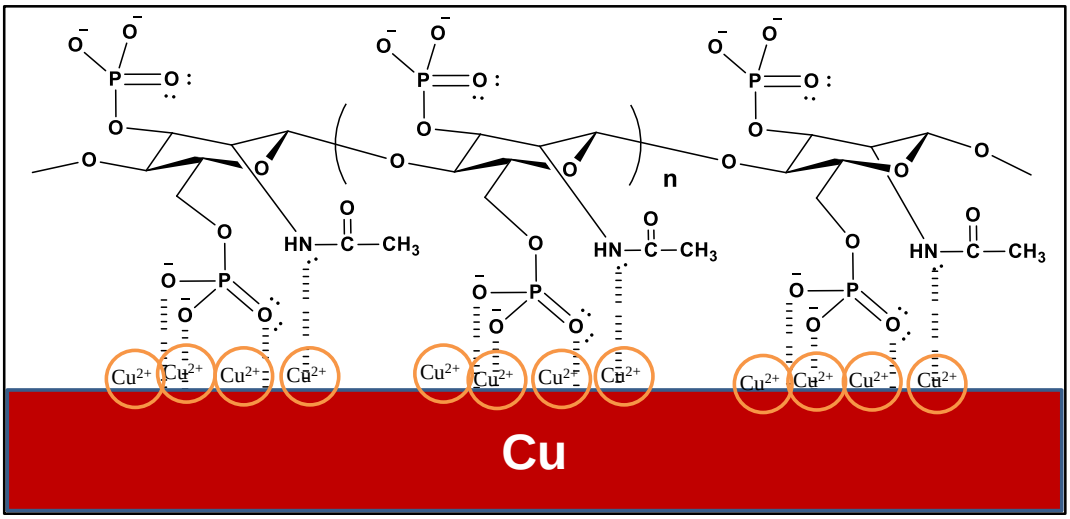


**Figure.IV.2.15:** Plausible orientation of the inhibitor molecule on the surface of copper after chemisorption.

**References:**


1. Amaral, I. F., Granja, P. L. & Barbosa, M. A. Chemical modification of chitosan by phosphorylation: an XPS, FT-IR and SEM study. *J. Biomater. Sci. Polym. Ed.* **16,** 1575–93 (2005).
2. Wang, K. & Liu, Q. Chemical structure analyses of phosphorylated chitosan. *Carbohydr. Res.* **386,** 48–56 (2014).
3. Jayakumar, R., Egawa, T., Furuike, T., Nair, S. V. & Tamura, H. Synthesis, characterization, and thermal properties of phosphorylated chitin for biomedical applications. *Polym. Eng. Sci.* **49,** 844–849 (2009).
4. Ravi Kumar, M. N. . A review of chitin and chitosan applications. *React. Funct. Polym.* **46,** 1–27 (2000).
5. Nishi, N., Maekita, Y., Nishimura, S., Hasegawa, O. & Tokura, S. Highly phosphorylated derivatives of chitin, partially deacetylated chitin and chitosan as new functional polymers: metal binding property of the insolubilized materials. *Int. J. Biol. Macromol.* **9,** 109–114 (1987).
6. Yoo, J. D., Ogle, K. & Volovitch, P. The effect of synthetic zinc corrosion products on corrosion of electrogalvanized steel. II. Zinc reactivity and galvanic coupling zinc/steel in presence of zinc corrosion products. *Corros. Sci.* **83,** 32–37 (2014).
7. Thornhill, R. S. Zinc, Manganese, and Chromic Salts as Corrosion,Inhibitors. *Ind. Eng. Chem.* **37,** 706–708 (1945).
8. Umoren, S. A., Ogbobe, O., Ebenso, E. E. & Ekpe, U. J. Effect of halide ions on the corrosion inhibition of mild steel in acidic medium using polyvinyl alcohol. *Pigment Resin Technol.* **35,** 284–292 (2006).
9. Gunasekaran, G., Palaniswamy, N. & Apparao, B. V. Synergistic effect of Zn2+ ions and 2-Carboxyethyl phosphonic acid on the corrosion inhibition of mild steel in neutral environment. *Bull. Electrochem.* **12,** 59–63 (1996).
10. Rao, B. V. A. & Christina, K. Ternary inhibitor system containing phosphonate , molybdate and Zn 2 + in corrosion control of carbon steel. *Indian J. Chem. Technol.* **13,** 275–282 (2006).
11. Gunasekaran, G. & Chauhan, L. . Eco friendly inhibitor for corrosion inhibition of mild steel in phosphoric acid medium. *Electrochim. Acta* **49,** 4387–4395 (2004).
12. Morad, M. S. An electrochemical study on the inhibiting action of some organic

phosphonium compounds on the corrosion of mild steel in aerated acid solutions. *Corros. Sci.* **42,** 1307–1326 (2000).

13. Keswani, M., Raghavan, S. & Deymier, P. A novel way of detecting transient cavitation near a solid surface during megasonic cleaning using electrochemical impedance spectroscopy. *Microelectron. Eng.* **108,** 11–15 (2013).
14. Rajendran, S., Apparao, B. V., Palaniswamy, N., Periasamy, V. & Karthikeyan, G. Corrosion inhibition by strainless complexes. *Corros. Sci.* **43,** 1345–1354 (2001).
15. To, X. H., Pebere, N., Pelaprat, N., Boutevin, B. & Hervaud, Y. A corrosion-protective film formed on a carbon steel by an organic phosphonate. *Corros. Sci.* **39,** 1925–1934 (1997).
16. Pech-Canul, M. a. & Bartolo-Pérez, P. Inhibition effects of N-phosphono-methyl-glycine/Zn2+ mixtures on corrosion of steel in neutral chloride solutions. *Surf. Coatings Technol.* **184,** 133–140 (2004).
17. Bouanis, F. Z., Bentiss, F., Traisnel, M. & Jama, C. Enhanced corrosion resistance properties of radiofrequency cold plasma nitrided carbon steel: Gravimetric and electrochemical results. *Electrochim. Acta* **54,** 2371–2378 (2009).
18. Sastri, V. S., Elboujdaini, M., Brown, J. R. & Perumareddi, J. R. Surface Analysis of Inhibitor Films Formed in Hydrogen Sulfide Medium. *Corrosion* **52,** 447–452 (1996).
19. Rao, B. V. A., Rao, M. V., Rao, S. S. & Sreedhar, B. Synergistic effect of N,N-bis(phosphonomethyl) glycine and zinc ions in corrosion control of carbon steel in cooling water systems. *Chem. Eng. Commun.* **198,** 1505–1529 (2011).
20. Babić-Samardzija, K., Lupu, C., Hackerman, N., Barron, A. R. & Luttge, A. Inhibitive properties and surface morphology of a group of heterocyclic diazoles as inhibitors for acidic iron corrosion. *Langmuir* **21,** 12187–96 (2005).
21. Cicileo, G. P., Rosales, B. M., Varela, F. e. & Vilche, J. R. Comparative study of organic inhibitors of coppercorrosion. *Corros. Sci.* **41,** 1359–1375 (1999).
22. Sherwood, P. M. A. Introduction to Studies of Phosphorus-Oxygen Compounds by XPS. *Surf. Sci. Spectra* **9,** 62–66 (2002).
23. Gu, Q. & Cheng, X. Tribological behaviors of lanthanum-based phosphonate 3-aminopropyltriethoxysilane self-assembled films. *Appl. Surf. Sci.* **253,** 6800–6806 (2007).
24. Viornery, C. *et al.* Surface modification of titanium with phosphonic acid to

improve bone bonding: Characterization by XPS and ToF-SIMS. *Langmuir* **18,** 2582–2589 (2002).

25. Keszthelyi, T. *et al.* Investigation of Solid Surfaces Modified by Langmuir−Blodgett Monolayers Using Sum-Frequency Vibrational Spectroscopy and X-ray Photoelectron Spectroscopy. *J. Phys. Chem. B* **110,** 8701–8714 (2006).
26. Felhősi, I. Effects of Bivalent Cations on Corrosion Inhibition of Steel by 1-Hydroxyethane-1,1-diphosphonic Acid. *J. Electrochem. Soc.* **146,** 961–969 (1999).
27. Nakayama, N. Inhibitory effects of nitrilotris(methylenephosphonic acid) on cathodic reactions of steels in saturated Ca(OH)2 solutions. *Corros. Sci.* **42,** 1897–1920 (2000).
28. Ochoa, N., Baril, G., Moran, F. & Pébère, N. No Title. *J. Appl. Electrochem.* **32,** 497–504 (2002).
29. Naumkin, A. V., Kraut-Vass, A., Powell, C. J. & Gaarenstroom, S. . NIST Standard Reference Database 20 version 4.1. *The National Institute of Standards and Technology NIST* 1–49 (2012). Available at: http://srdata.nist.gov/xps.
30. Deroubaix, G. & Marcus, P. X-ray photoelectron spectroscopy analysis of copper and zinc oxides and sulphides. *Surf. interface Anal.* **18,** 39–46 (1992).
31. Powell, C. J. *et al.* NIST data resources for surface analysis by X-ray photoelectron spectroscopy and Auger electron spectroscopy. *J. Electron Spectros. Relat. Phenomena* **114–116,** 1097–1102 (2001).
32. Loh, K.-S., Lee, Y., Musa, A., Salmah, A. & Zamri, I. Use of Fe3O4 Nanoparticles for Enhancement of Biosensor Response to the Herbicide 2,4-Dichlorophenoxyacetic Acid. *Sensors* **8,** 5775–5791 (2008).
33. Han, R. *et al.* 1D Magnetic Materials of Fe3O4 and Fe with High Performance of Microwave Absorption Fabricated by Electrospinning Method. *Sci. Rep.* **4,** 7493 (2015).
34. Liu, Y. *et al.* β-Cyclodextrin Modified Natural Chitosan as a Green Inhibitor for Carbon Steel in Acid Solutions. *Ind. Eng. Chem. Res.* **54,** 5664–5672 (2015).
35. Zou, C., Yan, X., Qin, Y., Wang, M. & Liu, Y. Inhibiting evaluation of β-Cyclodextrin-modified acrylamide polymer on alloy steel in sulfuric solution. *Corros. Sci.* **85,** 445–454 (2014).
36. Rao, B. V. A. & Rao, S. S. Electrochemical and surface analytical studies of

synergistic effect of phosphonate, Zn 2+ and ascorbate in corrosion control of carbon steel. *Mater. Corros.* **61,** NA-NA (2009).

37. Saker, S., Aliouane, N., Hammache, H., Chafaa, S. & Bouet, G. Tetraphosphonic acid as eco-friendly corrosion inhibitor on carbon steel in 3 % NaCl aqueous solution. *Ionics (Kiel).* **21,** 2079–2090 (2015).
38. Barsoukov, E. & Macdonald, J. R. *Impedance Spectroscopy*. *Impedance Spectroscopy: Theory, Experiment, and Applications* (John Wiley & Sons, Inc., 2005). doi:10.1002/0471716243
39. Cicileo, G. P., Rosales, B. M., Varela, F. e. & Vilche, J. R. Comparative study of organic inhibitors of coppercorrosion. *Corros. Sci.* **41,** 1359–1375 (1999).
40. McIntyre, N. S., Sunder, S., Shoesmith, D. W. & Stanchell, F. W. Chemical information from XPS—applications to the analysis of electrode surfaces. *J. Vac. Sci. Technol.* **18,** 714–721 (1981).
41. Chusuei, C. C., Brookshier, M. A. & Goodman, D. W. Correlation of Relative X-ray Photoelectron Spectroscopy Shake-up Intensity with CuO Particle Size. *Langmuir* **15,** 2806–2808 (1999).
42. Biesinger, M. C. *et al.* Resolving surface chemical states in XPS analysis of first row transition metals, oxides and hydroxides: Cr, Mn, Fe, Co and Ni. *Appl. Surf. Sci.* **257,** 2717–2730 (2011).
43. Yoshida, T. & Sawada, S. X-Ray Photoelectron Spectroscopy of EDTA. *Bull. Chem. Soc. Jpn.* **47,** 50–53 (1974).
44. Chadwick, D. & Hashemi, T. Adsorbed corrosion inhibitors studied by electron spectroscopy: Benzotriazole on copper and copper alloys. *Corros. Sci.* **18,** 39–51 (1978).
45. Meghana, S., Kabra, P., Chakraborty, S. & Padmavathy, N. Understanding the pathway of antibacterial activity of copper oxide nanoparticles. *RSC Adv.* **5,** 12293–12299 (2015).
46. Aslan, E., Patir, I. H. & Ersoz, M. Cu Nanoparticles Electrodeposited at Liquid-Liquid Interfaces: A Highly Efficient Catalyst for the Hydrogen Evolution Reaction. *Chem. - A Eur. J.* **21,** 4585–4589 (2015).
47. Kerber, S. J. *et al.* The Complementary Nature of X-Ray Photoelectron Spectroscopy and Angle-Resolved X-Ray Diffraction Part I: Background and Theory. *J. Mater. Eng. Perform.* **7,** 329–333 (1998).

48. Bastidas, J. Characterization of corrosion products on a copper-containing intrauterine device during storage at room temperature. *Biomaterials* **18,** 247–250 (1997).

49. Milosev, I., Pavlinac, J., Hodoscek, M. & Lesar, A. Amino acids as corrosion inhibitors for copper in acidic medium: Experimental and theoretical study. *J. Serbian Chem. Soc.* **78,** 2069–2086 (2013).

50. Cicileo, G. P., Rosales, B. M., Varela, F. e. & Vilche, J. R. Comparative study of organic inhibitors of coppercorrosion. *Corros. Sci.* **41,** 1359–1375 (1999).

51. Sastri, V. S., Perumareddi, J. R., Lashgari, M. & Elboujdaini, M. Application of Ligand Field Theory in Corrosion Inhibition. *Corrosion* **64,** 283–288 (2008).

# CHAPTER-V

## Chitosan- ascorbic acid- $Cu^{2+}$ inhibitor formulation for protection of mild steel in 1 M HCl environment

# TABLE OF CONTENTS

## Chapter V

# Chapter V

## Chitosan- ascorbic acid- $Cu^{2+}$ inhibitor formulation for protection of mild steel in 1 M HCl environment

### V.1: Preparation of chitosan ascorbate ketimine (CAK) inhibitor solutions:

Chitosan ascorbate ketimine solutions were prepared according to the procedure reported in the literature[1,2]. Different mole ratios of chitosan and ascorbic acid have been used in the preparation.

### Confirmation of formation of Chitosan ascorbate ketimine by FTIR spectroscopy:

The synthesized derivative of chitosan, namely chitosan ascorbate ketimine (CAK) was characterized by Fourier Transform Infrared spectroscopy (FTIR). The corresponding FTIR spectra are shown in the Figure V.1. The peaks appeared in the spectrum are compared with the literature values and the results are in good agreement with the literature values[1,2]. The FTIR spectrum of CAK (spectrum b) shows a peak at 1760 $cm^{-1}$ and another peak at 1711 $cm^{-1}$ along with the other bands generally found in the FTIR spectrum of chitosan. The additional peaks at 1760 and 1711 $cm^{-1}$ are assigned to unsaturated cyclic ketones, which are present in the CAK molecule. The peak at 1621 $cm^{-1}$ is assigned to acetamido group of the molecule. Since the spectrum of synthesized molecule shows the presence of aromatic carbonyls, and also that the peak intensity of the amino group is decreased, it can be inferred that chitosan reacts with dehydroascorbic acid to form ketimine derivative.

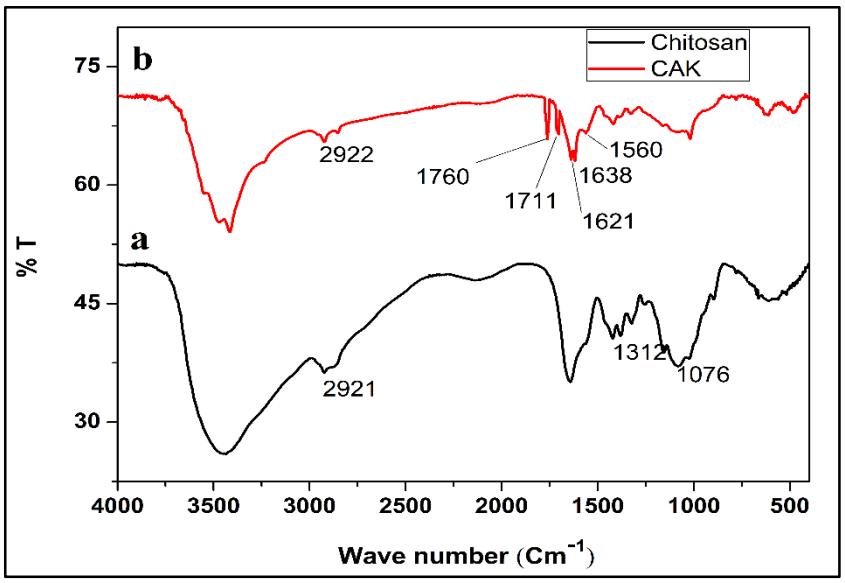


**Figure V.1:** FTIR spectra of (a) pure chitosan and (b) chitosan ascorbate ketimine (CAK).

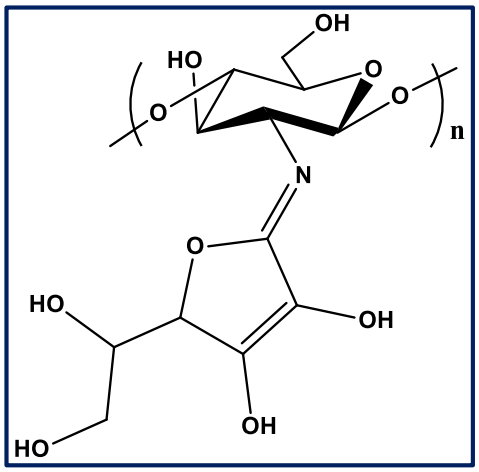


**Chitosan ascorbate ketimine**

**V.2: Analysis of the results of gravimetric studies of CAK as corrosion inhibitor:**

The experimental data of the corrosion rates and the inhibition efficiencies of CAK obtained from gravimetric studies are given in the tables V.1 and table V.2. The corrosion parameters of mild steel in 1M HCl in the absence and presence of chitosan and ascorbic acid mixture are given in the table V.1. Whereas, the table V.2 presents the results of gravimetric studies in the presence of chitosan, ascorbic acid and $Cu^{2+}$ mixture as corrosion inhibitor. Chitosan at 200 ppm concentration was taken and different concentrations of ascorbic acid have been used to dissolve chitosan as mentioned in chapter III. The dissolution of chitosan in ascorbic acid results in the formation of chitosan ascorbate ketimine (CAK) when the chitosan ascorbate solution was kept as such for 6 hours.

**Table V.1:** Corrosion parameters for mild steel in 1 M HCl in absence and presence of different mole ratios of chitosan and ascorbic acid (Temp. 30 ± 0.1 °C, immersion period of 24 h).

| S.No. | Concentration(ppm) | | $Cu^{2+}$(ppm) | Weight-loss(g) | Corrosion Rate(mmpy) | I.E.% |
|---|---|---|---|---|---|---|
| | Chitosan | Ascorbic acid | | | | |
| 1 | 0 | 0 | 0 | 0.8926 | 0.1752 | - |
| 2 | 200 | 200 | 0 | 0.6125 | 0.1202 | 31 |
| 3 | 200 | 300 | 0 | 0.5221 | 0.1024 | 42 |
| 4 | 200 | 400 | 0 | 0.4042 | 0.0471 | 64 |

**Table V.2**: Corrosion parameters for mild steel in 1 M HCl in absence and presence of Chitosan+ Ascorbic acid+ $Cu^{2+}$ (Temp. 30 ± 0.1 °C, immersion period of 24 h).

| S.No. | Concentration(ppm) | | $Cu^{2+}$(ppm) | Weight-loss(g) | Corrosion Rate (mmpy) | I.E.% |
|---|---|---|---|---|---|---|
| | Chitosan | Ascorbic acid | | | | |
| 1 | 0 | 0 | 0 | 0.8926 | 0.1752 | - |
| 2 | 200 | 400 | 0 | 0.4042 | 0.0471 | 64 |
| 3 | 200 | 400 | 25 | 0.2015 | 0.0358 | 77 |
| 4 | 200 | 400 | 50 | 0.1255 | 0.0150 | 86 |
| 5 | 200 | 400 | 100 | 0.1388 | 0.0152 | 84 |
| 6 | 0 | 0 | 25 | 0.8711 | 0.1709 | 2 |
| 7 | 0 | 0 | 50 | 0.8658 | 0.1699 | 3 |
| 8 | 0 | 0 | 100 | 0.8505 | 0.1669 | 4 |

The results show that the corrosion rate of mild steel in 1M HCl has decreased significantly in presence of inhibitor formulation when compared with the control. The highest inhibition efficiency of 64 % is obtained for the inhibitor consisting of 200 ppm chitosan and 400 ppm Ascorbic acid. When a relatively low concentration of $Cu^{2+}$ is added as an additive to the above solution of CAK (200 ppm chitosan+ 400 ppm ascorbic acid), corrosion rate of mild steel is further reduced and the highest inhibition efficiency is obtained when 50 ppm of $Cu^{2+}$ is added. This result indicates that the CAK has a synergistic relation with $Cu^{2+}$ions. The highest inhibition efficiency of 86 % is obtained at a combination of 200 ppm Chitosan, 400 ppm Ascorbic acid and 50 ppm $Cu^{2+}$. This inhibitor formulation acts as a good inhibitor to control the corrosion of mild steel in acidic chloride environment, namely 1M HCl.

The synergistic parameter (S) values for CAK (200 ppm chitosan+ 400 ppm ascorbic acid) and different concentrations of $Cu^{2+}$ are calculated to confirm the existence of synergistic effect between CAK and $Cu^{2+}$ions.

The synergistic parameter (S) has been calculated using the equation (1) given below[3],

$$\boldsymbol{S = \frac{1 - \emptyset_{1+2}}{1 - \emptyset'_{1+2}}} \ldots\ldots\ldots\ldots\ldots\ldots (\mathbf{1})$$

Here, $\emptyset_{1+2} = \emptyset_1 + \emptyset_2 - (\emptyset_1.\emptyset_2)$

$\emptyset_1$= surface coverage by $Cu^{2+}$,

$\emptyset_2$= surface coverage by CAK (200 ppm chitosan+ 400 ppm ascorbic acid)

$Ø'_{1+2}$ = surface coverage by CAK (200 ppm chitosan+ 400 ppm ascorbic acid) in combination with $Cu^{2+}$.

**Table V.3:** Synergistic parameters for CAK (200 ppm chitosan+ 400 ppm ascorbic acid) and $Cu^{2+}$.

| S.No. | Concentration (ppm) | | I.E.% | Synergistic parameter (S) |
|---|---|---|---|---|
| | Chitosan+ Ascorbic acid | $Cu^{2+}$ | | |
| 1 | 200 + 400 | 25 | 77 | 1.5 |
| 2 | 200 +400 | 50 | 86 | 2.4 |
| 3 | 200 + 400 | 100 | 84 | 2.2 |

The synergistic parameter (S) values are listed in the table V.3. The S value for all the inhibitor formulations is greater than one, which suggests that there exists a synergistic effect between CAK and $Cu^{2+}$ ions in inhibiting corrosion of mild steel in 1 M HCl solution.

**V.3: Analysis of the results of electrochemical studies:**

**Electrochemical Impedance Studies:**

The electrochemical impedance studies were performed at the open circuit potential in the absence and presence of different concentrations of inhibitor formulation. Figure V.2A depicts the Nyquist plots of the mild steel immersed in 1 M HCl solution in the presence and absence of inhibitor formulations. The corresponding Bode plots are shown in the Figure V.2B and Figure V.2C. In order to obtain different impedance parameters the experimental data have been fitted with appropriate equivalent circuits based on the physical model of the corroding system. The equivalent circuits used are depicted in the figure V.3. The corrosion parameters obtained from these plots are shown in the table V.4.

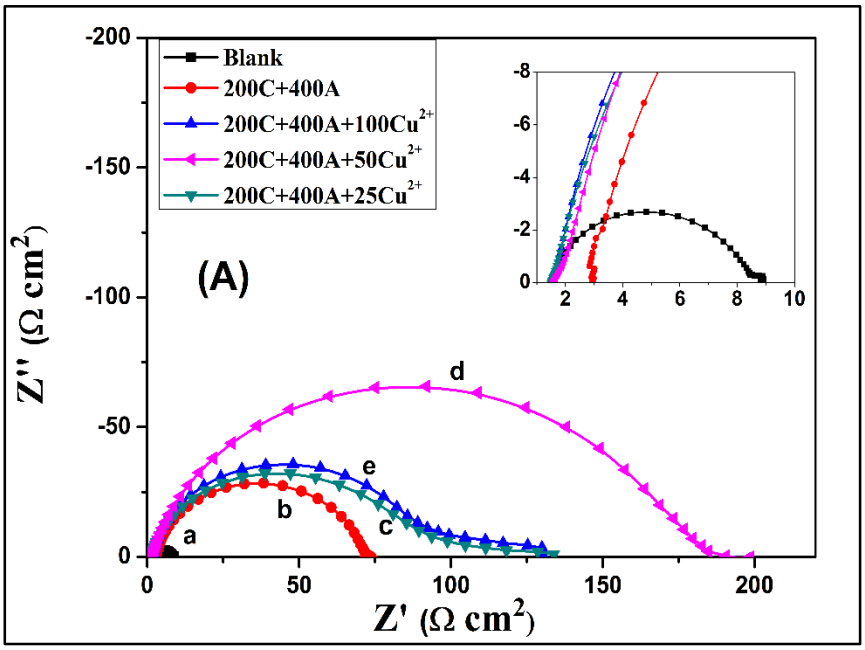


**Figure V.2A**: Nyquist plots for mild steel specimen in 1M HCl (a) in the absence of inhibitor formulation (b) In presence of 200 ppm C+ 400 ppm A (c) 200 ppm C + 400 ppm A + 25 ppm $Cu^{2+}$ (d) 200 ppm C + 400 ppm A + 50 ppm $Cu^{2+}$ (e) 200 ppm C + 400 ppm A + 100 ppm $Cu^{2+}$. **(C- chitosan, A- Ascorbic acid)**.

From figure.V.2A small depressed semicircles can be observed for control whose center is under the horizontal line and the charge transfer resistance value is 21.6 Ω $cm^2$. In the presence of inhibitor formulation consisting of 200 ppm chitosan and 400 ppm ascorbic acid, the diameter of the depressed semicircle has been increased significantly and it can be observed that two different semicircles overlapped to form a two time constant system and a charge transfer resistance value of 69.0 Ω $cm^2$ is obtained, which indicates a decrease in the rate of charge transfer from the metal into solution and solution to metal when compared to control. An inhibition efficiency of 69 % is obtained with this inhibitor formulation. Thus, this formulation protects the surface of the metal in the acid chloride aggressive environment. When different concentrations of $Cu^{2+}$ ions are employed as additive to the above formulation, the diameter of the semi-circle has been increased enormously and a maximum charge transfer resistance value of 197.2 Ω $cm^2$ is found with 50 ppm $Cu^{2+}$ as additive. The highest inhibition efficiency of 89 % is obtained with the combination of 200 ppm C+ 400 ppm A+ 50 ppm $Cu^{2+}$ inhibitor formulation. Results from impedance studies also support the evidence for the synergistic relationship between CAK and $Cu^{2+}$ in controlling corrosion of mild steel in 1M HCl environment.

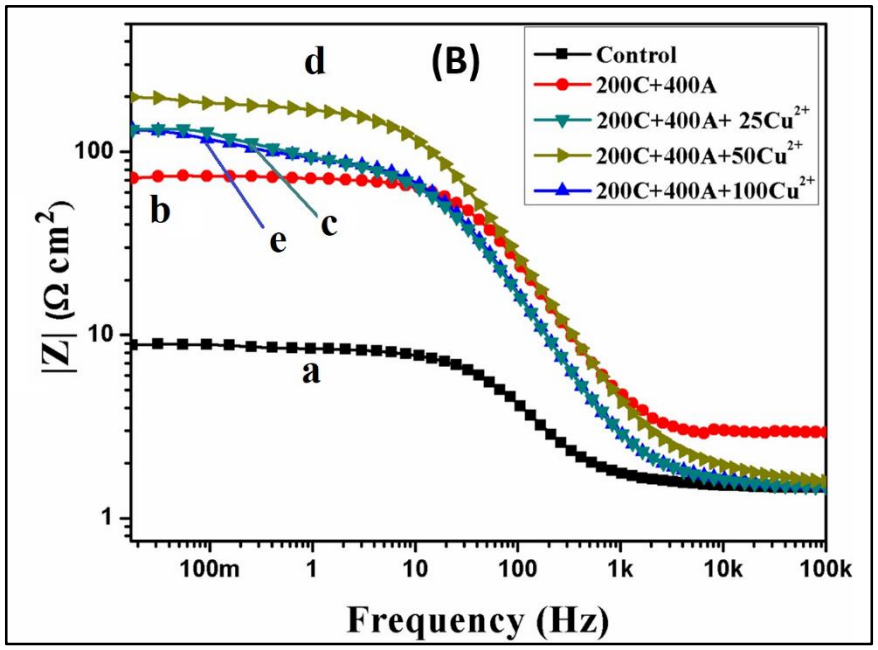


**Figure V.2B**: Bode plots (Total impedance) for mild steel specimen in 1M HCl (a) in the absence of inhibitor formulation (b) In presence of 200 ppm C+ 400 ppm A (c) 200 ppm C + 400 ppm A + 25 ppm $Cu^{2+}$ (d) 200 ppm C + 400 ppm A + 50 ppm $Cu^{2+}$ (e) 200 ppm C + 400 ppm A + 100 ppm $Cu^{2+}$. **(C- chitosan, A- Ascorbic acid).**

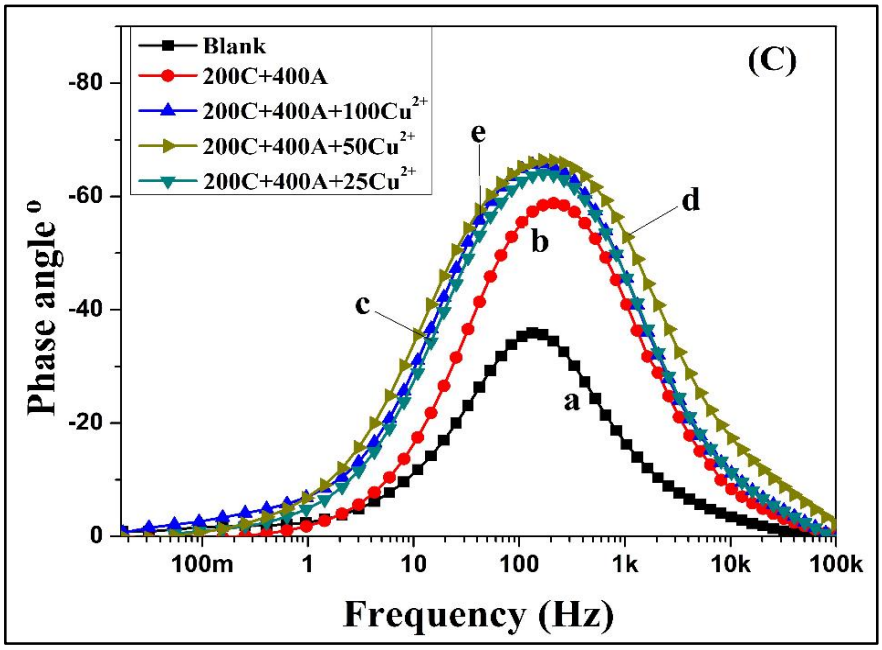


**Figure V.2C:** Bode plots (Phase angle) for mild steel specimen in 1M HCl (a) in the absence of inhibitor formulation (b) In presence of 200 ppm C+ 400 ppm A (c) 200 ppm C + 400 ppm A + 25 ppm $Cu^{2+}$ (d) 200 ppm C + 400 ppm A + 50 ppm $Cu^{2+}$ (e) 200 ppm C + 400 ppm A + 100 ppm $Cu^{2+}$. **(C- chitosan, A- Ascorbic acid).**

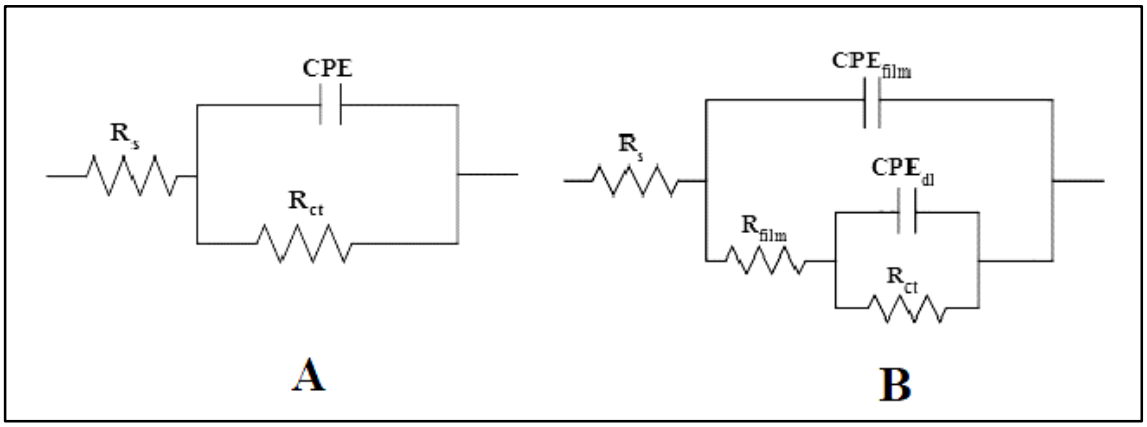


**Figure V.3:** Equivalent circuits used for mild steel immersed in 1 M HCl in EIS studies (A) without inhibitor (B) with the inhibitor formulation.

From figure.V.2B, it can be observed that in presence of inhibitor formulation the total impedance value of the system has increased in mid frequency (charge transfer region) and low frequency (diffusion region) range. Highest total impedance is obtained when the inhibitor formulation consists of 200 ppm chitosan + 400 ppm ascorbic acid + 50 ppm $Cu^{2+}$ ions. From figure.V.2C the phase angle maximum for the mild steel specimen immersed in 1 M HCl is increased in the presence of the inhibitor formulation compared to control (35°), and shifted to a maximum value of 71° for the combination of 200 ppm chitosan, 400 ppm ascorbic acid and 50 ppm $Cu^{2+}$. These results indicate an increase in the corrosion resistance of the film formed in the presence of inhibitor.

**Table V.4:** Corrosion parameters for mild steel in 1 M HCl in absence and presence of inhibitor formulation obtained from impedance studies. (A.A. - Ascorbic acid)

| **Chitosan (ppm)** | **A.A. (ppm)** | **$Cu^{2+}$ (ppm)** | **$R_{ct}$ ($\Omega$ $cm^2$)** | **CPE ($\mu F cm^{-2}$)** | **n** | **$R_{film}$ ($\Omega$ $cm^2$)** | **$CPE_{film}$ ($\mu F cm^{-2}$)** | **$n_{film}$** | **IE %** |
|---|---|---|---|---|---|---|---|---|---|
| 0 | 0 | 0 | **21.6** | 280.2 | 0.831 | - | - | - | - |
| 200 | 400 | 0 | **69.0** | 46.9 | 0.891 | 15.2 | 13.9 | 0.455 | **69** |
| 200 | 400 | 25 | **103.0** | 67.6 | 0.867 | 25.7 | 13.2 | 0.499 | **79** |
| 200 | 400 | 50 | **197.2** | 40.5 | 0.847 | 26.2 | 16.5 | 0.571 | **89** |
| 200 | 400 | 100 | **125.8** | 65.6 | 0.861 | 25.6 | 15.2 | 0.494 | **83** |

**Potentiodynamic polarization studies:**

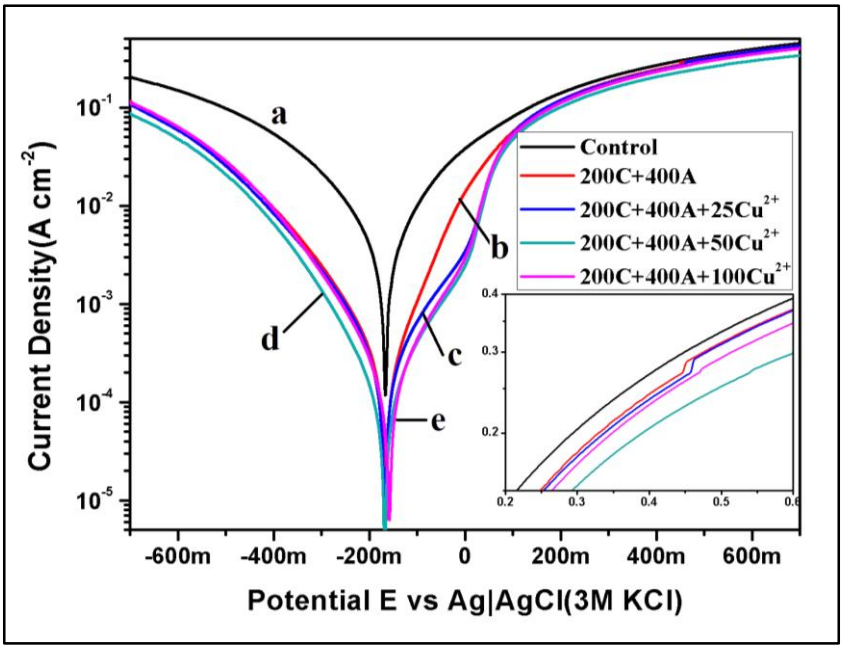


**Figure V.4**: Potentiodynamic polarization curves for mild steel specimen in 1M HCl (a) in the absence of inhibitor formulation (b) In presence of 200 ppm C+ 400 ppm A (c) In presence of 200 ppm C + 400 ppm A + 25 ppm $Cu^{2+}$ (d) In presence of 200 ppm C + 400 ppm A + 50 ppm $Cu^{2+}$ (e) In presence of 200 ppm C + 400 ppm A + 100 ppm $Cu^{2+}$. **(C-chitosan, A- Ascorbic acid).**

**TableV.5:** Corrosion parameters for mild steel in 1 M HCl in absence and presence of inhibitor formulation obtained from polarization studies. (A.A. -Ascorbic acid)

| S.No. | Concentration(ppm) | | | $E_{corr}$ (mV) | $J_{corr}$ (mA $cm^{-2}$) | βc ($mVdec^{-1}$) | βa ($mVdec^{-1}$) | I.E.% |
|---|---|---|---|---|---|---|---|---|
| | chitosan | A.A. | $Cu^{2+}$ | | | | | |
| 1 | 0 | 0 | 0 | -147.7 | 0.9 | -337 | 248 | - |
| 2 | 200 | 400 | 0 | -150.8 | 0.3 | -179 | 166 | 67 |
| 3 | 200 | 400 | 25 | -157.3 | 0.2 | -164 | 152 | 79 |
| 4 | 200 | 400 | 50 | -148.8 | 0.1 | -164 | 137 | 88 |
| 5 | 200 | 400 | 100 | -146.6 | 0.2 | -154 | 134 | 82 |

FigureV.4 shows the potentiodynamic polarization curves for mild steel specimen immersed in 1 M HCl solution in the absence and presence of different inhibitor formulations. Tafel extrapolation method has been used to calculate the corrosion

parameters from the polarization curves and the corresponding corrosion parameters are listed in the table V.5. From the curves it is quite evident that in the presence of inhibitor formulation (chitosan + ascorbic acid) the cathodic and anodic polarization curves are shifted towards lower current density values when compared with control and the current density values decreased even more when $Cu^{2+}$ has been used as an additive. The corrosion potential ($E_{corr}$) has shifted to more negative values for almost all the inhibitor formulations except for 200 ppm chitosan + 400 ppm ascorbic acid + 100 ppm $Cu^{2+}$ combination, although the shift in $E_{corr}$ is very less. From the table V.5 we can observe that the anodic and cathodic Tafel slopes (βa, βc) are significantly decreased in presence of all the inhibitor concentrations. The lowest βa value that has been observed, is 134.0 $mVdec^{-1}$ for 200 ppm chitosan + 400 ppm ascorbic acid + 100 ppm $Cu^{2+}$ combination. Whereas, the lowest βc value that has been observed, is -154 $mVdec^{-1}$. In the case of control the βa, βc values are 248.0 and -337 $mVdec^{-1}$ respectively.

The mild steel specimen immersed in 1 M HCl without inhibitor shows a corrosion current density value ($J_{corr}$) of 0.9 mA $cm^{-2}$. Whereas, in presence of all the inhibitor formulation systems the corrosion current density values are less than 0.2 mA $cm^{-2}$ as shown in the table. A considerable decrease in $J_{corr}$ value in the presence of inhibitor formulation infers that the dissolution of metal ions into the solution is hindered. That means, the corrosion rate is decreased.

Corrosion inhibition efficiencies are calculated using the corrosion current density values. A maximum inhibition efficiency of 88 % is obtained with 0.1 mA $cm^{-2}$ corrosion current density value for the combination of 200 ppm Chitosan, 400 ppm Ascorbic acid and 50 ppm $Cu^{2+}$. From the cathodic and anodic Tafel slopes, it can be interpreted that chitosan ascorbate ketimine and chitosan ascorbate ketimine in combination with $Cu^{2+}$ ions are considered as mixed type inhibitors since both the anodic and cathodic current densities are shifted towards lower values in presence of inhibitor formulation.

**V.4 Analysis of the results of surface morphological studies by SEM- EDX:**

The surface morphology of mild steel specimens immersed in 1 M HCl corrosive environment in the absence and presence of the inhibitor formulation for 24 h has been studied using scanning electron micrographs and the surface composition has been studied qualitatively by energy dispersive X-ray spectroscopy. Figure V.5 represents the SEM images and figure V.6 represents the EDX spectra.

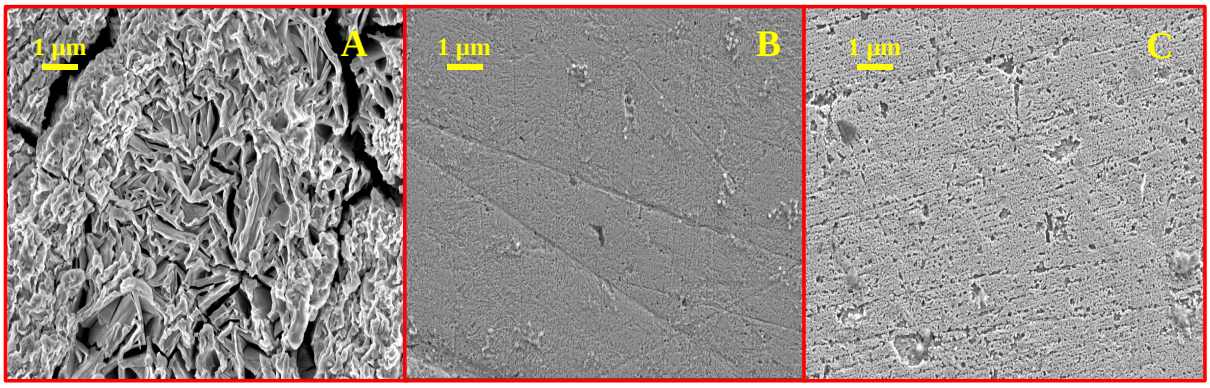


**Figure V.5:** SEM of mild steel surface immersed in 1 M HCl **(A)** in the absence, **(B)** in the presence of CAK (200 ppm Chitosan + 400 ppm ascorbic acid, **(C)** in presence of CAK (200 ppm Chitosan + 400 ppm ascorbic acid + 50 ppm $Cu^{2+}$). (Magnification: 10,000 X, immersion time 24 h).

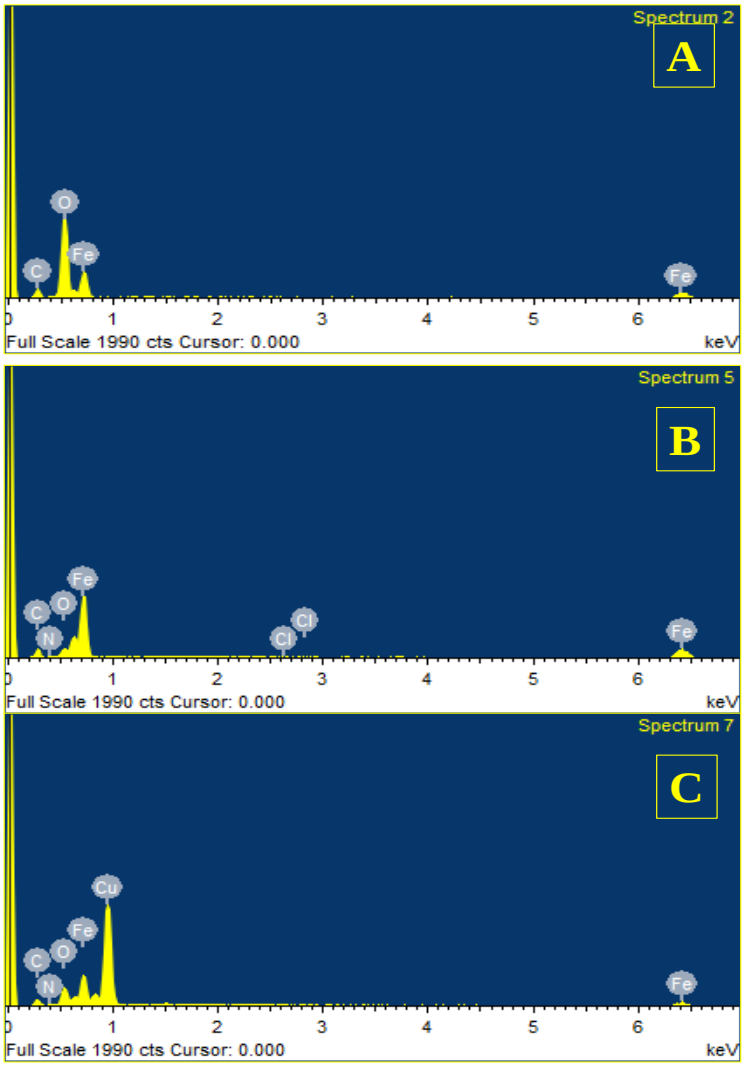


**Figure V.6:** EDX spectrum of mild steel surface immersed in 1 M HCl **(A)** in the absence, **(B)** in the presence of CAK (200 ppm Chitosan + 400 ppm ascorbic acid, **(C)** in presence of CAK (200 ppm Chitosan+400 ppm ascorbic acid+50 ppm $Cu^{2+}$). (24 h immersion time).

Figure.V.5A shows the SEM image of the mild steel specimen immersed in 1 M HCl in the absence of the inhibitor. It is evident that in the absence of the inhibitor the surface is badly damaged and the formation of pits and cracks can be seen. The surface is covered with the corrosion products. The corresponding EDX spectrum shown in figure V.6A illustrates that iron and oxygen are the main elements after corrosion. Presence of ferrous oxide, ferric oxide ($Fe_2O_3$, $Fe_3O_4$ and FeOOH) can be inferred from this spectrum. We also observed a small carbon peak, which may be because of the carbon present in the mild (carbon) steel. The bulk composition of mild steel contains small amount of carbon. In presence of 1M HCl, the extensive corrosion on the surface must have exposed the small amount of carbon. This could be the reason for the carbon peak in the EDX spectrum.

Figure V.5B represents the SEM image of the mild steel specimen immersed in 1 M HCl in the presence CAK (200 ppm chitosan + 400 ppm Ascorbic acid). The image shows that the surface is relatively smooth and does not exhibit any pit. The corresponding EDX spectrum shown in the figure V.6B reveals that the surface film consists of mostly iron and along with iron there is evidence for the presence of carbon, nitrogen, chlorine and oxygen. The intensity of the oxygen peak is reduced when compared to the oxygen peak of mild steel immersed in control. This infers the presence of less amount of oxides of iron on the surface. The presence of carbon and nitrogen reveal the presence of CAK in the surface film, which is responsible for protection. A small peak due to Cl infers that chloride ions from HCl diffused to the metal surface during the formation of protective film of chemisorbed CAK.

Figure V.5C represents the SEM image of the mild steel specimen immersed in 1 M HCl in presence CAK (200 ppm chitosan + 400 ppm Ascorbic acid) along with 50 ppm $Cu^{2+}$ions. From the microscopic image it can be seen that the surface is relatively smooth when compared with the control and formation of a protective film can be seen on the surface. The corresponding EDX spectrum shown in figure V.6C shows that along with iron there is presence of large amount of copper and some amounts of carbon, nitrogen and oxygen on the surface. The chlorine peak is absent. These results infer that cupric ions and CAK are present in the protective film. This might be because the inhibitor molecule CAK along with $Cu^{2+}$ formed a poly nuclear complex, [Fe(III), Cu(II) – CAK] as the CAK has the ability to form stable complexes with the metal ions and relatively high tendency to form complex with $Cu^{2+}$ ions[1]. There are two possibilities for this to happen. One possibility is that the $Cu^{2+}$-CAK complex formed in the solution phase, which diffuses

from the solution to the metal surface and participates in the formation of binuclear complex with the Fe(III) ions available on the surface due to initial corrosion. The second possibility is that the CAK and $Cu^{2+}$ ions diffuse independently to the metal surface where the binuclear complex formation takes place. Either way, a protective film is formed on the metal surface, which hindered the dissolution process of mild steel and thus reduced the corrosion rate of mild steel in 1M HCl.

**V.5: Surface analysis by X-ray photoelectron spectroscopic studies (XPS):**

The chemical composition of the film formed on the mild steel surface immersed in 1 M HCl solution in the presence and absence of inhibitor formulation has been studied using X-ray photoelectron spectroscopy. Figures V.7A and V.7B represent the corresponding XPS survey spectra in the absence and presence of 200 ppm Chitosan + 400 ppm ascorbic acid + 50 ppm $Cu^{2+}$.

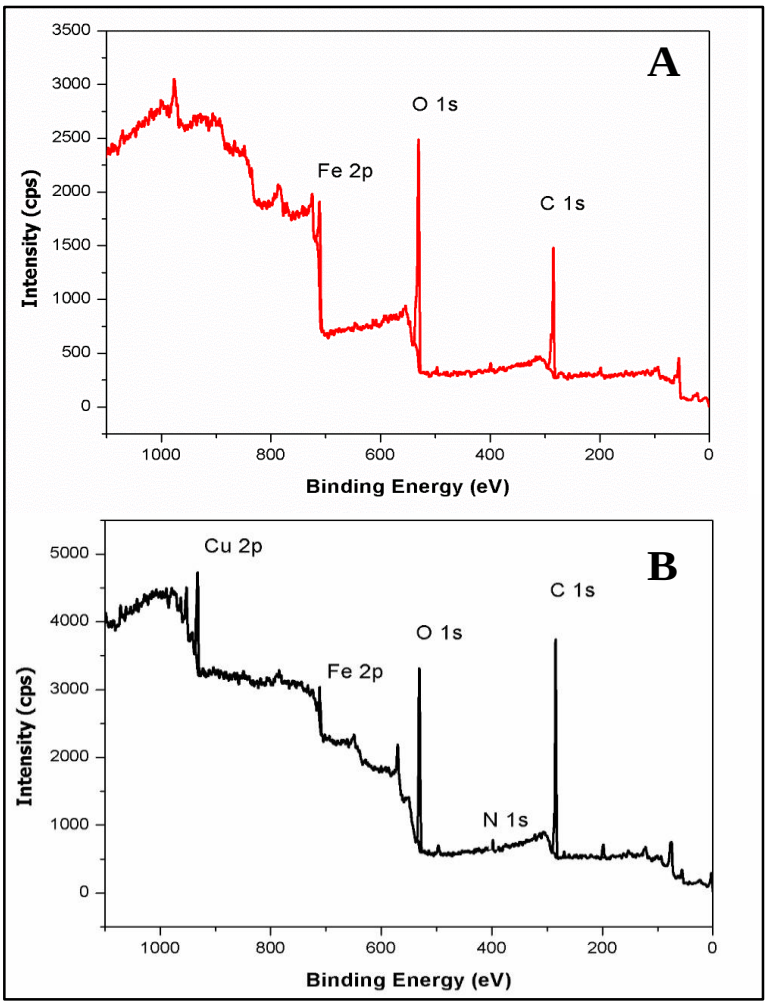


**Figure V.7:** XPS survey spectrum of mild steel specimen immersed in 1 M HCl **(A)** in the absence of inhibitor, **(B)** in the presence of 200 ppm Chitosan + 400 ppm ascorbic acid + 50 ppm $Cu^{2+}$. (24 h immersion time).

The XPS survey spectrum of the control indicates that the surface film consists of carbon, oxygen and iron. Whereas, the survey spectrum of mild steel immersed in the corrosive environment in presence of inhibitor formulation shows that the surface film contains carbon, oxygen, iron, copper and nitrogen. These two spectra infer that the inhibitor formulation is adsorbed on the metal surface. The corresponding deconvolution spectra for each of the elements is discussed hereunder.

Figure V.8A represents the computer deconvolution spectrum of C 1s in the case of control, which shows three distinct peaks one each at 284.5 eV, 285.1 eV and 288.1 eV. The peak at 284.5 eV can be interpreted as a contaminant carbon peak, which arises due to the cracking of vacuum oil used in the instrument[4]. The peaks at higher binding energy values are because of the carbon present in mild steel. The former peak at 285.1 eV may be ascribed to the carbon present in the oxide environment[5] and the later peak at 288.1 eV is attributed to the carbon bound to iron[6]. Whereas, In the presence of binary inhibitor formulation the carbon deconvolution spectrum shows four different peaks **(**Figure V.8B); one peak at the binding energy value of 284.6 eV with high intensity and three peaks of lower intensities at 285.6 eV and 288.3 eV and 289.6 eV respectively. The peak at 284.6 eV may be because of cracking of vacuum oil used in the instrument. The inhibitor formulation contains different types of carbon environments namely C=O, C – N, C=N, C – C and C – H, which explain the presence of multiple peaks in the deconvolution spectrum. The peak at 285.3 eV can be interpreted due to carbon present in the C – C and C – H bonding [7]. The peak at 288.3 eV is because of C=N which is present in the CAK molecule[7], the main linkage between the chitosan molecule and dehydroascorbic acid. The peak present at 289.6 eV can be assigned to C=O peak[8] which is present in the ascorbate ring of CAK molecule. These carbon peaks show an evidence for the presence of the CAK molecules in the surface film.

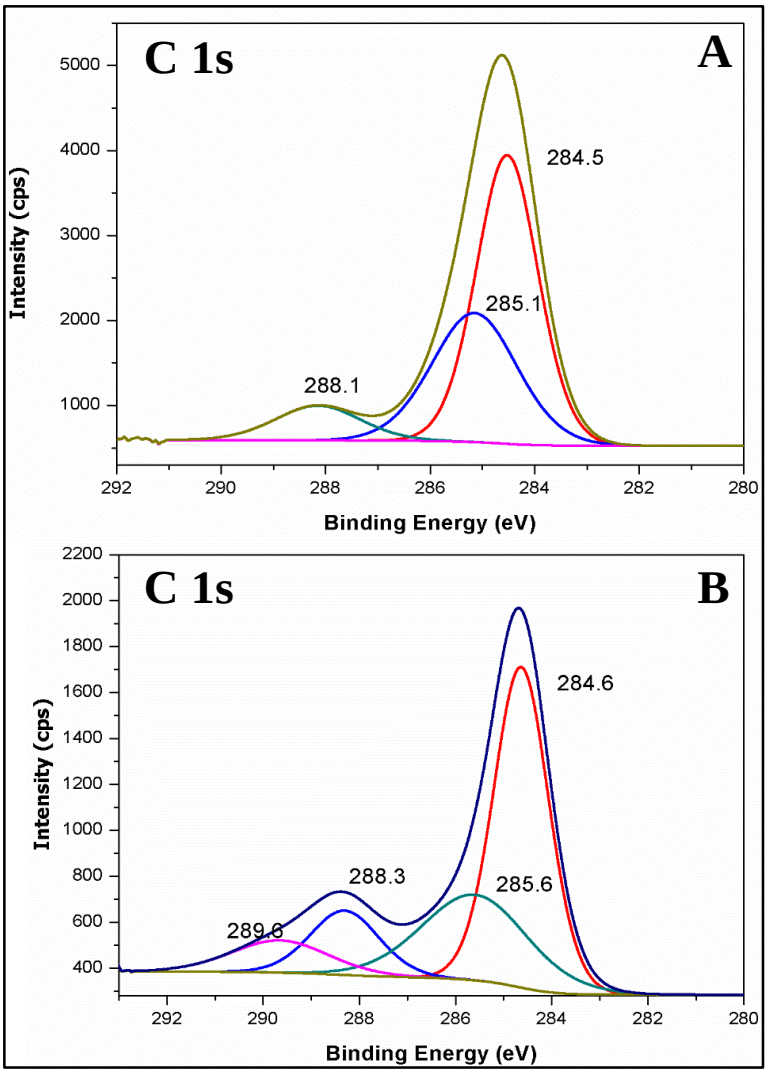


**Figure V.8:** XPS deconvolution spectra of C1s for mild steel sample immersed in 1 M HCl **(A)** in the absence of inhibitor **(B)** in the presence of 200 ppm Chitosan + 400 ppm ascorbic acid + 50 ppm $Cu^{2+}$. (24 h immersion time).

Figure V.9A represents the computer deconvolution spectrum of O 1s in the case of control, which shows a peak at 531.5 eV and another peak at 533.8 eV. The peak present at the lower binding energy value can be ascribed to $OH^-$ and is attributable to oxygen in hydrous iron oxides, such as FeOOH and $Fe(OH)_3$ [9]. The peak at 533.8 eV can be assigned to oxygen of adsorbed water molecules on the metal surface[10]. Figure V.9B represents the computer deconvolution spectrum of O 1s in presence of inhibitor formulation. The spectrum consists of five different peaks, at 529.7 eV, 531.3 eV, 532.5 eV, 535.4 eV and 536.9 eV respectively. The peak at 529.7 eV can be attributed to oxygen present in the oxides and hydroxides of Fe (III), in the form of $O^{2-}$. The peak at 531.3 eV can be interpreted to $OH^-$ and can be assigned to oxygen in hydrous iron oxides, such as FeOOH

and $Fe(OH)_3$ [9]. The peaks at 532.5 eV, 535.4 eV and 536.9 eV are ascribed to the oxygen present in the inhibitor molecules (CAK) in various forms such as C-O, C=O and C=N. The peak at 533.8 eV in the case of control, assigned to the adsorbed water molecules is absent in presence of inhibitor formulation. This may be because of the replacement of water molecules by the inhibitor molecules in presence of inhibitor formulation. The peak at 536.9 eV can be because of the C-O. The peak at 535.4 eV can be attributed to oxygen in the form of C=O, which is present in the ascorbate ring of CAK molecule. All these results also infer that the inhibitor molecule has adsorbed on the metal surface in the form of a film.

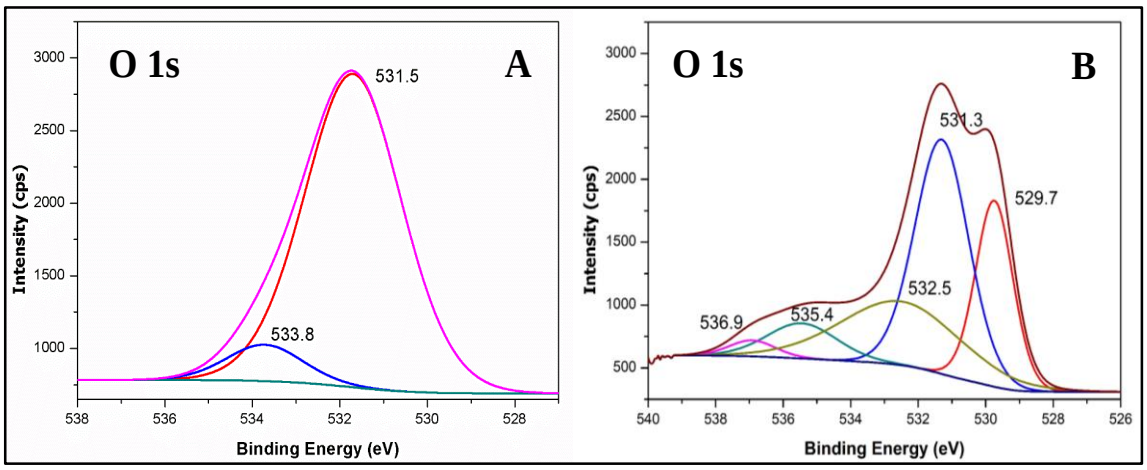


**Figure V.9:** XPS deconvolution spectra of O 1s for mild steel sample immersed in 1 M HCl **(A)** in the absence of inhibitor **(B)** in the presence of 200 ppm Chitosan + 400 ppm ascorbic acid + 50 ppm $Cu^{2+}$. (24 h immersion time)

The deconvolution spectrum of the Fe 2p of control consists of two peaks, one at 710.4 eV corresponding to Fe $2p_{3/2}$ and the other one at 725.6 eV corresponding to the Fe $2p_{1/2}$ electron (Figure V.10A). Generally Fe $2p_{3/2}$ is interpreted. In the present context there is a large shift in the binding energy value of Fe $2p_{3/2}$ from the characteristic elemental binding energy value of 707.0 eV. This shift of 3.4 eV confirms that iron is present as $Fe^{3+}$ in the form of ferric oxide and hydroxide. The ferric species is probably formed because of the oxidation of ferrous species. Indeed, the peak at a binding energy of 710.8 eV was attributed to ferric compounds such as $Fe_2O_3$, $Fe_3O_4$ and FeOOH in the literature[11–13]. In the presence of inhibitor formulation, in the Fe 2p3/2 spectrum (Figure V.10B), apart from the peak at 710.4 eV there is another peak at 712.3eV, which can be interpreted due to the formation of complex between Fe(III) and CAK molecules.

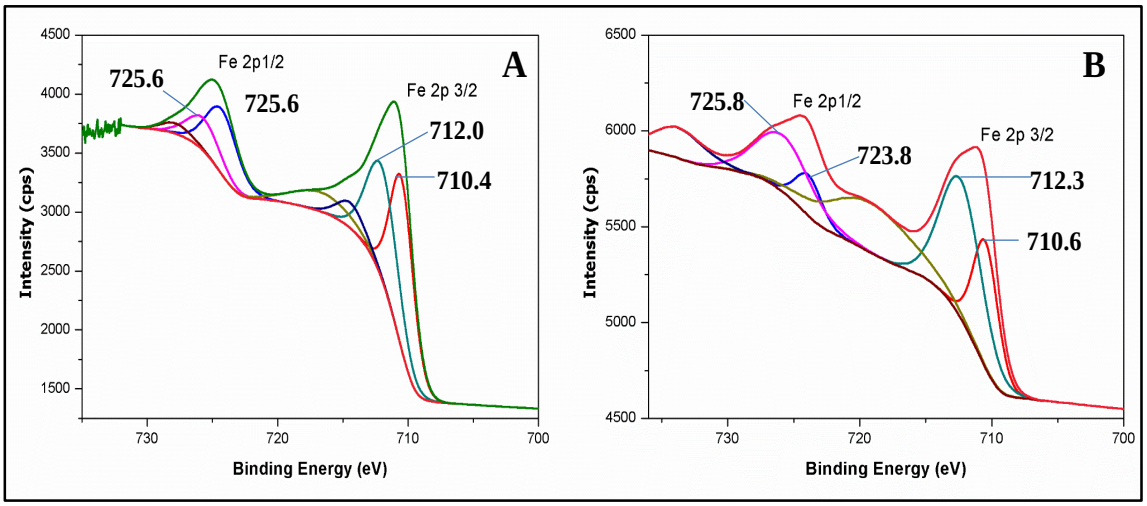


**Figure V.10:** XPS deconvolution spectra of Fe 2p for mild steel sample immersed in 1 M HCl **(A)** in the absence of inhibitor **(B)** in the presence of 200 ppm Chitosan + 400 ppm ascorbic acid + 50 ppm $Cu^{2+}$. (24 h immersion time)

Figure V.11 represents the Cu 2p peak in presence of the inhibitor formulation which is not observed in case of control. According to the standard reference data base Cu $2p_{1/2}$ and Cu $2p_{3/2}$ peaks for pure Cu appear at a binding energy of 952.45–952.56 eV and 932.20–933.1 eV, respectively[4]. We have observed the Cu $2p_{3/2}$ peak at 934.2 eV with a clear shift of 2 eV from that of pure Cu indicating the presence of Cu in double oxidation state form. Moreover, the presence of shakeup satellites also indicates that copper is present in the Cu(II) form. Interestingly, we have also observed a peak at 932.3 eV, which indicates the presence of elemental copper also on mild steel surface. This result can be explained as follows. Free $Cu^{2+}$ ions also diffuse to the metal surface and get reduced to elemental Cu as the reduction potential of $Cu^{2+}$/Cu system is very high. The protective film in the present context therefore may consists of the complex of inhibitor formulation namely [Cu(II),Fe(III)-CAK], elemental copper and also [Fe(III)-CAK] complex.

In addition to the above elements, the survey spectrum of the surface film on mild steel in presence of inhibitor formulation consists of nitrogen peaks. Figure V.12 represents the N 1s spectrum of mild steel surface in 1M HCl in presence of inhibitor formulation. The spectrum shows two distinct peaks, one at 398.9 eV and the other one at 402.1 eV. The former peak can be assigned to =N- (unprotonated nitrogen atom)[14], which is present in chitosan ascorbate ketimine molecule. Precisely it is the bond between chitosan and ascorbic acid. The later peak at 402.1 eV can be interpreted due to the

nitrogen atom which is bound to the mild steel (N-Fe) and because of this bond the binding energy is increased to higher values.

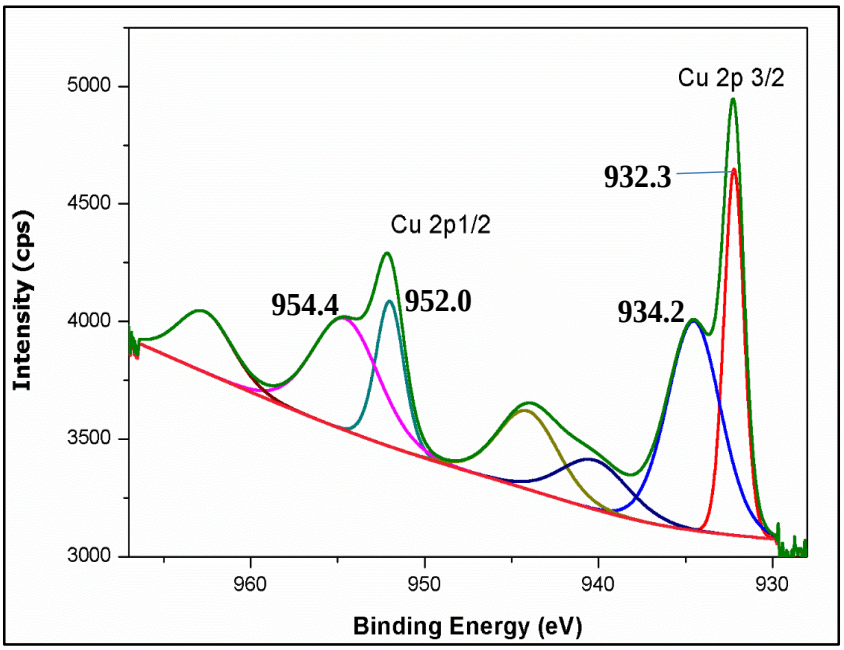


**Figure V.11:** XPS deconvolution spectra of Cu 2p for mild steel sample immersed in 1 M HCl in the presence of 200 ppm Chitosan + 400 ppm ascorbic acid + 50 ppm $Cu^{2+}$.(24 h immersion time).

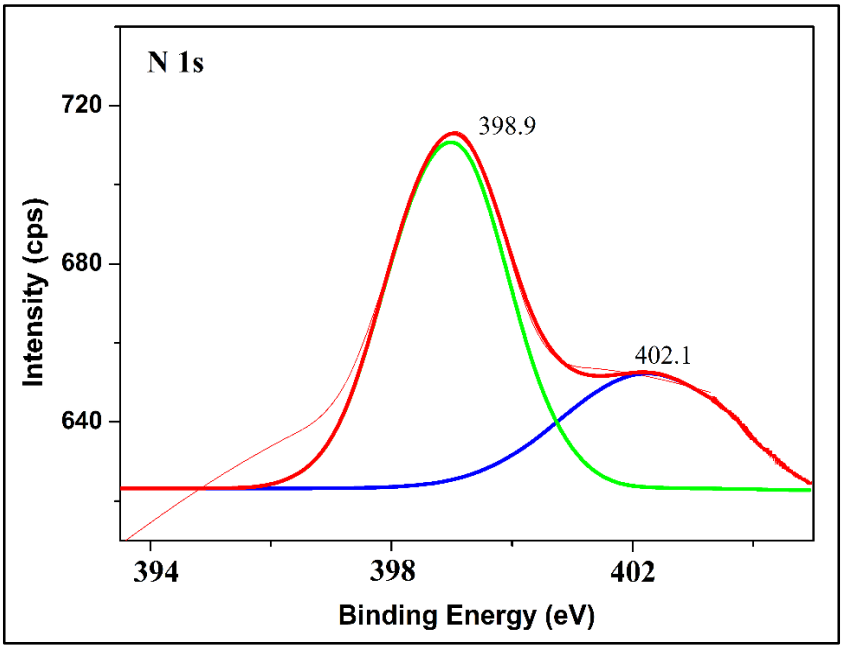


**Figure V.12:** XPS deconvolution spectra of N 1s for mild steel sample immersed in 1 M HCl in the presence of 200 ppm Chitosan + 400 ppm ascorbic acid + 50 ppm $Cu^{2+}$.(24 h immersion time).

**V.6: Analysis of the surface film by X- ray diffraction studies (XRD):**

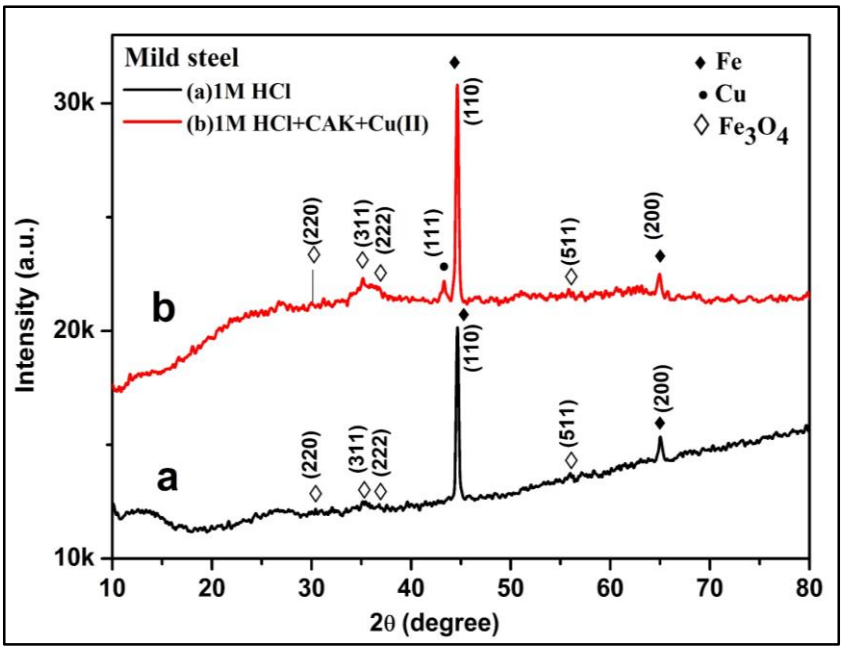


**Figure IV.2.13:** The X-ray diffraction patterns of the surface film formed on mild steel sample immersed in 1 M HCl (A) in the absence (B) in the presence of 200 ppm Chitosan + 400 ppm ascorbic acid + 50 ppm $Cu^{2+}$.(24 h immersion time).

Figure V.13(A) and V.13(B) shows the X-ray diffractograms of the surface of mild steel specimen immersed in 1 M HCl environment in the absence and presence of chitosan ascorbate ketimine (CAK) + $Cu^{2+}$. In both the cases, the iron (1 1 0) and (2 0 0) planes dominated the intensity of the spectrum[15], the peaks for the corrosion products ($Fe_2O_3$, $Fe_3O_4$,etc.) formed on the surface are almost submerged in the spectrum due to the high itensity of the iron peak. Apart from the iron peaks, in both the cases I have got very less intense peaks for $Fe_3O_4$. The planes present for $Fe_3O_4$ are (3 1 1), (2 2 2), (2 2 0) and (5 1 1). It may be noted that because of the aggressive nature of the corrosive environment, the corrosion products which are formed during the course of corrosion get dissolved in 1 M HCl solution. This is also one of the main reasons for the less intensities of the $Fe_3O_4$ peaks. In the presence of CAK+ $Cu^{2+}$ inhibitor formulation, the XRD pattern also shows a peak for Cu (1 1 1) plane. This is a very important information from the XRD pattern. The presence of the elemental copper peak supports the corroison inhibiton mechanism drawn from the XPS studies. The $Cu^{2+}$ ions present in the inhibitor solution diffuse to the metal surface and get deposited as elemetal copper on the mild steel surface. The XRD patterns confirm that in presence of CAK+$Cu^{2+}$ as inhibittor, the surface film contains copper.

**V.7: Plausible corrosion inhibition mechanism:**

The corrosion mechanism of mild steel in hydrochloric acid is well established by several authors[16,17]. The anodic and cathodic reactions are given in the following equations.

Anodic dissolution of mild steel follows the steps given in equation 2

$$Fe + Cl^- \rightleftharpoons (FeCl^-)_{ads} \quad (2a)$$

$$(FeCl^-)_{ads} \rightleftharpoons (FeCl)_{ads} + e^- \quad (2b)$$

$$(FeCl)_{ads} \rightleftharpoons (FeCl^+)_{ads} + e^- \quad (2c)$$

$$(FeCl^+)_{ads} \rightleftharpoons Fe^{2+} + Cl^- \quad (2d)$$

$$Fe^{2+} \xrightarrow{\text{oxidn,}} Fe^{3+} \quad (2e)$$

Hydrogen evolution at cathode follows the steps given in equation 3

$$Fe + H^+ \rightleftharpoons (FeH^+)_{ads} \quad (3a)$$

$$(FeH^+)_{ads} + e^- \longrightarrow (FeH)_{ads} \quad (3b)$$

$$(FeH)_{ads} + H^+ + e^- \longrightarrow Fe + H_{2(g)} \quad (3c)$$

The $Cl^-$ ions initially move to the positively charged metal surface and get adsorbed. In the presence of the inhibitor formulation, the $Cu^{2+}$ ions and chitosan ascorbate ketimine (CAK) form a complex and because of electrostatic attraction this complex will get adsorbed on to the metal surface (negatively charged) where $Cl^-$ ions are present. This adsorbed inhibitor complex then interacts with $Fe^{3+}$ which may be more plausible, and forms a binuclear complex [Fe(III),Cu(II)-CAK] which is insoluble and protects the mild steel surface from further attack of $Cl^-$ ions. Thus, the inhibitor protects mild steel from corrosion in 1M HCl solution.

$$Cu(II) + CAK \longrightarrow \left[Cu(II)\text{-}CAK\right] \text{ Complex} \quad (4)$$

$$Cu(II)\text{-}CAK + Fe(II) \longrightarrow [Cu(II), Fe(II)\text{-}CAK] \quad (5)$$

$$Cu^{2+} + 2e^- \longrightarrow Cu \quad (6)$$

There are several other processes that occur on the metal surface which also contributes to the corrosion inhibition. The free CAK molecules which are present in the solution may also diffuse to the metal surface where they form a complex with Fe(III) ions. So, the surface film may also consist of [Fe(III)-CAK] complex. Simultaneously, $Cu^{2+}$ ions may also diffuse to the metal and get reduced to elemental copper.

**References:**


1. Muzzarelli, R., Tanfani, F. & Emanuelli, M. Chelating derivatives of chitosan obtained by reaction with ascorbic acid. *Carbohydr. Polym.* **4,** 137–151 (1984).
2. Muzzarelli, R. A. A. Removal of uranium from solutions and brines by a derivative of chitosan and ascorbic acid. *Carbohydr. Polym.* **5,** 85–89 (1985).
3. Umoren, S. A., Ogbobe, O., Ebenso, E. E. & Ekpe, U. J. Effect of halide ions on the corrosion inhibition of mild steel in acidic medium using polyvinyl alcohol. *Pigment Resin Technol.* **35,** 284–292 (2006).
4. Cicileo, G. P., Rosales, B. M., Varela, F. e. & Vilche, J. R. Comparative study of organic inhibitors of coppercorrosion. *Corros. Sci.* **41,** 1359–1375 (1999).
5. Bennettand, H. & Ouver, G. J. High Resolution XPS of Organic Polymers: The Scienta ESCA300 Database (Beamson, G.; Briggs, D.). *J. Chem. Educ.* **70,** A25 (1993).
6. Barber, M., Connor, J. A., Derrick, L. M. R., Hall, M. B. & Hillier, I. H. High energy photoelectron spectroscopy of transition metal complexes. Part 2.—Metallocenes. *J. Chem. Soc., Faraday Trans. 2* **69,** 559–562 (1973).
7. Bentiss, F. *et al.* Corrosion control of mild steel using 3,5-bis(4-methoxyphenyl)-4-amino-1,2,4-triazole in normal hydrochloric acid medium. *Corros. Sci.* **51,** 1628–1635 (2009).
8. Barth, G., Linder, R. & Bryson, C. Advances in charge neutralization for XPS measurements of nonconducting materials. *Surf. Interface Anal.* **11,** 307–311 (1988).
9. Babić-Samardzija, K., Lupu, C., Hackerman, N., Barron, A. R. & Luttge, A. Inhibitive properties and surface morphology of a group of heterocyclic diazoles as inhibitors for acidic iron corrosion. *Langmuir* **21,** 12187–96 (2005).
10. Babić-Samardžija, K., Lupu, C., Hackerman, N., Barron, A. R. & Luttge, A. Inhibitive Properties and Surface Morphology of a Group of Heterocyclic Diazoles as Inhibitors for Acidic Iron Corrosion. *Langmuir* **21,** 12187–12196 (2005).
11. Pech-Canul, M. a. & Bartolo-Pérez, P. Inhibition effects of N-phosphono-methyl-glycine/Zn2+ mixtures on corrosion of steel in neutral chloride solutions. *Surf. Coatings Technol.* **184,** 133–140 (2004).
12. Bouanis, F. Z., Bentiss, F., Traisnel, M. & Jama, C. Enhanced corrosion resistance properties of radiofrequency cold plasma nitrided carbon steel: Gravimetric and

electrochemical results. *Electrochim. Acta* **54,** 2371–2378 (2009).

13. Zarrok, H. *et al.* Corrosion control of carbon steel in phosphoric acid by purpald – Weight loss, electrochemical and XPS studies. *Corros. Sci.* **64,** 243–252 (2012).
14. Lebrini, M. *et al.* Enhanced corrosion resistance of mild steel in normal sulfuric acid medium by 2,5-bis(n-thienyl)-1,3,4-thiadiazoles: Electrochemical, X-ray photoelectron spectroscopy and theoretical studies. *Appl. Surf. Sci.* **253,** 9267–9276 (2007).
15. Han, R. *et al.* 1D Magnetic Materials of Fe3O4 and Fe with High Performance of Microwave Absorption Fabricated by Electrospinning Method. *Sci. Rep.* **4,** 7493 (2015).
16. Li, W., He, Q., Pei, C. & Hou, B. Experimental and theoretical investigation of the adsorption behaviour of new triazole derivatives as inhibitors for mild steel corrosion in acid media. *Electrochim. Acta* **52,** 6386–6394 (2007).
17. Yurt, A., Balaban, A., Kandemir, S. U., Bereket, G. & Erk, B. Investigation on some Schiff bases as HCl corrosion inhibitors for carbon steel. *Mater. Chem. Phys.* **85,** 420–426 (2004).

# CHAPTER-VI

## Section VI.1: Chitin xanthate (CX) inhibitor to combat the corrosion of copper in neutral chloride environment

## Section VI.2. Phosphorylated xanthan gum (PXG) as an inhibitor to control the mild steel corrosion in neutral chloride environment

# TABLE OF CONTENTS

## Chapter VI

# Chapter VI

This chapter has been divided into two sections. Section VI.1 deals with the experimental results and discussion of the corrosion protection of copper in neutral chloride environment using Chitin xanthate (CX) inhibitor and section VI.2 consists of the experimental results and discussion of the corrosion protection of mild steel in neural chloride environment using phosphorylated Xanthan gum (PXG).

## VI.1. Chitin xanthate (CX) inhibitor to combat the corrosion of copper in neutral chloride environment:

### VI.1.1: Characterization of chitin xanthate (CX):

Chitin has been chemically modified to chitin xanthate using the method reported in the literature[1,2]. The preparative method has already been discussed in the 'materials and methods' chapter of this thesis. The xanthated derivative of chitin has been characterized by FTIR spectroscopy (KBr pellet method) in the wave number range of 4000 $cm^{-1}$ - 400 $cm^{-1}$. Results are in good agreement with the literature values [1,3].

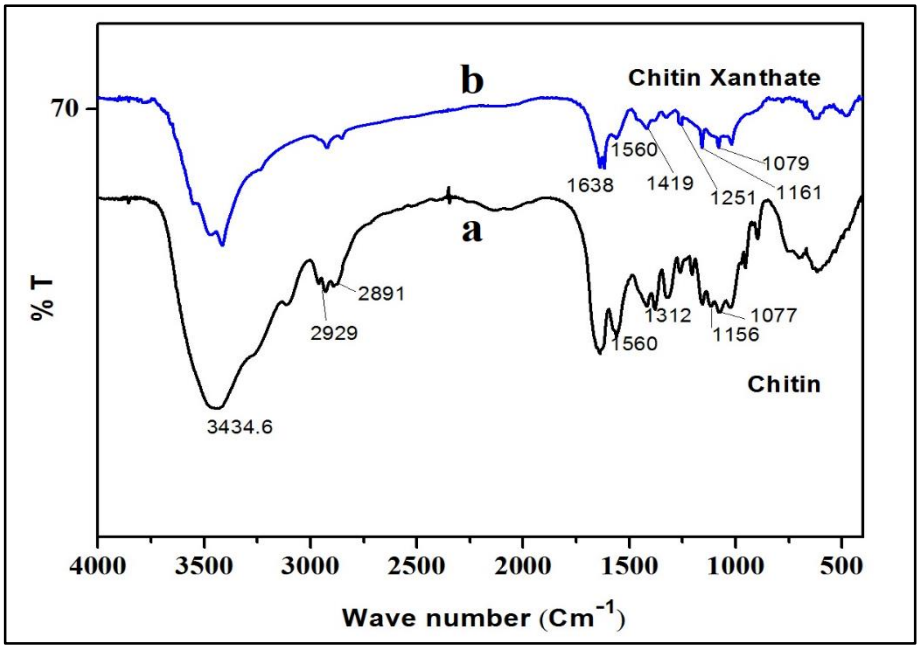


**Figure VI.1.1:** FTIR spectra of **(a)** pure chitin and **(b)** chitin xanthate (CX).

Figure VI.1.1(a) represents the FTIR spectrum of unmodified chitin and figure VI.1.1(b) represents the FTIR spectrum of chitin xanthate. After chemical modification new peaks appeared in the FTIR spectrum, which reveal that the xanthate group has been successfully introduced into the chitin moiety. The peaks at 1638 $cm^{-1}$, 1560 $cm^{-1}$ and 1490 $cm^{-1}$ are ascribed to the bending vibrations of the acetamide group[3]. The peak at 1260 $cm^{-}$

[1] is assigned to the –OH stretching vibration and the absorption bands at 1161 $cm^{-1}$ and 1079 $cm^{-1}$ are due to the –O-(CS)-$S^-$ (thiocarbonyl derivative) stretching vibrations. These peaks infer the formation of chitin xanthate.

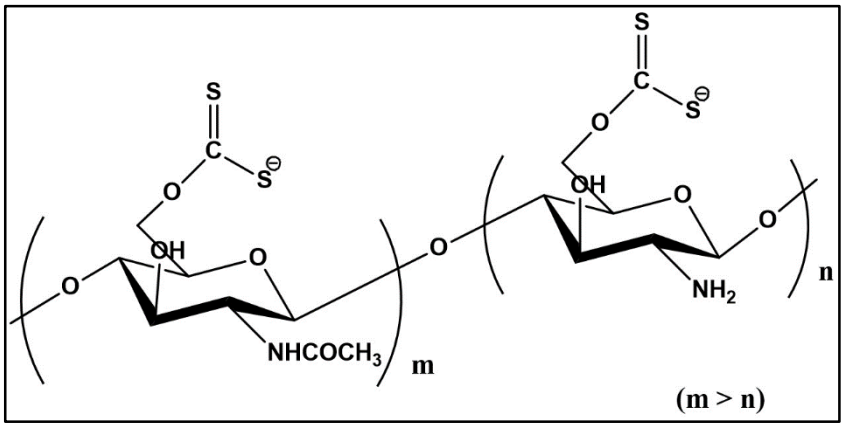


**Chitin xanthate**

Weight-loss studies, electrochemical impedance studies and potentiodynamic polarization studies were carried out in order to investigate the corrosion inhibition ability. SEM-EDX, XRD and XPS studies were employed for surface analytical studies.

### VI.1.2: Analysis of the results of weight-loss Studies:

The corrosion inhibition efficiency of the chemically modified chitin (CX) to combat the corrosion of copper in neutral chloride environment has been investigated using weight-loss studies at 30±0.1 °C after 10 days immersion period. The corrosion rates and the inhibition efficiencies obtained from the weight-loss data are given in the table VI.1.1. From the analysis of results it can be demonstrated that in presence of the inhibitor a significant decrease in the corrosion rate has been observed. The weigh-loss in the presence of the inhibitor is in the range of 0.5 to 0.3 mg when compared to the weight-loss observed in the case of control which is 6.52 mg. The corrosion rate is very much reduced from 0.0698 mmpy in case of control to 0.0038 mmpy by the addition of 30 ppm chitin xanthate. The inhibitor might have formed a film on the metal surface, which acts as a barrier between the metal and the corrosive environment and consequently the corrosion rate of the metal is decreased. As the concentration of the inhibitor is increased, the inhibition efficiency is also increased and a maximum inhibition efficiency of 95 % is obtained at a concentration of 30 ppm of chitin xanthate. This result shows that the surface coverage is increased with an increase in the inhibitor concentration and 30 ppm CX is the optimum concentration, where the surface is almost completely covered with the protective film. When the concentration of the inhibitor is further increased beyond 30

ppm, the inhibition efficiency remained the same.

**Table VI.1.1:** Corrosion rates of copper in 200 ppm NaCl (aq.) in the absence and presence of different concentrations of CX obtained from gravimetric method.(Temp. 30 ± 0.1 °C).

| S.No. | Concentration of chitin xanthate | Weight –loss (mg) | Corrosion Rate(mmpy) | I.E.% |
|---|---|---|---|---|
| 1 | 0 ppm | 6.52 | 0.0698 | - |
| 2 | 10 ppm | 0.50 | 0.0061 | 89 |
| 3 | 20 ppm | 0.47 | 0.0048 | 93 |
| 4 | 30 ppm | 0.30 | 0.0038 | 95 |
| 5 | 40 ppm | 0.30 | 0.0038 | 95 |
| 6 | 50 ppm | 0.30 | 0.0038 | 95 |

### VI.1.3: Analysis of the results of Electrochemical Studies:

### Electrochemical Impedance Studies:

Figure VI.1.2A presents the Nyquist plots of copper immersed in 200 ppm NaCl solution in the absence and presence of different concentrations of CX at a constant temperature of 30±0.1$^0$C and an immersion period of 24 h. The corresponding Bode plots are shown in the Figure VI.1.2B

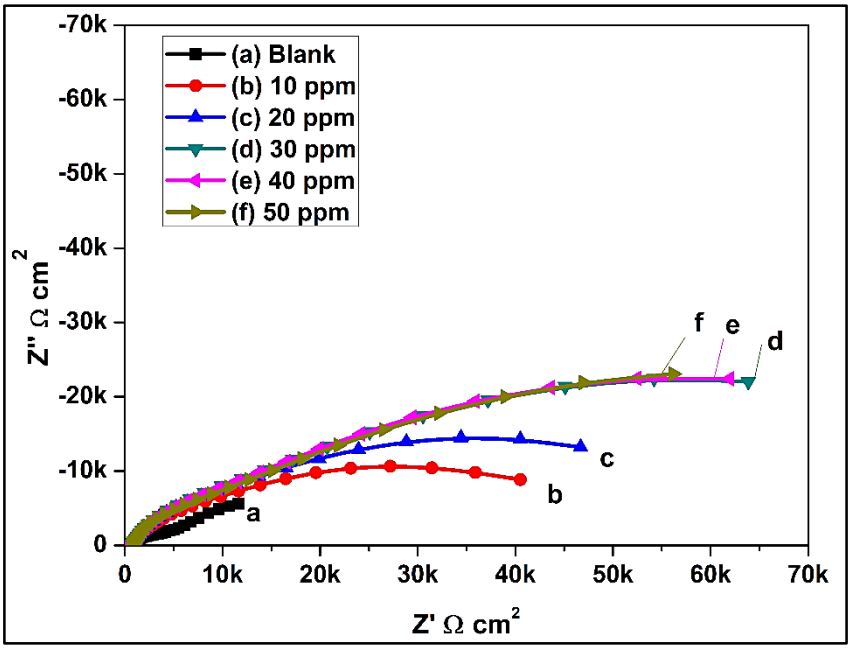


**Figure VI.1.2A**: Nyquist plots for copper specimen immersed in 200 ppm NaCl **(a)** in the absence of inhibitor, **(b)** In presence of 10 ppm CX, **(c)** In presence of 20 ppm CX, **(d)** In presence of 30 ppm CX, **(e)** In presence of 40 ppm CX, **(f)** In presence of 50 ppm CX.

Nyquist plots of copper immersed in 200 ppm NaCl without inhibitor showed Warburg behaviour in the low frequency region, which is primarily due to the diffusion of oxygen to the copper surface[4]. Whereas, the Nyquist plots of copper immersed in 200 ppm NaCl with different concentrations of chitin xanthate showed no signs of Warburg behaviour, indicating the absence of diffusion process and minimization of corrosion process. Moreover, the diameter of the depressed semicircle is increased considerably with an increase in the concentration of the inhibitor, acquiring higher charge transfer resistance ($R_{ct}$) values.

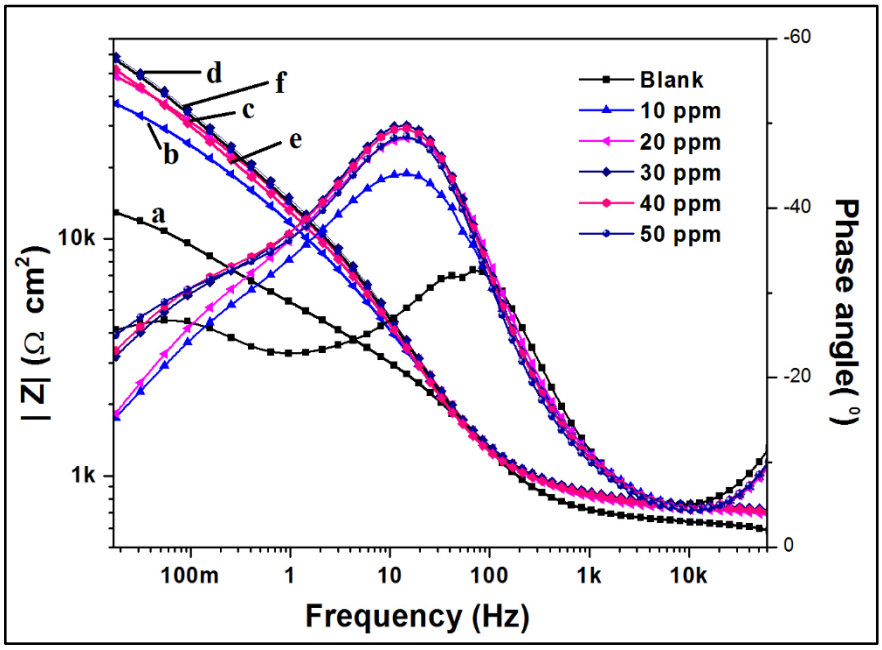


**Figure VI.1.2B**: Bode plots for copper specimen immersed in 200 ppm NaCl **(a)** in the absence of inhibitor, **(b)** In presence of 10 ppm CX, **(c)** In presence of 20 ppm CX, **(d)** In presence of 30 ppm CX, **(e)** In presence of 40 ppm CX, **(f)** In presence of 50 ppm CX.

Figure VI.1.2B shows the Bode plots for copper specimens immersed in 200 ppm NaCl without the inhibitor and with different concentrations of the inhibitor. The total impedance value increased with an increase in concentration of the inhibitor and the highest value is obtained for 30 ppm CX. The total impedance values for 30, 40, 50 ppm CX concentrations are close to each other and almost merged with each other in the mid-frequency region, which corresponds to charge transfer. These results indicate that the optimum concentration of CX required to form a uniform protective film and complete coverage of the surface is 30 ppm only. The phase angle maxima at the 30, 40 and 50 ppm concentrations of the inhibitor also merged with each other.

Appropriate equivalent circuits were used (Figure VI.1.3) which fitted well with the experimental data[5]. These circuits were used to obtain the charge transfer resistance ($R_{ct}$), double layer capacitance ($C_{dl}$), film resistance, CPE exponent and n. The impedance parameters are tabulated in the table VI.1.2. The charge transfer resistance ($R_{ct}$) value for copper specimen immersed in 200 ppm NaCl without inhibitor is 6.5 kΩ $cm^2$. There is a significant increase in the $R_{ct}$ value in the presence of chitin xanthate at all concentrations and a maximum value of 82.5 kΩ $cm^2$ is obtained at a concentration of 30 ppm CX. This is because of the formation of a protective film on the metal surface, which reduces the charge transfer at the metal/solution interface and minimizes the corrosion rate. The 'n' value is also increased in presence of chitin xanthate, indicating uniformity of the surface film on copper. An inhibition efficiency of 92 % is obtained at 30 ppm chitin xanthate.

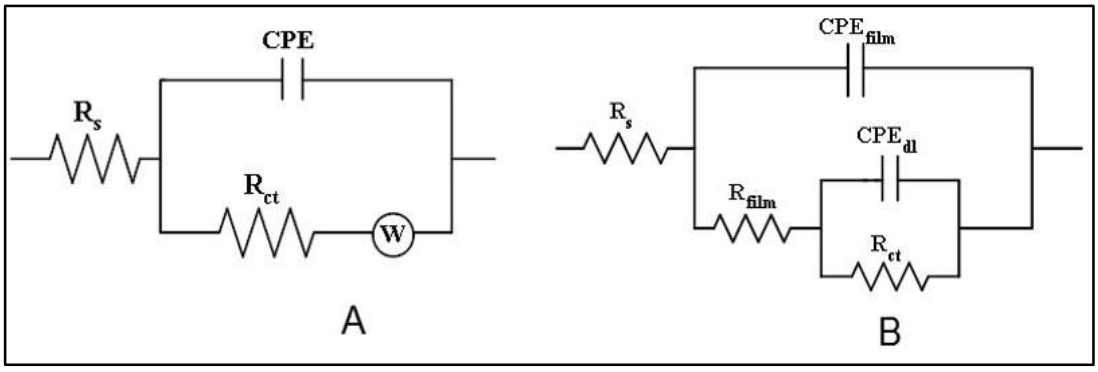


**Figure VI.1.3:** Equivalent circuits used for copper immersed in 200 ppm NaCl A) without inhibitor (B) with chitin xanthate inhibitor. $R_s$ – Solution resistance, $R_{ct}$ – Charge transfer resistance, CPE- constant phase element, $R_{film}$ – film resistance.

**Table VI.1.2:** Corrosion parameters for copper in 200 ppm NaCl (aq.) in the absence and presence of different concentrations of inhibitor obtained from electrochemical impedance method.

| **Chitin xanthate (CX) in ppm** | **$R_{ct}$ (kΩ $cm^2$)** | **$C_{dl}$ (μF $cm^{-2}$)** | **n** | **$R_{film}$ (kΩ $cm^2$)** | **$C_{film}$ (μF $cm^{-2}$)** | **$n_{film}$** | **IE %** |
|---|---|---|---|---|---|---|---|
| 0 | 6.5 | 5.5 | 0.538 | - | - | - | - |
| 10 | 44.9 | 0.8 | 0.722 | 15.2 | 0.4 | 0.245 | 85 |
| 20 | 56.3 | 1.0 | 0.770 | 17.2 | 0.4 | 0.266 | 88 |
| 30 | 82.5 | 0.9 | 0.814 | 17.9 | 0.5 | 0.291 | 92 |
| 40 | 80.7 | 1.1 | 0.810 | 15.4 | 0.5 | 0.285 | 92 |
| 50 | 78.7 | 1.1 | 0.819 | 13.8 | 0.6 | 0.272 | 92 |

**Potentiodynamic polarization studies:**

Figure VI.1.4 shows the potentiodynamic polarization curves for copper specimens immersed in 200 ppm NaCl solution at pH=7 and temperature of 30±0.1ºC without and with different concentrations of chitin xanthate. In the absence of inhibitor (blank) the potentiodynamic polarization curve shows a distinct profile. When the potential is scanned in the positive direction there is a decrease in the corresponding current density ($j_{corr}$), which can be explained as follows. At this anodic potential, copper dissolves to form $Cu^{+}$ ions [6] and these $Cu^{+}$ ions react with $Cl^{-}$ ions to form a passive film of CuCl. When the potential is increased further anodically, there is a progressive increase in the current density, which is because of the formation of soluble $CuCl_2^{-}$species [7]. With a further increase in potential, there is formation of $Cu_2O$, which leads to passivity again. This film is broken by further increase of the anodic potential. This phenomenon is also observed when CX is added as inhibitor at a concentrations of 10 ppm. However, at the concentration of 20 ppm CX, the polarization curve exhibits only one anodic peak; the second anodic peak is absent. In the case of higher concentrations of chitin xanthate such as 30 ppm and 40 ppm, the polarization curves do not exhibit any such anodic peaks as the inhibitor film is protective to stop the dissolution of copper into the solution.

It is evident that in the presence of chitin xanthate both the cathodic and anodic polarization curves are shifted towards lower current density values when compared with blank. However, the reduction in anodic current densities is much higher than the decrease in cathodic current densities. The calculated corrosion parameters from the polarization curves are depicted in the table VI.1.3**.** The copper specimen immersed in 200 ppm NaCl without inhibitor shows a corrosion current density value of 11.55 μA $cm^{-2}$. Whereas, the copper specimens immersed in 200 ppm NaCl containing the inhibitor show corrosion current densities of 2.5, 1.9, 1.6, 1.0 μA $cm^{-2}$ for 10, 20, 30, 40 ppm of CX respectively. Corrosion inhibition efficiencies are calculated using corrosion current density values. A maximum inhibition efficiency of 92 % is obtained from polarization studies at a concentration of 40 ppm CX.

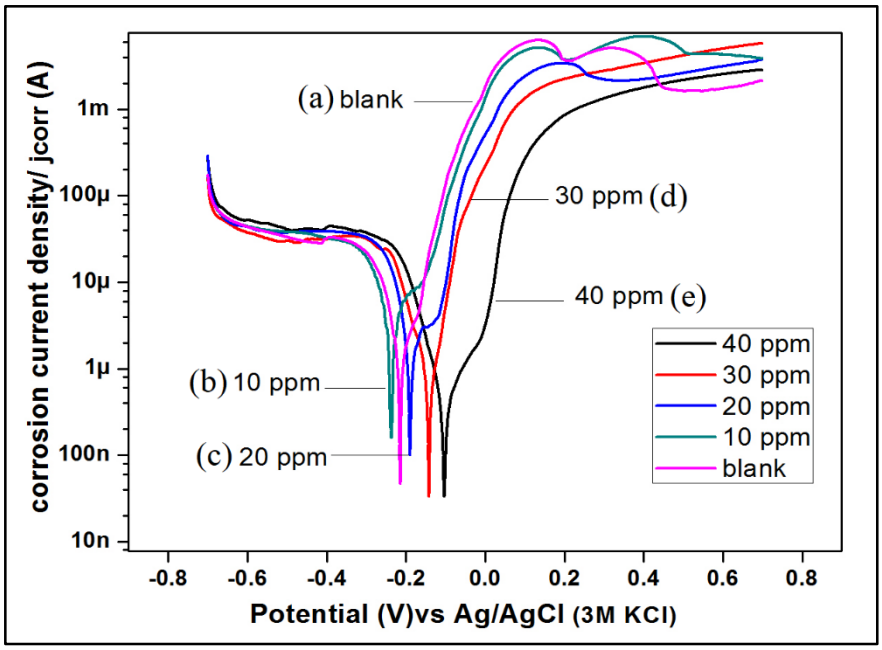


**Figure VI.1.4**: Potentiodynamic polarization curves for copper specimen immersed in aqueous 200 ppm NaCl **(a)** in the absence of inhibitor, **(b)** In presence of 10 ppm CX, **(c)** In presence of 20 ppm CX, **(d)** In presence of 30 ppm CX, **(e)** In presence of 40 ppm CX.

**Table VI.1.3:** Corrosion parameters for copper in 200 ppm NaCl (aq.) in the absence and presence of different concentrations of inhibitor obtained from potentiodynamic polarization studies.

| S.No. | Concentration of chitin xanthate (CX) | $E_{corr}$ (mV) | $J_{corr}$ ($\mu Acm^{-2}$) | βc ($mV\ dec^{-1}$) | βa ($mV\ dec^{-1}$) | I.E.% |
|---|---|---|---|---|---|---|
| 1 | 0 ppm | -216.0 | 11.6 | -275 | 220 | - |
| 2 | 10 ppm | -230.5 | 2.5 | -245 | 120 | 78 |
| 3 | 20 ppm | -196.2 | 1.9 | -202 | 98 | 84 |
| 5 | 30 ppm | -120.0 | 1.6 | -189 | 88 | 89 |
| 4 | 40 ppm | -89.20 | 1.0 | -125 | 77 | 92 |

From the polarization studies results it can be inferred that chitin xanthate is considered as a mixed type inhibitor since it controls both the anodic and the cathodic reactions. It may be noted that this method involves polarization of the electrode to much higher potentials (both anodic and cathodic). Therefore, the highest inhibition efficiency

is obtained at a somewhat higher concentration of 40 ppm in comparison to impedance studies and gravimetric studies. Nevertheless, even at 30 ppm CX, 89 % I.E. is obtained by potentiodynamic polarization studies also. The anodic and cathodic Tafel slopes (βa and βc) are decreased in presence of inhibitor (CX) and the lowest βa and βc values observed are 77 and -125 mV $dec^{-1}$ respectively for 40 ppm of chitin xanthate as inhibitor. Although both the anodic and cathodic current density ($j_{corr}$) values are shifted in presence of inhibitor, the anodic values have been more effected. Therefore, chitin xanthate functions as a mixed type inhibitor, predominantly anodic in nature.

**VI.1.4: Analysis of surface morphology and composition by SEM- EDX:**

Scanning electron microscopic images of the surfaces of the copper samples were taken in order to study the surface morphology after immersion in the corrosive environment for ten days in the absence and presence of the inhibitor. Figure VI.1.5A represents the surface of the polished copper specimen before immersing in the corrosive environment. The surface morphological images of the copper specimen immersed in 200 ppm NaCl in the absence and presence of 30 ppm of CX are shown in figures VI.1.5B and VI.1.5C respectively.

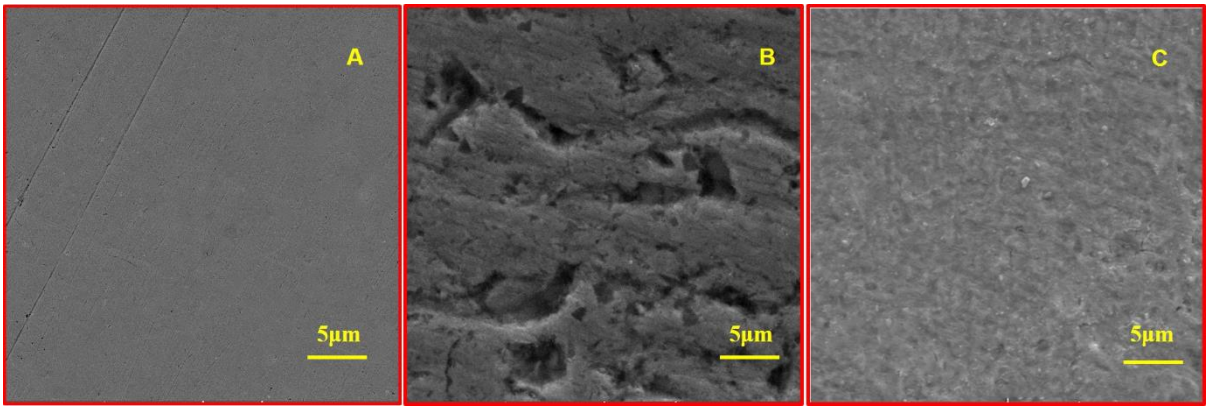


**Figure VI.1.5:** SEM images (10,000X magnification) of copper specimen immersed in 200 ppm NaCl (A) polished specimen (B) in the absence of inhibitor, (C) in presence of 30 ppm CX inhibitor after ten days immersion.

It is evident that in the absence of the inhibitor the surface is badly damaged and formation of pits is seen. The corresponding EDX spectrum shown in figure VI.1.6A indicates that copper and oxygen are the main elements after corrosion, suggesting the presence of cuprous and cupric oxides in the corrosion product. However, in the presence of the inhibitor (FigureVI.1.5C) the surface is relatively smooth and does not exhibit any pit. The corresponding EDX spectrum shown in figure VI.1.6B indicates that along with

copper and oxygen there is presence of carbon, nitrogen and sulphur on the surface. These elements are the main constituents of the inhibitor molecule. The intensity of the oxygen peak is much reduced in the presence of inhibitor. These results infer the formation of a protective film of CX on the copper surface, which is responsible for inhibition of corrosion of copper.

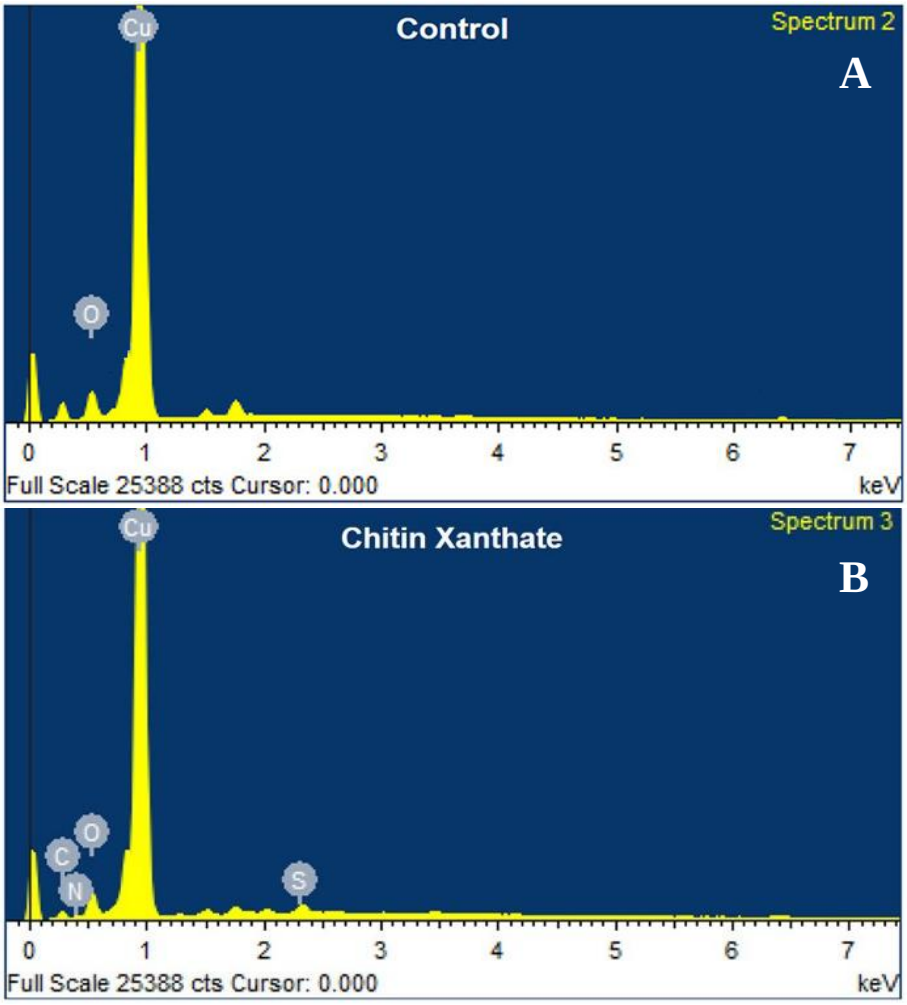


**Figure VI.1.6:** EDX spectrum of copper specimen immersed in 200 ppm NaCl (A) in the absence of inhibitor, (C) in presence of 30 ppm CX inhibitor after ten days immersion.

### VI.1.5: Analysis of the surface film by X-ray photoelectron spectroscopic studies (XPS):

Figure VI.1.7A presents the XPS survey spectrum of copper specimen immersed in the corrosive environment in the absence of CX. Whereas, the XPS survey spectrum of copper specimen immersed in the corrosive environment in the presence of the inhibitor is shown in the figure VI.1.7B.

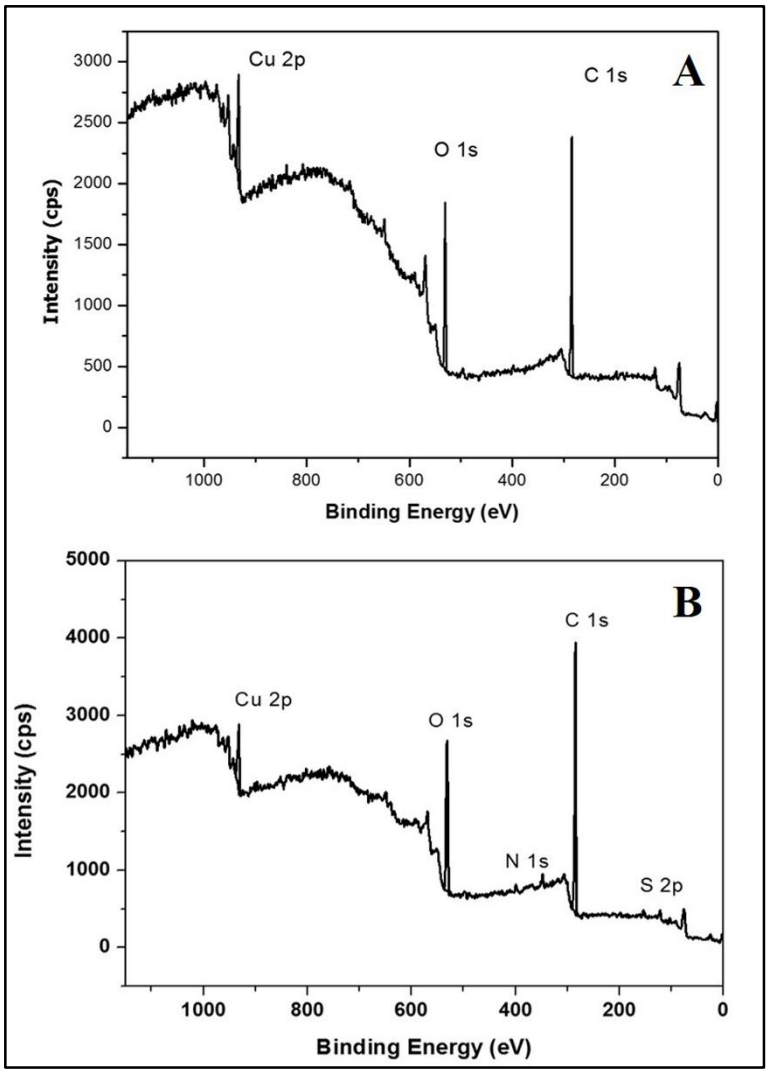


**Figure VI.1.7:** XPS Survey spectrum of copper specimen immersed in 200 ppm NaCl **(A)** in the absence of inhibitor **(B)** in presence of 30 ppm CX as inhibitor. (10 day immersion time).

In the absence of inhibitor, the surface film consists of carbon, oxygen and copper as the main elements. The presence of C 1s peak even in the absence of chitin xanthate is ascribed to contaminant carbon, which is due to cracking of vacuum oil during the operation of the instrument. Whereas, the surface film of copper specimen immersed in corrosive environment in presence of the inhibitor constitutes nitrogen and sulphur peaks along with carbon, oxygen and copper peaks. This result infers the presence of inhibitor molecules adsorbed on the copper surface since sulphur and carbon are the constituting elements of the inhibitor molecule. The computer deconvolution spectra for each element are interpreted separately.

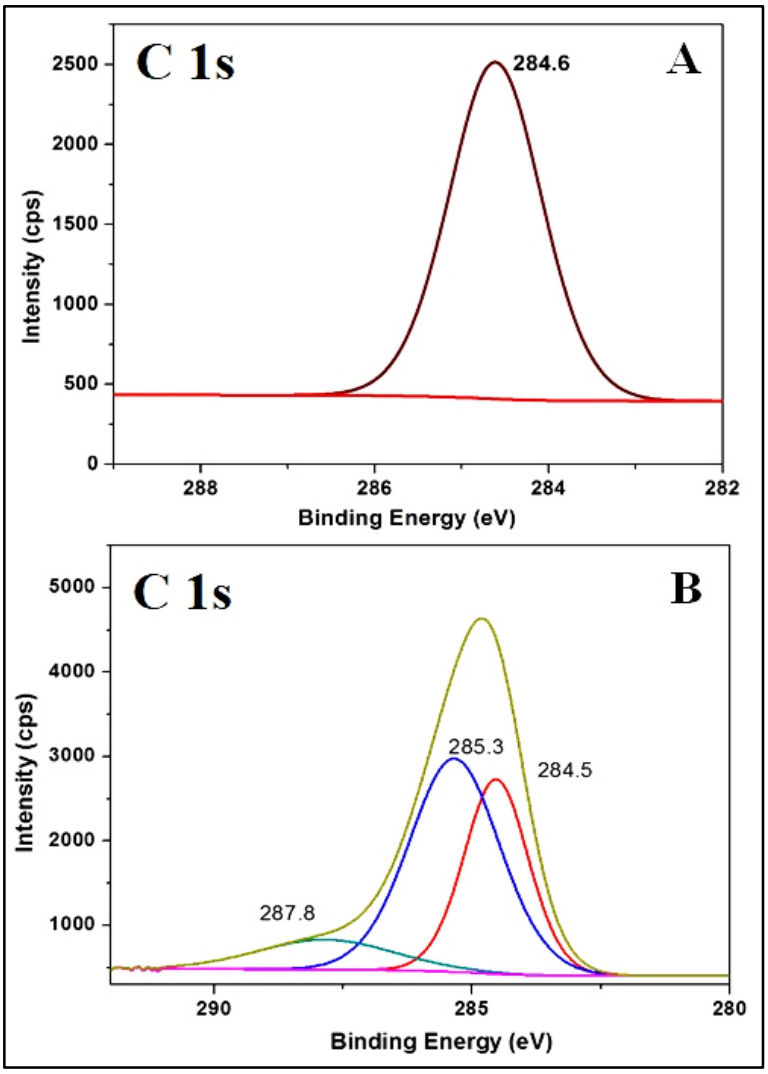


**Figure VI.1.8:** XPS deconvolution spectra of C 1s for copper sample immersed in 200 ppm NaCl **(A)** in the absence of inhibitor **(B)** in presence of 30 ppm CX as inhibitor. (10 day immersion time).

Figure VI.1.8A represents the computer deconvolution spectra for carbon in the absence of inhibitor (control) and figure VI.1.8B presents the C 1s spectrum in presence of 30 ppm CX as inhibitor. In the case of control, the deconvolution spectrum for C 1s **(**Figure VI.1.8A**)** shows a single peak at 284.6 eV. This peak corresponds to the contaminant carbon, which is mainly because of the cracking of vacuum oil used in the XPS instrument[8]. Whereas, in the case of inhibitor **(**figure VI.1.8B**)** three distinct peaks are observed one each at 284.5 eV, 285.3 eV and at 287.8 eV. These peaks can attributed to different types of carbon environment present in chitin xanthate namely C – O, C – N and C – S. This result is a clear evidence for the presence of inhibitor molecules in the surface film. The peak observed at 287.8 eV can be ascribed to the carbon in C–N bonds

present in chitin molecule and also to the carbon in C–S bond[9], which is present in the xanthated derivative of chitin.

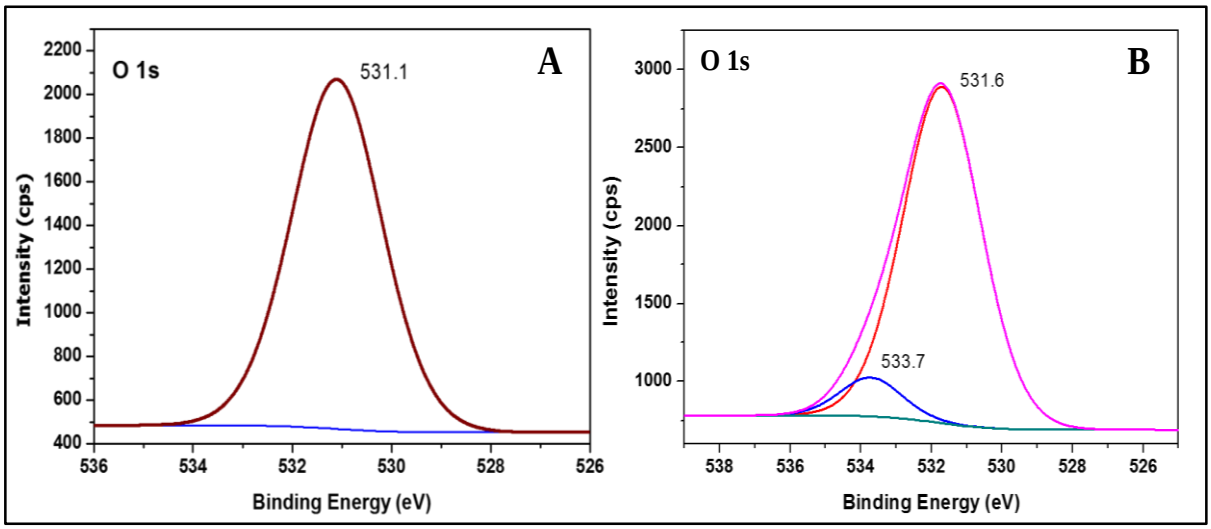


**Figure VI.1.9:** XPS deconvolution spectra of O 1s for copper sample immersed in 200 ppm NaCl **(A)** in the absence of inhibitor **(B)** in presence of 30 ppm CX as inhibitor. (10 day immersion time).

The O 1s deconvolution spectrum of copper immersed in control shows a single peak (Figure VI.1.9A), at a binding energy value of 531.1 eV. This peak can be assigned to oxygen in the oxidizing state of $O^{2-}$, which is mainly present in the form of cupric oxide (CuO), related to the bond with Cu (II)[10]. Copper oxide can exist in two different forms. But, cuprous oxide is further oxidised to cupric oxide[11] which is a consequence of the longer immersion time of the sample in the corrosive environment for ten days. In the case of O 1s deconvolution spectrum for copper immersed in corrosive environment with 30 ppm CX (Figure VI.1.9B), the spectrum shows two distinct peaks, one with high intensity at a binding energy value of 531.6 eV and the other peak at low intensity at a binding energy value of 533.7 eV. The former one can be interpreted as the oxygen present in the oxides and hydroxides of copper which are formed on the metal surface during the course of initial corrosion and the later one can be interpreted as oxygen present in the inhibitor molecule which is bound to carbon through formation of a complex with copper[11].

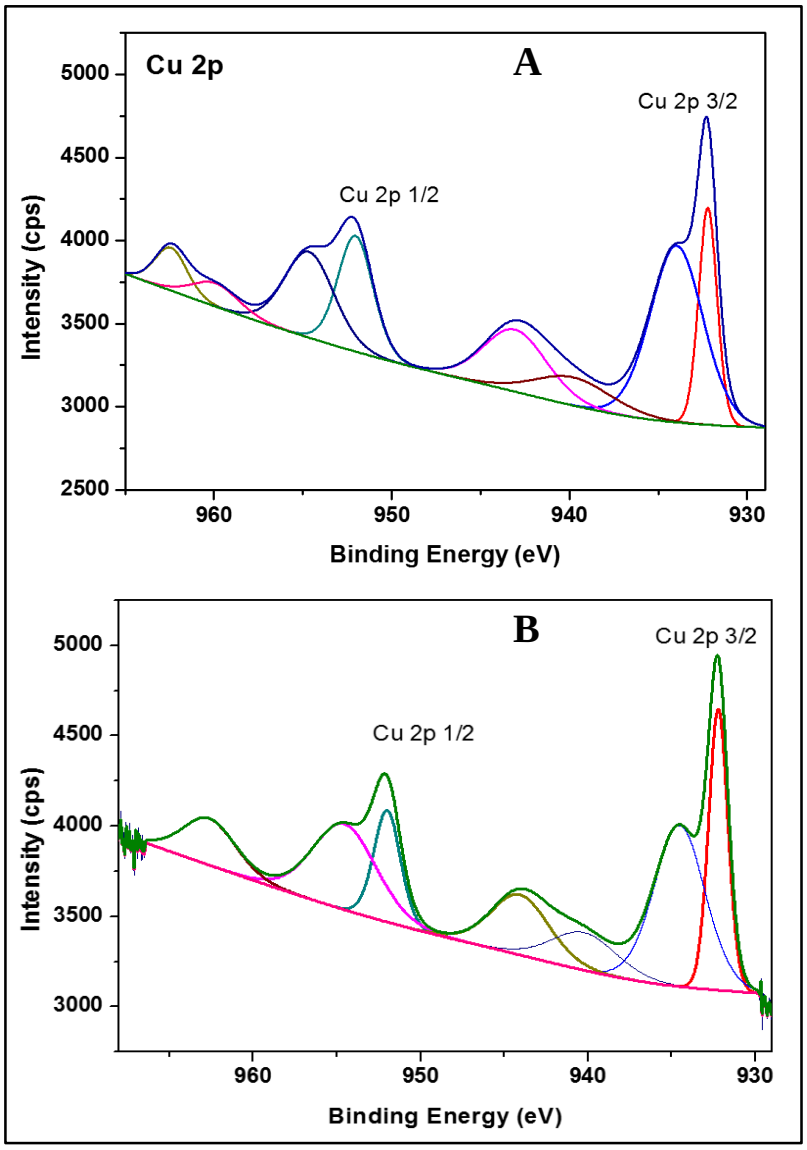


**Figure VI.1.10:** XPS deconvolution spectra of Cu 2p for copper sample immersed in 200 ppm NaCl **(A)** In the absence of inhibitor **(B)** in presence of 30 ppm CX as inhibitor. (10 day immersion time).

The deconvolution spectrum of copper in general consists of two peaks. One is attributed to Cu $2p_{3/2}$ and the other one to Cu $2p_{1/2}$. The Cu $2p_{3/2}$ peak is employed to investigate the oxidation state of copper. Figures VI.1.10A and VI.1.10B show the main and the satellite peaks of Cu $2p_{3/2}$ and Cu $2p_{1/2}$ of copper substrate immersed in corrosive environment without and with inhibitor respectively. Based on the standard reference data base, the binding energy values for Cu $2p_{1/2}$ and Cu $2p_{3/2}$ peaks for the pure Cu are located between 952.45–952.56 eV and 932.20–933.1 eV, respectively[10]. For control, we have observed the Cu $2p_{3/2}$ peak at 933.9 eV, which is higher by 2 eV in comparison to that of elemental copper. Therefore, it infers the presence of Cu in the form of Cu (II). Appearance

of strong satellite peaks further supports the presence of Cu (II). It is reported in the literature that the Cu $2p_{3/2}$ peak for the CuO is between 932.7 eV, 934.6 eV[10]. We have also observed another peak at 932.4 eV, which is ascribed to elemental copper.

In the presence of inhibitor, we have observed one Cu $2p_{3/2}$ peak at 934.2 eV. A clear positive shift of 2 eV from that of elemental Cu indicates the presence of Cu in Cu (II) form on the surface. This inference is further confirmed by the presence of shakeup satellites. In the present investigation, the most probable Cu(II) containing species are CuO, $Cu(OH)_2$.and [Cu (II)-CX] complex, which is also a constituent in the surface film. The other peak at 932.4 eV is interpreted due to the presence of elemental copper.

The XPS survey spectrum of the film on copper in the corrosive environment in presence of inhibitor also consists peaks due to two other elements namely nitrogen and sulphur. The deconvolution spectra for these elements are shown in the figures VI.1.11 and VI.1.12 respectively. Two distinct peaks are observed for N 1s at 398.9 eV and 400.2 eV indicating two different nitrogen environments present in the inhibitor molecule. The characteristic binding energy value for the nitrogen element is 398.0 eV[12,13]. Considerable shift in the binding energy value signifies the role of the nitrogen atom in the corrosion inhibition process by complex formation with metal. The lower binding energy value peak is ascribed to nitrogen bound to carbon (C-N) which is a possibility in the present inhibitor context (CX), and the higher binding energy value peak is attributed to nitrogen bound to copper. It donates its electron pair to $Cu^{2+}$ to form a coordination complex. Therefore, the binding energy of N 1s is increased. It is difficult to remove an electron from the outermost shell of nitrogen atom due to bond formation.

The S 2p deconvolution spectrum consists of two peaks, one at 161.8 eV and other one at 162.4 eV, which are ascribed to S $2p_{3/2}$ and S $2p_{1/2}$ respectively. These peaks interpret the presence of sulfur in the surface film. The binding energy value of S $2p_{3/2}$ (161.8 eV) indicates that sulphur is bound to copper [14–16].

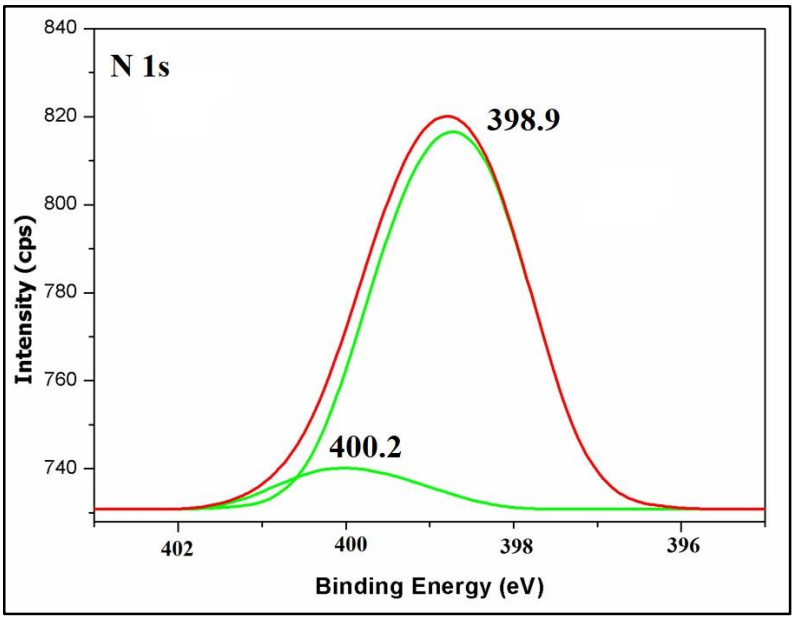


**Figure VI.1.11:** XPS deconvolution spectra of N 1s for copper sample immersed in 200 ppm NaCl in presence of 30 ppm CX as inhibitor. (10 day immersion time).

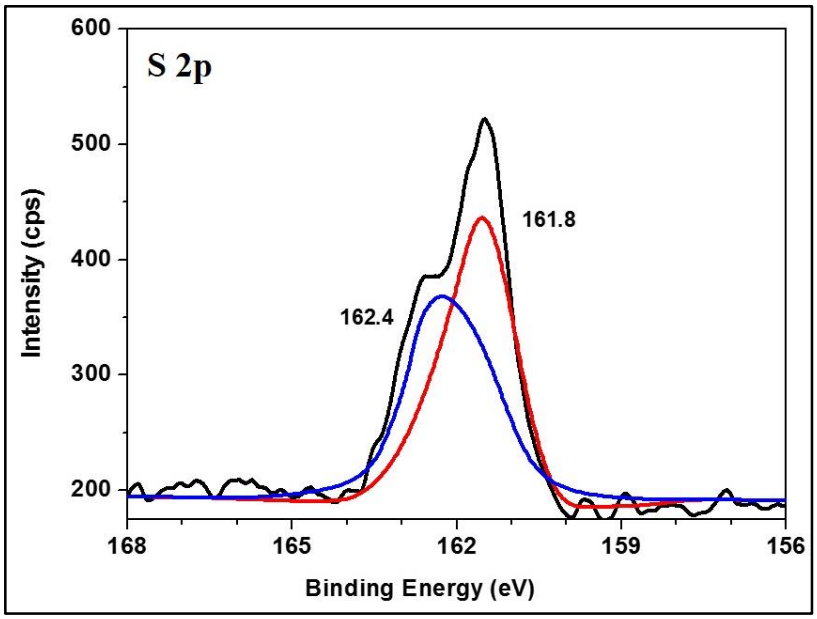


**Figure VI.1.12:** XPS deconvolution spectra of S 2p for copper sample immersed in 200 ppm NaCl in presence of 30 ppm CX as inhibitor. (10 day immersion time).

Thus, the XPS spectra confirm the formation of [Cu(II)- CX] complex by coordination between N and S atoms present in chitin xanthate with Cu (II).

**VI.1.6: Analysis of the surface film by X- ray diffraction studies (XRD):**

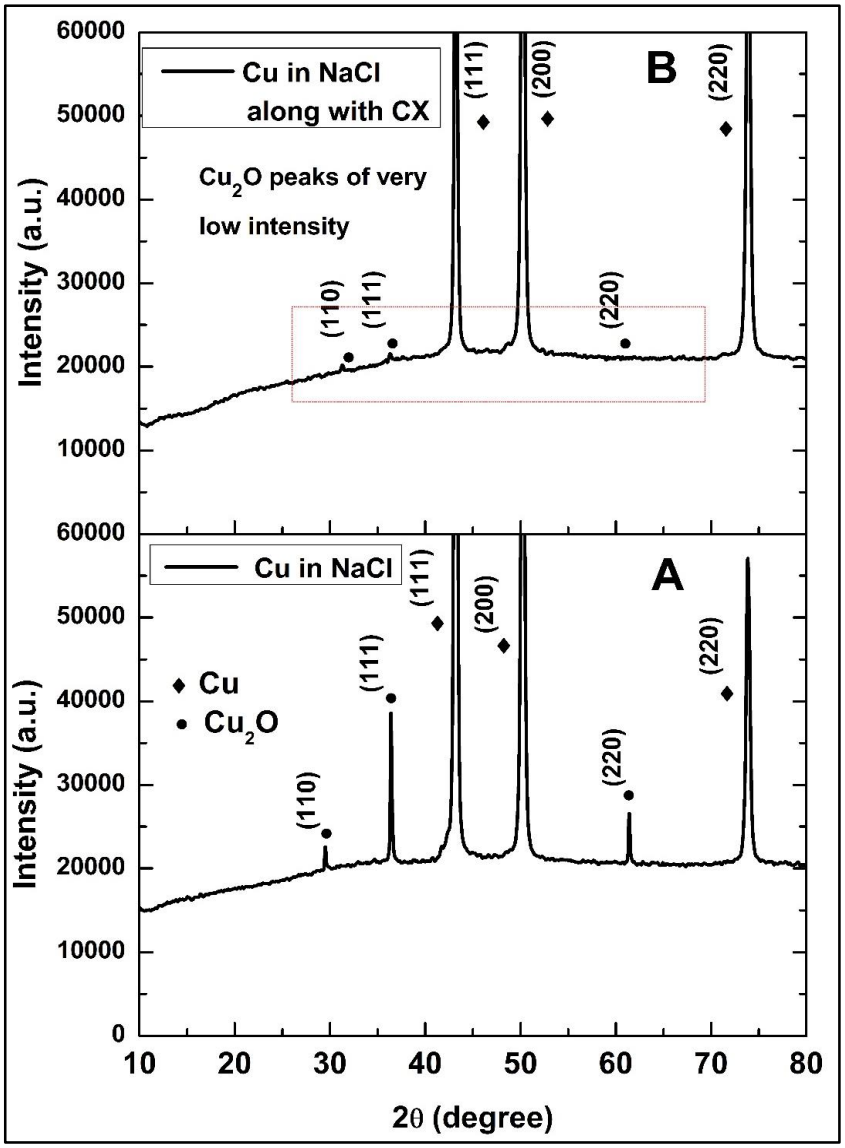


**Figure VI.1.13:** The X-ray diffraction patterns of the surface film formed on copper sample immersed in 200 ppm NaCl (A) in the absence (B) in the presence of CX (30 ppm).

Figure VI.1.13(A) and VI.1.13(B) presents the X-ray diffractograms of the surface of copper specimen immersed in 200 ppm NaCl environment in the absence and presence of chitin xanthate (CX) respectively. In the absence of inhibitor the difractogram shown peaks for base material copper and copper corrosion product ($Cu_2O$) [17,18]. The planes which represent $Cu_2O$ in the spectrum are (1 1 0), (1 1 1) and (2 2 0). The XRD pattern doesn't show any peak for CuO, which is the predominant corrosion product and is exhibited in XPS spectrum. This can be explained by the fact that the CuO is only present in the topmost layer of the film, XRD can analyse the film within about 10 µm of the surface[19]. In other words, the XRD can analyse the inner layers of the surface. Since, the

inner layers of the corrosion product on the copper surface only contain $Cu_2O$, the XRD pattern shows $Cu_2O$ peaks only[20].

In the presence of CX as inhibitor the difractogram shows peaks for base material copper and the intensities of the peaks of corrosion product $Cu_2O$.are extremely less Moreover, only peaks for planes (1 1 0), (1 1 1) are observed. There is no sign of (2 2 0) peak in the XRD pattern. This implies that the surface of copper consists of very less amount of corrosion product in presence of CX as inhibitor. This result infers that in the presence of chitin xanthate, corrosion rate of copper is controlled.

### VI.1.7: Langmuir adsorption isotherm:

The interaction between the inhibitor molecule (CX) and metal surface can give an idea about the inhibition mechanism. Different adsorption isotherm models were taken into consideration to understand the inhibition mechanism of CX. Among them, the Langmuir adsorption isotherm model is well fitted (based on the correlation coefficient value). The Langmuir adsorption is given in equation (1).

$$\frac{C}{\emptyset} = \frac{1}{K_{ads}} + C \ldots\ldots\ldots\ldots\ldots\ldots\ldots\ldots\ldots (1)$$

Here, $\emptyset$ is the surface coverage of the inhibitor molecule (Which is obtained by the relation, I. E. $\% = \emptyset\, X\, 100$), C is the concentration of CX (the monomer molecular weight is taken to calculate the concentration ) and $K_{ads}$ is the equilibrium constant.

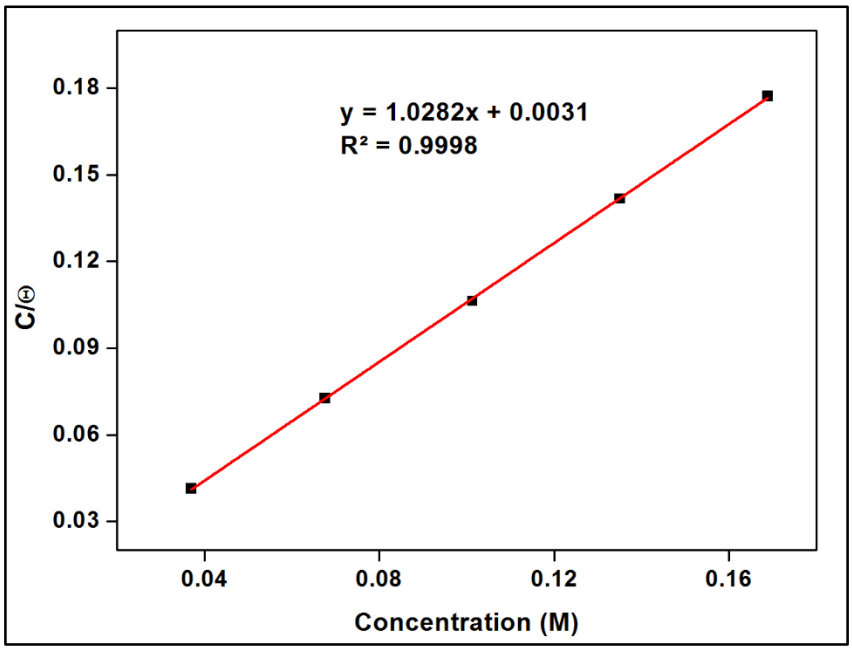


**Figure VI.1.14:** Langmuir adsorption isotherm for the adsorption of chitin xanthate on copper surface.

Figure VI.1.14 represents $C/\emptyset\ Vs\ C$ plot for adsorption of chitin xanthate on copper surface. A linear plot is obtained with a good correlation coefficient value ($R^2$= 0.9998), which infers that the adsorption process follows the Langmuir adsorption isotherm model.

**VI.1.8: Mechanistic aspects of corrosion and corrosion inhibition:**

The corrosion of metals whether it is mild steel or copper in neutral environment is well established [6,21]. However, the anodic and cathodic reactions are reproduced below.

At anode

$$Cu + Cl^- \rightleftharpoons CuCl + e^- \quad \text{(2) film formation reaction}$$

$$CuCl + Cl^- \rightleftharpoons CuCl_2^- \quad \text{(3) film dissolution reaction}$$

At cathode

$$H_2O + 1/2O_2 + 2e^- \longrightarrow 2OH^- \quad (4)$$

This cupric chloride complex further dissolved to form,

$$CuCl_{2\,(ads)}^- \rightleftharpoons Cu^{2+} + 2Cl^- + e^- \quad (5)$$

$$Cu^{2+} + 2OH^- \rightleftharpoons Cu(OH)_2 \quad (6)$$

When chitin xanthate (CX) is used as an inhibitor, the CX molecules get adsorbed on the copper surface through chemisorption. By adsorbing on the metal surface the inhibitor molecules form a protective film, by the formation of a coordination complex with Cu(II) ions available on copper surface due to initial corrosion. This protective film is responsible for the corrosion inhibition. This phenomenon is confirmed by the surface analytical studies, which gave a clear evidence for the presence of inhibitor molecule on the surface film. The protective film on the copper surface blocks the contact between metal and corrosive environment and minimizes the diffusion of ions and molecules to and from the metal surface, ultimately imparts corrosion protection of copper in aqueous chloride environment[22]. The plausible interaction mechanism of chitin xanthate with copper surface is given in figure VI.1.15.

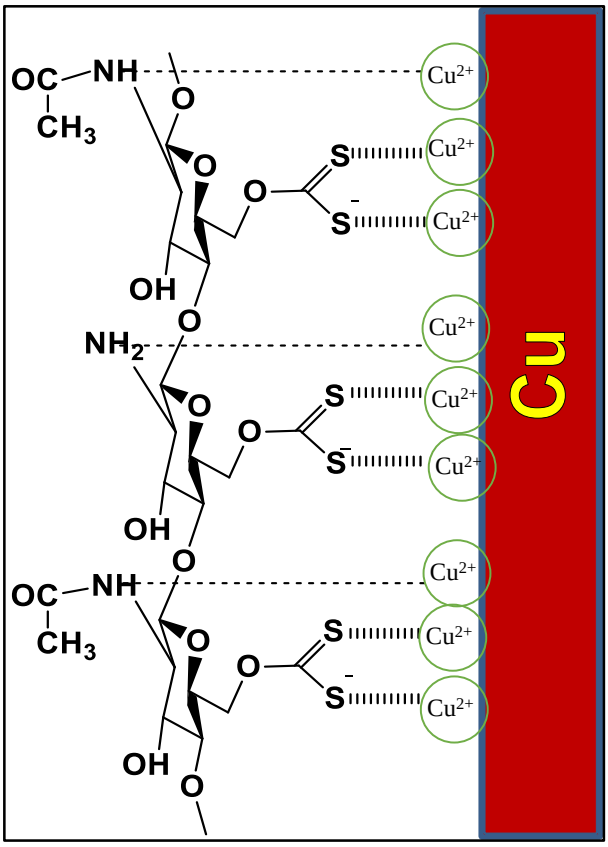


**Figure VI.1.15:** plausible interaction mechanism of chitin xanthate with copper.

# Chapter VI

## VI.2. Phosphorylated xanthan gum (PXG) as an inhibitor to control the mild steel corrosion in neutral chloride environment.

In this section we report the chemical modification of xanthan gum into phosphorylated xanthan gum and its influence in minimizing the corrosion of mild steel in neutral chloride environment.

### VI.2.1: Characterization of phosphorylated xanthan gum (PXG):

The synthetic procedure for the chemical modification of xanthan gum has been already discussed in the 'materials and methods' section of chapter III of this thesis. This synthesized phosphorylated derivative was characterized by Fourier Transform Infrared spectroscopy (FTIR). The FTIR spectra of xanthan gum and phosphorylated xanthan gum are shown in Figure VI.2.1.

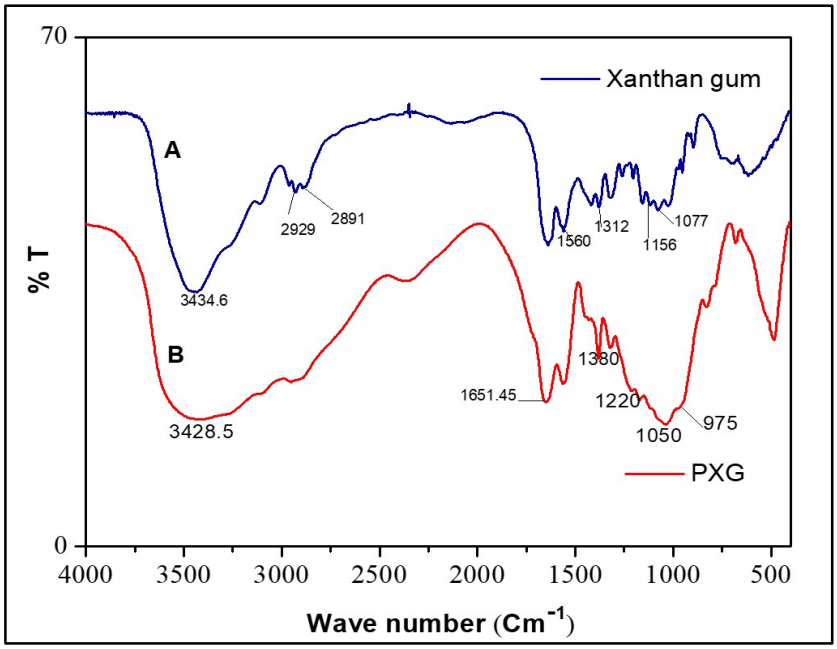


**Figure VI.2.1:** FTIR spectra of (A) xanthan gum and (B) Phosphorylated xanthan gum (PXG).

Figure VI.2.1A presents the FTIR spectrum of xanthan gum and figure VI.2.1B shows the FTIR spectrum of phosphorylated xanthan gum (PXG). In the spectrum of PXG, a broad band at 3428 $cm^{-1}$ is assigned to P-OH stretching vibrations. The peak at 1220 $cm^{-1}$ is attributed to phosphate group (P=O asymmetric stretching)[23], which infers that phosphate group has been successfully added on the xanthan gum backbone. The peak at 1050 $cm^{-1}$ can be attributed to C-O-P stretching in phosphate ester and the peak at

975 $cm^{-1}$ is due to P-OH stretching. Presence of a broad band between 900 $cm^{-1}$ to 1100 $cm^{-1}$ is also an indication of phosphorylation[24].

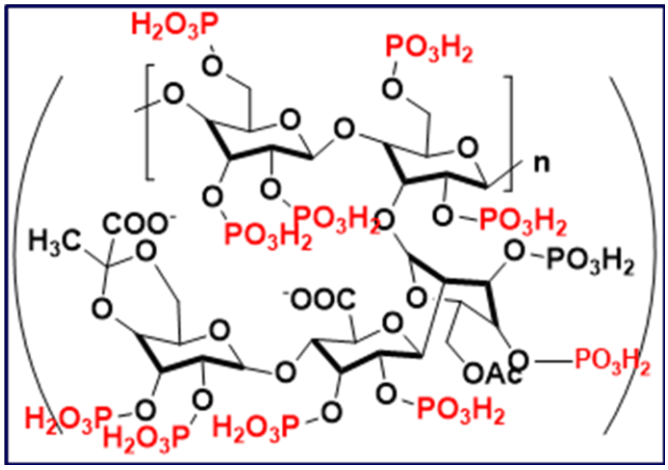


**Phosphorylated xanthan gum (PXG)**

Weight-loss studies, electrochemical impedance studies and potentiodynamic polarization studies were carried out to investigate the corrosion inhibition ability. SEM-EDX, XPS and XRD studies were employed for surface analytical studies.

### VI.2.2: Analysis of the results of weight-loss Studies:

The ability of phosphorylated xanthan gum (PXG) in inhibiting the corrosion of mild steel in 200 ppm NaCl environment has been investigated using the weight-loss studies at 30°C after 7 days immersion period. The corrosion rate and inhibition efficiency of PXG obtained through weight-loss studies are reported in the table VI.2.1. From the experimental data it can be deduced that in presence of PXG the corrosion rate of the mild steel in 200 ppm NaCl decreased considerably. This effect is observed in all the tested concentrations of PXG. This decrease in corrosion rate reveals that PXG can inhibit the corrosion of mild steel in neutral chloride environment. From the table VI.2.1, the weigh-loss of mild steel in the absence of any inhibitor is found to be 14.24 mg. When a small concentration (25 ppm) of PXG is added, the weight-loss of mild steel is decreased noticeably to 6.12 mg, acquiring an inhibition efficiency of 57 %. When the concentration of PXG is increased to 50 ppm the weight-loss is further decreased to 4.92 mg, with an inhibition efficiency of 65 %. For 100 ppm of PXG the weight-loss is 3.12 mg with an inhibition efficiency of 78 %. This decrease in weight-loss profile followed up to 150 ppm PXG as inhibitor and after that there is a slight increase in weight-loss for 200 ppm PXG as inhibitor. The highest inhibition efficiency of 88 % was obtained for 150 ppm PXG as inhibitor. This increase in inhibition efficiency as the concentration of inhibitor increased

can be explained by an increase in the extent of metal surface coverage by the inhibitor molecules. At 150 ppm PXG, the concentration of inhibitor was sufficient to cover the metal surface completely. As a consequence, the contact between metal surface and the corrosive environment has been efficiently blocked. When the concentration of PXG is further increased to 200 ppm, the weight-loss of mild steel is slightly increased and slightly higher corrosion rate is observed when compared to the case of 150 ppm PXG. This may be explained ass follows. 150 ppm PXG concentration is sufficient and optimum to form a protective film. At this concentration PXG molecules form a complex, [Fe(III)-PXG] on mild steel surface by interacting with $Fe^{3+}$ ions available due to initial corrosion of the metal. This complex along with iron oxides form a protective film, which completely covers the surface. When the concentration of PXG is increased to 200 ppm; 150 ppm PXG is sufficient to form the [Fe(III)-PXG] complex, and the remaining PXG molecules also compete for sites on the surface. Therefore, the surface film may consist of PXG molecules, [Fe(III)-PXG] complex and iron oxides. This film may not be as protective as the film consisting of [Fe(III)-PXG] complex and iron oxides.

**Table.VI.2.1:** Corrosion parameters for mild Steel in 200ppm NaCl in absence and presence of different concentrations of phosphorylated xanthan gum obtained from the gravimetric method.

| S.No. | Concentration of PXG (ppm) | Weight - loss(mg) | Corrosion Rate(mdd) | Corrosion Rate (mmpy) | I.E.% |
|---|---|---|---|---|---|
| 1 | 0 | 14.24 | 20.49 | 0.09513 | - |
| 2 | 25 | 6.12 | 8.80 | 0.04088 | 57 |
| 3 | 50 | 4.92 | 7.08 | 0.03282 | 65 |
| 4 | 100 | 3.12 | 4.49 | 0.02079 | 78 |
| 5 | 150 | 1.73 | 2.49 | 0.01151 | 88 |
| 6 | 200 | 2.51 | 3.61 | 0.01676 | 82 |

### VI.2.3: Analysis of the results of Electrochemical Studies:

### Electrochemical Impedance Studies

The electrochemical impedance studies were performed at the open circuit potential in the absence and presence of various concentrations of phosphorylated xanthan

gum (PXG) in neutral aqueous chloride environment. Although the impedance studies were done at different immersion periods in the range from 1 hour to 48 hours with a six hour interval. It was found that 24 h immersion time was adequate to afford the highest inhibition efficiency. Therefore, 24 h immersion time was fixed as the immersion time in the impedance studies.

The Nyquist plots for mild steel specimen immersed in 200 ppm sodium chloride environment in the absence and presence of different concentrations of phosphorylated xanthan gum (PXG) as inhibitor are presented in the figure VI.2.2. The corresponding Bode plots are presented in figure VI.2.3. Figure VI.2.3A represents the Bode plots in the form of total impedance vs frequency and figure VI.2.3B represents the Bode plots in the form of phase angle vs frequency. The experimental values have been fitted with different equivalent circuits in order to obtain the best fit and calculate various corrosion parameters. The experimental data fitted well with the simple Randles equivalent circuit with a very low error. The simple Randles circuit is shown in the figure VI.2.4. Similar equivalent circuit was also reported by other researchers[25,26] in this field. The equivalent circuit consists of solution resistance ($R_s$), charge transfer resistance ($R_{ct}$), and a constant phase element (CPE). The calculated corrosion parameters from EIS data are reported in the table VI.2.2.

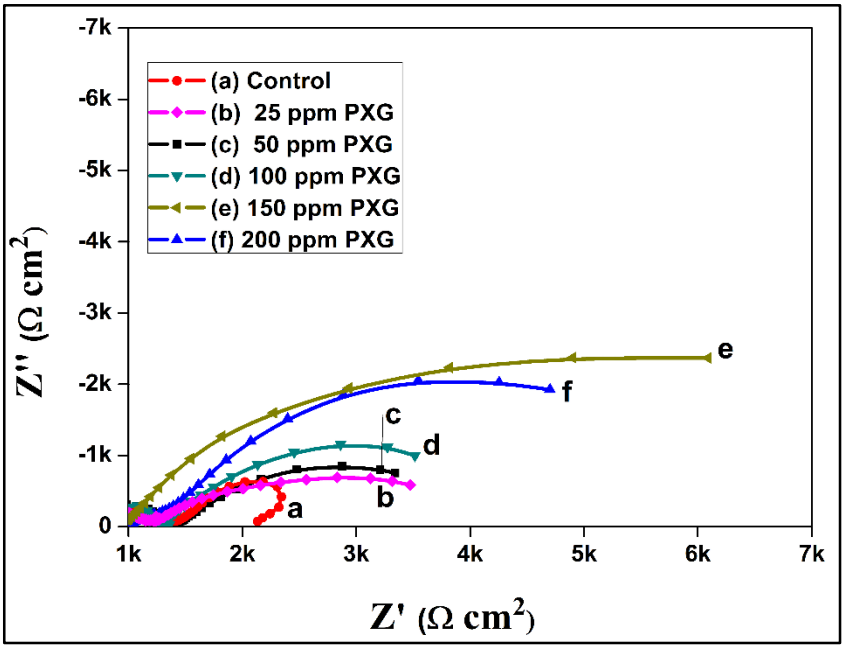


**Figure VI.2.2**: Nyquist plots of mild steel sample immersed in 200 ppm NaCl (a) control (b) in presence 25 ppm PXG (c) 50 ppm PXG (d) 100 ppm PXG (e) 150 ppm PXG (f) 200 ppm PXG (24 h immersion period).

From the figure VI.2.2, it can be observed that in all the cases, whether it is in the absence of inhibitor or in presence of various concentrations of PXG as inhibitor, the plots are of depressed semi-circular pattern whose centre is below the horizontal axis. In presence of inhibitor the diameter of the depressed semicircle is increased when compared to control. Moreover, the diameter of the depressed semi-circle is increased with an increase in concentration of the inhibitor. In the absence of inhibitor we have got a charge transfer resistance of 2.0 kΩ $cm^2$, which has been increased considerably in the presence of inhibitor at all concentrations. In the presence of 25 ppm PXG, the $R_{ct}$ value is increased to 4.1 kΩ $cm^2$ acquiring an inhibition efficiency of 50 %. As the concentration of the inhibitor is increased up to 150 ppm PXG, the $R_{ct}$ is increased even more in a linear profile. In the presence of 50 ppm PXG the value is further increased to 5.3 kΩ $cm^2$, with an inhibition efficiency of 61 %. Highest inhibition efficiency of 93 % is observed at 150 ppm of PXG concentration with a charge transfer value of 19.9 kΩ $cm^2$. The $R_{ct}$ value observed is slightly less when 200 ppm PXG is used as inhibitor, as compared to 150 ppm PXG. The reason for a slight decrease in the efficiency of the inhibitor with increase in concentration form 150 to 200 ppm PXG has already been explained in the section VI.2.2 under the 'analysis of results of weight-loss studies' The increase in the $R_{ct}$ value in presence of inhibitor is because of the minimization of metal dissolution in presence of inhibitor. This result is a consequence of the formation of a protective film by the inhibitor molecules. The addition of inhibitor decreased the double layer capacitance ($C_{dl}$). This decrease in $C_{dl}$ is attributed to the replacement of adsorbed water molecules on the metal surface by the inhibitor molecules, which have low dielectric constant. These results infer the adsorption of inhibitor on the metal | solution interphase.

Figure VI.2.3A represents the Bode plots from which we can observe that the total impedance value is increased significantly when PXG is added as the inhibitor. As the concentration of PXG is increased, the total impedance value is also increased indicating the minimization of charge transfer from metal to solution phase and from solution phase to metal. However, the total impedance is reduced with increase in concentration from 150 to 200 ppm. It is also interesting to note that the charge transfer region has shifted to low frequency range namely 1Hz to 10 mHz when high concentrations of PXG are used as inhibitor.

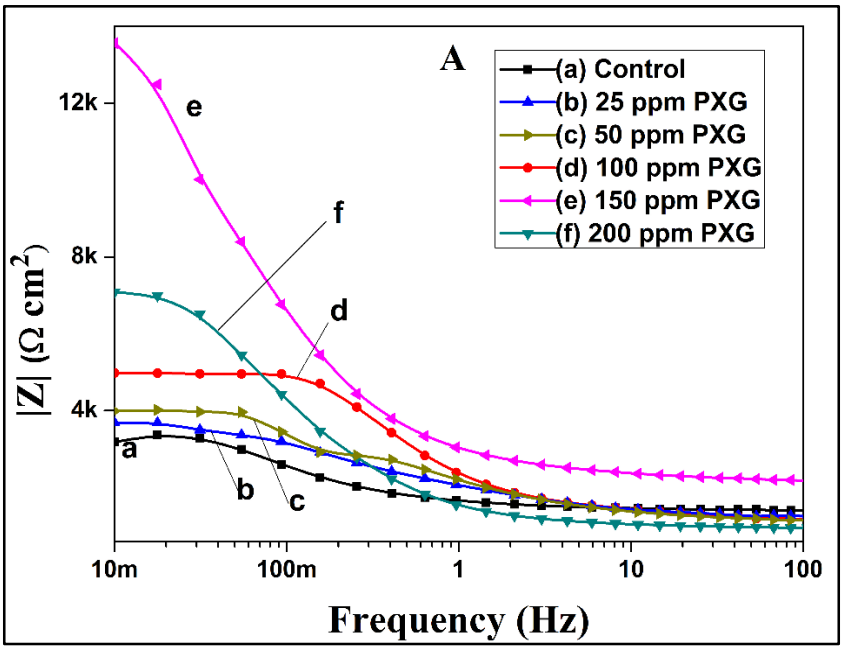


**Figure VI.2.3**: **(A)** Bode plots (Total impedance vs frequency) for mild steel specimen in 200 ppm NaCl **(a)** in the absence of inhibitor **(b)** in presence 25 ppm PXG **(c)** 50 ppm PXG **(d)** 100 ppm PXG **(e)** 150 ppm PXG **(f)** 200 ppm PXG (24 h immersion period).

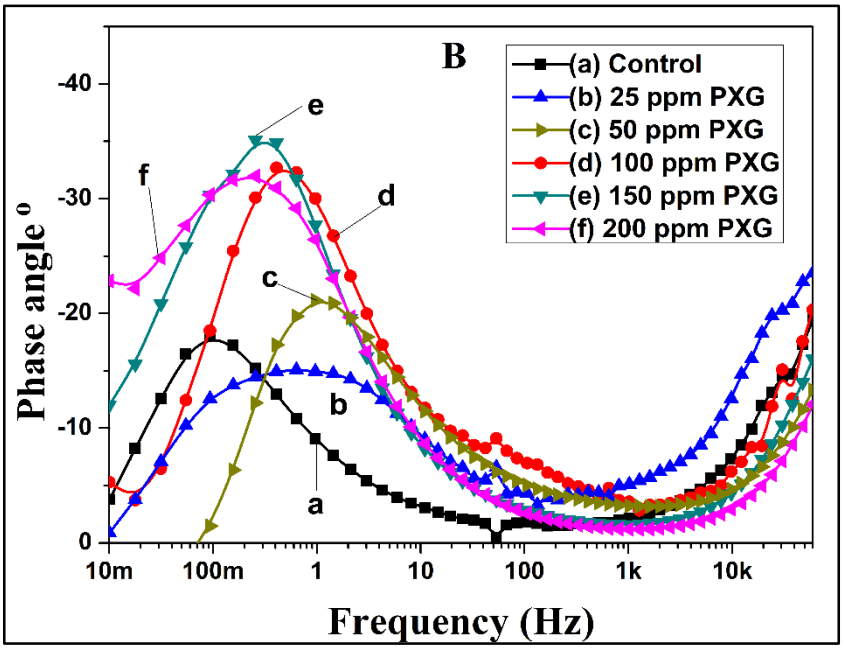


**Figure VI.2.3**: **(B)** Bode plots (Phase angle vs frequency), for mild steel specimen in 200 ppm NaCl (a) in the absence of inhibitor (b) in presence 25 ppm PXG (c) 50 ppm PXG (d) 100 ppm PXG (e) 150 ppm PXG (f) 200 ppm PXG (24 h immersion period).

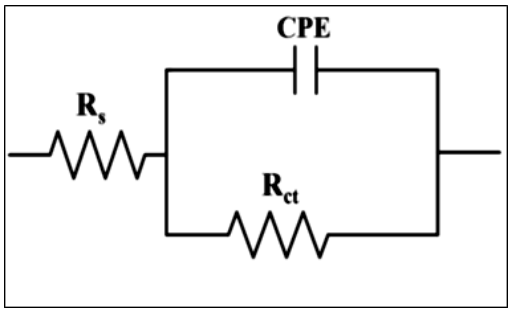


**Figure VI.2.4:** Equivalent circuit used (Simple Randles Circuit)

$R_s$- Solution Resistance, $R_{ct}$ - Charge transfer resistance, CPE - Constant phase element.

Figure VI.2.3B shows the Bode plots (Phase angle vs frequency). From the curves it can be interpreted that the addition of PXG as inhibitor increased the phase angle maximum to higher values. The phase angle maximum is around 35º in the case of control, which has been increased to 70º in presence of 150 ppm PXG as inhibitor. The formation of a protective film on the metal surface in presence of PXG contributed to increase in the phase angle maximum.

From the table VI.2.2, we can also observe an increase in the 'n' value when PXG is added as inhibitor when compared to control. The 'n' value for control is observed as 0.557. Such a low value of n indicates mass transport from metal to solution. Even in the presence of inhibitor the highest 'n' value observed is 0.726, which is however less than '1'. This result indicates significant improvement of the surface homogeneity in presence of PXG, which is a consequence of the adsorption of PXG molecule on the metal surface to form a protective film.

**Table VI.2.2**: Impedance parameters for mild steel in 200ppm aq. NaCl solution in the absence and presence of different concentrations of PXG.

| S.No. | Concentration of PXG (ppm) | $R_{ct}$(kΩ $cm^2$) | $C_{dl}$(µF $cm^{-2}$) | n | I.E.% |
|---|---|---|---|---|---|
| 1 | 0 | 2.0 | 21.5 | 0.557 | - |
| 2 | 25 | 4.1 | 20.1 | 0.630 | 50 |
| 3 | 50 | 5.3 | 15.6 | 0.708 | 61 |
| 4 | 100 | 7.1 | 14.9 | 0.726 | 71 |
| 5 | 150 | 27.4 | 13.8 | 0.677 | 93 |
| 6 | 200 | 19.9 | 13.5 | 0.659 | 90 |

**Potentiodynamic polarization studies:**

The cathodic and anodic Tafel curves for mild steel specimen immersed in 200 ppm NaCl environment in the absence and presence of different concentrations of PXG at a pH of 7 and a temperature of 30±0.1ºC are shown in the figure VI.2.5. The corrosion parameters have been calculated from the polarization curves by extrapolating the cathodic and anodic Tafel regions. The calculated corrosion parameters such as corrosion potential ($E_{corr}$), corrosion current density ($j_{corr}$), anodic Tafel slope (βa) and cathodic Tafel slope (βc) are listed in table VI.2.3. The corrosion current density ($j_{corr}$) values have been used to calculate the corrosion inhibition efficiencies in the presence of PXG as inhibitor.

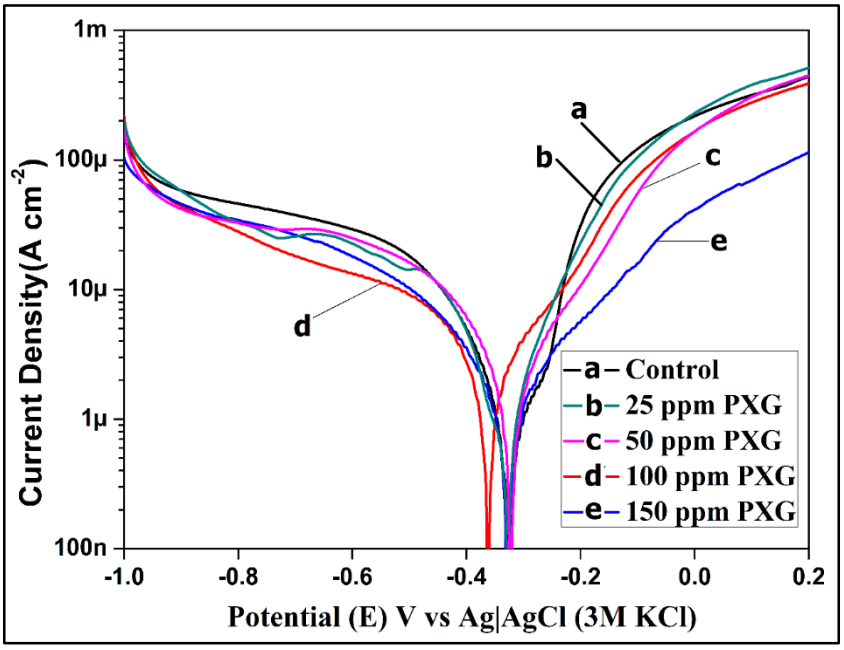


**Figure VI.2.5:** Potentiodynamic polarization curves for mild steel specimen immersed in 200 ppm NaCl solution **(a)** in the absence of inhibitor **(b)** in presence 25 ppm PXG **(c)** 50 ppm PXG **(d)** 100 ppm PXG **(e)** 150 ppm PXG.

From the potentiodynamic polarization curves, it can be observed that in presence of PXG as inhibitor, anodic and cathodic current densities are shifted towards lower values at all the concentrations of the inhibitor. This result indicates that PXG inhibits the corrosion of mild steel in 200 ppm NaCl environment. When the inhibitor is not used, the corrosion potential of mild steel specimen immersed in 200 ppm NaCl is found to be -359.9 mv vs Ag|AgCl (3M KCl) and the corresponding corrosion current density is 10.3 µA $cm^{-2}$. When PXG is used as inhibitor, the corrosion potential values are shifted from that of control but not in a regular manner. The corrosion current density values are

decreased considerably at all the concentrations and they are found to be in the range of 4.8 to 1.0 μA $cm^{-2}$. This result suggests that the current passed through the system by virtue of the metal dissolution and charge transfer from the solution to the metal surface has decreased in the presence of PXG. The lowest current density value was found to be 1.0 μA $cm^{-2}$ for 150 ppm of PXG as inhibitor, which affords the highest inhibition efficiency of 90 %.

**Table VI.2.3:** Corrosion parameters obtained from potentiodynamic polarization studies for mild steel specimen immersed in 200 ppm NaCl in absence and presence of various tconcentrations of PXG (Phosphorylated xanthan gum)

| **Concentration of (PXG) (ppm)** | **$E_{corr}$ (mV)** | **$J_{corr}$ (μA $cm^{-2}$)** | **βc (mV $dec^{-1}$)** | **βa (mV $dec^{-1}$)** | **I. E.%** |
|---|---|---|---|---|---|
| 0 | -359.9 | 10.3 | -281 | 186 | - |
| 25 | -355.4 | 4.8 | -188 | 175 | 54 |
| 50 | -320.8 | 3.5 | -220 | 125 | 66 |
| 100 | -371.1 | 1.7 | -146 | 139 | 84 |
| 150 | -319.7 | 1.0 | -129 | 101 | 90 |

When we compare the anodic and cathodic Tafel slopes (βa and βc) in presence of PXG as inhibitor with those of control, we can infer that in presence of inhibitor both the βa and βc values are decreased significantly. This result indicates clearly that, the inhibitor has controlled both the anodic and cathodic corrosion processes. By taking this result also into account, it can be inferred that PXG as inhibitor affects the kinetics of both iron dissolution and oxygen reduction. This nature of the inhibitor makes it as a mixed type inhibitor, which retards both the anodic and cathodic corrosion processes efficiently.

### VI.2.4: Analysis Surface morphology by scanning electron microscopy and EDX:

The surface topography of the mild steel specimens immersed in 200 ppm NaCl for 7 days in the absence and presence of 150 ppm PXG as inhibitor has been studied using scanning electron microscopy (SEM) and the surface films formed during corrosion and inhibition process have been analyzed by energy dispersive X-ray spectroscopy (EDX). Figure VI.2.6A shows the surface micrographic image of the polished mild steel specimen. Figure VI.2.6B depicts the SEM image of mild steel specimen after immersing it in 200 ppm NaCl for 7 days and the figure VI.2.6C represents the SEM image of mild steel

immersed in 200 ppm NaCl along with 150 ppm PXG as inhibitor. These SEM images show clear evidence that when the metal samples are immersed in the corrosive environment along with PXG, the surface does not show any damage and only the inhibitor film can be seen on the metal surface. Because of very less corrosion rate the smoothness of the surface is retained in presence of PXG.

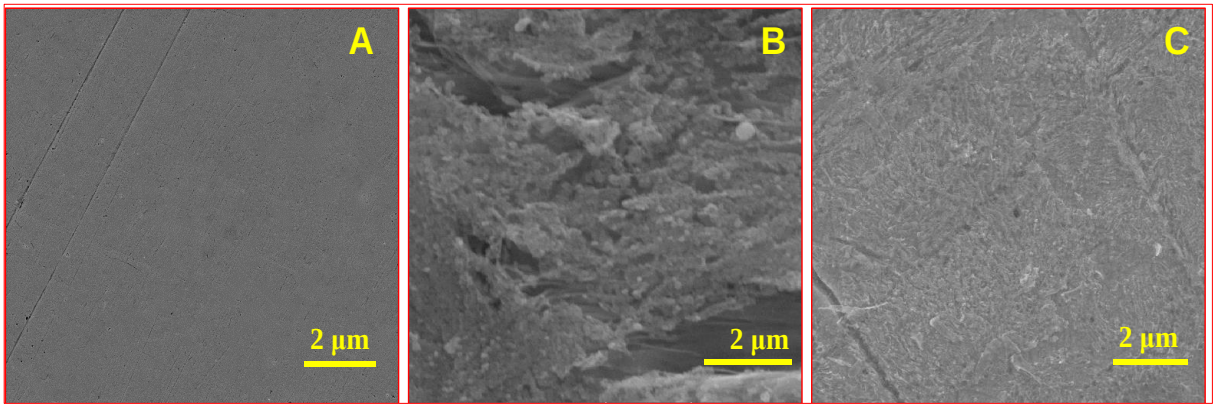


**Figure VI.2.6:** Scanning Electron Microscopic images of mild steel (A) polished sample (B) immersed in 200 ppm NaCl. (C) Immersed in 200 ppm NaCl with 150 ppm of PXG. (X10,000 magnification).

Figure VI.2.7A represents the energy dispersive X-ray spectrum (EDX) of the surface of mild steel specimen immersed in 200 ppm NaCl in the absence of any inhibitor. Whereas, figure VI.2.7B represents the energy dispersive X-ray spectrum of mild steel surface immersed in 200 ppm NaCl along with 150 ppm PXG as inhibitor. Both these spectra represent the composition of the surface film on the mild steel. In the absence of inhibitor, the intensity of the oxygen peak is much higher when compared to the oxygen peak in the presence of inhibitor. This result interprets the presence of iron oxides which are present in the corrosion product. Small peaks due to C and Mn are due to the elements present in mild steel. In presence of PXG (figure VI.2.7B), the surface film consists of carbon, oxygen and phosphorous along with iron. These three elements are the constituents of the inhibitor molecule namely phosphorylated xanthan gum. This result confirms that the surface film consists of the inhibitor molecule along with oxides and hydroxides of iron. However, as the intensity of the oxygen peak is much less than that of the control, the amount of oxides and hydroxides of iron is much less in the inhibited film. Moreover, it may also be noted that oxygen is also present in the structure of the xanthan gum. This oxygen also contributes to the oxygen peak intensity in EDX spectrum of the surface film.

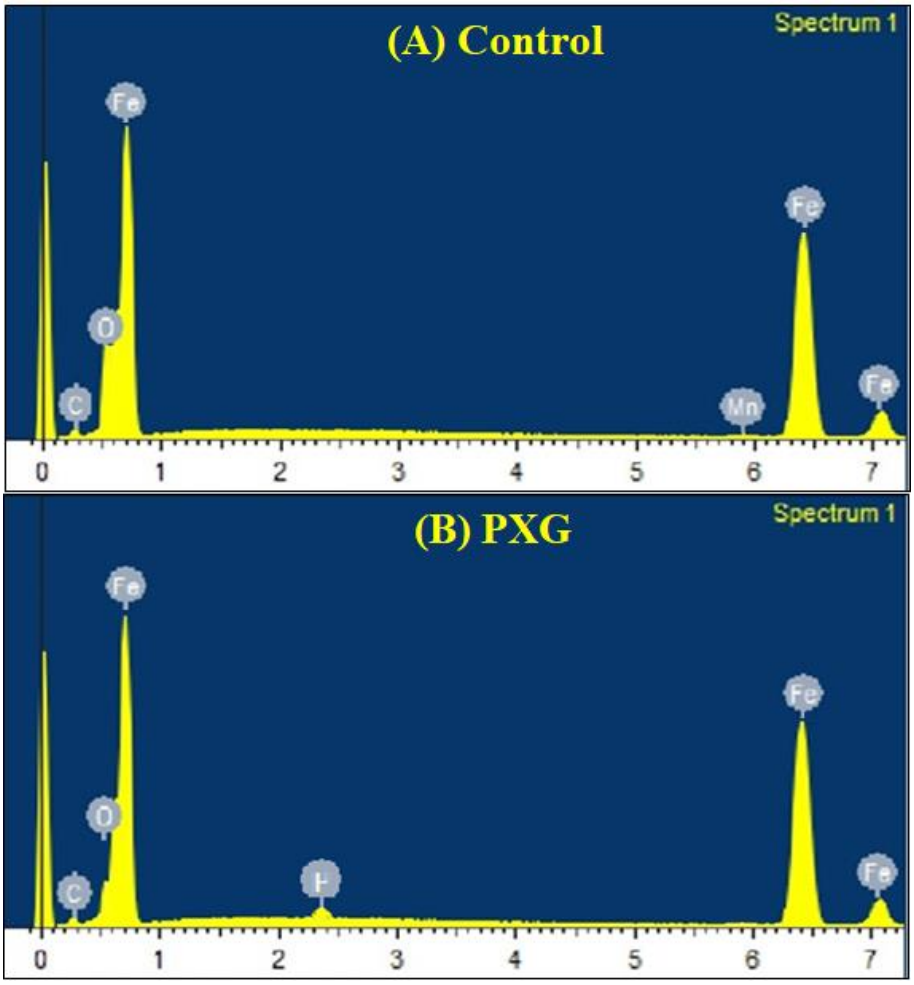


**Figure VI.2.7:** EDX spectrum of mild steel specimen immersed in 200 ppm NaCl environment (A) without inhibitor (B) With 150 ppm of PXG.

The SEM and EDX spectrum of mild steel in presence of PXG give a clear evidence that the surface smoothness has been retained even after 7 days of immersion in the corrosion environment and there is formation of a surface film which is protective in nature. This protective film constitutes the inhibitor molecule (PXG). This protective film prevents the metal surface from corrosion in the corrosive environment.

**VI.2.5: Surface analysis by X-ray photoelectron spectroscopic studies (XPS):**

The films formed on the mild steel surface during the seven days immersion in 200 ppm NaCl in the absence and presence of 150 ppm PXG have been characterized using X-ray photoelectron spectroscopy. Figures VI.2.8A and IV.2.8B present the survey spectra in the absence and presence of PXG respectively.

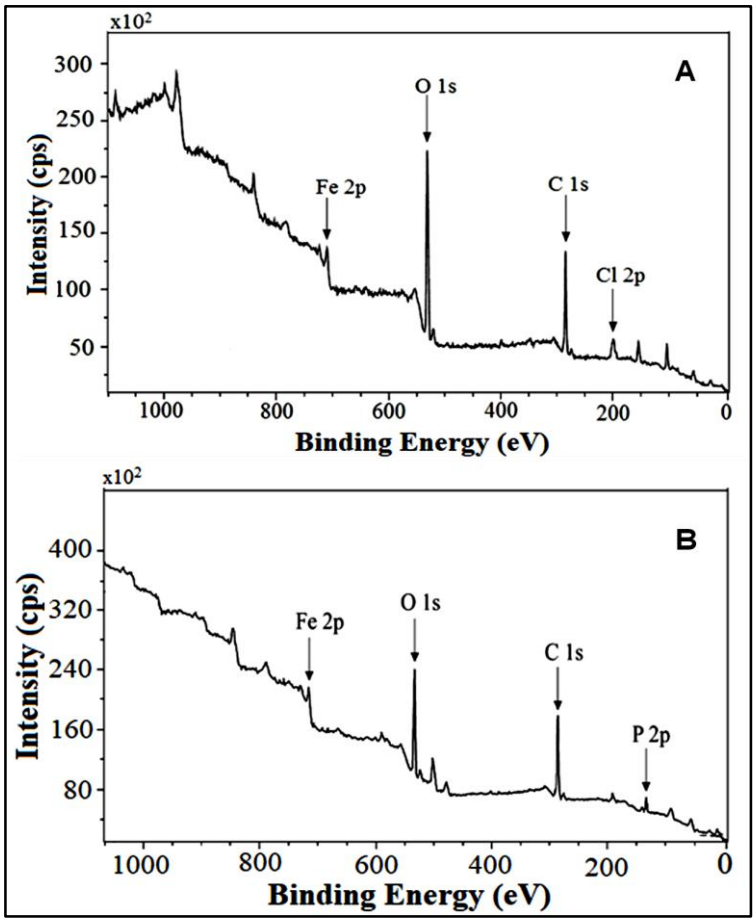


**Figure VI.2.8:** XPS survey spectrum of mild steel specimen immersed in 200 ppm NaCl (A) in the absence of inhibitor, (B) in the presence of 150 ppm PXG.

The survey spectrum of mild steel without any inhibitor comprises of carbon, oxygen, chorine and iron peaks. The carbon peak is only due to contamination in the vacuum chamber. This contamination is mainly because of the cracking of vacuum oil during recording of the XPS spectrum. Whereas, the survey spectrum of mild steel immersed in the corrosive environment in the presence of 150 ppm PXG shows the peaks of carbon, oxygen, iron and phosphorous. This result reveals that the surface film in the presence of inhibitor consists of inhibitor molecules. The corresponding deconvolution spectra for each of the elements are shown in the figures VI.2.9 to VI.2.12.

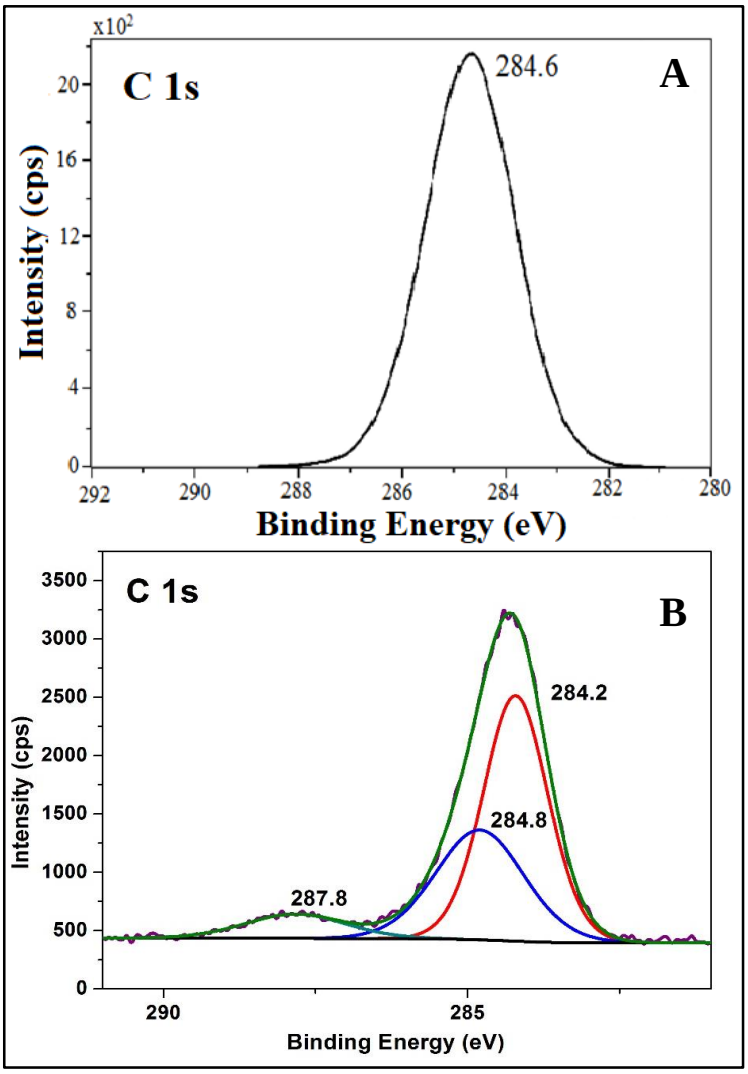


**Figure VI.2.9:** XPS deconvolution spectra of C 1s for mild steel sample immersed in **(A)** 200 ppm NaCl **(B)** 200 ppm NaCl along with 150 ppm PXG.

Figure VI.2.9A represents C 1s deconvolution spectrum for control which consists a single peak at a binding energy value of 284.6 eV, which is attributed to the contaminant carbon due to cracking of vacuum oil during the measurement[10]. Whereas, C 1s deconvolution spectrum in the presence of PXG consists of three distinguishable peaks. The first peak appeared at a binding energy value of 284.2 eV. The second peak appeared at 284.8 eV and the third peak with a low intensity appeared at 287.8 eV. Presence of three different peaks can be attributed to the presence of three different carbon environments in the protective film. The inhibitor molecule consists of different types of carbon environments mainly C-O, C-H, and C=O. The peak at 284.8 eV can be interpreted as the peak due to C – C and C – H [27] and the peak at 287.8 eV can be assigned to C=O peak [28] which is present in the backbone structure of xanthan gum molecule.

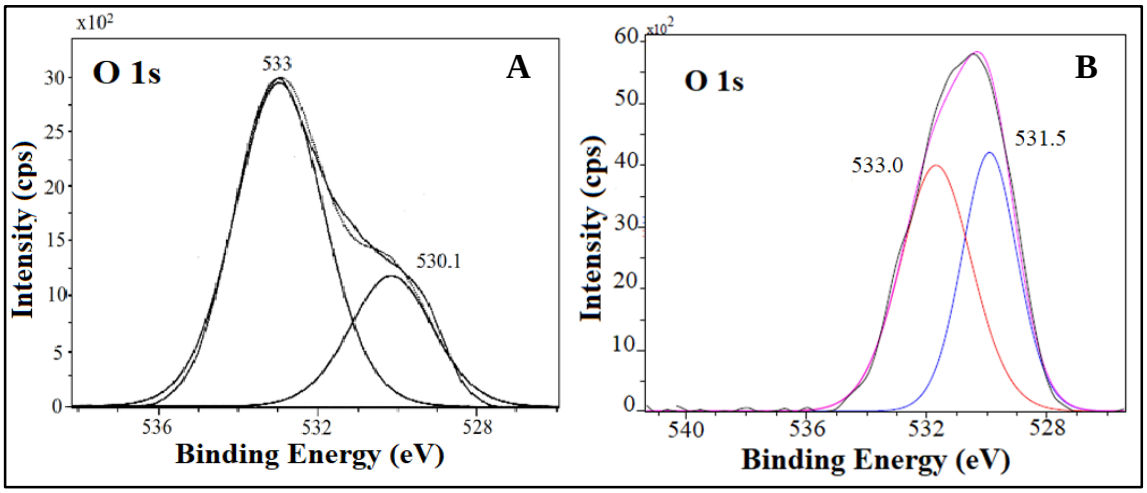


**Figure VI.2.10:** XPS deconvolution spectra of O1s for mild steel sample immersed in **(A)** 200 ppm NaCl **(B)** 200 ppm NaCl along with 150 ppm PXG.

Figure VI.2.10A represents the deconvolution spectrum of O 1s in the case of control, which consists of two peaks, one peak at a binding energy value of 530.1 eV and another one at a binding energy value of 533.0 eV. The peak located at a lower binding energy value (530.1 eV) can be attributed to $O^{2-}$ and can be related to the bond with $Fe^{3+}$ in iron oxides and hydroxides ($Fe_2O_3$, $Fe_3O_4$). The peak located at higher binding energy value (533.0 eV) can be ascribed to oxygen atoms of the adsorbed water molecules. Whereas, the O 1s deconvolution spectrum in presence of 150 ppm PXG as inhibitor consists of two distinguishable peaks, one at 531.5 eV and the other one at 533.0 eV. The former one can be due to oxygen in hydrous iron oxides, such as FeOOH, $Fe(OH)_3$ [29], and some contribution from the oxygen present in the PXG inhibitor molecule. The peak at 533 eV may be due to oxygen present in the PXG molecule, which contains different oxygen environments.

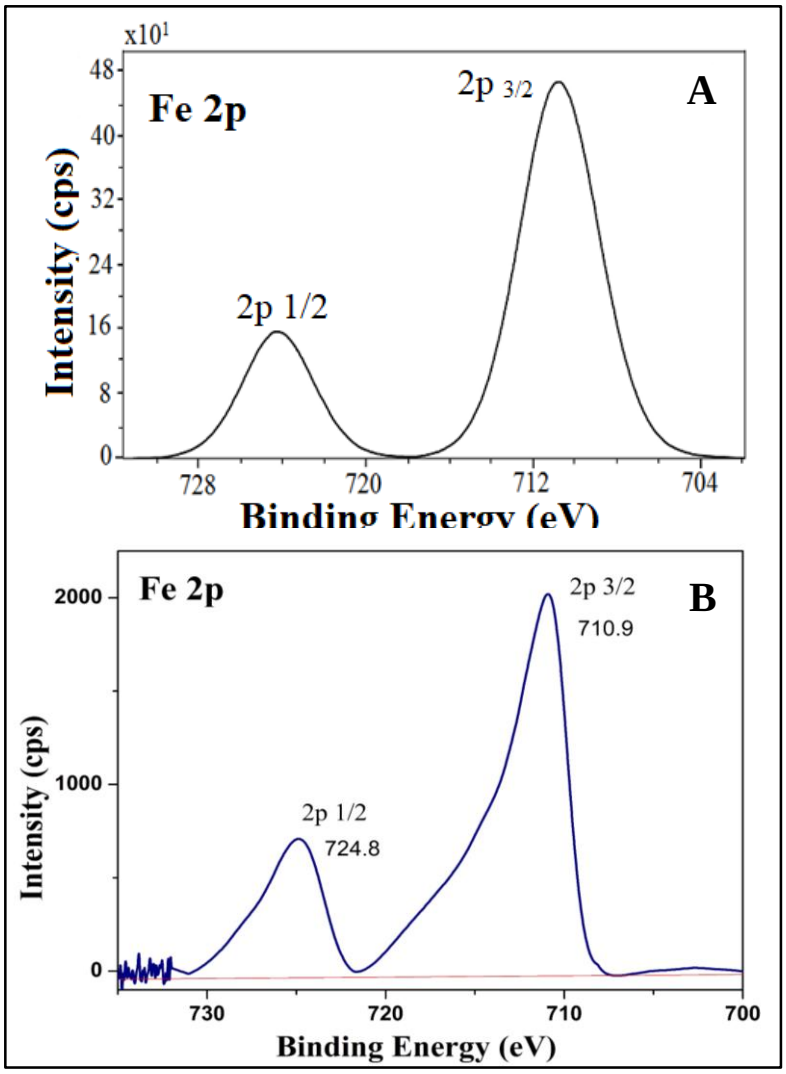


**Figure VI.2.11:** XPS deconvolution spectra of Fe 2p for mild steel sample immersed in **(A)** 200 ppm NaCl **(B)** 200 ppm NaCl along with150 ppm PXG.

The computer deconvolution spectrum of the Fe 2p of control is shown in figure VI.2.11A. The Fe $2p_{3/2}$ peak can be seen at 710.8 eV and a peak at 724.2 eV corresponds to the Fe $2p_{1/2}$. There is a large shift in the binding energy value of Fe $2p_{3/2}$ from the characteristic elemental binding energy value of 707.0 eV. This shift of 3.8 eV suggests that iron is present as Fe(III) in the form of ferric oxide and hydroxide. Indeed, the peak at a binding energy of 710.8 eV has been attributed to ferric compounds such as $Fe_2O_3$, $Fe_3O_4$ and FeOOH in the literature[30,31]. The peak located at 724.2 eV is attributed to the presence of a small concentration of $FeCl_3$ on the metal surface[32]. This can also be supported by the presence of a chlorine peak in the XPS survey spectrum. FigureVI.2.11B illustrates the Fe 2p deconvolution spectrum of the surface film in the presence of 150 ppm PXG, which also consists of two peaks, the Fe $2p_{3/2}$ peak at 710.9 eV and the Fe $2p_{1/2}$ peak at 724.8 eV.

The Fe $2p_{3/2}$ peak can be attributed to the iron present in the Fe(III)- PCT complex, and iron present in the oxides and hydroxides ($Fe_2O_3$, $Fe_3O_4$ and FeOOH), which may also be present in the surface film due to initial corrosion of iron. There is no peak due to elemental iron in the case of control or in the presence of the inhibitor formulation.

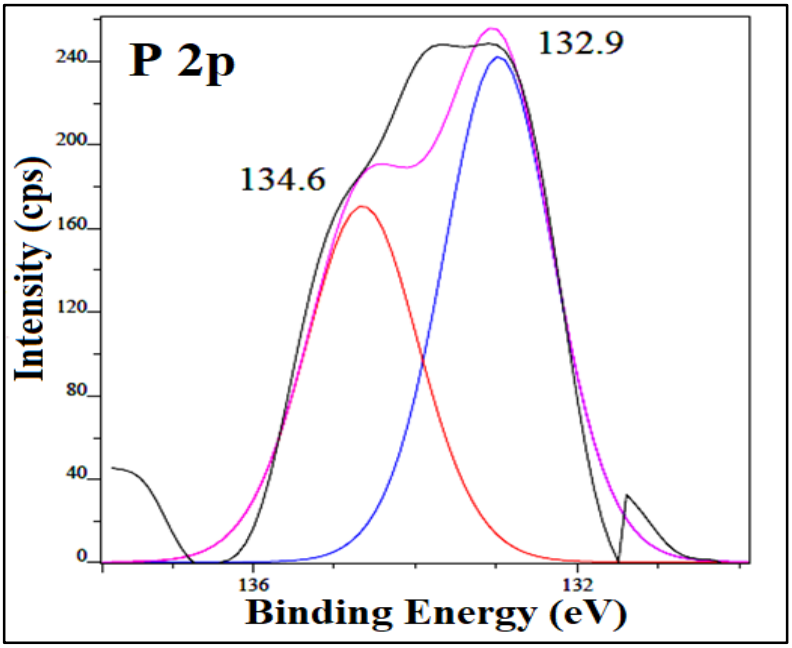


**Figure VI.2.12:** XPS deconvolution spectra of P 2p for mild steel sample immersed in 200 ppm NaCl along with 150 ppm PXG as inhibitor.

Figure VI.2.12 depicts the P 2p computer deconvolution spectrum of the surface film in the presence of 150 ppm PXG**.** The spectrum shows two peaks, one at 132.9 eV and the other one at 134.6 eV. The peak at 132.9 is mainly because of phosphate group present in the PXG molecule. The peak at 134.6 eV can be attributed to phosphates of iron(III) which are the main components of the complex in the protective film formed on the mild steel surface[33–36]. Based on the literature reports, the characteristic binding energy value of this coordinate phosphate is around 134.2 eV[37–39]. With all these evidences from the XPS deconvolution spectra of C, O, Fe and P in the present study, the presence of PXG in the protective film formed on mild steel surface is confirmed.

**VI.2.6: Analysis of the surface film by X- ray diffraction studies (XRD):**

Figures VI.2.13(A) and VI.2.13(B) show the X-ray diffractograms of the surface film formed on mild steel when immersed in 200 ppm NaCl environment without and with 200 ppm of PXG inhibitor respectively.

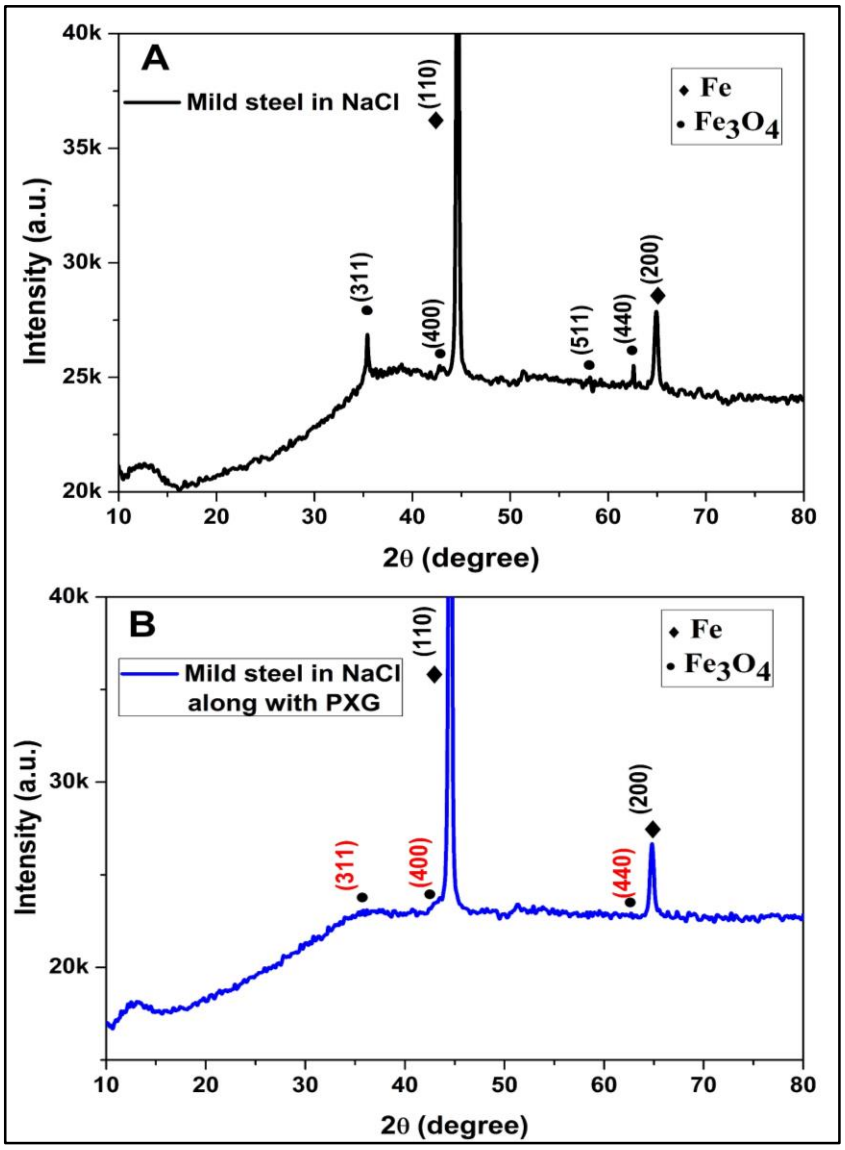


**Figure VI.2.13:** The X-ray diffraction patterns of the surface film formed on mild steel sample immersed in 200 ppm NaCl (A) in the absence (B) in the presence of PXG (150 ppm).

The XRD pattern shows prominent iron (Fe) peaks at (1 1 0) and (2 0 0) planes in both the cases, since mild steel is the alloy in the present study. Along with these iron peaks, the XRD pattern in control also shows peaks for corrosion product, $Fe_3O_4$ [40,41] in the planes (3 1 1), (4 4 0), (4 0 0) and (5 1 1). Whereas, The XRD pattern of mild steel surface in the presence of PXG shows almost, dissapearence of the $Fe_3O_4$ peaks as the intensities are so less when compared with the intensities of iron (1 1 0). This result infers that the surface is less corroded in presence of 200 ppm PXG. It is also intresting to note that the decrease in peak intensities is higher in presencce of PXG when compared

with the other inhibitor formulation namely PCT and $Zn^{2+}$ in controlling corrosion of mild steel in neutral chloride environment.

### VI.2.7: Langmuir adsorption isotherm:

The interaction of PXG molecule with mild steel surface can give an idea about the inhibition mechanism by PXG molecules. Different adsorption isotherm models were taken into consideration to understand the inhibition mechanism of PXG and among them Langmuir adsorption isotherm model is well fitted (based on the $R^2$ value). The Langmuir adsorption isotherm equation is already given in the equation (1) in this chapter.

In the present case $\emptyset$ is the surface coverage of the inhibitor molecule (Which is obtained by the relation, $\text{I. E.}\,\% = \emptyset\, X\, 100$), C is the concentration of PXG ($mgL^{-1}$) and $K_{ads}$ is the equilibrium constant.

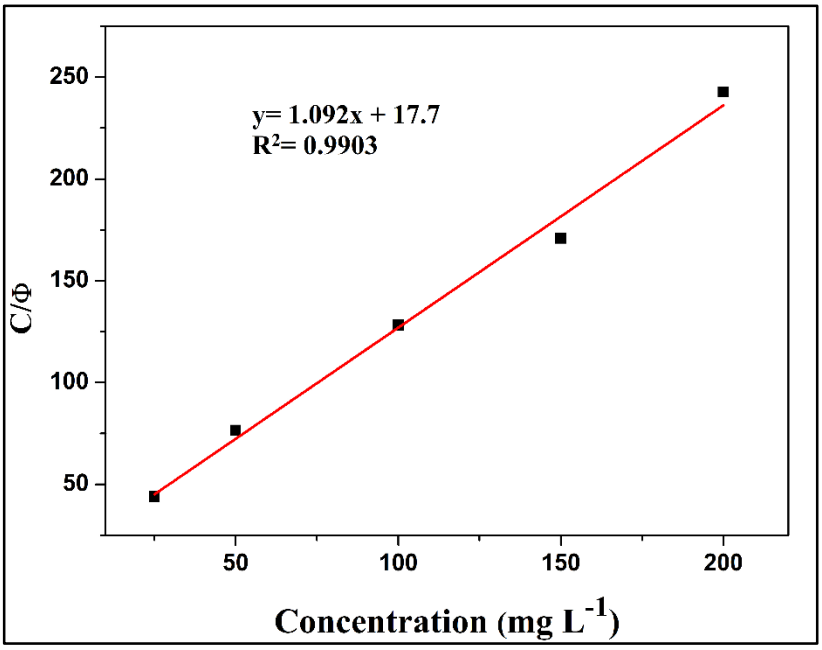


**Figure VI.2.14:** Langmuir adsorption isotherm for the adsorption of PXG on mild steel surface.

Figure VI.2.14 shows $C/\emptyset\, Vs\, C$ plot. A linear plot is obtained with a good correlation coefficient value ($R^2$= 0.9903), which infers that the adsorption process follows Langmuir adsorption isotherm model.

### VI.2.8: Mechanistic aspects of corrosion and corrosion inhibition:

The mechanism of corrosion of mild steel in nearly neutral aqueous medium in the absence of any inhibitor is well established[42,43]. However, the anodic and cathodic reactions are reproduced below.

At anode $Fe \longrightarrow Fe^{2+} + 2e^-$ (4)

At cathode $H_2O + 1/2\ O_2 + 2e^- \longrightarrow 2OH^-$ (5)

between anode and cathode $Fe^{2+} + 2OH^- \longrightarrow Fe(OH)_2$ (6)

$Fe(OH)_2 \xrightarrow{[O_2]} Fe(OH)_3$ (7)

When Phosphorylated xanthan gum (PXG) is added to the aqueous NaCl solution, the PXG molecules diffuse to the metal surface and get chemisorbed. The chemisorbed PXG molecule form a complex with Fe(III) ions present on the metal surface through the P and O donor atoms present in PXG. This complex film blocks the contact between the metal surface and the corrosive environment. This phenomenon minimizes the diffusion of ions or molecules to and from the metal surface and protects mild steel from corrosion.

PXG + Fe (III) $\longrightarrow$ [Fe (III)–PXG]…. (9)

The protective film may consist of the [Fe(III)-PXG] complex and ferric hydroxide.

**References:**


1. Hirano, S., Usutani, A. & Zhang, M. Chitin xanthate and some xanthate ester derivatives. *Carbohydr. Res.* **256,** 331–336 (1994).
2. Sankararamakrishnan, N. & Sanghi, R. Preparation and characterization of a novel xanthated chitosan. *Carbohydr. Polym.* **66,** 160–167 (2006).
3. Dong, T.-T., Chen, G.-H. & Gao, C.-J. Preparation of chitin xanthate/polyacrylonitrile NF composite membrane with cross-linking agent hydrogen peroxide and its characterization. *J. Memb. Sci.* **304,** 33–39 (2007).
4. MacDonald, D. D. Reflections on the history of electrochemical impedance spectroscopy. *Electrochim. Acta* **51,** 1376–1388 (2006).
5. ASTM. ASTM G102 - 89(2010) Standard Practice for Calculation of Corrosion Rates and Related Information from Electrochemical Measurements. in *Annual Book of ASTM Standards* **89,** 1–7 (2010).
6. Milosev, I., Pavlinac, J., Hodoscek, M. & Lesar, A. Amino acids as corrosion inhibitors for copper in acidic medium: Experimental and theoretical study. *J. Serbian Chem. Soc.* **78,** 2069–2086 (2013).
7. Kear, G., Barker, B. D. & Walsh, F. C. Electrochemical corrosion of unalloyed copper in chloride media—a critical review. *Corros. Sci.* **46,** 109–135 (2004).
8. Cicileo, G. P., Rosales, B. M., Varela, F. e. & Vilche, J. R. Comparative study of organic inhibitors of coppercorrosion. *Corros. Sci.* **41,** 1359–1375 (1999).
9. Outirite, M. *et al.* ac impedance, X-ray photoelectron spectroscopy and density functional theory studies of 3,5-bis(n-pyridyl)-1,2,4-oxadiazoles as efficient corrosion inhibitors for carbon steel surface in hydrochloric acid solution. *Electrochim. Acta* **55,** 1670–1681 (2010).
10. Naumkin, A. V., Kraut-Vass, A., Powell, C. J. & Gaarenstroom, S. . NIST Standard Reference Database 20 version 4.1. *The National Institute of Standards and Technology NIST* 1–49 (2012). Available at: http://srdata.nist.gov/xps.
11. Ghodselahi, T., Vesaghi, M. A., Shafiekhani, A., Baghizadeh, A. & Lameii, M. XPS study of the Cu@Cu2O core-shell nanoparticles. *Appl. Surf. Sci.* **255,** 2730–2734 (2008).
12. Beccaria, A. M. & Bertolotto, C. Inhibitory action of 3-trimethoxysilylpropanethiol-1 on copper corrosion in NaCl solutions. *Electrochim. Acta* **42,** 1361–1371 (1997).

13. Appa Rao, B. V., Iqbal, M. Y. & Sreedhar, B. Electrochemical and surface analytical studies of the self-assembled monolayer of 5-methoxy-2-(octadecylthio)benzimidazole in corrosion protection of copper. *Electrochim. Acta* **55,** 620–631 (2010).
14. Bruce, T. Interfacial reactions of ion beam deposited a-C films on ZnS. *J. Vac. Sci. Technol. A Vacuum, Surfaces, Film.* **12,** 1487 (1994).
15. Landry, C. & Barron, R. Synthesis of polycrystalline chalcopyrite semiconductors by microwave irradiation. *Science* **260,** 1653–1655 (1993).
16. Briggs, D. & Grant, J. T. Surface Analysis by Auger and X-Ray Photoelectron Spectroscopy. in *Surface Analysis by Auger and X-Ray Photoelectron Spectroscopy* 31–56 (2003). doi:10.1016/0378-5963(78)90014-4
17. Meghana, S., Kabra, P., Chakraborty, S. & Padmavathy, N. Understanding the pathway of antibacterial activity of copper oxide nanoparticles. *RSC Adv.* **5,** 12293–12299 (2015).
18. Aslan, E., Patir, I. H. & Ersoz, M. Cu Nanoparticles Electrodeposited at Liquid-Liquid Interfaces: A Highly Efficient Catalyst for the Hydrogen Evolution Reaction. *Chem. - A Eur. J.* **21,** 4585–4589 (2015).
19. Kerber, S. J. *et al.* The Complementary Nature of X-Ray Photoelectron Spectroscopy and Angle-Resolved X-Ray Diffraction Part I: Background and Theory. *J. Mater. Eng. Perform.* **7,** 329–333 (1998).
20. Bastidas, J. Characterization of corrosion products on a copper-containing intrauterine device during storage at room temperature. *Biomaterials* **18,** 247–250 (1997).
21. Cicileo, G. P., Rosales, B. M., Varela, F. e. & Vilche, J. R. Comparative study of organic inhibitors of coppercorrosion. *Corros. Sci.* **41,** 1359–1375 (1999).
22. Sastri, V. S., Perumareddi, J. R., Lashgari, M. & Elboujdaini, M. Application of Ligand Field Theory in Corrosion Inhibition. *Corrosion* **64,** 283–288 (2008).
23. Ravi Kumar, M. N. . A review of chitin and chitosan applications. *React. Funct. Polym.* **46,** 1–27 (2000).
24. Nishi, N., Maekita, Y., Nishimura, S., Hasegawa, O. & Tokura, S. Highly phosphorylated derivatives of chitin, partially deacetylated chitin and chitosan as new functional polymers: metal binding property of the insolubilized materials. *Int. J. Biol. Macromol.* **9,** 109–114 (1987).

25. Gunasekaran, G. & Chauhan, L. . Eco friendly inhibitor for corrosion inhibition of mild steel in phosphoric acid medium. *Electrochim. Acta* **49,** 4387–4395 (2004).
26. Morad, M. S. An electrochemical study on the inhibiting action of some organic phosphonium compounds on the corrosion of mild steel in aerated acid solutions. *Corros. Sci.* **42,** 1307–1326 (2000).
27. Bentiss, F. *et al.* Corrosion control of mild steel using 3,5-bis(4-methoxyphenyl)-4-amino-1,2,4-triazole in normal hydrochloric acid medium. *Corros. Sci.* **51,** 1628–1635 (2009).
28. Barth, G., Linder, R. & Bryson, C. Advances in charge neutralization for XPS measurements of nonconducting materials. *Surf. Interface Anal.* **11,** 307–311 (1988).
29. Babić-Samardzija, K., Lupu, C., Hackerman, N., Barron, A. R. & Luttge, A. Inhibitive properties and surface morphology of a group of heterocyclic diazoles as inhibitors for acidic iron corrosion. *Langmuir* **21,** 12187–96 (2005).
30. Pech-Canul, M. a. & Bartolo-Pérez, P. Inhibition effects of N-phosphono-methyl-glycine/Zn2+ mixtures on corrosion of steel in neutral chloride solutions. *Surf. Coatings Technol.* **184,** 133–140 (2004).
31. Bouanis, F. Z., Bentiss, F., Traisnel, M. & Jama, C. Enhanced corrosion resistance properties of radiofrequency cold plasma nitrided carbon steel: Gravimetric and electrochemical results. *Electrochim. Acta* **54,** 2371–2378 (2009).
32. Sastri, V. S., Elboujdaini, M., Brown, J. R. & Perumareddi, J. R. Surface Analysis of Inhibitor Films Formed in Hydrogen Sulfide Medium. *Corrosion* **52,** 447–452 (1996).
33. Sherwood, P. M. A. Introduction to Studies of Phosphorus-Oxygen Compounds by XPS. *Surf. Sci. Spectra* **9,** 62–66 (2002).
34. Gu, Q. & Cheng, X. Tribological behaviors of lanthanum-based phosphonate 3-aminopropyltriethoxysilane self-assembled films. *Appl. Surf. Sci.* **253,** 6800–6806 (2007).
35. Viornery, C. *et al.* Surface modification of titanium with phosphonic acid to improve bone bonding: Characterization by XPS and ToF-SIMS. *Langmuir* **18,** 2582–2589 (2002).
36. Keszthelyi, T. *et al.* Investigation of Solid Surfaces Modified by Langmuir−Blodgett Monolayers Using Sum-Frequency Vibrational Spectroscopy

and X-ray Photoelectron Spectroscopy. *J. Phys. Chem. B* **110,** 8701–8714 (2006).

37. Felhősi, I. Effects of Bivalent Cations on Corrosion Inhibition of Steel by 1-Hydroxyethane-1,1-diphosphonic Acid. *J. Electrochem. Soc.* **146,** 961–969 (1999).
38. Nakayama, N. Inhibitory effects of nitrilotris(methylenephosphonic acid) on cathodic reactions of steels in saturated Ca(OH)2 solutions. *Corros. Sci.* **42,** 1897–1920 (2000).
39. Ochoa, N., Baril, G., Moran, F. & Pébère, N. No Title. *J. Appl. Electrochem.* **32,** 497–504 (2002).
40. Loh, K.-S., Lee, Y., Musa, A., Salmah, A. & Zamri, I. Use of Fe3O4 Nanoparticles for Enhancement of Biosensor Response to the Herbicide 2,4-Dichlorophenoxyacetic Acid. *Sensors* **8,** 5775–5791 (2008).
41. Han, R. *et al.* 1D Magnetic Materials of Fe3O4 and Fe with High Performance of Microwave Absorption Fabricated by Electrospinning Method. *Sci. Rep.* **4,** 7493 (2015).
42. Rao, B. V. A. & Rao, S. S. Electrochemical and surface analytical studies of synergistic effect of phosphonate, Zn 2+ and ascorbate in corrosion control of carbon steel. *Mater. Corros.* **61,** NA-NA (2009).
43. Saker, S., Aliouane, N., Hammache, H., Chafaa, S. & Bouet, G. Tetraphosphonic acid as eco-friendly corrosion inhibitor on carbon steel in 3 % NaCl aqueous solution. *Ionics (Kiel).* **21,** 2079–2090 (2015).

# CHAPTER-VII

## Summary and Conclusions

# TABLE OF CONTENTS

**CHAPTER – VII**

# CHAPTER – VII

# SUMMARY AND CONCLUSIONS

During the course of this research study, we have developed five different eco-friendly corrosion inhibitor systems based on naturally occurring polymers. To develop these inhibitor systems, we have chemically modified three selected biopolymers namely chitin, chitosan and xanthan gum. We have studied the corrosion inhibition ability of the inhibitor formulations based on these chemically modified biopolymers for mild steel and copper in selected corrosive environments as per the details shown in the table below.

| **S.No.** | **New inhibitor formulation developed in the present study** | **Metal/alloy** | **Corrosive environment** |
|---|---|---|---|
| 1 | Phosphorylated Chitin (PCT) (PCT) + $Zn^{2+}$ ions | Mild steel | aq. NaCl (200 ppm) |
| 2 | Phosphorylated Chitin (PCT) | Copper | aq. NaCl (200 ppm) |
| 3 | Chitosan Ascorbate Ketimine (CAK) + $Cu^{2+}$ ions | Mild Steel | 1M HCl |
| 4 | Chitin Xanthate (CX) | Copper | aq. NaCl (200 ppm) |
| 5 | Phosphorylated Xanthan gum (PXG) | Mild steel | aq. NaCl (200 ppm) |

The synergistic effect of phosphorylated chitin (PCT) and $Zn^{2+}$ ions was studied in controlling the corrosion of mild steel in aqueous 200 ppm NaCl environment. We have studied the synergistic effect of chitosan ascorbate ketimine (CAK) and $Cu^{2+}$ ions in controlling the corrosion of mild steel in 1 M HCl environment.

The methodologies employed to study the corrosion inhibition ability of the selected inhibitor formulations, are gravimetric studies (weight-loss studies), electrochemical impedance studies (EIS) and potentiodynamic polarization studies. The surface morphological studies were carried out using scanning electron microscopy (SEM) and the analysis of the films formed during the course of corrosion and inhibition processes has been carried out using energy dispersive X-ray spectroscopy (EDX), X-ray photoelectron spectroscopy (XPS) and X- ray diffraction (XRD).

The synergistic effect of PCT and $Zn^{2+}$ in controlling the corrosion of mild steel in neutral chloride environment was studied using weight-loss (gravimetric) measurements. The results of weight-loss studies established the synergistic effect of PCT and $Zn^{2+}$ in

controlling corrosion of mild steel in neutral chloride environment. The binary system consisting of 200 of ppm PCT and 100 ppm of $Zn^{2+}$ ions afforded an inhibition efficiency of 93 %.

From the EIS results, the Nyquist plots obtained are depressed semi-circles with one time constant. From the results, it is also quite evident that PCT possesses excellent synergism with $Zn^{+2}$ ions. The inhibition efficiency increased from 83 % in case of 200 ppm PCT to 94 % in case of 200 ppm PCT+100 ppm of $Zn^{+2}$. From the potentiodynamic polarization studies, it can be inferred that in presence of inhibitor the corrosion potential values are shifted towards more negative direction with respect to the control. Both the anodic and cathodic current density values are reduced and both the anodic and cathodic Tafel slopes are changed in the presence of inhibitor formulation. These results infer that the inhibitor formulation acts as a mixed inhibitor, predominantly cathodic in nature. The polarization studies showed that PCT+$Zn^{2+}$ combination afforded an inhibition efficiency of 93 %. Thus, weight-loss studies, impedance studies and polarization studies confirmed that the PCT+$Zn^{2+}$ is a promising corrosion inhibitor for mild steel in neutral chloride (200 ppm) environment.

The SEM images of mild steel after immersing in corrosive environment with 200 ppm P-Chitin, and 200 ppm P-Chitin in combination with 100 ppm $Zn^{2+}$ clearly show the retention of surface smoothness and absence of any corrosion product, when compared with the SEM images of mild steel immersed in control. Analysis of the XPS deconvolution spectra of the individual elements present in the surface film formed on the mild steel in presence of binary inhibitor formulation inferred that the protective film consists of the complex, ($Fe^{3+}$-$Zn^{2+}$-P-chitin), $Zn(OH)_2$ as well as small amounts of oxides and hydroxides of Fe(III). The adsorption process obeys Langmuir adsorption isotherm model with an excellent regression coefficient value of 0.9999. Based on all the experimental results the plausible mechanism of the corrosion inhibition process has been discussed, in which we have tried to explain the reasons for inhibition effect and synergistic effect between PCT and $Zn^{2+}$ ions.

The second inhibitor system developed in the present study was phosphorylated chitin (PCT) as a corrosion inhibitor to control the corrosion of copper in neutral chloride environment. The weight-loss studies inferred that PCT inhibited the dissolution of copper in chloride environment and an inhibition efficiency of 88 % has been obtained with 200 ppm of PCT. Further increase in the concentration of the PCT has no effect on the

inhibition efficiency.

The Nyquist plots obtained from impedance studies are depressed semi-circles with two time constant. Analysis of the results of EIS studies inferred that PCT exhibited good inhibition efficiency for copper corrosion in neutral chloride environment. We have obtained a maximum inhibition efficiency of 92 % when 200 ppm PCT was used as an inhibitor. Polarization studies indicated that by the addition of different concentrations of PCT, the corrosion rate of copper is decreased significantly, with highest inhibition efficiency of 89 % for 200 ppm PCT. Polarization studies also indicated that PCT acts as a mixed type inhibitor for copper corrosion in neural chloride environment.

The SEM studies revealed that in the presence of 200 ppm PCT the copper surface retained its smoothness even after 10 days of immersion in corrosion environment. The EDX studies inferred that in the presence of 200 ppm PCT, the composition of the protective film consists of phosphorous, nitrogen, carbon and oxygen, which are present in the adsorbed inhibitor molecule. Analysis of the XPS survey spectrum showed additional peaks of P and N in the presence of inhibitor along with C 1s, O 1s and Cu 2p peaks. The XPS deconvolution spectra of the individual elements present in the surface film formed on the copper in presence of inhibitor (200 ppm) inferred that the protective film consists of the complex, (Cu(II)-P-chitin), as well as oxides and hydroxides of Cu(II).

Langmuir adsorption isotherm model is well fitted in this case also with a regression coefficient value of 0.9968. Based on all the experimental results a plausible mechanism of the corrosion inhibition process has been discussed, in which we have tried to explain the reasons for the inhibition effect.

The third inhibitor system developed in the present study was chitosan and ascorbic acid along with $Cu^{2+}$ ions to combat the corrosion of mild steel in 1 M HCl environment. The weight-loss studies established the synergistic effect between chitosan ascorbate ketimine (CAK) and $Cu^{2+}$ ions. When chitosan and ascorbic acid are mixed with each other, there is formation of chitosan ascorbate ketimine (CAK). From results of weight-loss studies it is found that chitosan ascorbate ketimine (CAK) decreases the corrosion rate of mild steel in 1 M HCl when compared with the control. Moderate inhibition efficiency was observed in presence of CAK. Whereas, the corrosion rate of carbon steel is even more reduced and highest inhibition efficiency of 86 % is obtained when 50 ppm of $Cu^{2+}$ ions were added to the CAK solution. This result indicates that the CAK has a synergistic relation with $Cu^{2+}$ions in controlling the corrosion of mild steel in 1 M HCl.

From the EIS studies, the Nyquist plots showed depressed semicircle whose centre is under the horizontal line with two-time constant system. Analysis of EIS studies inferred that CAK showed excellent synergistic relation with $Cu^{2+}$ in controlling the corrosion of mild steel in 1 M HCl environment. The inhibition efficiency increased from 69 % (200 ppm chitosan + 400 ppm ascorbic acid) to 89 % (200 ppm chitosan + 400 ppm ascorbic acid+ 50 ppm $Cu^{+2}$). From the results of potentiodynamic polarization studies, it can be inferred that CAK and CAK+ $Cu^{2+}$ systems act as mixed type inhibitors. Potentiodynamic polarization studies also revealed very good corrosion inhibition of mild steel in 1 M HCl in the presence of CAK+$Cu^{2+}$.

The SEM studies of the mild steel surface indicate that the surface retained its smoothness in presence of CAK as well as CAK+ $Cu^{+2}$ formulations when compared to control. The corresponding EDX spectra inferred that the surface film comprises of the elements of the inhibitor formulation. Analysis of the XPS survey spectrum in presence of inhibitor formulation shows additional peaks for N, Cu and an increase in the intensity of oxygen peak. The XPS deconvolution spectra of the individual elements present in the surface film infer that in the presence of inhibitor formulation the protective film may consist of [Fe(III),Cu(II)-CAK] complex, [Cu(II)-CAK] complex and [Fe(III)-CAK] complex. Based on all the experimental results a plausible mechanism of the corrosion inhibition has been discussed, in which we have tried to explain the reasons behind synergistic effect and process of inhibition.

The fourth inhibitor system developed in the present study was chitin xanthate (CX) as a corrosion inhibitor to combat corrosion of copper in neutral chloride environment. From the analysis of weight-loss studies, it is established that chitin xanthate works efficiently in controlling the corrosion of copper in 200 ppm NaCl environment. An inhibition efficiency of 95 % was obtained at a concentration of 30 ppm of CX.

The Nyquist and Bode plots of copper immersed in 200 ppm NaCl along with different concentrations of chitin xanthate (CX) showed no signs of Warburg behaviour, indicating the absence of diffusion process. Whereas, in control solution Warburg behaviour was observed. There is a significant increase in the $R_{ct}$ value in presence of chitin xanthate at all concentrations. An inhibition efficiency of 92 % was obtained at 30 ppm chitin xanthate. From the potentiodynamic polarization studies, it is inferred that the CX acts as a mixed type inhibitor, predominantly anodic in nature. The highest inhibition efficiency of 91 % was obtained for the 30 ppm CX from the polarization studies.

The surface morphological study by SEM revealed that in the presence of chitin xanthate, the surface is relatively smooth and does not exhibit any pit nor any sign of corrosion. From the corresponding EDX spectrum it was found that carbon, nitrogen and sulphur are present along with copper in the surface film. Analysis of the results of XPS studies inferred that in the presence of chitin xanthate the surface films formed consists of a complex of Cu(II)-CX along with oxides and hydroxides of copper. The adsorption of CX on copper obeys Langmuir adsorption isotherm model with a regression coefficient value of 0.9998. Based on all the experimental results a plausible mechanism of corrosion inhibition process has been discussed.

The fifth inhibitor system developed in the present study was phosphorylated xanthan gum (PXG) as inhibitor for the corrosion of mild steel in neutral chloride environment. The results of the weigh-loss studies inferred that PXG inhibited the corrosion of mild steel in neutral chloride environment and showed the highest inhibition efficiency of 88 % at a concentration of 150 ppm PXG.

The Nyquist plots are depressed semi-circles with one time constant. From analysis of the results it can be concluded that PXG works excellently in controlling the corrosion of mild steel. An inhibition efficiency of 93 % was obtained when 150 ppm PXG is used. Polarization studies indicated that PXG acts as a mixed type inhibitor, and the maximum inhibition efficiency of PXG (150 ppm) was found to be 90 %.

The surface morphological studies of mild steel specimens by SEM inferred that the surface has retained its smoothness in presence of 150 ppm PXG as inhibitor. The corresponding EDX spectrum showed the presence of phosphorus peak in presence of inhibitor along with carbon, oxygen and iron peaks. From the analysis of the results of XPS studies and deconvolution spectra of individual elements, it is inferred that the inhibitor molecules (PXG) are the major constituents of the surface film formed on the mild steel. Adsorption of PXG on mild steel surface follows Langmuir adsorption isotherm model with a regression coefficient value of 0.9903. The mechanistic aspects were discussed.

The newly developed inhibitor systems in the present study along with the corresponding metal, corrosive environment and inhibition efficiencies obtained from different methods are presented in table VII.1.

It may be noted that in the weight-loss studies, the immersion period was 7 days for mild steel in the said corrosive environments and it was 10 days for copper in the said

corrosive media. However, the immersion period in impedance studies, polarization studies was 24 h only.

**Table VII.1:** Newly developed inhibitor systems and their inhibition efficiencies from different methods.

| S.No. | Inhibitor formulation | Metal/alloy | Corrosive environment | Inhibition efficiency | | |
|---|---|---|---|---|---|---|
| | | | | Weight-loss Studies | EIS Studies | Polarization Studies |
| 1 | PCT+ $Zn^{2+}$ | Mild steel | aq. NaCl | **92 %** | **94 %** | **93 %** |
| 2 | PCT | Copper | aq. NaCl | **88 %** | **92 %** | **89 %** |
| 3 | CAK+ $Cu^{2+}$ | Mild Steel | 1M HCl | **86 %** | **89 %** | **88 %** |
| 4 | Chitin Xanthate | Copper | aq. NaCl | **96 %** | **92 %** | **92 %** |
| 5 | Phosphorylated Xanthan gum | Mild steel | aq. NaCl | **88 %** | **93 %** | **90 %** |

## CONCLUSIONS OF THE PRESENT STUDY

1. All the five newly developed inhibitor systems are proved to be excellent corrosion inhibitors for the respective metal or alloy in the selected corrosive environment. All the inhibitor formulations afforded very high inhibition efficiencies. Thus, one of the objectives of the present study, i.e. development of environment-friendly corrosion inhibitors based on naturally occurring polymers is achieved.
2. From the present study, the synergistic relationship between phosphorylated chitin and $Zn^{2+}$ ions in controlling the corrosion of mild steel in 200 ppm NaCl is established. The formulation works excellently in controlling the corrosion.
3. The synergistic relationship between chitosan ascorbate ketimine (CAK) and $Cu^{2+}$ ions in controlling the corrosion of mild steel in 1 M HCl is established.
4. From the Nyquist plots obtained in EIS studies, a single time constant was identified for the inhibitor formulations namely, PCT+$Zn^{2+}$ for mild steel corrosion in 200 ppm NaCl and PXG for the corrosion of mild steel in 200 ppm NaCl. Whereas, two time constant was identified for the inhibitor formulations namely, PCT for corrosion of copper in 200 ppm NaCl, CX for corrosion of copper in 200 ppm NaCl and CAK+$Cu^{2+}$ for corrosion of mild steel in 1 M HCl.

5. Potentiodynamic polarization studies show that all the inhibitor systems function as mixed type inhibitors by retarding both the anodic and cathodic corrosion processes.
6. SEM-EDX and XPS studies inferred that all the inhibitor systems have formed protective films on the metal or alloy surface. These films have successfully hindered the contact between metal and corrosive environment and thus protected the metal or alloy from corrosion.
7. The results of surface analytical studies namely SEM, EDX, XPS and XRD provide a comprehensive understanding of the protective film and the mechanistic aspects of corrosion protection by each of the new inhibitors developed in the present study.
8. In all the inhibitor formulation studied, the adsorption process of the inhibitor molecules on the metal surface follows Langmuir adsorption isotherm model.
9. The mechanistic aspects of corrosion control of mild steel and copper by the new inhibitor formulations have been discussed. In case of all the inhibitor formulations the inhibitor gets chemisorbed on the metal surface and forms an insoluble coordinated complex with the metal ions.

# TABLE OF CONTENTS

## LIST OF PUBLICATIONS

**Publications in Peer-Reviewed/Refereed International Journals**

1) *"Chemically modified biopolymer as an eco-friendly corrosion inhibitor for mild steel in a neutral chloride environment"* **Vimal Kumar K.,** B. V. Appa Rao*.
**New Journal of Chemistry.** 2017, **41**, 6278-6289 (DOI: 10.1039/c7nj00553a).

2) *"Phosphorylated chitin as a chemically modified polymer for eco-friendly corrosion inhibition of copper in aqueous chloride environment".* **Vimal Kumar K.,** B. V. Appa Rao*, Neha Yeshwanta Hebalkar. **Research on Chemical Intermediates** (2017) **43**, 5811–5828 **(**DOI 10.1007/s11164-017-2964-x**).**

3) *"Corrosion control of mild steel in 1 M HCl by synergistic effect of chitosan ascorbate ketimine and $Cu^{2+}$ ions".* **Vimal Kumar K.,** B. V. Appa Rao*, Neha Yeshwanta Hebalkar. **ACS sustainable chemistry and engineering (under review).**

4) "Chitin xanthate, a chemically modified biopolymer as an eco-friendly inhibitor to combat corrosion of copper in aqueous chloride environment". Vimal Kumar K., B. V. Appa Rao*, Neha Yeshwanta Hebalkar[#]. **Polymer Journal (under review)**

**Publications in Peer-Reviewed/Refereed International Conference Proceedings**

1) *"Corrosion control of mild steel in 1 M HCl by synergistic effect of chitosan ascorbate ketimine and $Cu^{2+}$ ions"* **Vimal Kumar K. and B. V. Appa Rao* won the Best Paper Award in the Young Scientist forum of the International conference 'CORCON-2015'** organized by NACE International Gateway India section, 19-21 November 2015, Chennai Trade Centre, Chennai.

2) *"Chemically modified biopolymer as an eco-friendly corrosion inhibitor for mild steel in cooling water systems"* B. V. Appa rao, **Vimal Kumar K**. Presented at International Corrosion Prevention symposium for research scholars (**CORSYM-2013**) organized by NACE Nigis South Zone Student Section, held at Hotel GRT Grand, Chennai, during 28th February to 2nd March 2013.

3) *"Chitin xanthate, an eco-friendly inhibitor to combat corrosion of copper in aqueous chloride environment"* **Vimal Kumar K.** and B. V. Appa Rao. Presented at "Fourth International Conference on Natural Polymers, Bio-Polymers, Bio-Materials, their Composites, Nanaocomposites, Blends, IPNs, Polyelectrolytes and Gels: Macro to Nano Scales (ICNP – 2015) during April 10, 11 & 12, 2015 at Mahatma Gandhi University, Kottayam, Kerala, India".

4) *"Phosphorylated chitin: an eco-friendly corrosion inhibitor for copper in aqueous chloride environment"* B. V. Appa Rao*, **Vimal Kumar K.** 4th Annual meeting Indian chitin and chitosan society (ICCS) National Conference on Application of the derivatives of Chitin and Chitosan (ADCC-2014). During August 22- 23, 2014.

## PERSONAL INFORMATION

**VIMAL KUMAR K.**

Research Scholar, Department of Chemistry,
National Institute of Technology Warangal, Telangana, India. PIN-506004

+91-9849204754

vimalnitw@gmail.com,

Web Link: https://scholar.google.co.in/citations?hl=en&user=7V9s6-YAAAAJ

Gender: Male | Date of birth: 05-08-1985 | Nationality: Indian

Languages known: English, Telugu and Hindi Marital status: UNMARRIED

## EDUCATION

**July 2011 –Present**

**Ph.D. Thesis submitted**
NIT Warangal, India (http://www.**nitw**.ac.in/)

- Full time Research Scholar in **Department of Chemistry**.
- **Thesis Title: "Studies on *chemically modified biological polymers as environmental friendly corrosion inhibitors*".**

***Course Work :*** As a part of PhD programme, a mandatory Course works have been undergone on the following relevant subjects for one semester

1. Principles of corrosion and corrosion inhibition
2. Advanced Electrochemical Methods
3. Advanced Analytical Techniques
4. Surface Analytical Techniques
5. English for Scientific Communication

**July 2007 – June 2009**

**Master of science in Chemistry (Modern Methods of Chemical Analysis)**
NIT Warangal, India (http://www.**nitw**.ac.in/)
Cumulative Grade Point Average (CGPA): **8.14 (First Division with Distinction)**

**July 2002– June 2005**

**Bachelor of Science ( Mathematics, Physics, Chemistry)**
Kakatiya Univesity, (www.**kakatiya**.ac.in/)
Percentage of marks : **72.5 % (First Division with Distinction)**

**July 2000 – June 2002**

**Intermediate (Mathematics, Physics and Chemistry)**
Board of intermediate Education, A.P., India. (http://**bieap**.gov.in/)
Percentage of marks : **72.2 % (First Division with Distinction**)

**July 1999 – June 2000**

**Secondary School Certificate (High School)**
Board of Secondary Education, A.P., India. (http://**bseap**.org/)
Percentage of marks : 84.5 % **(First Division with Distinction)**

## HONOURS AND AWARDS

- **Won the best paper award** in an international conference CORCON -2015 organised by NACE International, Gate Way India Section,19-21 November 2015, Chennai Trade Centre, Chennai' the title of the paper is 'Corrosion control of mild steel in 1M HCl by synergistic effect of chitosan ascorbate ketimine and $Cu^{2+}$ ions, Vimal Kumar, K and B.V.Appa Rao.
- Qualified joint CSIR-UGC /NET test for junior research fellowship under UGC fellowship scheme held on 17/06/2012.
- Qualified in Graduate Aptitude Test in Engineering (GATE) 2011.
- Qualified Andhra Pradesh state Eligibility test (APSET-2012) for Assistant professor/lectureship.